Copper Electrodeposition in the Presence of Guar or Activated Polyacrylamide

Thesis submitted by
CESIMIRO P FABIAN
In August 2005

for the degree of Doctor of Philosophy
in the Chemical Engineering Department,
School of Engineering
James Cook University

STATEMENT OF ACCESS

I, the undersigned, author of this work, understand that James Cook University will make this thesis available for use within the University Library and, via the Australian Digital Theses network, for elsewhere.

I understand that, as an unpublished work, a thesis has significant protection under the Copyright act and;

I wish this work to be embargoed until 25 July 2006.

_____ _____

Signature **Date**

STATEMENT OF SOURCES

DECLARATION

I declare that this thesis is my own work and has not been submitted in any form for another degree or diploma at any university or other institution of tertiary education. Information derived from the published or unpublished work of others has been acknowledged in the text and a list of references is given.

Signature _____ **Date** _____

ABSTRACT

In the copper electrodeposition industry, it is essential to dose very small concentrations of additives including chloride ions to control the physical and chemical properties of the copper deposit. It is also widely recognized in the industry that the adsorption of these additives at electrode surfaces significantly influences the current-potential relationships. This thesis presents the development of a new organic additive for copper electrowinning and electrorefining. This thesis also presents the comparison between the new organic additive 'activated polyacrylamide' and Guartec (Guar), the industry-standard organic additive for electrowinning under industrial conditions.

The first half of the thesis presents the results of bulk electrolysis experiments using either a rotating cylinder electrode (RCE) or parallel plate electrodes. The RCE was selected since it yields an uniform current distribution. In these experiments, the effectiveness of both organic additives in the presence of chloride ions was determined by directly measuring the surface roughness of the copper deposit. The second half presents Cyclic Voltammetry and Electrochemical Impedance Spectroscopy data using a rotating cylinder electrode to measure and quantify the behaviour of Guar and APAM at the electrolyte/electrode interface also in the presence of chloride ions.

It has been found from the literature review that polyacrylamide hydrolysis in weakly acidic solutions produces block copolymers. The diffusion layer thickness was determined from experimental limiting current density data. In this thesis/work, a

15million Dalton molecular weight polyacrylamide was dissolved in full-strength electrolyte (Cu, 36g/L; H_2SO_4, 160 g/L and chloride ions, 25mg/L) and in solutions with systematically halved concentrations, and in water and alkaline solutions at 50^{o}C for two hours under stirring. The effect of the preparation media of polyacrylamide was tested by measuring the surface roughness of the copper deposits obtained after 6-hours electrowinning at 50^{o}C using a rotating cylinder electrode. The statistically significant lowest surface roughness (6.59μm ± 0.49) was obtained when polyacrylamide was prepared in 16-fold diluted electrolyte (10g/L sulfuric acid and 2.25g/L cupric ions and 1.56mg/L chloride ions). The chemical structure of the polyacrylamide was examined after the preparation in 16-fold electrolyte using NMR. The NMR indicated that less than 10% of the non-ionic polyacrylamide was hydrolysed and it appears to consist of a block copolymer of polyacrylamide and polyacrylic acid. The new organic additive was named activated polyacrylamide (APAM)[1].

A comprehensive study on the effect of Guarfloc66 (Guar), the 40-year-old industry-standard organic additive, on copper electrowinning was lacking prior to this thesis. Guar was used as a basis against which to compare the effectiveness of APAM.

This study provides an industrial-relevant baseline against which the new additive was compared. Therefore, the fundamental processes occurring at the stainless steel/copper metal-electrolyte interface in the presence and absence of Guar and APAM were investigated. Fractional factorial experimental designs for copper electrowinning (EW) were conducted in which the effect of current density, temperature, diffusion layer thickness, Guar and APAM on surface roughness was studied. The evolution of dendrite formation was evaluated using Peaks-per-Centimeter and surface roughness. These above tests were verified by experimental design tests up to 12-hours EW time. The overall results indicated that a more uniform surface and lower roughness was obtained using APAM than Guar.

Cyclic voltammetry (CV) was used to understand the polarization behaviour of Guar and APAM at the interface of the copper electrolyte/copper cathode. Cyclic

[1] A property rights application (PCT/AU2005/001262) for this material has been filed with Intellectual Property, Australia.

voltammetry tests on the ageing of 2mg/L Guar in the electrolyte at 45°C indicated that Guar *depolarized* the electrode. At 300A/m^2 current density about 14mV maximum depolarization was obtained at 2-3 hours residence time whether the working electrode was stainless steel or freshly pre-plated copper metal. In contrast, CV tests showed that the presence of 2mg/L APAM *polarized* the electrode at 45°C and 65°C. At 300A/m^2 current density and 45°C the presence of APAM resulted in a significant polarization of the electrode on pre-plated copper over a 5-hour period, i.e., 13 mV at 5-hours residence time. This polarization value at 65°C was achieved after 1-hour residence time and the electrode remains significantly polarized over a 7-hour period.

Electrochemical Impedance Spectroscopy (EIS) tests were also conducted to characterize the electrode processes in the presence and absence of Guar and APAM. The electrochemical kinetics of the process was evaluated in terms of the charge-transfer resistance (or polarization resistance) and the double-layer capacitance. The electrochemical system of copper deposition in the presence and absence of Guar and APAM is described theoretically in terms of an equivalent circuit. The EIS experimental data was fitted to the equivalent circuit using complex nonlinear least-squares (CNLS) technique with LEVM and ZSimpWin™ software packages. The electrode process in the presence of Guar or APAM was quantitatively characterized using the high frequency loop only since it represents the kinetic control of the process. The low frequency loop that represents the mass-transfer control was used qualitatively only.

EIS tests indicate that Guar *decreased* the charge-transfer resistance values obtained from equivalent circuit modelling from about 0.83ohm.cm^2 in its absence to 0.74ohm.cm^2 at 2mg/L, -490mV versus the Hg/Hg_2SO_4 saturated in K_2SO_4, (MSE) for about 5-hours therefore *increasing* the electrochemical kinetics. The maximum reduction was determined to be 0.086ohm.cm^2 at 2-3hours residence time of Guar in the electrolyte. Therefore, electrowinning using the RCE, CV and EIS indicated that the role of Guar during the deposition process is to act as a *depolarizer*.

The presence of APAM in the electrolyte, in contrast, indicated that the charge-transfer resistance *increased* from about 0.79-ohm.cm^2 to 1-ohm.cm^2 for over 7-hours at 45°C and -490mV vs. MSE. The maximum increase in the charge-transfer resistance

value was 0.23-ohm.cm^2 at 3-5hours residence time. These set of tests with APAM were also repeated at -470mV vs. MSE and 45^{o}C, the results also indicated that APAM *increased* the charge-transfer resistance under these conditions. At this potential, a maximum increase of 0.42-ohm.cm^2 was determined at 3-5hours. When these tests were also repeated at electrorefining temperature (65^{o}C) and -445mV vs. MSE, the presence of APAM in the electrolyte also *increased* the charge-transfer resistance from about 0.39 up to 0.69-ohm.cm^2 for over 5-hours. The maximum increase of 0.34-ohm.cm^2 was at 2-hours for 65^{o}C. Electrowinning tests using the RCE, CV and EIS overall results with APAM were found to be consistent. In summary, APAM was found to *decrease* the electrochemical kinetics and that the role of APAM is as a levelling agent during the deposition process.

Guar and APAM decreased the double-layer capacitance but the equivalent circuit simulation data indicated that while the maximum reduction for Guar was 0.46 x 10^{-5} μF/cm^2, the maximum reduction for APAM was 1.2 x 10^{-5} μF/cm^2 at 45^{o}C and 6.8 x 10^{-5} μF/cm^2 at 65^{o}C. The overall EIS results may indicate that APAM is adsorbed more specifically than Guar.

It was also shown that the effect of temperature on the ageing sequence of APAM is consistent with reaction kinetics, i.e., it is faster at 65^{o}C than at 45^{o}C as would be expected. Results were presented for the rotating disc electrode (RDE) also. The EIS data at 65^{o}C and 45^{o}C are consistent with the CV data whether the RCE or RDE was used. However, the EIS data with the RDE was not amenable to being modelled using the most commonly referred equivalent circuit for electrochemical systems.

Bench-scale *continuou*s electrowinning tests using parallel plate electrodes where APAM and Guar were also dosed continuously and independently also indicated that APAM produces smoother deposits than Guar. The cross sections of the copper deposits were examined using scanning electron microscopy (SEM) and showed that Guar produced *porous* deposits and APAM produced *slightly columnar* deposits.

It is therefore concluded that the results of electrowinning, CV and EIS tests correlate: Guar *depolarizes* the electrode enhancing *depolarization* of the electrode by chloride ions and therefore increasing the growth rate with simultaneous formation of

voids and porosity. APAM *polarizes* the electrode or decreases the rate of the deposition process and therefore assists the nucleation rate and produces purer copper deposits. Voids and porosity are probably reduced by the continuous formation of crystallites and their coalescence as indicated by x-ray diffraction data. The overall results indicate that APAM is more specifically *adsorbed* than Guar at the electrolyte/copper-metal interface and APAM acts as a levelling agent.

Acknowledgments

I would like to express my deep gratitude to my supervisors Dr. Michael Ridd, Dr. Gregory Griffin and Dr. Madoc Sheehan for their support, trust and enthusiasm during the duration of this project. I am especially grateful to Dr. M. Ridd for his patient guidance throughout the duration of this endeavour.

I would also like to thank Dr. Sherryl Robertson, with whom I spent great moments discussing hydrometallurgy and in particular electrodeposition for her friendliness and advice.

I would like to thank my parents Buenaventura and Emilia who I came to fully appreciate after leaving my country of birth. Their belief in the value of education for their children as well as their thoughts and love guides me through life. To my wife Ana Luz and my children Irma, Fiorella and Joshua for their support.

Finally, I would like to thank Mount Gordon Operations of Western Metals Copper Ltd. for their financial support for the duration of this project.

TABLE OF CONTENTS

LIST OF TABLES

LIST OF FIGURES

CHAPTER 1

INTRODUCTION

This Section briefly describes the background to the project described in this thesis. Electrometallurgy is the last process for the recovery, and therefore production of copper metal from the mining industry. Copper electrometallurgy includes electrorefining and electrowinning depending on whether the copper mineral was processed through pyrometallurgy or hydrometallurgy. A 2003 world survey[1, 2] indicated that the production of electrolytic copper was about 13,066 kilotonnes per year of which about 2,375 kilotonnes per year proceeded from electrowinning operations.

Recent advances in hydrometallurgy led Mount Gordon Operations of Western Metals Copper Ltd., Australia to treat some copper sulphide ores directly in an autoclave reactor. Mount Gordon Operations (Mt. Gordon) was the first hydrometallurgical plant in the Western World to produce copper cathode using a mild-pressure autoclave ferric ion-sulfuric acid leach[3, 4]. The Mt. Gordon flowsheet is depicted in Figure 1-1. Initially, the feed to the plant was chalcocite ore, but later, it was a semi-concentrate with about 12 percent copper content. Mt. Gordon had occasionally produced the smoothest copper cathode ever known in the industry and also experienced premature detachment of the copper cathode from the stainless steel substrate, known as “pre-stripping” in the industry.

Nonionic polyacrylamide (MW 15 million Dalton, Magnafloc® 800HP, approx. theoretical length 10-50μm) from Ciba was dosed as flocculant to the hydroclassifiers and pinned bed clarifiers. It was highly likely that occasionally polyacrylamide (PAM) passed through the solvent extraction stage and then reached the electrowinning plant where it may have acted as an organic additive. Thus, the electrolyte contained two organic additives: Guarfloc66 (Guar), the industry-standard organic additive and PAM. These organic additives may have *occasionally* assisted to Mt. Gordon into the production of *highly smooth* copper cathodes. However, it was unclear, at this time, whether this smoothness was the effect of polyacrylamide by itself or its combination with Guar. The smoothness of the copper cathode led to the development of this thesis to study polyacrylamide as an organic additive for copper electrowinning.

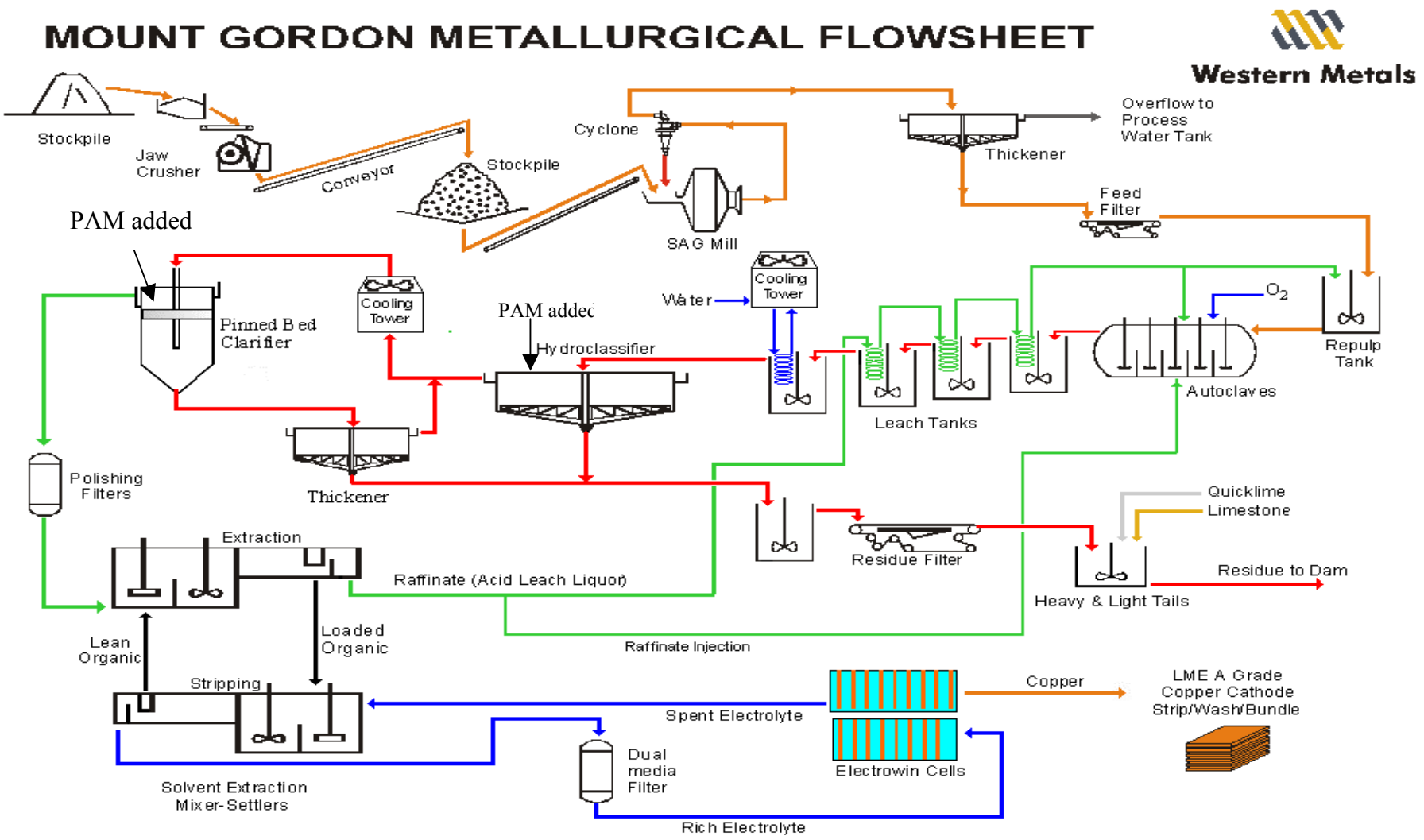

Figure 1-1: Mount Gordon Operations Flowsheet[4, 5]

1.1 Problem Statement

It is widely recognized that the initial process of electrochemical crystal growth and subsequent formation of monolayers are affected by the crystallographic properties of the substrate and metal deposit itself. It is therefore necessary to use additives to control nucleation and growth during the deposition process. These additives enable the production of smooth copper deposits free of voids and porosity. Such copper deposits also routinely achieve a higher level of polycrystalinity and ductility. In the absence of additives, the morphology of the copper deposit will be columnar, containing large crystals which enhance dendrite growth. Such morphology is counter-productive to achieving a high quality copper cathode and plant productivity.

The recent literature has widely discussed the advances in copper electrodeposition for the damascene process in the fabrication of interconnects (IC) and printed circuit boards (PCB). These studies consistently indicate that a levelling agent (often also called an inhibitor), an accelerator (also often called a grain refiner in electrometallurgy) and chloride ions should be dosed to produce "superconformal" growth. It is also known that animal glue, a leveller; thiourea (a grain refiner) and chloride ions have been dosed in copper electrorefining for more than 100 years. However, only guar gum (Guar) and chloride ions have been dosed in copper *electrowinning* for the last 40 years. Guar is known as a weak levelling agent in the industry. Table 1-1 briefly summarizes these industry-standard additives used in copper electrodeposition and their typical concentrations and their respective roles.

Research and development on the effects of Guar (often also known as a "weak polarizer" and/or "brightener" within the industry) and chloride ions in copper electrowinning has been neglected, notwithstanding that about 20% of the copper cathodes produced around the World comes from electrowinning operations. It appears that the mature technology of copper electrometallurgy knows only glue as a levelling agent throughout the World. It is a concern within the industry that additives other than Guar may affect the components of the organic solvent extractant (LIX®984 or ACORGA®M5640 and kerosene type diluent). Moreover, it also appears to be an understanding in the industry that the highly purified copper electrolyte after solvent

extraction does not require a levelling agent and grain refiner. However, commercial laboratories for the fabrication of PCB and IC not only use reagent grade copper sulfate and sulfuric acid but also a levelling agent. Surfactants such as PEG and a grain refiner or accelerator are used to obtain void-free "superfilling" or "superconformal" growth of nanometer scale trenches and vias.

Table 1-1: Industry-Standard Additives Used in Copper Electrodeposition

Role of the Additive	Electrorefining		Electrowinning		Microelectronics, PCB and IC	
	Additive	mg/L	Additive	mg/L	Additive	mg/L
Leveller	glue	1	Nil	Nil	PEG*	100-300
Brightener**			Guar	0.25-5		
Grain refiner	thiourea	2	Nil	Nil	SPS&JGB/MPSA*	1&1/1, respectively
Depolarizer	Cl^-	50-60	Cl^-	20-25	Cl^-	40-60

*PEG, polyethylene glycol; SPS, bis(3-sulfo-propyl) disulfide; JGB, Janus Green B (safranine dye); MPSA, 3-mercapto-1-propanesulfinate. **Guar is also known as weak polarizer in the industry.

The polarizer/inhibitor/leveller controls the vertical growth to produce smooth deposits by conferring preferential adsorption on the peaks or active sites. The grain refiner/accelerator may predominantly control the nucleation process or promote the formation of new nuclei to possibly form new crystallites at the recesses. This synergistic process between the inhibitor and grain refiner is aimed at improving the overall quality of the copper deposit: purity, smoothness and plant productivity i.e., elimination/reduction of short-circuits caused by dendrites

1.2 Thesis Objectives

The aim of this thesis project is to compare and understand the fundamental events at the solid-electrolyte interface during the electrodeposition of copper in the presence of Guar and a *new* organic additive developed in this thesis. This thesis will characterise and compare Guar and the newly developed organic additive in terms of their roles as levelling agents and/or grain refiners during the deposition process.

A smooth copper cathode improves the plant productivity in terms of current efficiency. It may also assist to increase the current density and the purity of the copper cathode by reducing entrainment of solid particles. A London Metal Exchange Grade "A" copper (less than 0.0065% total impurities excluding O, C, and H) attracts

premium. This thesis also attempts to bring together and apply the knowledge gained on copper deposition for the fabrication of PCB and IC with the experience gained from the mature industry of copper electrometallurgy.

CHAPTER 2

LITERATURE REVIEW

2.1 Electrodeposition Process Fundamentals

Electrodeposition is the formation of a new solid phase on a substrate immersed in an ionic conducting electrolyte under the influence of an electric field [6-10]. The electrolyte generally consists of an electro-active species and a supporting electrolyte to improve its conductivity. The overall reaction process involves the following individual steps[7]:

(i) Mass transfer of the reactants from the bulk solution to the electrode/electrolyte interface via diffusion and convection,

(ii) Formation of metal adatoms, M_{ads}, on a same-metal substrate, M, or on foreign substrate, S, via adsorption and transfer of electrons from the cathode to the reactant,

(iii) Two-dimensional (2D) and three-dimensional (3D) metal phase formation via nucleation and growth.

In the following sections, the convective diffusion equation is developed for strong electrolyte solutions such as a cupric ions-sulfuric acid electrolyte to develop a physicochemical model. The mass transfer for cupric ions based on the equation

developed for the rotating cylinder electrode is also discussed to show the importance of the type of the supporting electrolyte such as sulfuric acid.

2.2 Transport Processes in Electrolytic Solutions

A review of the overall experimental/laboratory based literature on electrodeposition of metals shows that a rotating disc electrode (RDE) has been more often used than a rotating cylinder electrode (RCE). However, copper electrorefining and electrowinning at commercial scale takes place in parallel plate electrodes where a uniform current distribution is prevalent since the insulator forms an angle close to 90^o (right angle) with the electrode[10]. As the primary and mass-transfer-limited current distribution are more uniform on a RCE than a RDE[10, 11]; Newman[10] suggests that perhaps more attention should be devoted to the possibility of using a RCE rather than RDE. This problem with the RDE becomes more serious for fast reactions and large current densities[10].

The hydrodynamics for the RDE[10] are well understood possibly due to its critical Reynolds number[12] of 10^5 and it is therefore most often used in the laminar regime, i.e., 300-500rpm. The critical Reynolds number for the RCE is about 200[12] and therefore turbulent flow is achieved at low speeds of rotation. However, the ohmic potential drop and concentration change at the electrode can be accurately calculated even in turbulent flow when the RCE is used[10]. Therefore, the RCE may be the preferred electrochemical cell to study copper deposition at 300-400A/m^2 to measure and quantify the effect of additives due to its uniform current distribution. Moreover, the hydrodynamics in commercial copper electrowinning may also be simulated more closely using a RCE than RDE.

2.2.1 Mass Transfer

Step (*i*) in Section 2.1, mass transfer, is governed by the hydrodynamic transport law for dilute solutions and can also be generalized for strong solutions to express the molar flux (mole/s) of an ionic species[10]. The flux density N_i of a species *i* is equal to its velocity multiplied by its concentration.

$$N_i = -z_i u_i F c_i \nabla\Phi - D_i \nabla c_i + c_i v_i \qquad (2\text{-}1)$$

The first term on the RHS of Equation 2-1 represents the flux due to electric field migration where z_i is the charge number of the ion, u_i its mobility, F the Faraday constant, c_i concentration of species i, and $\nabla\Phi$ the electric field. The second term represents the diffusion flux due to a concentration gradient: the species will diffuse from regions of high concentration to regions of low concentration, and the third term represents the convection flux due to motion of the solution with bulk velocity, ν.

The transient material balance is given by:

$$\frac{\partial c_i}{\partial t} = -\nabla \cdot N_i + R_i \qquad (2\text{-}2)$$

where the term on the LHS is the accumulation rate, the first term on the RHS is the net input differential volume element and R_i is the production (in homogeneous chemical reactions) in mol/cm^3.s. The differential volume element is simply the time rate of concentration change. In electrochemical systems, the reaction is frequently restricted to electrode surfaces, in which case R_i is zero. As the solution is also electrically neutral except in a thin double charge layer near the electrode and other boundaries, it is reasonable to adopt Equation 2-3 in the context of the electroneutrality of the bulk solution.

$$\sum_i z_i c_i = 0 \qquad (2\text{-}3)$$

In the presence of a supporting electrolyte such as sulfuric acid and due to the incompressibility of the electrolyte ($\nabla\cdot\nu = 0$), the flux Equation 2-1 above can be combined with Equation 2-2 to produce Equation 2-4. The supporting electrolyte is frequently added to increase the conductivity of the solution and thereby reduce the electric field.

$$\frac{\partial c}{\partial t} + \nu\nabla c_i = z_i F \nabla(u_i c_i \nabla\Phi) + \nabla(D_i \nabla c_i) + R_i \qquad (2\text{-}4)$$

Equation 2-4 can be used to determine the concentration distribution when the fluid velocity and potential distributions are known. A further simplification of Equation 2-4 can be applied when migration is neglected and the requirement of electroneutrality allows the potential to be eliminated[10, 13]. Thus, the mass transfer is primarily due to diffusion and convection, therefore the concentration distribution is governed by the known *convective diffusion*, Equation 2-5 for a constant diffusion coefficient[10] and strong electrolyte solutions.

$$\frac{\partial c_i}{\partial t} + v \cdot \nabla c_i = D_i \nabla^2 c_i \qquad (2\text{-}5)$$

where

c_i is the concentration of species i, mol/cm^3

v is the mass-average velocity, cm/s

D_i is the diffusion coefficient of species i, cm^2/s

Equation 2-5 can be used to develop a physicochemical model for copper electrodeposition.

2.3 Rotating Cylinder Electrodes

The mass transfer of reactants from the bulk solution to the electrode/electrolyte interface via diffusion and convection stated in Equation 2-5 for the overall reaction process will be discussed using the hydrodynamic properties of the RCE. Although the turbulent flow cannot yet be fully analyzed from fundamental principles; the rotating cylinder electrode has been studied and analysed by many authors[10, 14-18]. The RCE was selected for this thesis to approximate the fluid flow of the electrolyte during commercial scale copper electrowinning[19].

If the cathodic current density is much less than the limiting, mass transfer controlled current density, for a cathodic reaction, neglecting the reverse, oxidation reaction, the limiting diffusion current density, i_L is given by Fick's first law, Equation 2-6, with a surface concentration of zero[20].

$$i_L \equiv \frac{nFDC_b}{\delta} \qquad (2\text{-}6)$$

where δ, cm, is the diffusion layer thickness.

Mass transfer between concentric cylinders, the inner of which is rotating with an angular speed ω has been studied[10, 14, 16]. The limiting current density for the RCE is described as follows according to Eisenberg et al.[14].

$$i_L = 0.0791\frac{nFDC_b}{di}(\mathrm{Re})^{0.7}(Sc)^{0.356} \qquad (2\text{-}7)$$

where

i_L is the limiting current density, mA/cm^2,

n is the number of electrons transferred in the electrode reaction,

F, Faraday's constant, 96,487C/equivalent and,

D, diffusion coefficient of electrolyte, cm^2/s,

C_b is copper concentration in the bulk solution, mol/cm^3,

di is the diameter of the inner, rotating cylinder, cm,

Re is the Reynolds number, ($\omega d^2/2\nu$),

ω is the rotation speed in rad/s,

ν is the kinematic viscosity, cm^2/s,

Sc is the dimensionless Schmidt number, (ν/D)

Equating Equations 2-6 and 2-7, the Nernst diffusion model for the RCE can be expressed as[14]:

$$\delta = 12.64\frac{di^{0.30}\nu^{0.344}D^{0.356}}{U^{0.70}} \qquad (2\text{-}8)$$

Eisenberg et al.[14] developed the empirical Equation 2-7 using the hexacyanoferrate (II) and hexacyanoferrate (III) in 2M NaOH as supporting electrolyte at 25^{o}C.

Arvia et al[15] also developed an equation for the RCE, Equation 2-9, using 1.5-3.5 g/L cupric ions in 1.5M sulfuric acid at 18°C. The experimental RCE of Arvia et al.[15] had the inner, rotating electrode as anode and a fixed cathode as the outer electrode. This experimental set up was opposite to that of Eisenberg et al.[14] and to the experimental set up for this thesis. The limiting current density for the RCE can also be calculated using the equation developed by Arvia et al[15]. The difference between Equations 2-7 and 2-9 possibly reflect the effect of sulfuric acid in Arvia et al[15] experiments.

$$i_L = 0.0791\, nFC_b \left(\frac{di}{\nu}\right)^{-0.30} (U)^{0.70} \left(\frac{do}{di}\right) (Sc)^{-0.644} \qquad (2\text{-}9)$$

where U is the peripheral velocity, *di* and *do* are the inner, rotating and outer-static cylinders diameters, respectively. The other variables are described as above.

The addition of sulfuric acid as supporting electrolyte in copper electrodeposition has several effects on the behaviour of the system. First, the conductivity is increased; thereby reducing the electric field in solution for a given current density and, second, the transference number of the cupric ion is reduced[10]. Therefore, the role of migration in the transport of cupric ion and the ohmic potential drop in solution are greatly reduced; the importance of diffusion in the transport of cupric ion is increased[10]. Since migration is reduced, the supporting electrolyte decreases the limiting current density. The conductivity of 6.3 g/L cupric ions will increase from 0.00872S/cm to 0.548S/cm when 150g/L H_2SO_4 is added to the copper electrolyte but the limiting current density will decrease from 79mA/cm^2 using the equation developed by Eisenberg et al.[14] to 48mA/cm^2 using a RCE at 900rpm[10]. If the concentration of cupric ions is increased from 6.3 to 44.5g/L in 150g/L sulfuric acid, the conductivity still will be about 0.0375S/cm.

The rotation of one electrode in the RCE electrochemical cell can produce flow patterns that assist in reducing the concentration gradient and contribute to the transport of materials to the electrode surface. Very low rotation speeds lead to simple laminar flow in concentric circles in which the fluid velocity is perpendicular to the direction of

mass transfer. This simple flow pattern becomes unstable at higher rotation speeds, particularly if the inner electrode rotates and Taylor vortices or laminar flow with vortices can be obtained resulting in an enhanced mass transfer[10]. Moreover, in the laminar flow Taylor vortices region, there is a radial and axial motion, inward at one point and outward at different axial position superimposed to the tangential motion. At higher rotation speeds, the flow becomes turbulent with Taylor vortex flow[21] with further enhancement of the mass transfer. Wang[21] recently studied the Taylor-Couette flow and indicated the disappearance and reappearance of azimuthal waves depending on the ratio of the Reynolds number to the Reynolds critical number.

The fluid flow at rotating cylinder electrodes can be described using the Reynolds and Taylor numbers. Reynolds number, Re has been expressed differently in the literature if $d_{Rotating}$=di, Re=U*d/ν =ω*ri*di/ν > Re= ω*di^2/ν > Re=ω*di^2/2ν = U*di/ν where ω is the rotation speed, rad/s, *di* is the inner rotating diameter, *ri* is the inner rotating radius, d is radius of the outer cylinder minus radius of the inner cylinder (ro-ri) and U is the peripheral velocity in cm/s. The first equality was used by Schlichting[22] and Wang et al.[21], respectively. The second equation was used by Silverman[23]. The third equality was used by Newman[10], Gabe[12], Eisenberg et al.[14] and Arvia et al.[15]. These Reynolds numbers are slightly different as shown in Appendix A. This difference is due to the selection of the radius, diameter and/or inter-electrode distance as the characteristic length for the rotating cylinder electrode.

The predominance of Taylor vortices is given by the Taylor number [Ta, Ta= (U*d/ν*√d/ri)][22, 23]. However, this Taylor number appears to be only valid for small inter-electrode gap, e.g. 0.19cm, and the Taylor vortices may vary from 41.3 to 400. For larger electrode gaps, e.g., 3.2cm, such as is used in this thesis, the fluid flow at the RCE appears to be most often described by the Reynolds number (Re = ω*di^2/2ν), and the Taylor number, Ta = [(Re^2)(d/ri)]. Newman in 1973[24] defined that turbulent flow prevails for Reynolds numbers greater than 3960 or Taylor numbers greater than about $3x10^6$. Using the above Reynolds equation described above, the critical Reynolds number for a RCE is 200[12].

At currents below, but at a significant fraction of the limiting current, it is necessary to calculate the concentration variations near the electrode. The surface concentration can be calculated using the following equation[10]:

$$\frac{i_n}{i_L} = 1 - \frac{C_o}{C_b} \qquad (2\text{-}10)$$

and if Equation 2-6 is inserted in Equation 2-10, the surface concentration of cupric ions is given by Equation 2-11 to develop a physicochemical model:

$$C_o = C_b - \delta \frac{i_n}{2DF} \qquad (2\text{-}11)$$

where

C_o is the surface concentration at the electrode surface, mol/cm^3,
C_b is the bulk concentration of cupric ions, mol/cm^3,
δ is the diffusion layer thickness, cm,
i_n is the normal current density at electrode surface, A/cm^2,
D is the diffusion coefficient of cupric ions, cm^2/s,
F is the Faraday's constant, 96,487, C/equiv.

The equations developed by Eisenberg et al.[14] and Arvia et al.[15] will be compared with the experimental data produced in this thesis. Computational fluid dynamics of the electrolyte fluid flow around the electrode during copper electrowinning indicate that the hydrodynamic boundary layer varies between 250 and 300 μm[19].

2.4 Electrochemical Kinetics Fundamentals

The first task of electrode kinetics is to explain the sequence of partial reactions constituting the overall electrode reaction or reaction mechanism and the second task is the determination of electrode reaction rates or the application of Faraday's law[6]. The dependence of current density, the reaction rate, on the electrode potential, the

concentration of reactants and other variables such as temperature and transport processes must also be determined.

In summary, the analysis of the behaviour of electrochemical systems seeks to formulate the relationship between the current density and electrode potential, surface overpotential, and the composition adjacent to the electrode surface as well as the temperature.

Copper dissolution and deposition are widely regarded as being composed of two elementary steps, each of which involves the transfer of an electron:

$$\begin{array}{lcll} & & & E^o(V) \\ & k_1 & & \\ Cu^{2+} + e^- & \rightleftharpoons & Cu^+_{(ads)} \quad \text{(slow)} & 0.159^{25} \qquad (2\text{-}12) \\ & k_{-1} & & \\ & k_2 & & \\ Cu^+_{(ads)} + e^- & \rightleftharpoons & Cu^o \quad \text{(fast)} & 0.520^{25} \qquad (2\text{-}13) \\ & k_{-2} & & \end{array}$$

The first reduction step is much slower than the second step.[10, 26] Mattsson and Bockris[26] studied the deposition and dissolution of copper in acid sulfate electrolyte by a galvanostatic technique and found that the overall reaction obeys the Butler-Volmer equation, Equation 2-14. This equation is valid irrespective of the presence and absence of additives and it is related to surface overpotential, η_s; F, Faraday's constant; i_n, the normal component of the faradic current density which is related to the normal component of the flux of cupric ions and, i_o, exchange current density. The number of electrons transferred is n.

$$i_n = i_o[\exp(\frac{\alpha_a F}{RT}\eta_s) - \exp(-\frac{\alpha_c F}{RT}\eta_s)] \qquad (2\text{-}14)$$

α_a and α_c are two additional kinetic parameters termed as the *transfer coefficients* and the theoretical values are 1.5 and 0.5, respectively and their sum, $\alpha_a + \alpha_c$, equal to 2[10, 26]. The symmetry factor β_3 ($\alpha_a = 2-\beta_3$ and $\alpha_c = \beta_3$) for Equation 2-14 is

equal to 0.5[26]. Newman[10] further examined Mattsson and Bockris[26] data and suggested that β_3 in the exponent of composition dependence of the exchange current density, γ, ($\gamma = (2-\beta_3)/2$) has a value 0.42 rather than 0.50. It is therefore ascertained that the exchange-current density, i_o depends strongly on the composition at the interface[10] as

$$i_o = \left(\frac{c_{Cu^{2+}}}{Cu^{\infty}_{Cu^{2+}}} \right)^{\gamma} i_o\left(c^{\infty}_{Cu^{2+}}\right).$$

The probability for simultaneous electron transfer in a single step is extremely low since the time scale for an electron transfer event, ca. 10^{-16} s is much smaller than the time scale of the fastest chemical reorganization in the metal-ligand vibration scale, 10^{-13} s or slower[27]. The rate constants k_1 and k_2 have been explained to have different kinetics with $i_{o,1}$ and α_1 and $i_{o,2}$ and α_2, characterising each process, respectively. The general expression for a sequential two-electron reaction derived by Vetter[6, 27] is:

$$i = -2i_{o,1} \exp(-\frac{(1-\alpha_1)}{RT} F\eta) \times \frac{1-\exp(\frac{2F}{RT}\eta)}{1+(\frac{i_{o,1}}{i_{o,2}})\exp[\frac{(1+\alpha_1-\alpha_2)}{RT}F\eta]} \qquad (2\text{-}15)$$

where η=E-E^o and E^o is the standard electrode potential for the overall two-electron process. The two rate-limiting cases are described below:

1. The first electron-transfer step is the rate determining step ($k_2 \gg k_{-1}$).The forward rate coefficient is $k_f \approx k_1$ and the backward rate coefficient is $k_b \approx \left(\frac{k_2}{k_{-2}} \right) / k_{-1}$.
2. The second electron-transfer step is the rate determining step ($k_2 \ll k_{-1}$) then $k_f \approx \left(\frac{k_1}{k_{-1}} \right) k_2$ and $k_b \approx k_{-2}$.

The first limiting case was demonstrated to be the rate determining step in copper electrodeposition in the presence of a supporting electrolyte[10, 26].

2.5 Effect of Additives on Copper Electrocrystallization

2.5.1 Introduction

The process of electrochemical crystal growth cannot be achieved under "ideal" conditions, i.e., without additives, due to the crystallographic properties of the substrate and depositing metal. In the copper deposition industry in general, chloride ions and organic additives need to be dosed to produce smooth deposits, free of voids or porosity and as a result its morphology can be changed and, polycrystalinity and highly ductility can also be achieved. It has been widely acknowledged that organic additives significantly influence the current-potential relationship due to their interactions for surface coverage with the components of the electrolyte system including with chloride ions. These interactions take place since some species in solution may have a preference for being near the solid.

Electrocrystallization denotes formation of new nuclei and crystal growth in electrochemical systems under the influence of an electric field. Nucleation is a very important process; the first step of metal-deposition is the formation of nuclei of the depositing metal on a foreign substrate or on a substrate of the same metal. The competition between nucleation and growth determine the smoothness of the deposit: higher nucleation rates yield smaller crystallite sizes[7].

On the other hand, the forms of the growing crystals determine the physical appearance and structure of the depositing metal. Thus a high growth rate of the crystal size normal to the substrate yields (*i*) a more fibrous or columnar microstructure and (*ii*) a brightening effect is achieved from large developed crystal faces parallel to the substrate. Therefore, the kinetics of nucleation and growth play a dominant role in determining the overall deposition kinetics, as well as the appearance, structure and properties of the deposit.

The literature on copper deposition in the presence of additives indicates that the type of adsorption onto the metal substrate is critical in affecting the deposition process. The whole array of charged species and oriented dipoles existing at the metal-electrolyte interface is called the *electrical double-layer* as described in Figure 2-2.

Figure 2-2 indicates that some components of the electrolyte bath are more closely adsorbed at the electrode interface, i.e., within the inner and outer Helmholtz planes (IHP and OHP) than other components. The electrolyte component more closely adsorbed is defined to be more *specifically adsorbed* and the component less closely adsorbed is defined to be *non-specifically adsorbed*[9, 10].

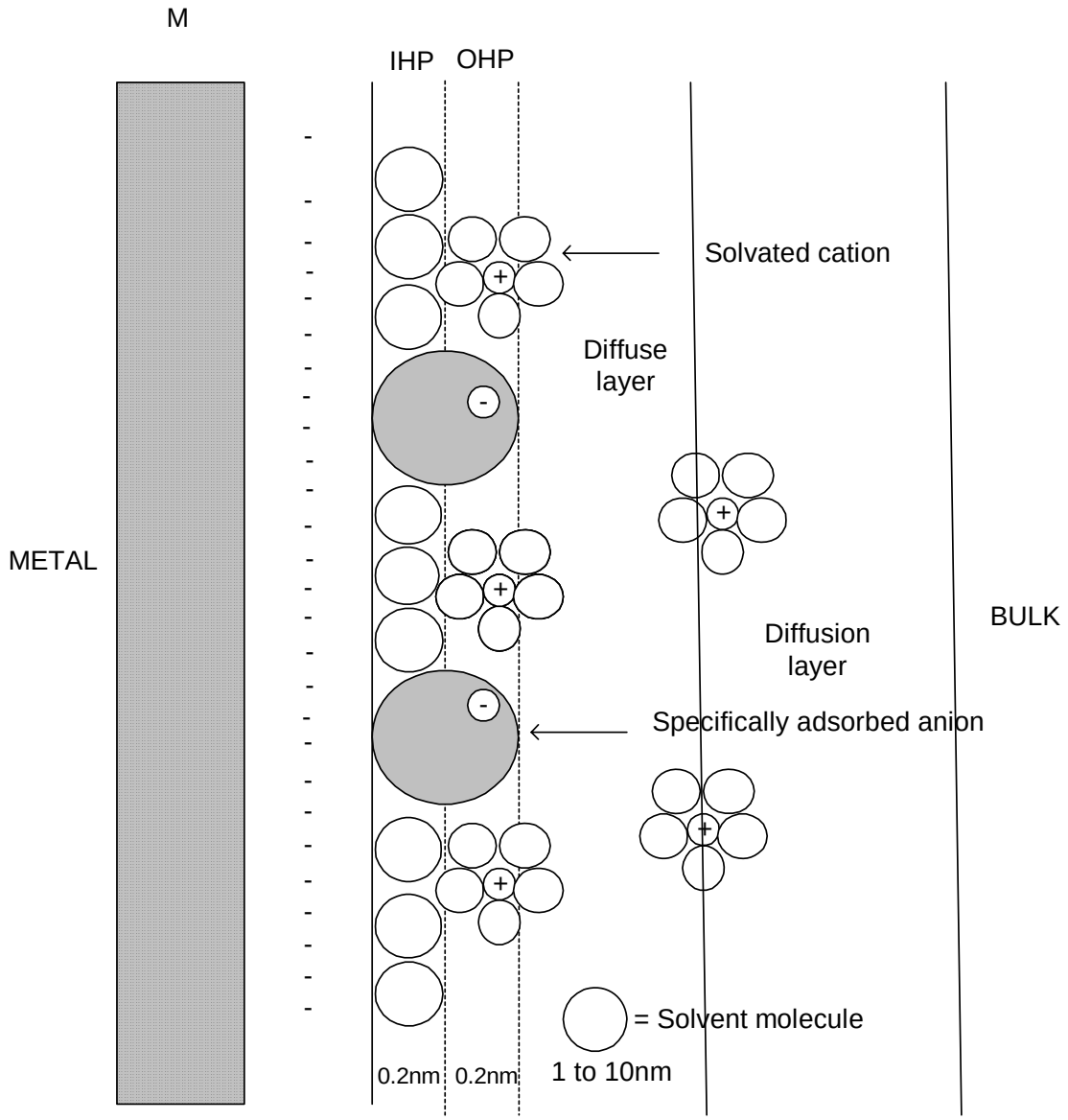

Figure 2-2: Schematic representation of the structure of the double-layer in electrolyte solution during electrochemical reactions where anions are specifically adsorbed.

The indicative dimensions of the IHP, OHP and diffuse layer represent mercury electrode[10]. Specifically adsorbed ions or molecules are located at the IHP while solvated adsorbed ions are located beyond (but not quite at) the OHP[9, 10].

2.5.2 Effect of Chloride Ions on Nucleation and Growth

The use of additives in copper electrodeposition is extremely important owing mainly to effects produced on the growth and microstructure such as brightening of the deposit, reducing crystallite size, reducing the tendency to grow dendrites, increasing the current density range, and changing the mechanical and physical properties and reducing stress[28].

Sun and O'Keefe[29] and Zhou and O'Keefe[30] studied the nucleation and growth of copper on stainless steel substrates using 40g/L Cu^{2+} and 180g/L H_2SO_4 at 40°C in the presence and absence of chloride ions, respectively. Sun and O'Keefe[29] found that irrespective of the presence or absence of chloride ions on a 304 stainless steel RDE seems to promote *progressive* nucleation, 3-D growth and diffusion control at various rotation speeds (0-1600rpm). In contrast, Zhou and O'Keefe[30] found that in the absence of chloride ion the copper nucleation mechanism on 316L substrate plate (as-received) appears to be *instantaneous* and diffusion controlled. It is therefore concluded that the initial nucleation and growth mechanism on stainless steel is not clear possibly due to the non-uniform current distribution of the RDE. Moreover, Sun and O'Keefe[29] also reported that in the presence of 40 mg/L chloride ions:

(i) the current density was 30 percent higher at a fixed potential than in the absence of chloride ions. This effect is defined as the *depolarizing* effect of an additive - in this case of chloride ions.

(ii) a decreasing number of nuclei and an enhanced redistribution of copper crystals was observed, that is coalescence of small crystals towards large crystals possibly due to binding[8] and surface energy differences[31] between the copper metal and stainless steel,

(iii) Secondary nucleation takes place preferably on already formed copper crystals rather than on the stainless steel substrate possibly due to the crystallographic misfit[8], and

(iv) The secondary nucleation leaves large portions of the stainless steel uncovered, and produces lacy copper or discontinuous deposits possibly due to surface diffusion[7].

Ilgar and O'Keefe[32] also studied the effect of chloride ions and indicated that it increased the surface roughness of the copper deposit. Chloride ions strongly adsorb on the surface of the cathode and the reduction of Cu^{+} to Cu becomes the rate limiting step instead of the reduction of Cu^{2+} to cuprous ion[33, 34]. A recent study also indicates that chloride ion is a depolarizer[35]. It can be seen that these independent studies agree to conclude that chloride ions have a *depolarizing* effect leading to non-uniform discontinuous deposits and higher levels of contained impurities[29].

2.5.3 Effect of Organic Additives on Nucleation and Growth

Copper deposition in the presence of polyethylene glycol (PEG), chloride ions, Janus Green B (JGB) and bis-(3-sulfopropyl) disulfide (SPS) in the electrolyte bath increased the progressive nucleation rate and nucleus density but the Volmer-Weber, Figure 2-3(a), growth mode was unchanged on n-Si(111) substrate[36]. It is widely known[7] that the growth mode depends on the binding energy (ψ) of adsorbed metal ions, M_{ads} on the substrate, S compared to that of M_{ads} on same M substrate and on the crystallographic misfit given by the inter-atomic distances $d_{o,M}$ and $d_{o,S}$ of 3D M and S bulk phases, respectively. The Volmer-Weber growth mode shown in Figure 2-3(a) indicates (3D M island formation) for ψM_{ads}-S « ψM_{ads}-M, independent of the ratio $(d_{o,M} - d_{o,S})/d_{o,S}$).

An ideal levelling agent and grain refiner at their correct concentrations including those of chloride ions can start the deposition process on 316L stainless steel with the Volmer-Weber and/or Stranski-Krastanov growth modes, Figures 2-3(a) and 2-3(c), respectively. These Figures show 3D M (metal) island formation prevail due to the crystallographic misfit given by inter-atomic distances between the depositing metal and the substrate and their binding energy differences. However, after about 20 monolayers of the depositing metal where the effect of the substrate on the depositing metal ceases[7] the Frank-van der Merwe growth mode, shown in Figure 2-3(b), where a layer-by-layer growth form prevails, is obtained.

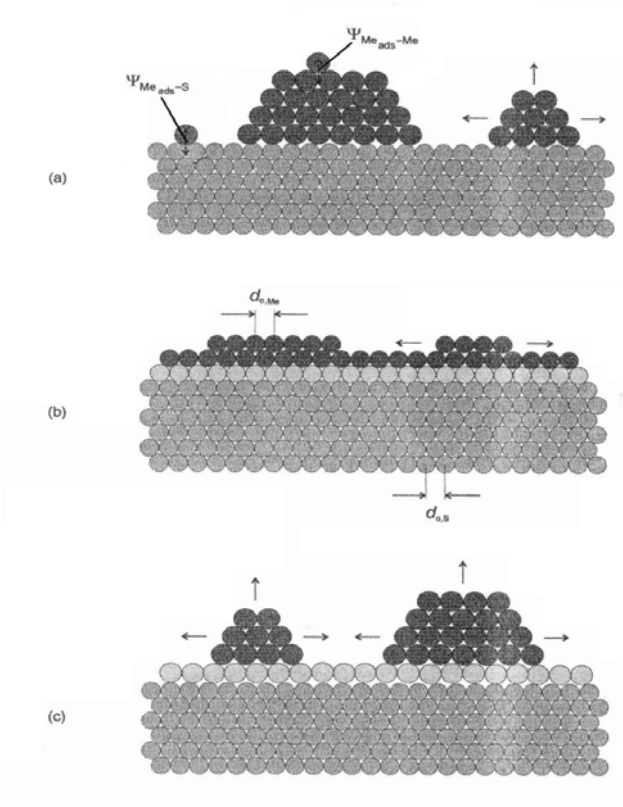

Figure 2-3: Schematic Representation of Different Growth Modes in Metal Deposition on Foreign Substrates.

(a) Volmer-Weber; (b) Frank-van der Merwe and (c) Stranski-Krastanov[7].

Deposition of copper on highly oriented pyrolytic graphite from additive-free solutions lead to rough surface textures due to diffusion limited 3D nucleation and growth. The addition of benzotriazole, a levelling agent, to the above bath inhibited the vertical growth and the lateral growth was charge-transfer limited. This process smoothes the deposit by diminishing surface diffusion[37].

It appears that there is also an overall consensus in the literature that the grain refiner/accelerator plays an important role in electrorefining and in the microelectronics industry. This role was recently described using atomic force microscopy and indicated that surface roughness of copper deposits obtained from PEG + SPS and chloride ions are nearly one-third those grown from SPS + chloride alone[38]. The PEG + SPS and Cl^- system also produces smaller features than the SPS + Cl^- alone. This effect of SPS appears to be a result of its interaction with Cl^-.

Thiourea [$(H_2N)_2C=S$] in copper *electrorefining* acts as grain refiner. Surface-enhanced Raman Scattering (SERS) spectroscopy indicates that sulfur atoms of thiourea and sulfate ions, but not bi-sulfate ions, cooperate rather than compete to bond onto copper atoms possibly at the most active sites[39]. This process possibly increases the number of new nuclei where new metal could grow or in other terms increases the rate of nucleation.

It has been shown in this Section that the presence of chloride ions and organic additives can change the nucleation and growth mode of copper deposition. It has been also shown that a levelling agent and a grain refiner/accelerator are dosed with chloride ions during copper deposition in electrorefining and in the microelectronics industry.

2.5.4 Copper Electrowinning in the Presence of Organic Additives

An extensive literature review revealed very few publications related to organic additives in copper *electrowinning* even though the industry is about 40 years old. In the first publication, Pye and Schurz (1957)[40] patented the electrowinning of zinc and copper in the presence of acrylamide polymer (homopolymer and copolymers of acrylamide). It was claimed that acrylamide polymer can be dissolved in *water* or *electrolyte* or may be added in a solid form to the copper electrolyte. The concentration of the acrylamide polymer in the electrolyte was claimed to vary from 25 to 150 mg/L to accomplish an improved deposition of the metal of concern. This patent also claims that the electrolyte contains 20-70 grams/L copper with a substantial proportion of sulfuric acid and it is essentially *free of chloride ions* to obtain smooth bright copper deposits after 5, 13 and 16 hours of electrowinning at 25^{o}C and 172 A/m^2 current density.

In a second publication, Vereecken and Winand (1976)[41] compared the influence of nonionic and cationic polyacrylamides with Guar Gum (Guar) on the quality of copper deposits using "industrial" copper sulphate solution at 200 Amp/m^2 and 50^{o}C. The electrolyte composition was (g/L): copper, 50; Mn, 10; Mg, 4; Co, 1.5; phosphate ions, 10 and sulfuric acid, 50. it should be noted that chloride ions were not reported to be present in the electrolyte and the sulfuric acid concentration is lower than that in

current plant practice. Moreover, it is unclear in the publication whether the nonionic and cationic polyacrylamides were prepared in water or in a solution of pH 3. Every 12 hours, 1mg/L of PAM was dosed for 48 hours of electrowinning. The conclusion of this study was that the quality of the copper deposits obtained with Guar was always better than those obtained with both nonionic and cationic polyacrylamides. It is stated by Vereecken that "the polarization curve was recorded for the reduction of Cu^{2+} ions on copper cathode with 1mg/l of the *different inhibitors*. This low concentration does not significantly change the overpotential of the cathode reduction. This confirms the results obtained during the electrolysis: the cathodic galvanic potential in all the experiments was equal to *+200mV/NHE* (the cell voltage was about 2V)". Vereecken and Winand[41] observed the depolarization behaviour of nonionic and cationic polyacrylamides, and Guar prepared in water or in a solution of pH 3.

The "active" concentration of Glue[42] and Guarfloc66[43], the industry-industry organic additives dosed in copper electrorefining and electrowinning, respectively were measured using CollaMat™. This technique determines the rate of polarization change by measuring the potential over short-time periods on platinum wire (diameter: ~1mm) correlated with the inhibitor concentration. It concluded that Guar activity was about 70 percent lower than Glue activity under the same conditions and indicated that Guar is a weak levelling agent.

2.5.5 Physicochemical Properties of Guar

Guar gum (Guar) is a naturally occurring galactomannan polymer, a polysaccharide, used as flocculant and coagulant with typical molecular weights ranging from $2x10^5$ to $5x10^5$ Dalton. Guar is a linear D-mannose sugar with a D-galactose sugar chain on every other mannose as shown below (Figure 2-5)[44].

Very little information was found on Guar hydrolysis and adsorption other than to say that it forms colloidal dispersions when hydrated in cold water[44]. No information was found on its adsorption mechanism on stainless steel or copper or any other substrate.

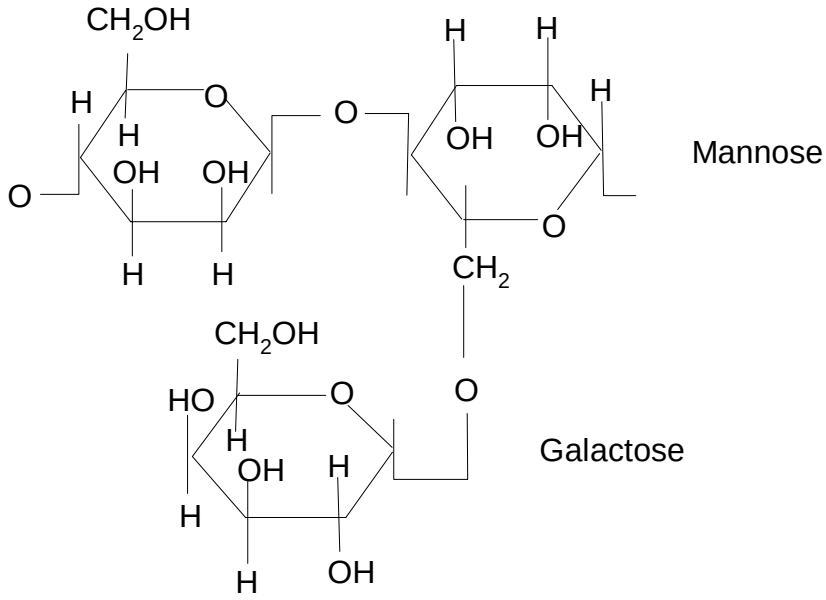

Figure 2-4: The chemical structure of Guar[44]

2.6 Polyacrylamide Hydrolysis and Adsorption

2.6.1 Introduction

(iv) This section presents an overview of the literature on polyacrylamide hydrolysis reactions and its molecular adsorption at electrified and non-electrified solid surfaces. Recent developments in surface electrochemistry explore the phenomena at the electrified solid-liquid interface by a combination of electrochemical, spectroscopic, diffraction and surface imaging techniques[45]. The knowledge gained from these studies is relevant to copper electrometallurgy, to study the coordination at electrode surfaces. The adsorption of an organic additive is a sought-after occurrence in copper electrometallurgy to produce smooth, void-free and low porosity copper deposits[29, 46, 47]. Smoothness assists to increase the purity of the copper deposit by reduction of particle and electrolyte entrainment, and results in an increase in plant productivity. In this thesis, the use of polyacrylamide as an organic additive is investigated.

Polyacrylamide is highly soluble in water but its solution viscosity limits its concentration to very low values, nevertheless among other polymers, it has a unique position for industrial applications due to its adsorption properties[48]. In general, the rheological behaviour of aqueous polyacrylamide solutions is pseudoplastic[44], i.e., the apparent viscosity decreases with increasing shear rate at relatively low shear rates.

A literature search showed that while a lot of information was found on the behaviour of polyacrylamide as a flocculant and coagulant in weak acid and alkaline conditions, less information was found on the behaviour of polyacrylamide in strong acid solutions such as copper electrolytes in 1.5-1.8M sulfuric acid.

Macromolecules such as high-molecular weight polyacrylamide such as 15 million Dalton Ciba Magnafloc® 800HP with theoretical lengths 10-50 μm, are used as flocculants and thickeners. Low-molecular-weight (co)polymers are used as coagulants and mud stabilizers due to their exceptional adsorption properties[48, 49]. Polyacrylamide adsorption onto solid surfaces may involve one or more of a number of interactions, listed below:

(i) Chemical short distance interactions, i.e., covalent bonding, coordination bonding, and hydrogen bonding;

(ii) Physical longer-range forces, i.e., electrostatic bonding, dipole attraction, London-van der Waals attraction;

(iii) Hydrophobic associations, i.e., surface hydrophobicity and substitutional adsorption with water, and endothermic adsorption process; and

(iv) Chemical nature of the surface, the presence of solutes and functional groups in the polymer[48].

Neutral or nonionic polyacrylamide, shown in Figure 2-5, confers adsorption through hydrogen bonding from the acrylamide functional group ($-CONH_2$). *Hydrolysed polyacrylamide,* shown in Figure 2-6, is frequently referred to as anionic polyacrylamide and consists of acrylamide-acrylic acid copolymers.

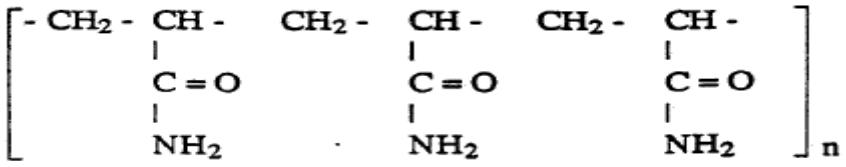

Figure 2-5: Nonionic polyacrylamide

It should be noted that while under neutral conditions nonionic polyacrylamide is stable; but under acidic or basic conditions it undergoes hydrolysis. The hydrolysis mechanisms are discussed in the next Sections.

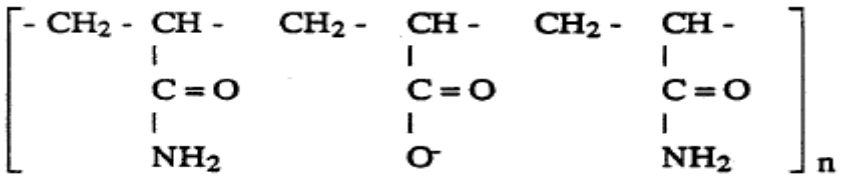

Figure 2-6: Anionic or hydrolysed polyacrylamide

2.6.2 Polyacrylamide Hydrolysis Mechanisms

Polyacrylamide undergoes hydrolysis in alkaline and acid solutions and the reaction product differs[50]. It is also known that that the kinetics of polyacrylamide hydrolysis depends on temperature, media and degree of shear. Hydrolysis of non-ionic polyacrylamide (described below) is the transformation of the amide functional group ($CONH_2$) of the polyacrylamide molecules to produce carboxyl functional group ($COO–$) and ammonia[51]. The percent of hydrolysis, τ is be defined as the number of carboxyl groups replacing amide groups divided by the total number of macromolecule groups, $\tau = 100y/(x + y)$ as described below:

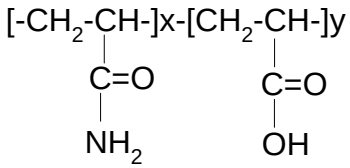

The number of negative charges on the polymer chain increases as a result of the polymer hydrolysis. This depends on the pH.

2.6.2.1 Polyacrylamide Hydrolysis in Neutral and Alkaline Solutions

Hydrolysis in water at room temperature is negligible (<2 percent)[52]. Polyacrylamide hydrolysis under basic reaction conditions at 60-100°C involves a nucleophilic addition of hydroxide to the amide carbonyl followed by the elimination of the amide ion ($-NH_2$) to afford an acrylic acid residue[50]. The amide ion then removes a proton from the acrylic acid residue to form a more stable carboxylate anion and ammonia as it is shown in the reaction pathway 1 below.

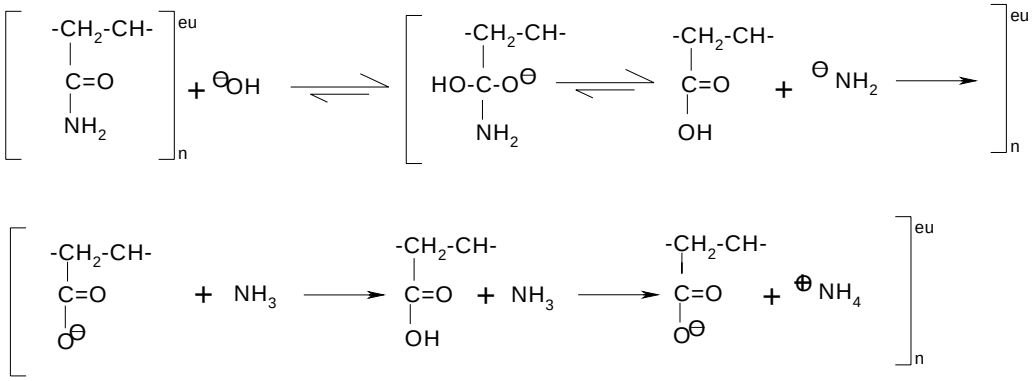

eu (either/unknown): polymer repeat pattern

Reaction Path 2.1: Hydrolysis of Polyacrylamide Under Alkaline Conditions[50]

Atkins[53] patented the hydrolysis of polyacrylamide to produce polyacrylic acid in sodium hydroxide at 50°C and reported a conversion of 30 and 61% after two and three hours residence time, respectively. Caulfield[50] reported that hydrolysis becomes extremely slow when the residual amide content falls below about 30% in the polyacrylamide.

2.6.2.2 Polyacrylamide Hydrolysis in Acid Solutions

Under acid conditions, polyacrylamide hydrolysis involves the nucleophilic addition of water to the protonated amide followed by the loss of ammonia as shown in the reaction pathway 2 below[50].

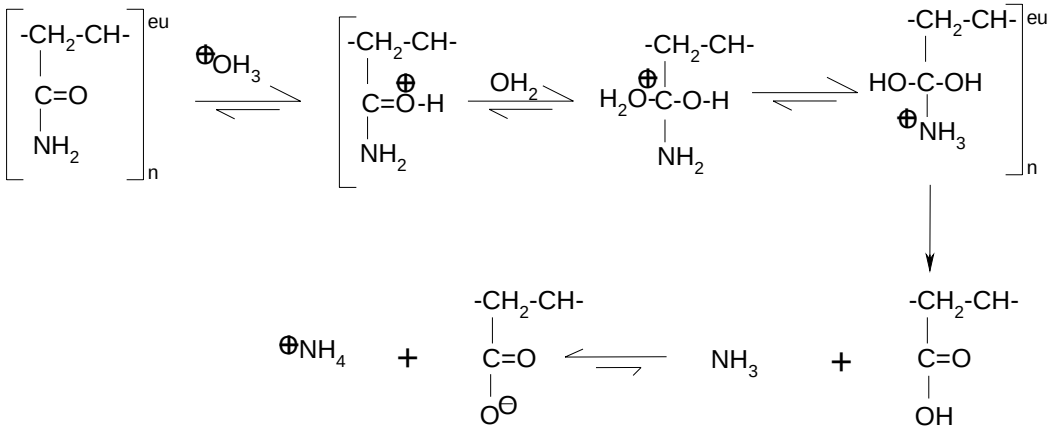

Reaction Path 2.2: Hydrolysis of Polyacrylamide under Acidic Conditions

Hydrolysis of polyacrylamide in strong acid solution can also lead to the formation of polyacrylimide (imide)[54, 55] shown in Figure 2-7. The *imide* is an insoluble gel induced in polyacrylamide either thermally or by mineral acids[56, 57].

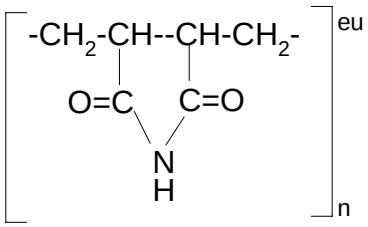

Figure 2-7: Polyacrylimide Molecule

The rapid initial reaction was characterised by the transient appearance of an absorption band at 235nm which was attributed to the formation of cyclic imide intermediate[50]. The imide quickly decomposed to form the acrylic acid residue. The proposed reaction pathway for the initial hydrolysis of polyacrylamide is presented below[50].

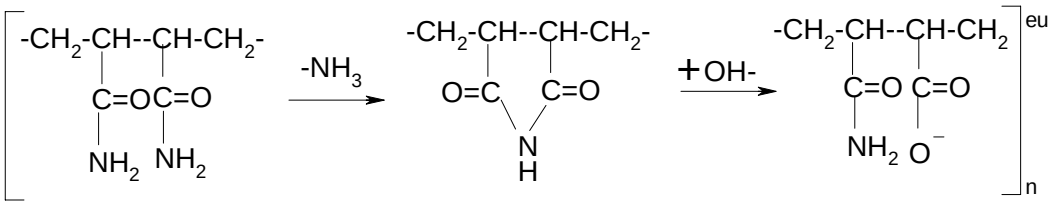

Reaction Path 2.3: Proposed Reaction Pathway for the Initial and Fast Hydrolysis of Polyacrylamide[50]

Minsk et al.[55] presented results for acid hydrolysis in the temperature range from below zero, 15, 38.5, 53.5, 65 and 73°C and for up to 22-hours. The *imide* content increased from 8.5 to 34.5% and the acrylic acid from 1.57% to 11.10%.

Moradi-Araghi et al.[54] presented similar data at 90°C, as summarised in Table 2-2. It can be seen that the per cent population of *imide* in concentrated acid increased steadily over 9 days and the carboxylate structure increases in a dilute base but the amide is the predominant functional group at any pH. In weakly acid solutions both authors reported very low concentrations of carboxylic acid and imide.

Table 2-2: Effect of Hydrolysis Media on the Population of Various Structures Starting from Non-hydrolysed Polyacrylamide[54]

Media	Ageing Time	Population, %		
	Days	Amide	Carboxylate	Imide
Dilute Base	0	84.5	14.2	1.3
Dilute Base	3	73.1	25.3	1.6
Dilute Base	0	84.5	14.2	1.3
Dilute Base	3	73.1	25.3	1.6
Dilute Acid	0	95.2	0.6	4.2
Dilute Acid	3	89	3	8.1
Dilute Acid	0	91.9	5	3.1
Concentrated Acid	0	94.4	0.8	4.7
Concentrated Acid	2	79	2.4	18.6
Concentrated Acid	9	71.7	2.5	25.8

Halverson et al[56] investigated the structural changes of polyacrylamide macromolecule from acid and alkaline hydrolysis using ^{13}C NMR and derived a sequence length of carboxyl groups in the polyacrylamide chain. These authors described structural characteristics within the polymer chain, with the implicit understanding that many chains are present, using the notation 'A' for the acrylamide functional group in the polymer and 'B' for the acrylic acid functional group (whether

in acid or base form). Additionally, the mole fraction of A units having only A units as nearest neighbours are denoted by F(AAA), the mole fraction of A units having one A unit and one B unit as nearest neighbours by F(AAB) or F(BAA) and so forth were named.

Table 2-3 shows the structural difference between alkaline and acid hydrolysis of polyacrylamide at 110^{o}C after 24-hours[56, 58]. It can be seen that 57 per cent hydrolysis at pH 2 predominantly produced blocks of continuous acrylic acid or acrylamide segments, i.e., AAA and BBB functional groups but alkaline hydrolysis contains ABB, BAB, ABA triads. The B segments (acrylic acid functional group) from alkaline hydrolysis are well distributed along the chain with an average sequence length of 1.4. This average sequence length of carboxyl groups from pH 2 acid hydrolysis was 14[58]. Moreover, the blocky polymers obtained at pH 2 acid hydrolysis appear to exhibit adsorption by covalent bonding or "salt linkage" where electrons are transferred from the acrylate group to multivalent cations like calcium and iron present in or on the mineral surface[56, 58]. The presence of polyacrylimide was also insignificant under both conditions of hydrolysis.

Table 2-3: Hydrolysis Level and Triad Mole Fractions[56, 58]

Media	Hydrolysis,%	AAA	AAB	BAB	ABA	ABB	BBB	Imide
Mild Alkaline	56	0.00	0.10	0.32	0.22	0.36	<0.01	---
Acid pH 2	57	0.31	0.07	0.00	0.00	0.08	0.49	0.04

As the pH 2 acid hydrolysis time for Table 2-3 was 24 hrs, it would be expected that the conversion of F(AAA) to F(BBB) in few hours of hydrolysis would be less complete, i.e., F(AAA) higher than 31%.

In slightly acidic solutions the rate of polyacrylamide hydrolysis increased with increasing temperature and decreasing pH and indicated conformation or structural changes of the polymer in solution upon degradation[59]. Light scattering data also under slightly acidic condition, suggested that the molecular weight of the polymer remained relatively "static" during the hydrolysis[59].

2.6.3 Polyacrylamide Adsorption Mechanisms

This section examines the adsorption of polyacrylamide predominantly onto either oxide or quartz surfaces in mildly acidic or alkaline conditions or onto gold and mild steel surfaces in strong acid solutions.

Neutral or nonionic polyacrylamide (PAM) confers adsorption through hydrogen bonding from the acrylamide functional group as shown in Figure 2-8[48, 60]. This was confirmed using the Scheutjens-Fleer adsorption isotherm in which the participation of segments as trains, loops and tails were calculated[18]. Increasing of the MW of PAM increases adsorption on hematite but its adsorption decreases from pH 3 to 9[61].

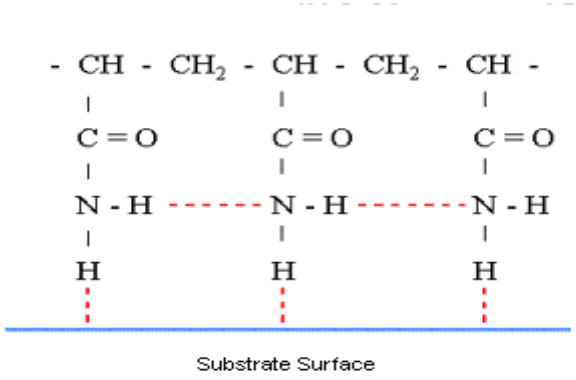

Figure 2-8: Hydrogen Bonding of Non-ionic Polyacrylamide

The presence of positively charged, negatively charged, and neutral chain segments in hydrolysed PAM confers amphoteric character on the polymer chain. The specific amphoteric interaction, typical of nonionic polyacrylamide, progressively disappears as the hydrolysis conversion increases until the non-selective interfacial surface coverage of polyacrylic acid takes place[48]. Therefore, the *number and distribution of –COOH groups* in polyacrylamide macromolecules determines the polymer chain conformation at the interface and directly influences the adsorption amount of polyacrylamide[48, 49, 51, 61]. Adsorption of polyacrylamide with few –COOH groups onto negatively charged surfaces is reduced due to the electrostatic repulsion between negatively charged carboxyl groups of the polymer and negative surface sites[49].

Polyacrylamide with blocks of carboxyl groups spaced along the polymer chain exhibit some adsorption properties which are different from their counter parts with carboxyl groups more widely distributed along the polymer chain particularly in the presence of divalent ions[58, 62]. This type of adsorption is shown in Figure 2-9. Moreover, adsorption takes place only if the energy of a segment-surface interaction is lower than that of a solvent-surface interaction, given by the adsorption energy, and is proportional to the number of adsorbed segments[63].

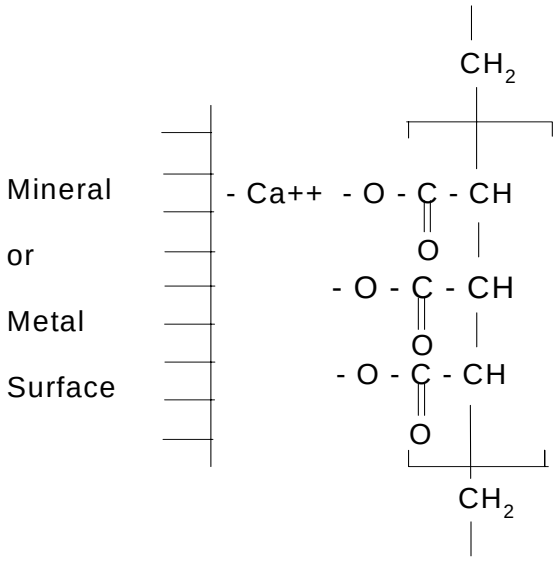

Figure 2-9: Blocky polyacrylamide may exhibit covalent bonding with divalent ions Calcium and Iron [64]

2.6.3.1 Polyacrylamide Adsorption onto Metals and Metal Alloy

It appears from the literature that only Grchev et al.[64-66] studied nonionic polyacrylamide adsorption in strong acid solutions. These authors indicated that adsorption of polyacrylamide on *gold* and *mild steel* in 0.5M sulfuric acidic solution strongly depends on the molecular weight of the polymer, electrode potential and temperature and it appears to be better described by the Frumkin isotherm than by the Langmuir isotherm[64-66]. The following conclusions were drawn from these studies:

(i) Polyacrylamide with a molecular weight of $5x10^3$ (g/mol) produced a surface coverage on gold close to 1 at 20°C and decreased to 0.25 surface coverage at 80°C. Adsorption at E=0 V (vs. MSE) and 40°C of 20 mg/L of $5x10^5$ Daltons

polyacrylamide yielded coverage value of approximately 0.6 and with $1.5x10^6$ molecular weight yielded 0.5. Similar values were obtained for mild steel in 1.6M HCl.

(ii) The value of the maximum coverage at about 20mg/L polyacrylamide and in the temperature range from 20 to 80^oC remains almost unaffected by the polymer molecular weight. Therefore, it is possible that the thickness of the adsorbed layer is not influenced by the polymer molecular weight and probably a flat orientation of the adsorbed parts of the polymer molecules on the metal surface takes place.

(iii) The surface coverage at 2-3mg/L polyacrylamide concentration decreased from about 0.52 to 0.02 as the polyacrylamide molecular weight increased from $5x10^3$ to $1.5x10^6$, respectively.

(iv) The effects of the adsorption of polyacrylamide on gold and mild steel were explained in terms of substitutional absorption of the polymer on a bare metal surface followed by a significant de-sorption of water molecules from the surface[51, 64-66]. The inhibition (adsorption) efficiency drastically decreased after 5-10 hours.

AFM studies of polyacrylamide adsorption on mica have been reported[67, 68]. Nonionic Polyacrylamide with 5.71 x 10^5 Dalton MW was synthesised to have $–SCH_2COOH$ as one end and $–CH_3$ as the other end confers covalent bonding with gold surfaces via the gold-sulfur bond and the rest of the macromolecules confers hydrogen bonding with mica in water. As the force-distance measurements between gold and sulfur were one order of magnitude greater than that between hydrogen bonding with mica and gold, the gold-sulfur bond was called *specific adsorption* and the hydrogen bonding as *non-specific adsorption*.

Polyacrylamide with 1500 and 10,000 Dalton MW at 100ppm concentration and pH 3 gave 1.22 and 1.84nm, respectively of adsorption layer thickness on hematite and the number of segments remained almost unchanged from about 2 to 10^{61}. Polyacrylic acid (PAA) with 2000 and 240,000 MW also at 100ppm concentration and pH 3 gave

1.73 and 2.65nm of adsorption layer thickness and an increase in the number of segments from 3 to 141[61], respectively. Chibowski et al.[61] therefore concluded that the length of both loops and tails may influence the adsorption layer thickness of PAM on hematite surfaces[61] and in contrast mainly tails of PAA are responsible for the increase of adsorption layer with the increase of MW.

2.6.3.3 Cleavage of Polyacrylamide

Polyacrylamide degradation defined as cleavage of the backbone chain can be initiated by different radicals, e.g., sulfate ions $SO_4^{=}$ or OH radicals obtained from decomposition of potassium and ammonium persulfate, H_2O_2-$FeSO_4$ in water, and temperature[69]. These radicals *abstract* an H atom from the "weak" units of the chain, primarily from the head-to-head structure polymer chain, which at low polymer concentration results in cleavage of C-C bond in the backbone. Oxygen also affects the stability of polyacrylamide solutions, i.e., oxidative degradation of polyacrylamide also occurs in the presence of oxygen[69]. Since copper EW electrolyte contains oxygen at its saturated concentration due to the dissociation of water, it may also contribute to the cleavage of PAM.

2.6.3.4 Adsorption Mechanism of Polyacrylamide

A general example of polyacrylamide adsorption has been reported as it is shown in Figure 2-10[63]. It proposes that in order to minimise the adsorption energy the adsorbed layer consists of polymer chains (amide group functionalities) with several stretches of segments in the surface layer (trains). Some trains stick out into the solution (loops rich in carboxylic acid functional groups). Moreover, at the chain ends, freely dangling tails may protrude into the solution.

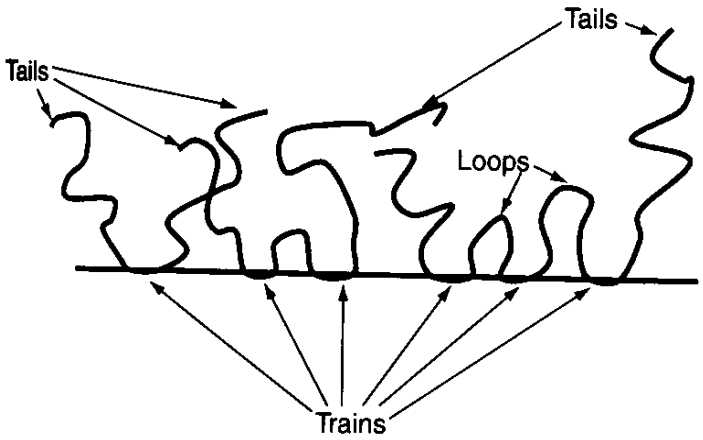

Figure 2-10: Postulated Structure of Adsorbed Partially Hydrolysed Polyacrylamide Layer at the Copper-Electrolyte Interface

However, this example needs to be re-examined to account for the charge density of a block copolymer and random polymer, and of the substrate. It was stated by Panzer and Halverson[58, 62] that polyacrylamide with blocks of carboxylic groups spaced along the polymer chain exhibit different adsorption properties, i.e., covalent bonding, particularly in the presence of divalent ions than random copolymers. Moreover, nonionic polyacrylamide, synthesized with sulfur at one tail to give $-SCH_2COOH$, exhibited covalent bonding or specific adsorption between the sulfur and a gold-plated cantilever during atomic force microscopy (AFM) studies[68].

There appears to be no published work studying the adsorption of block or random copolymers derived from polyacrylamide on copper metal. It would be enormously useful if research would be undertaken to determine if the findings of Halverson et al.[56] and Panzer and Halverson[58] could be extended to the adsorption of block and random polymers on copper. It is important to describe the adsorption mechanism to understand the observation that Mt. Gordon occasionally produced unusually smooth copper cathode when polyacrylamide was contacted with the pregnant leach solution at a pH value of about 1.5.

2.7 Summary

The aim of this chapter is to primarily highlight the importance of the addition of additives in copper electrodeposition. The nucleation and growth of copper electrodeposits needs to be controlled by the addition of carefully selected and properly concentrated organic additives to eliminate the formation of dendrites. In summary, the mechanism and electrochemical action of Guar and chloride ions have been poorly documented in the literature compared with those of glue, thiourea and chloride ions for electrorefining operations. Studies of the effect of polyacrylamides on copper electrodeposition are lacking. Therefore, a better understanding of the influence of polyacrylamide and Guar on copper electrocrystallization is particularly important. Chloride ions depolarize the electrode, in other terms increases the rate kinetics of the electrode-transfer and consequently increases surface roughness since it enhances growth rate rather than nucleation rate[32].

It is shown in Table 1-1 that only *two* additives are used in copper electrowinning: Guar, known in the industry as a "weak levelling agent" and chloride ions instead of *three* additives in copper electrorefining and *four* additives in the microelectronics industry. It may be due to the belief that the highly purified electrolyte solution obtained after solvent extraction does not require a levelling agent and the concern that a new organic additive may affect the solvent extraction reagent. However, it is known that in the damascene process[70] reagent grade electrolyte is used, but nevertheless a levelling agent, grain refiner and chloride ions are also dosed. Since the damascene process uses three additives (inhibitor, accelerator and chloride ions) rather than the two additives in conventional electrowinning it is concluded that electrowinning may be improved through the use of a levelling agent and grain refiner besides chloride ions to control dendrite growth and minimize the level of impurities in the copper cathode. At the commencement of the work described in this thesis, it was not known whether polyacrylamide behaved as a levelling agent or grain refiner or both.

Vereecken and Winand[41] concluded that the quality of the copper deposits obtained with Guar was always better than those obtained with both nonionic and cationic polyacrylamides. Vereecken and Winand[41] also observed the depolarization

behaviour of nonionic and cationic polyacrylamides, and Guar prepared in water or in a solution of pH 3.

The physicochemical properties of polyacrylamide can be summarized as follow:

(i) Polyacrylamide adsorption onto solid surfaces may involve both chemical and physical adsorption. The adsorption of polymers also depends on the solution pH, chemical nature of the surface, the presence of solutes and the functional groups of the polymer.

(ii) The reaction pathway and therefore product from alkaline hydrolysis is different to that from acid hydrolysis. Polyacrylamide in a strong acid medium is attached to the surface through hydrogen bonds. Hydrolysis increases the number of carboxyl functional groups in the polymer.

(iii) The reaction product of non-ionic polyacrylamide hydrolysed in strong acid conditions is polyacrylimide upon ageing. However, the presence of polyacrylimide was insignificant under slightly acidic conditions.

(iv) Light scattering data indicates that under slightly acidic condition the molecular weight of the polymer remained relatively "static" during the hydrolysis process.

(v) Hydrolysis at pH value of 2 predominantly produces blocks of acrylic acid and acrylamide segments with an average sequence length of carboxyl groups of 14 instead of 1.4 obtained from alkaline hydrolysis.

(vi) In general, the *initial hydrolysis* of polyacrylamide is faster than the remainder[50].

(vii) Literature on the adsorption of PAM on copper metal and 316L stainless steel appears to be nonexistent. However, the free energy of the overall adsorption process of the polyacrylamide pre-treated at pH value of 1.5 must be favourable if it is going to be a useful organic additive in copper electrowinning and electrorefining.

(viii) The adsorption process of non-ionic and anionic PAM and also polyacrylic acid depends on their molecular weight (MW), solution pH, hydrophobicity characteristics of the substrate[71] and the presence of some metal chlorides[61].

2.8 References

1. Robinson T, Davenport WG, Quinn J, Karkas G. Electrolytic Copper Refining - 2003 World Tankhouse Operating Data. In: Dutrizac JE, Clement CG, editors. *Copper 2003 - Cobre 2003*; 2003; Santiago, Chile: Canadian Institute of Mining, Metallurgy and Petroleum; 2003. p. 3-66.

2. Robinson T, Rasmussen S, Davenport WG, Jenkings J, King M. Copper Electrowinning - 2003 World Tankhouse Operating Data. In: Dutrizac JE, Clement CG, editors. *Copper 2003 - Cobre 2003 Copper Electrorefining and Electrowinning*; 2003; Santiago, Chile; 2003. p. 421-472.

3. Baxter K, Kaiser C, Richmond GD. Design of the Mt. Gordon Chalcocite Project. In: *Alta Copper Sulfides Symposium*; 1999 September 5-10; 1999. p. 1-21.

4. Richmond G, Christie M. The Commissioning and Operation of a Copper Sulfide Pressure Oxidation Leach Process at Mt. Gordon. In: ALTA, editor. *Alta Copper Sulfides Symposium*; 1999 September 5-10; 1999. p. 1-9.

5. Richmond G, Dreisinger D; inventors. Western Metals Copper Limited, assignee. Processing Copper Sulfide Ores. Australia patent 749257. 1999.

6. Vetter K. *Electrochemical Kinetics, Theoretical and Experimental Aspects*. New York: Academic Press; 1967.

7. Budevski E, Staikov G, Lorenz W. *Electrochemical Phase Formation and Growth, an Introduction to the Initial Stages of Metal Deposition*. New York: VCH; 1996.

8. Paunovic M, Schlesinger M. *Fundamentals of Electrochemical Deposition*: John Wiley & Sons, Inc.; 1998.

9. Bard AJ, Faulkner L. *Electrochemical Methods, Fundamentals and Applications*. Second ed. Brisbane: John Wiley & Sons, Inc.; 2001.

10. Newman J, Thomas-Alyea KE. *Electrochemical Systems*. Third ed. Hoboken, New Jersey: John Wiley & Sons, Inc.; 2004.

11. Grabowski A, Newman J. *Current and Potential Distributions on a Cylinder Electrode*. J. Electrochem. Soc. 1993;140(6):1625-1631.

12. Gabe D. *Rotating Electrodes for Use in Electrodeposition Process Control*. Plating & Surface Finishing 1995;9:69-76.

13. Podlaha E, Landolt D. *Induced Codeposition Ii. A Mathematical Model Describing the Electrodeposition of Ni-Mo Alloys*. J. Electrochem. Soc. 1996;143(3):893-899.

14. Eisenberg M, Tobias C, Wilke C. *Ionic Mass Transfer and Concentration Polarization at Rotating Electrodes*. Journal of the Electrochemical Society 1954;101(6):306-319.

15. Arvia AJ, Carrozza JSW. *Mass Transfer in the Electrolysis of Cuso4-H2so4 in Aqueous Solutions under Limiting Current and Forced Convection Employing a Cylindrical Cell with Rotating Electrodes*. Electrochimica Acta 1962;7:65-78.

16. Barkey D, Muller R, Tobias C. *Roughness Development in Metal Electrodeposition I. Experimental Results*. Journal of the Electrochemical Society 1989;138(8):2199-2207.

17. Gabe D, Wilcox G, Gonzalez-Garcia J, Walsh F. *The Rotating Cylinder Electrode: Its Continued Development and Application*. Journal of Applied Electrochemistry 1998;28(8):759-780.

18. Maciel J, Agostinho S. *Construction and Characterization of a Rotating Cylinder Electrode for Different Technological Applications*. Journal of Applied Electrochemistry 1999 Jun;29(6):741-745.

19. Filzwieser A, Hein K, Hanko G. Application of Two Phase Hydrodynamic Modeling to an Electrowinning Cell. In: Dutrizac JE, Ji J, Ramachandran V, editors. *Copper 99 - Cobre 99 International Conference*; 1999: The Minerals, Metals & Materials Society; 1999.

20. Manzanares JA, Kontturi K. Diffusion and Migration. In: Calvo EJ, editor. *Interfacial Kinetics and Mass Transport*: Wiley-VCH; 2003. p. 81-121.

21. Wang L, Olsen M, Vigil R. *Reappearance of Azimuthal Waves in Turbulent Taylor-Couette Flow at Large Aspect Ratio*. Chemical Engineering Science 2005;60:5555-5568.

22. Schlichting H. *Boundary-Layer Theory*. Sydney: McGraw-Hill; 1968.

23. Silverman DC. *The Rotating Cylinder Electrode for Examining Velocity-Sensitive Corrosion - a Review*. Corrosion 2004;60(11):1003-1022.

24. Newman J. *Electrochemical Systems*. Second ed. London: Prentice-Hall International; 1991.

25. Bard AJ, Parsons R, Jordan J. *Standard Potentials in Aqueous Solution*. New York: Marcel Dekker, Inc; 1985.

26. Mattsson E, Bockris JOM. *Galvanostatic Studies of the Kinetics of Deposition and Dissolution in the Copper+Copper Sulphate System*. Transaction Faraday Soc. 1959;55:1586-1601.

27. Calvo EJ. The Current-Potential Relationship. In: Bard AJ, Stratmann M, editors. *Encyclopedia of Electrochemistry, Volume 2: Interfacial Kinetics and Mass Transport*: Wiley-VCH; 2003. p. 3-30.

28. Dini J. *Electrodeposition, the Materials Science of Coatings and Substrates*. New Jersey: Noyes Publications; 1993.

29. Sun M, O'Keefe T. *The Effect of Additives on the Nucleation and Growth onto Stainless Steel Cathodes*. Metallurgical Transaction B 1992;23B:591-599.

30. Zhou Z, Okeefe T. *Electrodeposition of Copper on Thermally Oxidized 316 L Stainless Steel Substrates*. Journal of Applied Electrochemistry 1998(4):461-469.

31. Kinaci F. Nucleation and Growth in Electrodeposition of Thin Copper Films on Pyrolytic Graphite [MS]. Berkeley: University of California; 1992.

32. Ilgar E, O'Keefe T. Surface Roughening of Electrowon Copper in the Presence of Chloride Ions. In: Dreisinger D, editor. *Aqueous Electrotechnologies: Progress in Theory and Practice*; 1997: The Minerals Metals and Materials Society; 1997. p. 51-62.

33. Wu Q, Barkey D. *Faceting and Roughening Transitions on Copper Single Crystals in Acid Sulfate Plating Baths with Chloride*. Journal of the Electrochemical Society 2000 Mar;147(3):1038-1045.

34. Chassaing E, Wiart R. *Epitaxial Growth and Electrode Impedance of Copper Electrodeposits*. Electrochimica Acta 1984;29(5):649-660.

35. Gabrielli C, Mocoteguy P, Perrot H, Wiart R. *Mechanism of Copper Deposition in a Sulfate Bath Containing Chlorides*. Journal of Electroanalytical Chemistry 2004;572(2):367-375.

36. Radisic A, West A, Searson P. *Influence of Additives on Nucleation and Growth of Copper on N-Si(111) from Acidic Sulfate Solutions*. Journal of the Electrochemical Society 2002;149(2):C94-C99.

37. Schmidt W, Alkire R, Gewirth A. *Mechanic Study of Copper Deposition onto Gold Surfaces by Scaling and Spectral Analysis of in-Situ Atomic Force Microscopic Images*. J. Electrochem. Soc. 1996(10):3122-3132.

38. Kang M, Gross ME, Gewirth AA. *Atomic Force Microscopy Examination of Cu Electrodeposition in Trenches*. Journal of the Electrochemical Society 2003;150(5):C292-C301.

39. Hope GA, Woods R. *Transient Adsorption of Sulfate Ions During Copper Electrodeposition*. J. Electrochem. Soc. 2004;151(9):C550-553.

40. Pye D, Schurz G; inventors. The Dow Chemical Company, assignee. Electrowinning of Metals. United States patent 2,798,040. 1957 July 2, 1957.

41. Vereecken J, Winand R. *Influence of Polyacrylamides on the Quality of Copper Deposits from Acidic Copper Sulphate Solutions*. Surface Technology 1976; 4:227-235.

42. Langner BE, Stantke P, Reinking EF; inventors. Norddeutsche Affinerie Aktiengesellschaft (Hamburg, DE), assignee. Method of Measuring the Effective Inhibitor Concentration During a Deposition Process of Metal from Aqueous Electrolytes and Test Apparatus Therefore patent 4,834,842. 1989.

43. Stantke P. *Guar Concentration Measurement with the Collamat System*. Proceedings of the COPPER 99-COBRE 99 International Conference 1999;3:643-651.

44. Mark H, Gaylord N, Bikales N. *Encyclopedia of Polymer Science and Technology*; 1969.

45. Lipkowski J. *1998 Alcan Award Lecture - Surface Electrochemistry - Surface Science with a Joy Stick*. Canadian Journal of Chemistry 1999;77(7):1163-1176.

46. Saban M, Scott J, Cassidy R. *Collagen Proteins in Electrorefining: Rate Constants for Glue Hydrolysis and Effects of Molar Mass on Glue Activity*. Metallurgical & Materials Transactions B-Process Metallurgy & Materials Processing Science 1992;23B:125-133.

47. Plieth W. *Additives in the Electrocrystallization Process*. Electrochimica Acta 1992;37(12):2115-2121.

48. Pefferkorn E. *Polyacrylamide at Solid/Liquid Interfaces*. Journal of Colloid & Interface Science 1999;216:197-220.

49. Drzymala J, Fuerstenau D. *Adsorption of Polyacrylamide, Partially Hydrolyzed Polyacrylamide and Polyacrylic Acid on Ferric Oxide and Silica*. Process Technology Proceedings 1987;4(Flocculation Biotechnol. Sep. Syst.):45-60.

50. Caulfield MJ, Qiao GG, Solomon DH. *Some Aspects of the Properties and Degradation of Polyacrylamides*. Chemical Reviews 2002;102(9):3067-3083.

51. Ghannam M. *Wetting Behavior of Aqueous Solutions of Polyacrylamide over Polyethylene Substrate*. Journal of Chemical and Engineering Data 2002;47(2):274-277.

52. Tackett J; inventor. Marathon Oil Company, assignee. A Method for Inhibiting Hydrolysis of Polyacrylamide patent WO 92/07881. 1992.

53. Atkins M, Biggin I, Kidd D; inventors. BP Chemicals Limited, assignee. Hydrolysis of Polymers. United States patent 5,081,195. 1992 January 14, 1992.

54. Moradi-Araghi A, Hsieh E, Westerman I. *Role of Imidization in Thermal Hydrolysis of Polyacrylamides*. Water-Soluble Polym. Pet. Recovery, [Proc. Natl. Meet. ACS] 1988:271-8.

55. Minsk L, Kotlarchik C, Meyer G, Kenyon W. *Imidization During Polymerization of Acrylamide*. Journal of Polymer Science 1974;12:133-140.

56. Halverson F, Lancaster J, O'Connor M. *Sequence Distribution of Carboxyl Groups in Hydrolyzed Polyacrylamide*. Macromolecules 1985;18(6):1139-44.

57. Haas H, Macdonald R. *Imidization Reaction in Polyvinylamides*. Journal of Polymer Science 1971;9(A-1):3583-3593.

58. Panzer H, Halverson F. Blockiness in Hydrolyzed Polyacrylamide. In: Moudgil B, Scheiner B, editors. *Flocculation Dewatering, Proc. Eng. Found. Conf.*; 1988; Palm Coast Florida, USA; 1988. p. 239-49.

59. Muller G, Fenyo J, Selegny E. *High Molecular Weight Hydrolyzed Polyacrylamides. Iii. Effect of Temperature on Chemical Stability*. Journal of Applied Polymer Science 1980;25:627.

60. Kuz'kin SF, Nebera VP, Zolin SN. *Aspects of the Theory of Suspension Flocculation by Polyacrylamides*. Intern. Mineral Process. Congr., Tech. Papers, 7th, New York City, 1964 1965;1:347-57.

61. Chibowski S, Wisniewska M. *Study of Electrokinetic Properties and Structure of Adsorbed Layers of Polyacrylic Acid and Polyacrylamide at Ferric Oxide-Polymer Solution Interface*. Colloids and Surfaces A: Physicochemical and Engineering Aspects 2002;208(1-3):131-145.

62. Panzer H, Halverson F, Lancaster J. *Carboxyl Sequence Distribution in Hydrolyzed Polyacrylamide*. Polymeric Materials Science and Engineering 1984;51:268-71.

63. Holmberg K, editor. *Handbook of Applied Surface and Colloid Chemistry*: John Wiley & Sons, Ltd.; 2002.

64. Grchev T, Cvetkovska M. *Electrochemically Initiated (Co)Polymerization of Acrylamide and Acrylonitrile on a Steel Cathode - Electrochemical and Impedance Study*. Journal of Applied Electrochemistry 1989;19(3):434-42.

65. Grchev T, Cvetkovska M, Stafilov T, Schultze J. *Adsorption of Polyacrylamide on Gold and Iron from Acidic Aqueous Solutions*. Electrochimica Acta 1991;36(8):1315-1323.

66. Grchev T, Cvetkovska M, Schultze JW. *The Electrochemical Testing of Polyacrylic Acid and Its Derivatives as Inhibitors of Corrosion*. Corrosion Science 1991;32(1):103-12.

67. Haschke H, Miles MJ, Sheppard S. *Adsorption of Individual Polyacrylamide Molecules Studied by Atomic Force Microscopy*. Single Molecules 2002;3(2-3):171-172.

68. Haschke H, Miles MJ, Koutsos V. *Conformation of a Single Polyacrylamide Molecule Adsorbed onto a Mica Surface Studied with Atomic Force Microscopy*. Macromolecules 2004;37(10):3799-3803.

69. Kurenkov V, Hartan H, Lobanov F. *Degradation of Polyacrylamide and Its Derivatives in Aqueous Solutions*. Russian Journal of Applied Chemistry 2002;75(7):1039-1050.

70. Vereecken PM, Binstead RA, Deligianni H, Andricacos PC. *The Chemistry of Additives in Damascene Copper Plating*. IBM Journal of Research and Development 2005;49(1):3-19.

71. Broseta D, Medjahed F. *Effects of Substrate Hydrophobicity on Polyacrylamide Adsorption*. Journal of Colloid and Interface Science 1995;170(2):457-465.

CHAPTER 3

EFFECT OF PREPARATION MEDIA OF POLYACRYLAMIDE ON SURFACE ROUGHNESS

3.1 Introduction

As discussed in the previous Chapter it is generally accepted that the mechanisms of polyacrylamide hydrolysis and the reaction products in acid and alkaline media are different. This difference mainly corresponds, to the distribution of the polyacrylic acid moieties in the polyacrylamide molecular chain: block copolymers appears to be obtained in slightly acidic solutions, i.e., pH 2 and random copolymers in alkaline solutions. However, in strong acid solutions the amount of polyacrylimide becomes a significant product upon ageing.

In the work described in this Chapter, the equipment required to carry out bulk electrolysis, a rotating cylinder electrode, was built and its characteristics in terms of diffusion layer thickness and surface roughness of electrowon copper were compared with those published in the recent literature. A rotating cylinder electrode (RCE) was selected as the electrode for copper electrowinning trials because at low rotation speeds this *large* electrode configuration appears to achieve *turbulent* flow with vortices described in Appendix A, a uniform current distribution and therefore mass transfer[1, 2]. The RCE allows the hydrodynamics of a commercial scale copper electrowinning cell to

be approximated at low speeds of rotation. The RCE primarily imposes horizontal forced convection thus minimizing the effect of the vertical free convection due to changes in density at the electrode/electrolyte interface.

It has been described in Chapter 1 that Mt. Gordon occasionally produced the smoothest copper cathode ever known in the industry. Therefore, the aim in this Section was to indirectly explore the range of hydrolysis products of polyacrylamide to achieve the smoothest copper deposit surface. Thus, polyacrylamide was prepared in both acid solutions (including diluted solutions of the full-strength electrolyte) and alkaline solutions. The experiments were designed to evaluate the effect of polyacrylamide preparation media on the surface roughness of the copper deposit obtained from copper electrowinning.

3.2 Experimental

3.2.1 Design and Construction of Rotating Cylinder Electrode for Copper Electrowinning

A rotating cylinder electrode was designed and constructed at the Engineering Workshop of James Cook University similar in design to that described by Barkey, Muller and Tobias[3]. Figures 3-11 and 3-12 present the design of the top and bottom sections of the rotating cylinder electrode, respectively. The main feature of the rotating cylinder electrode design is that it resembles a typical commercial scale operation in terms of (i) the distance between the electrodes, 40mm, (ii) the use of the industry-standard cathode material (316L stainless steel) and (iii) the hydrodynamics of the electrolyte.

The rotating cylinder electrode (RCE) for this thesis, consisted of a 4.445 cm diameter 15 cm overall height 316L stainless steel rod (Sandvik). This electrode was bounded tightly with 3mm thickness PTFE sleeves to suppress edge effects and to leave a 2cm active height of stainless steel exposed. A dimensionally stable anode (DSA) sourced from Eltech Systems Corporation (USA) was used for the anode of the RCE. The RCE with the DSA concentrically arranged around it was located within a 5L Pyrex beaker. Eight PTFE baffles (200 x 20 x 5 mm) within the beaker maintained the DSA mesh at a distance of 40 mm from the RCE surface through a PVC lid. The RCE electrowinning cell rested in a thermostated water bath.

The active area of the RCE was 27.91cm^2 and the number of coulombs applied to each test varied from 12,000 to 36,000C. The rate of rotation of the RCE was controlled using a Movitrac controller and 0.37kW motor (RF27DT71D4) using a gear box sourced from SEW Eurodrive.

In the experiments described in this Chapter, the dependent variable was the surface roughness of the copper electrodeposit produced.

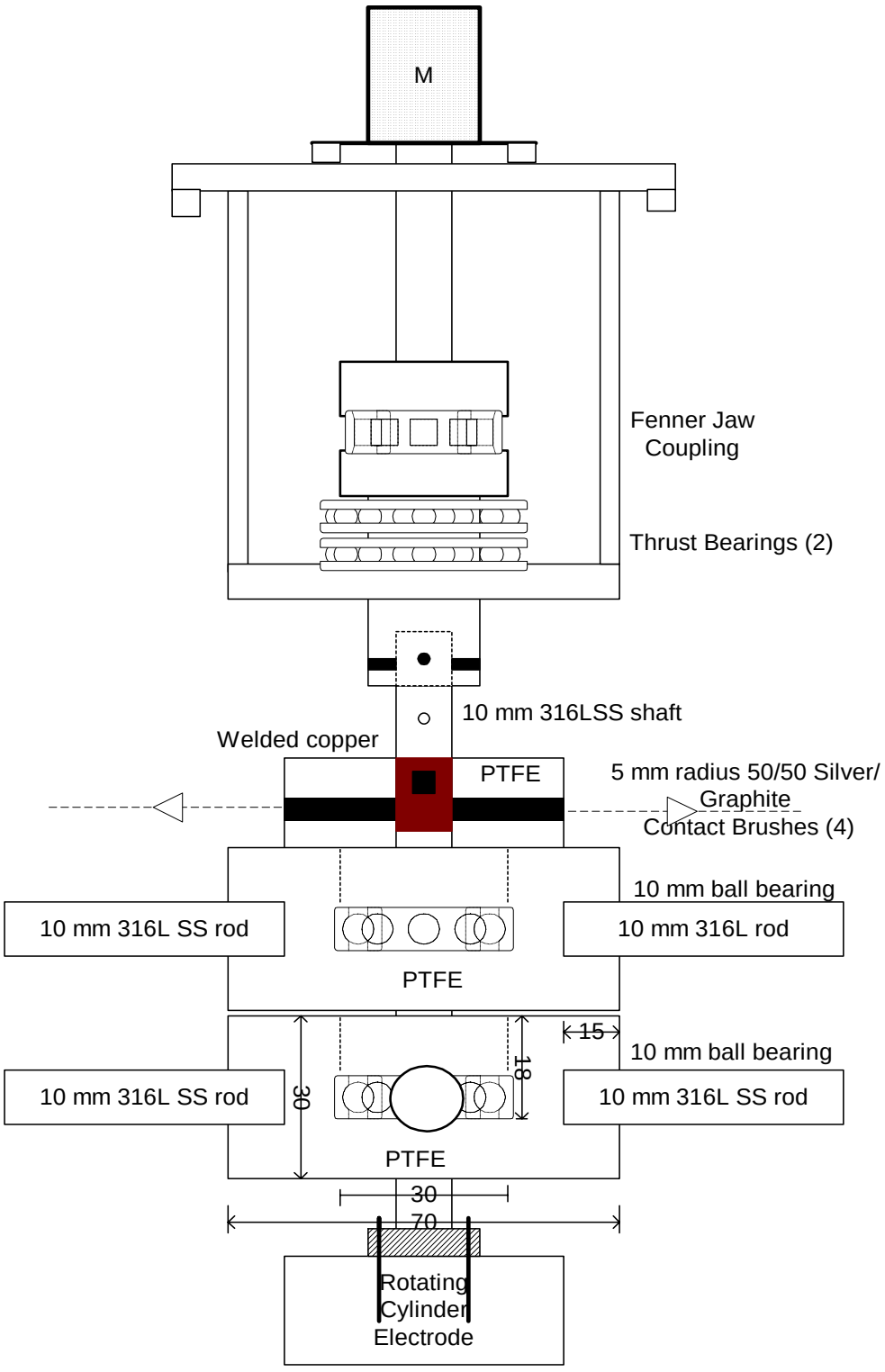

Figure 3-11: Rotating Cylinder Electrode – Top Section

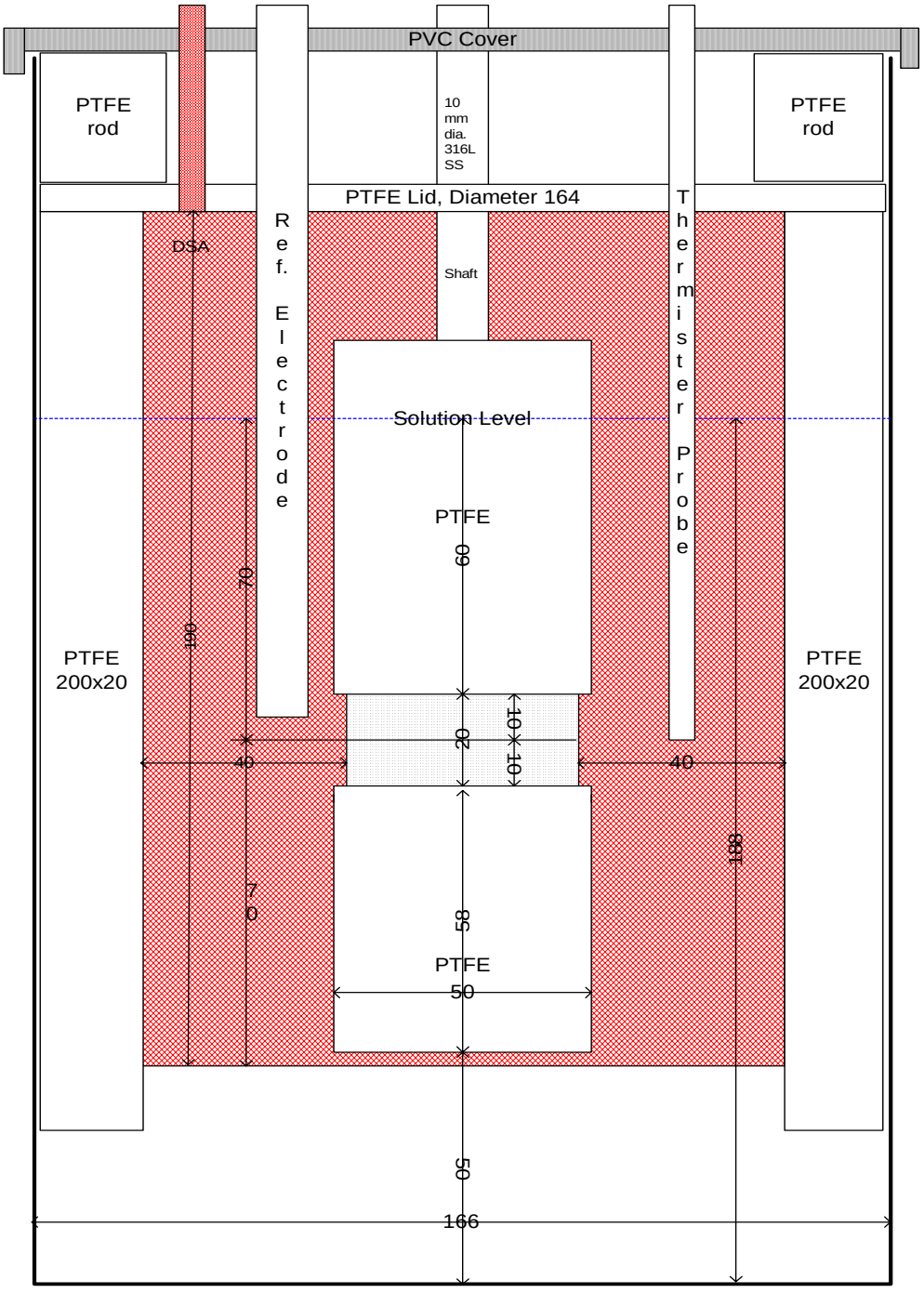

Figure 3-12: Rotating Cylinder Electrode – Bottom Section

The surface roughness was collected using a Mahr Perthometer M1[4] with a 2μm stylus tip radius. It was calibrated with its PGN-3 (Rz = 2.9μm, Ra = 0.79μm) standard. The surface roughness measurement was conducted before the copper deposit was detached from the rotating cylinder electrode along the height of the electrode. This measurement process was *repeated 8 times* around the cylinder electrode on equidistantly distributed lines. Figure 3-13 shows the setup of the rotating cylinder electrode and the M1 Mahr Perthometer to measure the surface roughness. Direct current to the RCE electrowinning cell was applied using a 0-18VDC, 0-20A digital power supply sourced from Cole-Parmer Extech Equipment Pty. Ltd., USA.

The copper deposit, a ring, was removed from the rotating cylinder electrode once the surface roughness measurements were obtained. The copper deposit ring was gently forced out using a stainless steel ring specially machined with an internal diameter of few microns larger than that of the RCE and a 2inch diameter stainless steel pipe (~20cm height). The stainless steel pipe was made to sit on the top of the stainless steel ring and hammered vertically using a mallet while the RCE sat on a 60mL plastic sampler (<4cm diameter). This procedure may occasionally produce few scratches onto the RCE but is does not affect the surface roughness measurement and it is a better technique than that used by Barkey et al. [3] who machined the RCE to have a slope of a few microns which could affect the current density distribution.

The RCE was polished with 1μm and 0.25μm diamond paste and had an initial surface roughness of 0.15 ± 0.04 μm. Once the copper was detached from the RCE, the RCE was immersed in 10% nitric acid for about 60 seconds, polished with 0.25μm diamond paste, washed with distilled water, immersed again in the nitric acid solution for another 60 seconds and completely washed with distilled water. This sequence was repeated after each test and the stainless steel maintained its brightness.

Figure 3-13: M1 Mahr Perthometer Measuring the Surface Roughness of Electrowon Copper

3.2.3 Determination of Limiting Current Density and Diffusion Layer Thickness

The aim in this section is to discuss the limiting current density, i_L technique to determine the diffusion layer thickness, δ for copper electrodeposition. The value of the diffusion layer thickness is then correlated with surface roughness in Section 3.2.4.

The δ was calculated in the literature either by measuring i_L for copper deposition[4-6] or by measuring the i_L for added silver[7, 8]. As silver is reduced at more positive potentials than copper by 0.462mV, it should plate at its mass transfer controlled (limiting) current density at the normal operating cathode potential (-100 to -300mV vs. Hg/H_2SO_4). The accuracy of both techniques may be limited by both the electrocrystallization mechanism on the particular substrate in terms of underpotential deposition and type of nucleation and growth[9-11]. It also is argued against the i_L technique applied directly to copper deposition that at current densities close to the i_L it gives powdery material increasing the active area of the working electrode and therefore

affecting the results[7]. In this thesis the i_L was measured using the copper electrodeposition method.

The large active area (27.91 cm^2) of the large rotating cylinder electrode used for all the testwork in this Chapter and Chapter 4 was an impediment to measure directly the i_L on that electrode due to the one ampere capacity of the instrumentation for this test. Therefore, i_L and δ were determined using a *small* RCE described and used in Chapter 5 – Figure 5-3. Appendix A shows that the i_L and δ are similar for both the large and small RCE. The electrolyte composition is described in Table 3-4. The first cycle of Cyclic Voltammograms at 1mV/sec with the RCE at 0, 10, and 25rpm and 45°C and 65°C in the absence of additives were used to determine the i_L. Figures 3-14, 3-15 and 3-16 show the results.

Table 3-4: Electrolyte Composition and Other Variables

Copper, g/L	36
Sulfuric acid, g/L	160
Chloride ions, mg/L	25
Active cathode surface area, cm^2	1.5
Electrolyte volume, mL	500
Inter-electrode distance, mm	32

The i_L for this thesis was also calculated using the equations developed by Eisenberg et al.[12] and Arvia et al[13], discussed in Section 2.3, and these equations are replicated as Equations 3-16 and 3-17, respectively. Although the equation of Eisenberg et al.[12] is valid for Reynolds numbers from 112 to 162,000 and Schmidt numbers from 2230 to 3650, it is known to be in error by as much as 8.3 percent[2].

$$i_L = 0.0791 \frac{nFDC_b}{di} (\mathrm{Re})^{0.7} (Sc)^{0.356} \qquad (3\text{-}16)$$

$$i_L = 0.0791\, nFC_b \left(\frac{di}{\nu}\right)^{-0.30} (U)^{0.70} \left(\frac{do}{di}\right) (Sc)^{-0.644} \qquad (3\text{-}17)$$

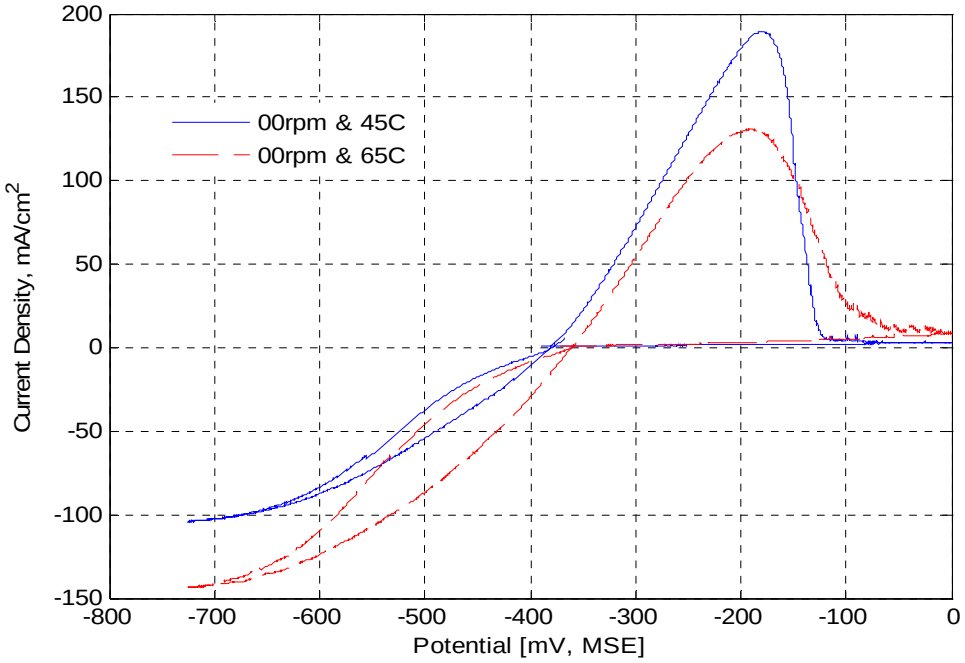

Figure 3-14: Current-Potential Curve – First Cycle Starting on pre-plated copper at 1mV/sec with the RCE at 0rpm (Free Convection) and 45°C and 65°C in the Absence of Additives to determine the Limiting Current Density (1037 and 1432 A/m^2).

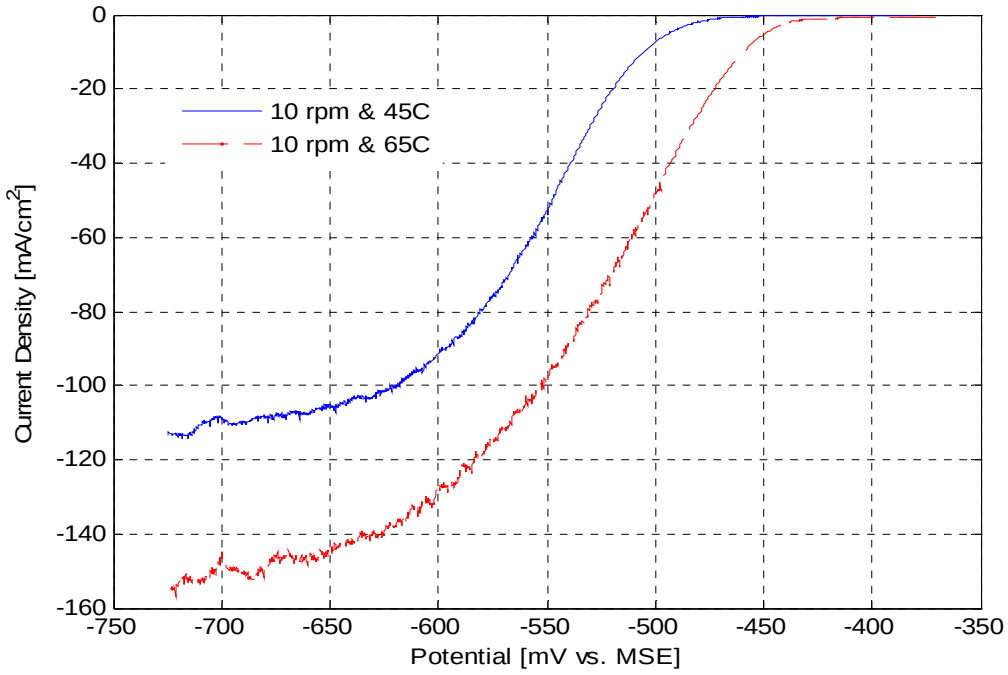

Figure 3-15: Current-Potential Curve – Initial Cycle Starting on Bare Stainless Steel at 1mV/sec with the RCE at 10rpm and 45 and 65°C in the Absence of Additives to determine the Limiting Current Density (1118 and 1497 A/m^2).

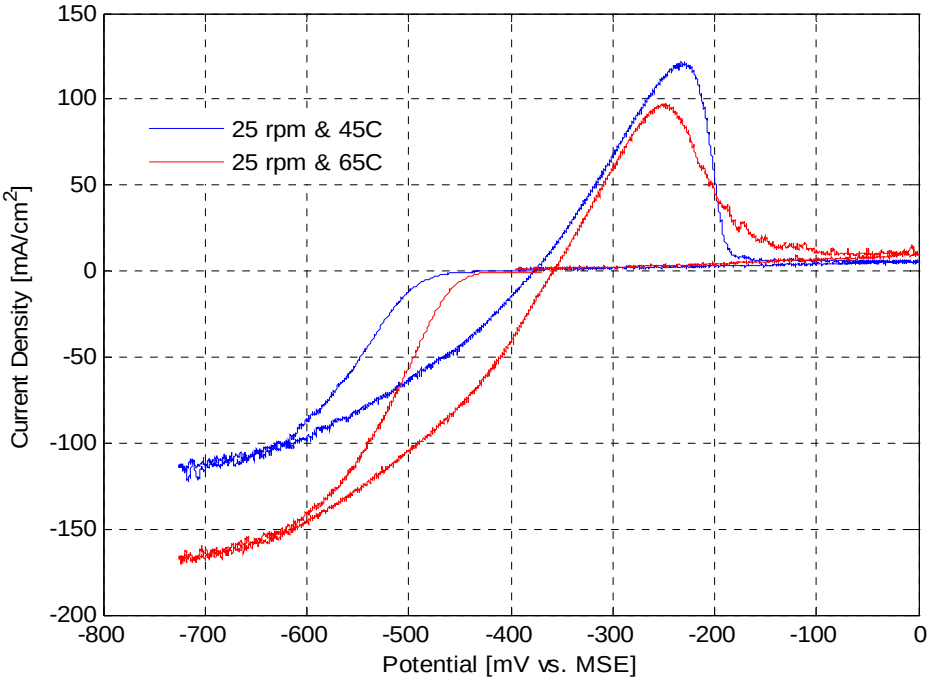

Figure 3-16: Current-Potential Curve – First Cycle Starting on Bare Stainless Steel at 1mV/sec with the RCE at 25rpm and 65°C in the Absence of Additives to determine the Limiting Current Density (1155 and 1666 A/m^2).

i_L is given by Fick's first law with a surface concentration of zero described in Equation 3-18[14].

$$i_L \equiv \frac{nFDC_b}{\delta} \tag{3-18}$$

where δ is the diffusion layer thickness. Recombination of equations (3-16) or (3-17) and (3-18) allows the diffusion layer thickness to be calculated. The δ is schematically shown in Figure 3-17. The concentration of cupric ions at the electrode/electrolyte interface is zero at the limiting current density.

It is shown in Appendix A that Arvia et al.'s[13] equation produces similar δ for both the large and small rotating cylinder electrodes used in this thesis and hence it is used to present the calculated value of δ.

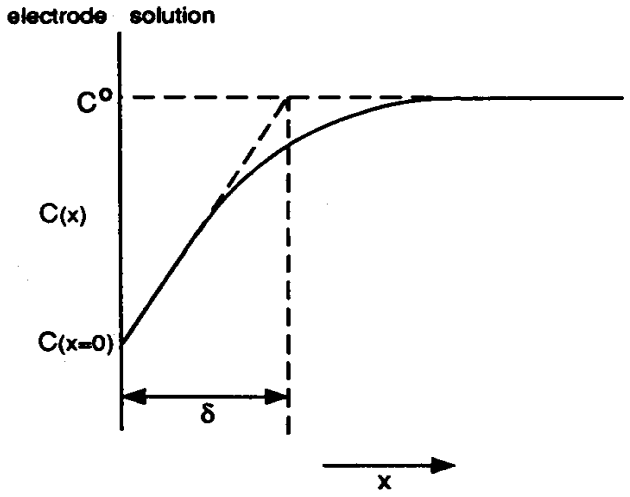

Figure 3-17: Schematic Presentation of the Concentration Profile of Cupric Ions (C^o at the bulk electrolyte) at the Electrode/ electrolyte Interface and the Diffusion Layer Thickness, δ.

In order to apply Equations 3-16 and 3-17 to calculate the diffusion layer thickness the kinematic viscosity and diffusion coefficient of cupric ions at different temperatures were required. The viscosity and electrolyte density for 35 g/L copper and 165 g/L sulfuric acid were obtained from Price et al.[15] to derive the kinematic viscosity at different temperatures as plotted in Figure 3-18. The diffusion coefficient of cupric ions was collected from various authors[1, 8, 16] for different temperatures and plotted in Figure 3-19. An exponential line of the best fit was used to fit the data and the diffusion coefficient at any temperature was determined by interpolation.

Appendix A presents the calculations to determine the diffusion layer thickness. Table 3-5 and Figure 3-20 present the summary of the results. The results obtained by using the equation developed by Arvia et al.[13] more closely replicate the experimental data than those obtained by using the equation developed by Eisenberg et al.[12]. These findings are consistent with an effect of sulfuric acid discussed in Section 2.3. Therefore diffusion layer thicknesses obtained using Arvia et al.'s[12] equation were compared with the data for this thesis as depicted in Figure 3-20.

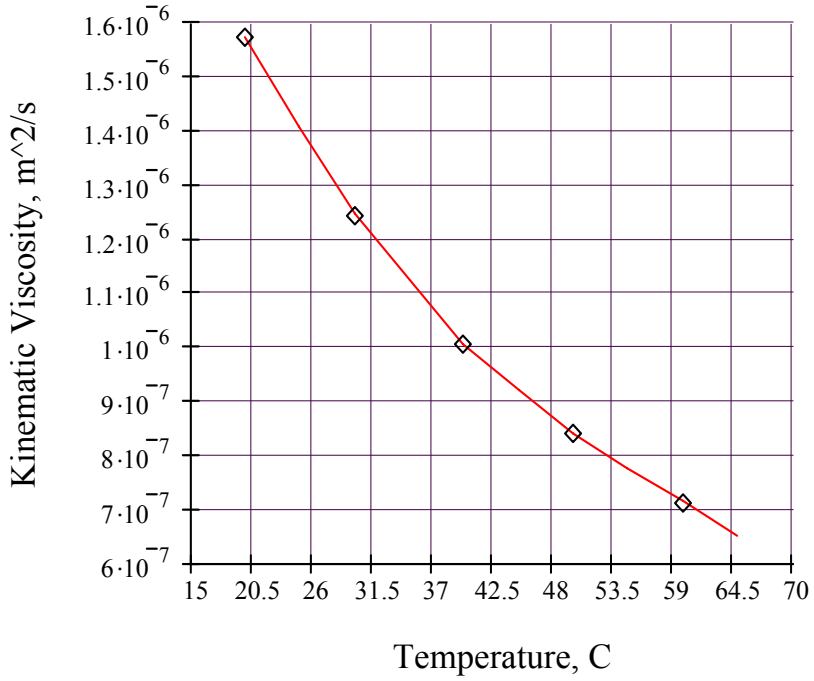

Figure 3-18: Variation in Kinematic Viscosity with Temperature

◊ represents Price et al.'s[15] data for a copper electrolyte containing 35 g/L copper and 165 g/L sulfuric acid. Line represents the line of best fit.

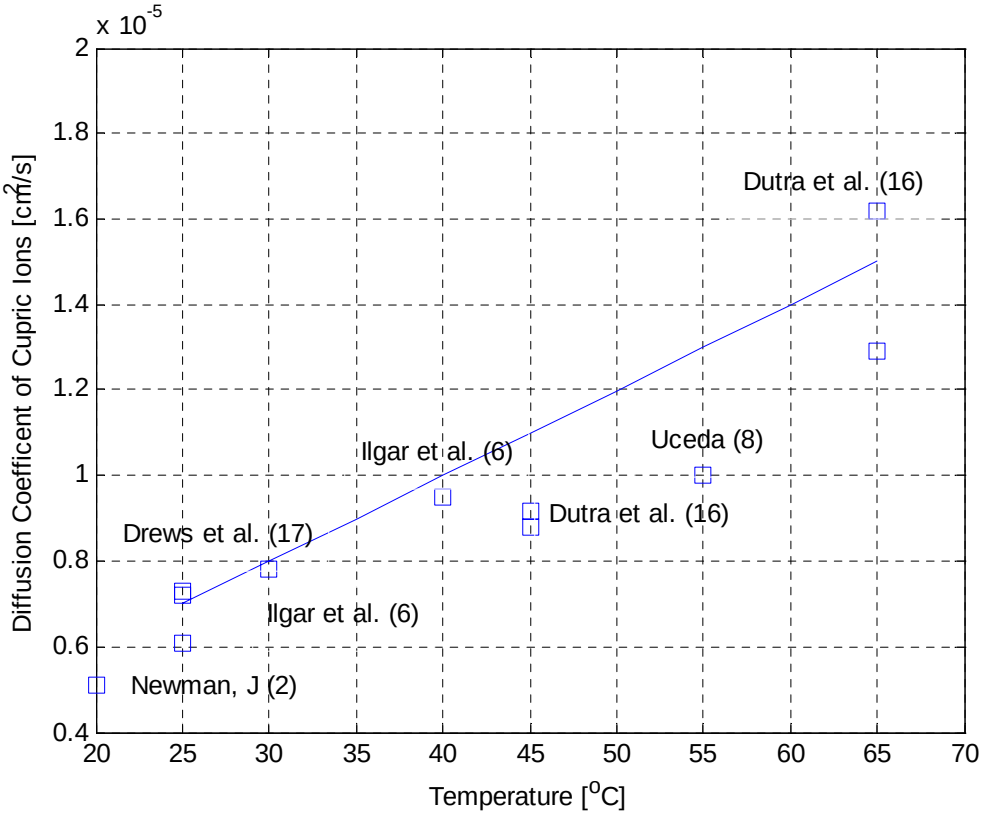

Figure 3-19: Variation of Diffusion Coefficient of Cupric Ions as a Function of Temperature

Legend: □ = original data from the literature stated in Appendix A and line = linear fitting.

Table 3-5: Effect of RPM and Temperature on Diffusion Layer Thickness

RPM	Temperature	Calculated		Experimental	
	°C	i_L, A/m^2	δ, µm	i_L, A/m^2	δ, µm
0	45	--	--	1037	97
0	65	--	--	1432	115
10	45	1070	94	1118	90
10	65	1655	99	1497	110
25	45	2032	49	1155	87
25	65	3143	52	1666	99

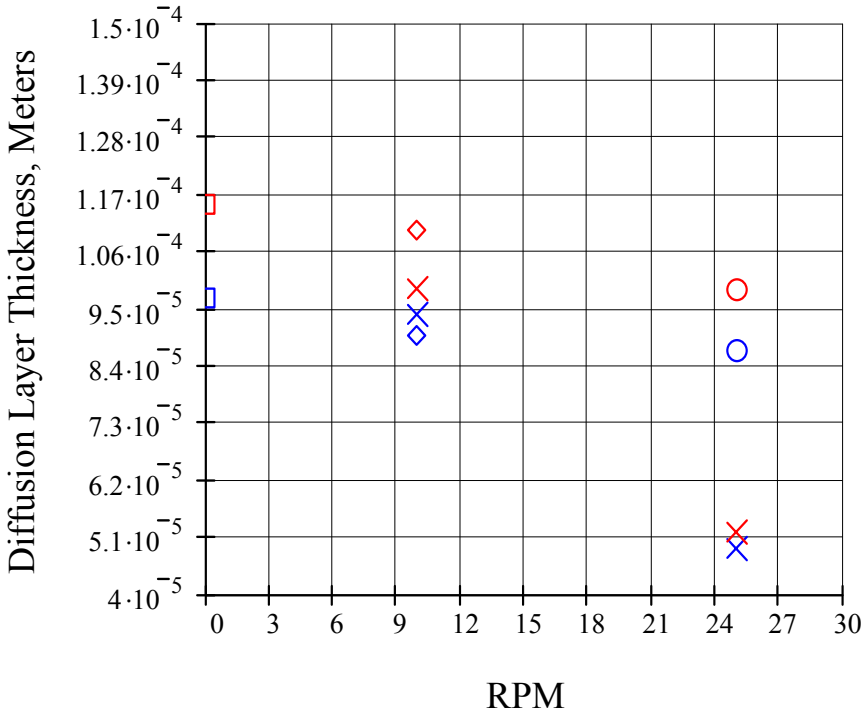

Figure 3-20: Effect of RPM on Calculated and Experimental Diffusion Layer Thickness at 45°C and 65°C

Legend: blue=45°C; red=65°C; x=Calculated using Arvia et al.'s LCD Equation; □= Experimental Free Convection; ◊ = Experimental at 10 rpm and o = Experimental at 25 rpm

The experimental diffusion layer thicknesses are greater at 0rpm, followed by 10rpm and 25rpm as expected. It is important to note that Arvia et al.'s[13] equation is more relevant for turbulent flow than for laminar flow with 2-3 vortexes, the flow regime in this thesis, and for temperatures from 16°C to 37°C. Therefore the discrepancy between the experimental and calculated values at 65°C in Table 3-20 is less significant.

3.2.4 Effect of Fluid Flow on Surface Roughness of Electrowon Copper

Preliminary tests were conducted to evaluate the rotating cylinder electrode by comparing results produced with those of Ilgar and O'Keefe[6] since the electrolyte compositions used in both works are similar as shown in Table 3-6. Minor differences between both electrolyte compositions occur in the sulfuric acid and chloride ions concentrations. This electrolyte composition for this thesis closely resembles that used in commercial practice. The number of coulombs per square centimetre applied in this testwork also closely replicates Ilgar and O'Keefe[6] data. The electrolyte composition shown in Table 3-6 was used throughout the testwork for this thesis.

Table 3-6: Electrolyte Composition and Other Variables

	This work	Ilgar and O'Keefe[6]
Copper, g/L	36	36
Sulfuric acid, g/L	160	150
Chloride ions, mg/L	25	20
Active cathode surface area, cm^2	27.91	12
Electrolyte volume per test, L	3.75	0.2
Inter-electrode distance, mm	40	30

Ilgar and O'Keefe[6] used this electrolyte composition to study the effect of chloride ions on the copper cathode surface roughness.

3.2.5 Experimental Results

Table 3-7 presents the results of the effect of the RCE rotation rate on surface roughness and these results are compared with those obtained by Ilgar and O'Keefe[6] in the absence of organic additives. The diffusion layer thickness reported in Table 3-7 was derived from Figure 3-20 above.

It can be seen in Table 3-7 that the measurement of average surface roughness obtained in this testwork is consistent with those results obtained with Ilgar and O'Keefe[6] given the differences in experimental design, temperature and electrolyte

composition. The effect of the minor differences in the electrolyte composition, the number of Coulombs applied and temperature are difficult to assess independently. The δ of 175μm at 30°C and 40°C for natural convection reported by Ilgar and O'Keefe[6] shown in Table 3-7 is about twice higher than the δ of 97μm at 45°C and 115μm at 65°C δ obtained at 0rpm (natural convection) for this thesis, shown in Table 3-5. However, these experimental δ values obtained for natural convection in this thesis more closely agrees with Drews et al.[17] who conducted Monte Carlo simulation using 78μm[4] for natural convection at 25°C. The δ presented in this thesis is below the average between δ values presented by Ilgar and O'Keefe[6] and Drews et al[17]. It could be therefore assumed that δ values determined in this thesis for 10 and 25 rpm agree with the above references.

Table 3-7: Effect of Diffusion Layer Thickness on Surface Roughness

	Ilgar and O'Keefe[6]		This study	
Electrowinning Cell Type	Parallel Plate Electrode		RCE	RCE
RCE rpm			25	10
Reynolds Number			225	90
Diffusion L. Thickness, μm	65	175*	88	94
Electrowinning Time, Hrs	5.5 or 4	5.5 or 4	4	4
Current Density, mA/cm^2	25 and 35	25 and 35	30	30
Temperature, °C	30 and 40	30 and 40	50	50
Coulombs, C/cm^2	500	500	434	434
Number of Fine Needles	N.A.**	N.A.**	None	50
Surface Roughness, Ra, μm	3.9±0.50	6.4-12.5±0.50	4.31±0.16	5.51±0.41

*Natural convection; **Not reported

The δ value of 65μm reported by Ilgar and O'Keefe[6] for highly stirred solutions agrees with the δ value of 94μm at 25rpm obtained *experimentally* in this thesis. The surface roughness reported by Ilgar and O'Keefe[6] accords with those measured in this thesis. Accordingly, it was possible to compare the results obtained in this thesis on the RCE with those of Ilgar and O'Keefe[6] on a parallel plate electrode assembly.

3.3 Effect of Polyacrylamide Preparation Media on Surface Roughness of Electrowon Copper

3.3.1 Introduction

It will be recalled that Mt. Gordon produced unusually smooth copper deposits and that it was suggested that it was caused by the presence of adventitious PAM. Therefore, the effect of polyacrylamide preparation in both mild alkaline and acidic solutions on the copper deposit surface roughness obtained from electrowinning tests was evaluated in the following Sections. It also compares the new additive derived from polyacrylamide with polyacrylic acid.

3.3.2 Experimental Conditions

Since PAM is known to undergo both acid and alkaline hydrolysis discussed in Section 2.6.2, a set of experiments were undertaken in which the acidity or alkalinity of PAM solution were systematically varied to see any difference in the surface roughness of copper electrowon under controlled conditions.

The preparation media for acid solutions was conducted by systematically halving the 160 g/L sulfuric acid concentration in the electrolyte. Therefore, polyacrylamide was prepared in full-strength electrolyte (160), 80, 40, 20 and 10 g/L sulfuric acid. The initial copper (36g/L) and chloride ions (25mg/L) concentrations were also halved in the same manner giving 2.25g/L and 1.56 mg/L, respectively in the last dilution. Polyacrylamide was also prepared in distilled water.

The polyacrylamide was also prepared in mildly alkaline aqueous solution. A maximum pH value of 8.5 was selected due to the impracticality of adding additional sodium hydroxide to the electrolyte of a commercial plant. At higher pH values than 8.5, sodium sulfate may unnecessarily increase the total sulfate ions in the electrolyte for copper electrorefining and therefore promote anode passivation. It can be seen in

Table 3-8 that polyacrylamide was prepared at pH value of 8.5 for Tests 1 and 2 at 50^{o}C and, for 3 and 2 hours, respectively.

The polyacrylamide (PAM) used was a high-molecular weight PAM i.e., 15 million Dalton Ciba Magnafloc® 800HP known as neutral or non-ionic PAM throughout this thesis. PAM was prepared in a 150mL glass long-necked beaker where 100mg PAM was weighed and then 100mL solution media added. This beaker sat in a thermostated water bath at 50^{o}C. Gentle stirring was applied through a 6cm height x 1.5cm diameter Teflon rod cut in a cross at one end to simulate an impeller. A 6mm diameter stainless steel shaft was inserted at the other end of the Teflon rod and to the stirrer. Therefore, the concentration of PAM in the preparation media was 1mg/mL. An Eppendorf pipette was used to dose 3.75mL of the polyacrylamide solution in 3.75L of electrolyte held at constant temperature in another water bath to achieve a final concentration of 1mg/L. The polyacrylamide once prepared was named "activated polyacrylamide" (APAM).

3.4 Experimental Results on the Effect of Polyacrylamide Preparation Media on Surface Roughness of Electrowon Copper

The experiments were designed to detect the effect of hydrolysis of polyacrylamide on the surface roughness of electrowon copper. Therefore, these experiments indirectly evaluate the adsorption of the hydrolysed polyacrylamide onto the stainless steel substrate and copper metal during the electrodeposition process. Some tests were replicated 2, 3 or 4 times to assess the hydrolysis conditions presented in the literature and thus to validate the results of this study.

Table 3-8 presents the summary of the experimental conditions and results. The one-way ANOVA between groups was analysed using SPSS software (version 11, 2003). Figure 3-21 shows the error bar plot of the surface roughness of the copper deposits produced as a function of preparation media. The error bars show the 95% confidence interval (CI). Since 8 replicate measurements of each test sample were collected, the number of replicate tests can be determined by dividing N (at the bottom of the graph) by 8. Thus it can be seen that the electrowinning test with PAM prepared

in water (Test 3) was repeated three times and in full-strength electrolyte two times (Test 8) and in 4-fold diluted electrolyte (Test 6) two times.

Despite the variety of mechanisms that are proposed for the smoothening effect of additives[18], a consensus exists that adsorption of the additive on the substrate plays the determining role[19, 20]. It can then be inferred from the above results that the type of copolymer, random or block copolymer, degree of PAM hydrolysis and its molecular weight have a strong effect on adsorption on stainless steel and copper metal and therefore on surface roughness of the copper deposits.

Table 3-8: Effect of Polyacrylamide Preparation Media on Surface Roughness

Test No.	1	2	3	4	5	6	7	8
Sulfuric Acid Conc., g/L	alkaline		Water	10	20	40	80	160
No. of Replicates	1	1	3	4	1	2	1	2
pH Preparation Media	8.5	8.5	6	1.5	1.25	1.14	1	<1
APAM Preparation Temp., ^{o}C	50	50	25	50	50	50	50	50
APAM Preparation Time, Hrs	3	2	2	2	2	2	2	2
EW PAM/APAM Conc. mg/L	1	1	1	1	1	1	1	1
Electrowinning Time, Hrs	6	6	6	6	6	6	6	6
Electrode Voltage Drop, V	1.46	1.42	1.45	1.35	1.4	1.38	1.36	1.33
Current Density, mA/cm^2	30	30	30	30	30	30	30	30
Electrolyte Temperature, ^{o}C	50	50	50	50	50	50	50	50
RCE rpm	10	10	10	10	10	10	10	10
Surface Roughness, Ra µm	8.47	7.03	7.09	6.59	7.11	7.09	7.29	7.32
Ra Standard Deviation, µm	0.93	0.43	0.44	0.47	0.41	0.85	0.49	0.61
Test4 One-Way ANOVA Sig.*	0.00	0.54	0.04		0.32	0.11	0.06	0.00
Dendrites<0.1mm length	10	Nil	Nil	Nil	Nil	Nil	Nil	Nil
S. Steel spots<1x1mm	Nil	Nil	Nil	Nil	Nil	1	Nil	Nil

*One- way ANOVA significance for Test 4, Tuckey, HSD.

The APAM used in Test 4 was prepared with 16-fold diluted electrolyte (sulfuric acid, 10 g/L or pH 1.5; copper, 2.25g/L) and produced a surface with a significantly lower roughness (6.59 ± 0.47 µm) than PAM prepared in water, full-strength electrolyte and alkaline hydrolysis (3hours preparation time). In Table 3-8, the significance of the difference in surface roughness between each test and Test 4 is

presented. In acid solutions, the significantly different mean surface roughness sequentially increase as the concentration of sulfuric acid increases indicating the true effect of acid concentration on the hydrolysis of polyacrylamide.

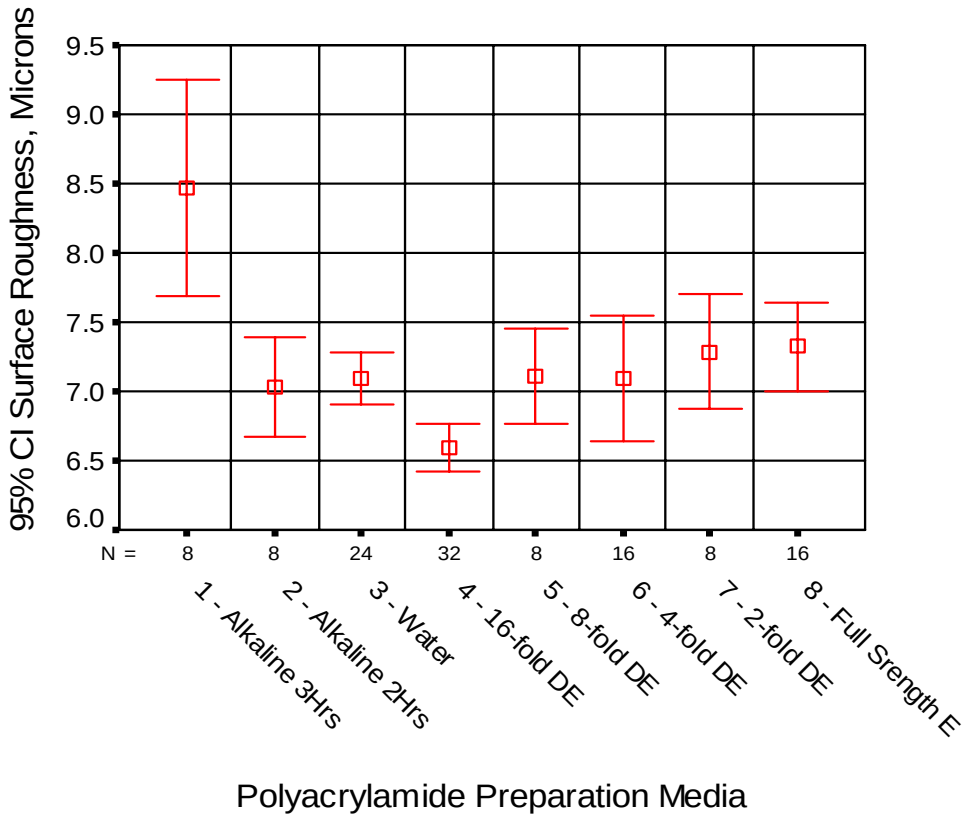

Figure 3-21: Error bar plot of the effect of preparation media on surface roughness of the copper deposits.

The average sequence length obtained from sequential mild alkaline hydrolysis followed by acid hydrolysis at pH 2 for 24 hours at 110^{o}C was 14[21] and this structure is known as a block copolymer. This suggest that PAM prepared for test 4 at a pH value of 1.5 also undergoes hydrolysis to form a block copolymer and cleavage in the backbone and therefore its 15million Dalton molecular weight was possibly also reduced due to the initial and fast acid hydrolysis reaction of PAM discussed in Section 3.2.1.2.

Grchev et al.[22] showed that surface coverage of 2-3mg/L polyacrylamide concentration in 0.5M sulfuric acid on gold and mild steel decreased from about 0.52 to 0.02 as the polyacrylamide molecular weight increased from 5x10^{3} to 1.5x10^{6} in the

temperature range from 20 to 80°C[22]. Because APAM preparation media influences surface roughness, it can be assumed that cleavage of the APAM backbone can occur and therefore the MW of APAM varies depending on the ageing of APAM in the electrolyte. Thus, the findings obtained from Test 4 can agree with the work of Grchev et al.[22]

The adsorption of polyacrylamide on gold and mild steel were explained in terms of substitutional absorption of the polymer on a bare metal surface followed by a significant desorption of water molecules from the surface[22]. Since surface roughness is directly related to adsorption, it is assumed that APAM prepared for Test 4 confers the highest adsorption.

Test 1 in which PAM was prepared at pH value of 8.5 at 50°C for 3 hours produced the highest surface roughness (8.47 ± 0.93 μm) compared with any test. Test 2 in which PAM was prepared at the same pH at 50°C for 2 hours gave a surface roughness of 7.03 ± 0.43 μm. It appears that under alkaline conditions surface roughness increases as PAM hydrolysis increases.

It was reported by Atkins[23] that at 50°C and 3 hours residence time the conversion of PAM into polyacrylic acid in alkaline solution was 61% while at 2 hours, this conversion was 31%. Surface roughness from hydrolysis of PAM in mildly alkaline solutions was the highest possibly due to the fast kinetics of polyacrylamide alkaline hydrolysis which suggests neighbouring-group catalysis superimposed on a general electrostatic effect[21, 24, 25]. These studies suggest that the rate constants for attack of an hydroxyl ion, OH^- at a polymer amide group with zero, one or two nearest-neighbour carboxylate groups exhibit relative rate constants $k_o > k_1, k_2$. Therefore, segments of acrylic acid functional groups are well distributed along the chain with an average sequence length of 1.4 from mild alkaline hydrolysis followed by strong alkaline hydrolysis[21] and this polymer structure is known as a random copolymer. Overall, the results obtained from Tests 1 and 2 from mild PAM hydrolysis are unlikely to be used in plant practice since it appears to produce a highly hydrolysed and random copolymer which is a detriment to the smoothness of the copper deposit.

In summary, it is assumed that that APAM undergoes cleavage in the backbone at 50^{o}C electrolyte temperature and block copolymers form at pH 1.5 which may also act as a small PAM molecular weight. These properties give PAM prepared for Test 4 the highest adsorption and therefore surface coverage than PAM prepared in water and full-strength electrolyte.

The polyacrylamide prepared in Test 4 is the discovery in this thesis and it is named "activated polyacrylamide" (APAM). This newly developed organic additive for copper electrowinning and possibly also for electrorefining will be compared with polyacrylic acid and Guar, the industry-standard additives, using electrowinning, Cyclic Voltammetry and Electrochemical Impedance Spectroscopy. .

3.4.1 NMR Analysis of Activated Polyacrylamide

Characterization of the activated polyacrylamide structure was determined by both ^{1}H and ^{13}C NMR spectroscopy in sulfuric acid and deuterium oxide (D_2O). All spectra were recorded on a Varian Mercury Console 300MHz spectrometer. ^{1}H spectra were obtained at 300MHz while ^{13}C spectra were obtained at 75 MHz. The NMR spectra were obtained using the polyacrylamide sample with about 15million Dalton molecular weight Ciba Magnafloc® 800HP *as received* from Mount Gordon Operations, Australia. Five wt% polyacrylamide was dissolved in 10g/L sulfuric acid and few drops of deuterium oxide (D_2O) at 50^{o}C for 2 hours in the absence of cupric ions. These conditions correspond to a solution of acid concentration similar to 16-fold diluted electrolyte (Test 4). Sonication was conducted for 30 minutes before NMR reading to obtain good quality spectra. Approximately 10^6 transients (over a weekend) were accumulated for the spectrum.

The raw data indicates that only the amide carbonyl carbon was detected in the 100-220ppm range and Figure 3-22 shows part of this section. Therefore it is suggested that carboxyl ions may be present only at relatively low concentrations, i.e., less than 10 mol %. Halverson et al.[21] and Feng et al.[26] reported ^{13}C NMR spectra for 10 mol % hydrolysed polyacrylamide and the relative intensity ratio of the amide carbonyl carbon to acid carbonyl carbon was about 6:1. This ratio decreases from about 5.25:2.3 to

3.5:2.5 for 22% and 33% hydrolysis, respectively. There must be acid carbonyl carbon present in APAM. Moreover, from the NMR spectra this is less than the instrument noise or least a 7:1 ratio. Had the acid carbonyl resonances exceeded approximately 10% of the amide carbonyl it would have been detected. The C^{13} NMR spectra presented in Figure 3-22 indicates that the proportional polyacrylamide hydrolysis must be less than 10%.

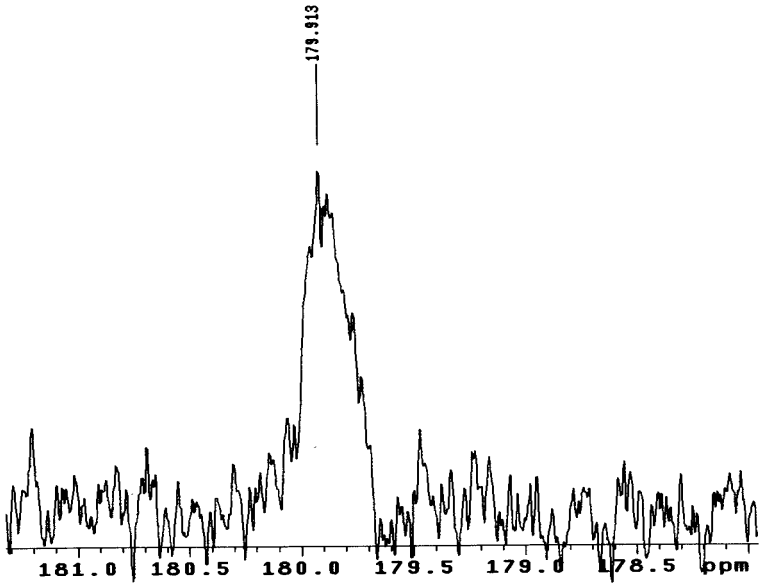

Figure 3-22: ^{13}C NMR signal intensity of activated polyacrylamide prepared in 10g/L sulfuric acid and deuterium oxide (D_2O) solutions at 50°C for 2 hours.

3.5 Effect of Activated Polyacrylamide Ageing on Surface Roughness

Tests were undertaken to determine the effect of ageing APAM in 16-fold diluted electrolyte (DE) and in full-strength electrolyte. The study in full-strength electrolyte was designed to estimate the effect of in-situ APAM hydrolysis in the electrowinning cells. Tests were also undertaken to verify the effect of ageing of APAM in 16-fold DE at room temperature for over 24 hours. This experiment was designed to determine if APAM could be stored prior to use. This test was also designed to verify whether an additional ageing in the electrolyte at 50°C following the

24-hours in 16-fold diluted electrolyte at 25°C could reduce surface roughness due to "as a matter of course" hydrolysis. Therefore, Test 1 was run with fresh APAM. Test 2 was run with APAM aged for 24 hours at 25°C in 16-fold DE. The electrolyte bath from Test 2 was maintained at 50°C for 24 hours and then Test 3 was run without adding any fresh APAM. Table 3-9 and Figure 3-23 show the results for this testwork.

Table 3-9: Effect of APAM Degradation in 16-fold DE and Full-Strength Electrolyte

Test No.	1	2	3
Number of Tests	1	1	1
pH Preparation Media	1.5	1.5	1.5
Preparation Temperature, oC	50	25	50
Residence Time in 16-fold DE, Hours	2	24	24
Residence Time in Electrolyte, Hours	0	0	24
Sulfuric Acid Concentration, g/L	10	10	10 & 160
APAM Conc. in Electrolyte, mg/L	1	1	1
Electrowinning Time, Hours	6	6	6
Electrode Voltage Drop, V	1.34	1.39	1.41
Current Density, mA/cm^2	30	30	30
Electrolyte Temp., °C	50	50	50
Diffusion Layer Thickness, µm (10rpm)	140	140	140
Surface Roughness, Ra µm	6.23	6.89	7.46
Ra Standard Dev., µm	0.41	0.68	0.86
Peaks per Centimetre	82.63	78.13	77.75
Peaks-per-Centimeter Std. Dev.	10.6	9.61	9.90
Dendrites Formation	Nil	Nil	Nil

Test 1 showed the lowest surface roughness with 2 hours prepared PAM in 16-fold diluted electrolyte followed by Test 2 with 24 hours residence time in 16-fold diluted electrolyte at 25°C. The surface roughness produced from Test 3 was the highest and indicated that an additional hydrolysis in the electrolyte at 50°C for 24 hours after 24 hours degradation in 16-fold diluted electrolyte at 25°C, increased surface roughness. Additional ageing or hydrolysis in the electrolyte increases the surface roughness possibly due to the decomposition of the active species, and/or formation of less adsorbent copolymers, such as imides.

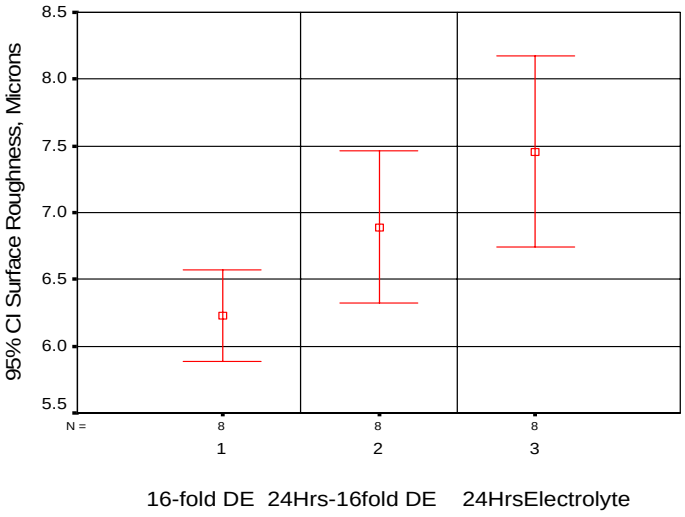

Figure 3-23: Degradation of Polyacrylamide in 16-fold Diluted Electrolyte and Full-Strength Electrolyte

Tests 1 and 2 are not statistically different indicating that APAM could be prepared for up to 24 hours without affecting significantly the surface roughness. However, based on the data shown in Figure 3-23, it may be better to prepare it every 12 or 6 hours and continuously dosed.

3.6 Comparison of Polyacrylic Acid and Activated Polyacrylamide

3.6.1 Introduction

The United States Patent 5,733,429 in the name of S. Martin and N. Nebeker[27] described the use of polyacrylic acid (repeating polymeric units having the structural formula of $-(CH_2\text{-}CH(COOX)\text{-}CH_2)_n$- wherein X=H, periodic table group 1 or group 2 element salts, an ammonium salt or mixture thereof) as an organic additive for copper electrowinning. US Patent 5,733,429 discusses the formation of dendrites or surface nodes on the cathodes and the increased potential to short-circuit the cell. The patent also claims that the use of polyacrylic acids, alone, prevent the formation of dendrites, minimizes anode flaking and prevents shorts in the circuit. The disadvantage with the process as described in US Patent 5,733,429 is that the preferred concentration of polyacrylic acid in electrolyte is between 10 and 200 mg/L. Such a high level of

dissolved organic material in electrolyte is known to cause significant carbon and hydrogen contamination of the copper cathode[28] when animal glue and thiourea are also used as additives.

Electrowinning tests were carried out to determine the comparative effectiveness of polyacrylic acid (PAA) and polyacrylamide prepared in 16-fold diluted electrolyte at 50^{o}C for 2 hours under stirring (APAM). This work was undertaken to compare the efficiency of APAM with PAA in minimizing the surface roughness of electrowon copper. The effectiveness of these organic additives in copper electrowinning was determined by directly measuring the surface roughness of the copper deposit. A high measurement of surface roughness would be indicative of a low effectiveness of the organic additive.

3.6.2 Comparison of Polyacrylic Acid and Activated Polyacrylamide in 4 Hour Electrowinning Test

Unless otherwise stated, polyacrylamide was dissolved in 16-fold diluted synthetic electrolyte (sulfuric acid, 10 g/L; copper, 2.25 g/L after dilution). PAA was prepared in a solution of sodium hydroxide at pH 11.5 at 50^{o}C of a concentration of 1000 mg/L for 2 hours.

Tests were undertaken to study the extent to which the efficacy of these two additives changed when held in full-strength electrolyte under plant conditions. Over a 12-hour test period, EW was undertaken for the first and last 4-hours. In the intermediate time (4-hours), the electrolyte temperature was kept constant at 50^{o}C. The first tests were carried out just after the 2-hours preparation at 50^{o}C at a pH 11.5 in sodium hydroxide for PAA and in 16-fold diluted electrolyte (i.e., 10 g/L H_2SO_4) for APAM. The results are presented in Table 3-10.

These experiments demonstrate that PAA consistently produced higher surface roughness than APAM. Moreover, PAA lost its efficacy at a much greater rate than APAM. It is noteworthy that APAM maintains its ability to produce smooth copper deposit over a period of at least 12-hours under conditions typical of contemporary

electrowinning and electrorefining plants. This has important practical benefits as it minimizes the dosing rate of the organic additive.

Table 3-10: Surface Roughness Using Polyacrylic Acid and Activated Polyacrylamide

	Polyacrylic Acid		**APAM**	
EW Test	0-4 Hrs	8-12 Hrs	0-4 Hrs	8-12 Hrs
Test No.	80A	80B	79A	79B
PAA/PAM Prep. Res. Time, Hrs	2	2	2	2
PAA/APAM Conc., mg/L	1	1	1	1
Electrowinning Time, Hours	4	4	4	4
Current Density, mA/cm^2	30	30	30	30
Electrolyte Temperature, ^oC	50	50	50	50
RCE rpm	10	10	10	10
Dendrite Observation	None	None	None	None
Surface Roughness, Ra, μm	5.70±0.20	7.78±1.20	5.06±0.52	5.50±0.66

3.6.3. Comparison of Polyacrylic Acid and Activated Polyacrylamide in 12-Hours Continuous Electrowinning

A continuous electrowinning test was conducted over a period of 12 hours continuous to further compare the effectiveness of APAM over PAA. A concentration of 10 mg/L was selected as described by Martin et al.[27] and for the purposes of comparison, both APAM and PAA were dosed at the same concentration. Table 3-11 summarises the results of this comparison.

Table 3-11 indicates that it was not possible to measure the surface roughness of the copper deposit produced by polyacrylic acid due to the presence of fine dendritic needles stopping the travel of the stylus tip. Qualitatively, the copper deposit produced by PAA was rougher compared to the copper deposit produced using APAM. Table 3-11 clearly shows that over 12-hours EW time, APAM is more effective at eliminating dendrite formations than polyacrylic acid.

Table 3-11: Comparison of PAA and APAM in 12 Hours Continuous EW

	Polyacrylic Acid	Activated PAM
Test No.	84	85
PAA/APAM Prep. Residence Time, Hrs	2	2
Concentration of PAA or APAM, mg/L	10	10
EW Time, Hrs	12	12
Current Density, mA/cm^2	30	30
Electrolyte Temperature, ^oC	50	50
RCE RPM	10	10
Dendrite	Numerous	None
Surface Roughness, Ra, μm	>20	10.5±1.

3.7 Discussion and Conclusions

It has been shown that the surface roughness obtained with the RCE built for this project agrees with the results obtained by Ilgar and O'Keefe[6] in the absence of organic additives.

It was therefore concluded that the use of the RCE for the testwork observed in this thesis would provide results consistent with those described in the literature. It appears that the use of surface roughness measurements to study the effect of organic additives under simulated commercial electrowinning and electrorefining conditions presented in this project thesis is the first of its kind. From this work, the following conclusions are drawn:

Despite the variety of mechanisms proposed for the smoothening effect of additives[18], a consensus exists that *adsorption* of the additive on the substrate plays the determining role[19, 20]. It is then be inferred from the results in this Chapter that the type of copolymer, random or block copolymer, degree of PAM hydrolysis and its molecular weight have a strong effect on adsorption on stainless steel and copper metal and therefore on surface roughness of the copper deposits.

It was shown that when 15 million MW polyacrylamide was prepared in 16-fold diluted electrolyte at 50^{o}C for 2-hours the surface roughness of the copper deposit was statistically lower than when PAM was either prepared in water, where hydrolysis is

insignificant, full-strength electrolyte or alkaline solution at pH 8.5 (3 hours preparation time).

Halverson et al.[21] showed that PAM dissolved at pH 2 for 24 hours at 110^{o}C was 57% hydrolysed to form a block copolymer with a polyacrylic acid sequence length of 14. In this work, NMR data suggests that polyacrylamide prepared for Test 4 at pH equal to 1.5 at 50^{o}C under stirring for 2-hours was less than 10% hydrolysed. These data are mutually consistent since the experimental hydrolysis at 110^{o}C in 24-hours would be much greater than that observed at 50^{o}C for 2-hours. It is therefore assumed that the APAM produced in this work is a block copolymer as described schematically below:

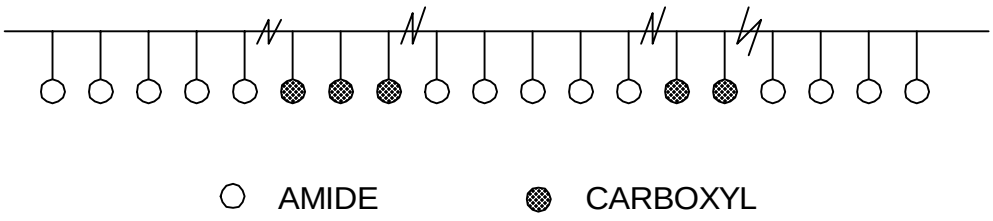

PAM prepared in water, where hydrolysis is insignificant, and in full-strength electrolyte produces similar hydrolysis reactions and products. These hydrolysis products may adsorb statistically less than the APAM possibly due to polyacrylimide formation discussed in Chapter 2.

Grchev et al.[22] showed that surface coverage of 2-3mg/L polyacrylamide concentration in 0.5M sulfuric acid on gold and mild steel decreased from about 0.52 to 0.02 as the polyacrylamide molecular weight increased from 5x103 to 1.5x106 in the temperature range from 20 to 80oC. Because APAM preparation media influences surface roughness, it can be assumed that cleavage of the APAM backbone can occur and therefore the MW of APAM varies depending on the ageing of APAM in the electrolyte. Thus, the findings obtained with APAM can agree with the work of Grchev et al.[22]

Since surface roughness is directly related to adsorption, APAM prepared in 16-fold electrolyte at 50^{o}C and under stirring for 2-hours gives the highest adsorption and

therefore surface coverage than PAM prepared in water and full-strength electrolyte. The adsorption mechanism of APAM appears to conform to partially hydrolysed block copolymer through hydrogen and covalent bonding as discussed in Chapter 2.

PAM hydrolysed in alkaline media is much less effective than 'APAM'. Therefore, based on these results and literature[21, 24, 25] the hydrolysis product in alkaline solutions is a random copolymer as schematically described below:

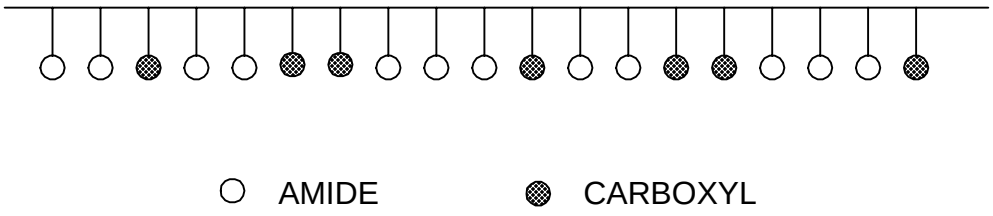

APAM is more effective at eliminating dendrite formations than polyacrylic acid up to 12 hours electrowinning. APAM can be maintained in 16-fold diluted electrolyte without significantly affecting surface roughness.

3.8 References

1. Baker DR, Verbrugge MW, Newman J. *A Transformation for the Treatment of Diffusion and Migration. Application to the Simulation of Electrodeposition onto Microelectrode Geometries*. Proceedings - Electrochemical Society 1992;92-3(Proc. Int. Symp. Electrochem. Microfabr., 1st, 1991):279-90.

2. Newman J, Thomas-Alyea KE. *Electrochemical Systems*. Third ed. Hoboken, New Jersey: John Wiley & Sons, Inc.; 2004.

3. Barkey D, Muller R, Tobias C. *Roughness Development in Metal Electrodeposition I. Experimental Results*. Journal of the Electrochemical Society 1989;138(8):2199-2207.

4. Wilke C, Eisenberg M, Tobias C. *Correlation of Limiting Currents under Free Convection Conditions*. J. Electrochem. Soc. 1953;100(11):513-523.

5. Landau U. Determination of Laminar and Turbulent Mass Transport Rates in Flow Cells by the Limiting Current Technique. In: *Lectures in Electrochemical Engineering*: The American Institute of Chemical Engineers; 1981. p. 75-87.

6. Ilgar E, O'Keefe T. Surface Roughening of Electrowon Copper in the Presence of Chloride Ions. In: Dreisinger D, editor. *Aqueous Electrotechnologies: Progress in Theory and Practice*; 1997: The Minerals Metals and Materials Society; 1997. p. 51-62.

7. Ettel V, Tilak B, AS G. *Measurement of Cathode Mass Transfer Coefficients in Electrowinning Cells*. J. Electrochem. Soc. 1974;121(7):867-872.

8. Uceda D. Determination of Mass Transfer Characteristics in the Electrolysis of Copper [PhD Thesis]. Missouri-Rolla: University Missouri-Rolla; 1988.

9. Obretenov W, Schmidt U, Lorenz W, Staikov G, Budevski E, Carnal D, Muller U, Siegenthaler H, Schmidt E. *Underpotential Deposition and Electrocrystallization of Metals*. J. Electrochem. Soc. 1993;140(3):692-703.

10. Budevski E, Staikov G, Lorenz W. *Electrochemical Phase Formation and Growth, an Introduction to the Initial Stages of Metal Deposition*. New York: VCH; 1996.

11. Schmidt W. In Situ Studies of Copper Electrodeposition in the Presence of Organic Additives Using Atomic Force Microscopy [PhD]. Urbana-Champaign: University of Illinois; 1996.

12. Eisenberg M, Tobias C, Wilke C. *Ionic Mass Transfer and Concentration Polarization at Rotating Electrodes*. Journal of the Electrochemical Society 1954;101(6):306-319.

13. Arvia AJ, Carrozza JSW. *Mass Transfer in the Electrolysis of Cuso4-H2so4 in Aqueous Solutions under Limiting Current and Forced Convection Employing a Cylindrical Cell with Rotating Electrodes*. Electrochimica Acta 1962;7:65-78.

14. Manzanares JA, Kontturi K. Diffusion and Migration. In: Calvo EJ, editor. *Interfacial Kinetics and Mass Transport*: Wiley-VCH; 2003. p. 81-121.

15. Price D, Davenport W. *Physico-Chemical Properties of Copper Electrorefining and Electrowinning Electrolytes*. Metallurgical & Materials Transactions B-Process Metallurgy & Materials Processing Science 1981;12B:639-643.

16. Dutra A, O'Keefe T. *Copper Nucleation on Titanium for Thin Film Applications*. Journal of Applied Electrochemistry 1999;29:1217-1227.

17. Drews T, Ganley J, Alkire R. *Evolution of Surface Roughness During Copper Electrodepositon in the Presence of Additives*. J. Electrochem. Soc. 2003;150(5):C325-C334.

18. Onicio L, Muresan L. *Some Fundamental Aspects of Levelling and Brightening in Metal Electrodeposition*. Journal of Applied Electrochemistry 1991;21:565-574.

19. Jordan K, Tobias C. *The Effect of Inhibitor Transport on Leveling in Electrodeposition*. J. Electrochem. Soc. 1991;138(5):1251-1259.

20. Chung D. Localized Adsorption of Organic Additives During Copper Electrodeposition [Ph.D.]. Urbana-Champaign: University of Illinois; 1996.

21. Halverson F, Lancaster J, O'Connor M. *Sequence Distribution of Carboxyl Groups in Hydrolyzed Polyacrylamide*. Macromolecules 1985;18(6):1139-44.

22. Grchev T, Cvetkovska M, Stafilov T, Schultze J. *Adsorption of Polyacrylamide on Gold and Iron from Acidic Aqueous Solutions*. Electrochimica Acta 1991;36(8):1315-1323.

23. Atkins M, Biggin I, Kidd D; inventors. BP Chemicals Limited, assignee. Hydrolysis of Polymers. United States patent 5,081,195. 1992 January 14, 1992.

24. Panzer H, Halverson F, Lancaster J. *Carboxyl Sequence Distribution in Hydrolyzed Polyacrylamide*. Polymeric Materials Science and Engineering 1984;51:268-71.

25. Panzer H, Halverson F. Blockiness in Hydrolyzed Polyacrylamide. In: Moudgil B, Scheiner B, editors. *Flocculation Dewatering, Proc. Eng. Found. Conf.*; 1988; Palm Coast Florida, USA; 1988. p. 239-49.

26. Feng Y, Billon L, Grassl B, Khoukh A, Francois J. *Hydrophobically Associating Polyacrylamides and Their Partially Hydrolyzed Derivatives Prepared by Post-*

Modification. 1. Synthesis and Characterization. Polymer 2002;43(7):2055-2064.

27. Martin S, Nebeker N; inventors. Enthone-OMI, Inc, assignee. Polyacrylic Acid Additives for Copper Electrorefining and Electrowinning. United States patent 5,733,429. 1998.

28. Chia D, Patel G. *Copper Rod and Cathode Quality as Affected by Hydrogen and Organic Additives*. Wire Journal International 1992(Nov.):67-75.

CHAPTER 4

EXPERIMENTAL DESIGNS FOR COPPER ELECTROWINNING

4.1. Introduction

It has been shown that polyacrylamide prepared in 16-fold diluted electrolyte at 50^{o}C for 2-hours under stirring has a statistically significantly lower mean surface roughness than either polyacrylamide prepared in water or in full-strength electrolyte. It also produced lower surface roughness than polyacrylic acid. This result may be interpreted to mean that this method of preparation results in a higher surface coverage of the copper metal and stainless steel substrates than the preparation media in water and full-strength electrolyte. It is widely recognised in the literature that surface coverage of an organic additive in metals electrodeposition and corrosion is directly related to its adsorption onto the substrate[1, 2].

In the work described in this Chapter, the following studies were conducted to evaluate Guar and APAM. The electrowinning time was the most important variable to follow on the evaluation of both additives.

(i) Two fractional factorial experimental designs were devised to evaluate whether Guar, the industry-standard additive for copper electrowinning, or APAM act independently or perform the same role as levelling agent.

(ii) The role of Guar and APAM was studied using an extended ratio of Guar to APAM concentrations in a 2^2 experimental design to determine whether an optimum concentration ratio exists to effectively reduce surface roughness.

(iii) Guar and APAM were directly compared in a Guar or APAM 2^2 experimental design to evaluate their effectiveness on the surface roughness of the copper deposit at 4.64, 6 and 12 Hours EW time.

The variables in commercial copper electrowinning and electrorefining are the flow rate of the feed electrolyte into the electrolytic cells, electrolyte temperature, current density, and copper, sulphuric acid, chloride ions and fresh organic additive(s) concentrations. An increment of the electrolyte flow rate into the electrolytic cell also increases the velocity of the bulk electrolyte closest to the cathode and therefore may also decrease the value of the diffusion layer thickness. The experimental designs selected for this work use high and low levels of these variables, including Guar and APAM to closely replicate the industry-standard operating conditions of commercial copper electrowinning. Fractional factorial experimental designs are a variation of a basic factorial design in which only a subset of the runs are made to minimize the number of experiments but include all the process variables[3].

The two fractional factorial experimental designs have low and high temperature levels of 45^{o}C and 55^{o}C and, 45^{o}C and 64^{o}C to evaluate APAM at electrolyte temperatures similar to commercial copper electrowinning and electrorefining conditions.

4.2 Experimental Conditions

Table 4-12 shows the electrolyte conditions and the preparation media for polyacrylamide described in Section 3.3. APAM was prepared in 16-fold diluted electrolyte at 50^{o}C for 2 hours under stirring conditions. The evaluation of Guar and APAM was carried out using the rotating cylinder electrode described also in Section 2.3.

The Guar concentration used at Mt. Gordon was approximately 0.52mg/L electrolyte at the new tankhouse or 175 grams Guar/tonne copper cathode. This concentration was used as the low level factor in the experimental design and the high level was set at 1mg/L electrolyte. Guar was prepared in water at room temperature as per commercial operation and under similar stirring conditions described for APAM. Guar was dosed *twice* throughout the testwork. The first dose was added at the beginning and the second at one at approximately half EW time (2hours 10minutes or 2hours 21minutes) depending on the current density. The total electrowinning time was 4hrs 21 minutes at a current density of 320A/m^2 and 4hrs 58 minutes at 280A/m^2.

Table 4-12: Electrolyte Composition and Additives Preparation Media

Copper, g/L	36
Sulphuric Acid, g/L	160
Chloride Ions, mg/L	25
PAM Preparation Media – 16 fold Diluted Electrolyte, Temp. ^oC	50
Guar Preparation Media, water, Temperature, ^oC	25
Number of Coulombs per cm^2	500

The organic additives, once dosed to the electrolyte, were subjected to 15 minutes mixing at 40 rpm and 5 minutes at the rpm value to be evaluated (10, 17.5 or 25) before the application of the desired current to the electrolytic cell. Therefore the total residence time of the organic additives in the electrolyte was *20 minutes* in addition to the electrowinning times at 45^{o}C, 50^{o}C or 65^{o}C ± 0.5^{o}C. APAM was dosed *once* during this testwork. Figure 4-24 shows the rotating cylinder electrode in operation.

The surface roughness was collected using a Mahr Perthometer M1[4] with a 2μm stylus tip radius. A detailed description about this measurement was given in Section 3.2.1. The surface roughness evaluation includes analysis of variance (ANOVA) and statistical inference procedures using Design-Expert® software (Stat-Ease, Version 6.0.10, 2003)[5]. The adequacy of the models was checked using residual analysis as described by Montgomery[3].

The cross-section of the copper deposits was prepared for Scanning Electron Microscopy (SEM). The samples were embedded in an epoxy resin and the cross-

section cut with 600 grit silicon carbide powder on a round table. It was then sequentially polished with 3, 1 and 0.25µm diamond paste from Struers. It was finally etched with a solution of 5 g of ferric chloride and 5mL hydrochloric acid in 90mL ethanol for 20-25 seconds.

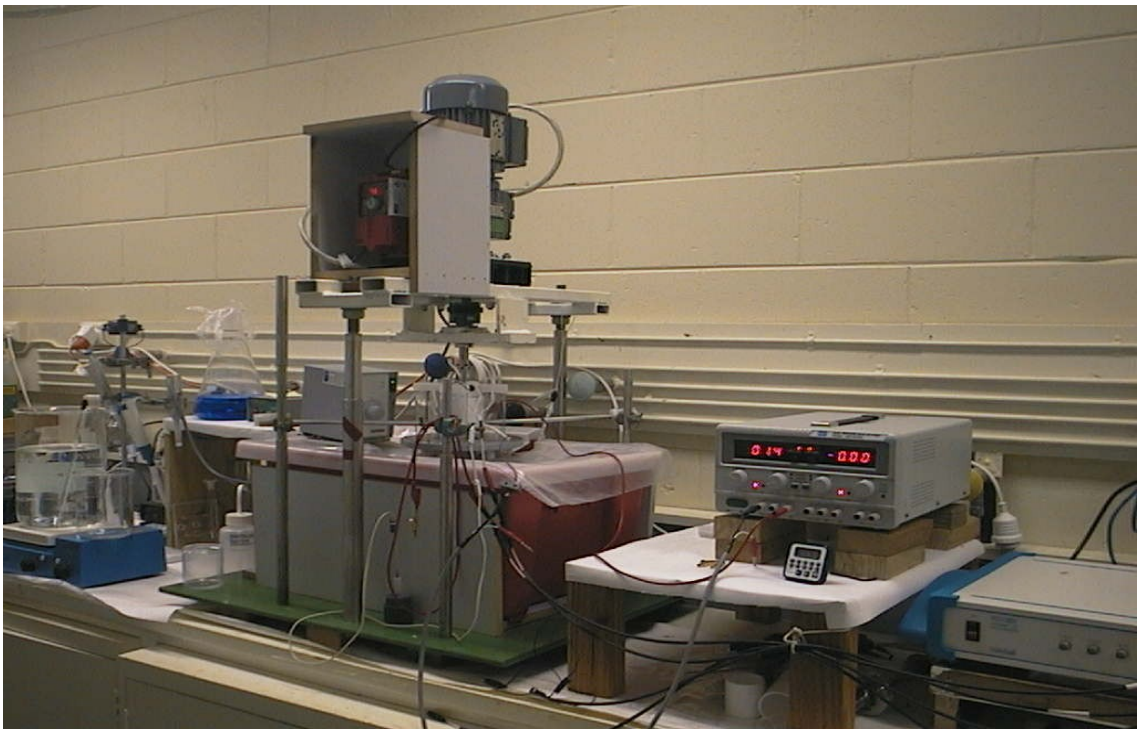

Figure 4-24: Rotating Cylinder Electrode Equipment

4.2.1 Copper Electrowinning and the Effect of its Main Operating Variables

Table 4-13 shows the two 2^{5-2} fractional factorial experimental designs. The factors at low level are common for both designs. The factors at high level differ in temperature only. The values of the limiting current density and diffusion layer thickness were derived using the equation developed by Arvia et al.[6] and Fick[7], respectively, using Mathcad 12[8] as described in Chapter 3 – Section 3.2.3. It should be noted that variations in temperature affect the diffusion layer thickness are linked through the Schmidt number (ν/D).

Table 4-13: Two 2^{5-2} Fractional Factorial Experimental Designs

Factors		Factor Level		
		Low	High	
A	T (Temperature, ^{o}C)	45	55	65
B	i (Current Density, A.m^{-2})	280	320	320
C	L (Guar, mg/L)	0.5	1	1
D	S (APAM, mg/L)	0.5	1	1
E	δ (Diffusion Layer Thickness, μm)	87 (25rpm)	108 (10rpm)	110 (10rpm)

4.3 Experimental Results

4.3.1 2^{5-2} Experimental Design Results at 45^{o}C - 55^{o}C

Table 4-14 presents the results indicating the effect of temperature (A), current density (B), Guar concentration (C), APAM concentration (D) and diffusion layer thickness (E) on surface roughness.

The regression model obtained from this testwork is shown in Equation 4-19. An F-value of 9.41 implies that the model is significant. There is only a 0.01% chance that the model F-value this large could occur due to noise. If the "Prob > F value" (α) is very small (less than 0.05), then the terms in the model have a significant effect on the response[3, 5].

Surface Roughness (μm) =

$$+6.26+0.27*B-0.053*C-0.056*D+0.25*E-0.62*B*C-0.38*B*E \quad (4\text{-}19)$$

It can be seen that the surface roughness is strongly influenced by an increment of the current density B, (α=0.0180) and diffusion layer thickness E, (α=0.0247). In addition, it is evident that there are two strong interacting terms involving B*C (Current Density*Guar, α<0.0001) and B*E (Current Density*Diffusion Layer Thickness, α=0.0009) which decreases the surface roughness. APAM (D, α=0.6098) and Guar (C, α=0.6316) have an insignificant effect on reducing surface roughness in this temperature range. The regression analysis also indicates that APAM and Guar are not

aliased -that is no C*D term appears in Equation 4-19, APAM appears to act independent of Guar[3].

Figure 4-25 shows the effect of the aliased and significant variables Current Density and Diffusion Layer Thickness on surface roughness. It clearly indicates that at high rotational speed of the cylinder and low current density the smoothest surface roughness is achieved.

Table 4-14: 2^{5-2} Fractional Factorial Experimental Results–Temperature Levels 45°C-55°C

	A	B	C	D=A*B#	E=A*C#	Mean Surface	Std.
Run	Temp.,	C.Density	Guar	APAM	DLayerT	Roughness	Dev.
Std	°C	mA/cm^2	mg/L	mg/L	µm	Ra, µm	
1	45	28	0.50	1.00	108	5.95	0.47
2	55	28	0.50	0.50	87	4.90	0.42
3	45	32	0.50	0.50	108	7.08	1.38
4	55	32	0.50	1.00	87	7.33	1.09
5	45	28	1.00	1.00	87	5.83	0.72
6	55	28	1.00	0.50	108	7.31	1.08
7	45	32	1.00	0.50	87	5.99	0.66
8	55	32	1.00	1.00	108	5.71	0.68
CP	50	30	0.75	0.75	97.50	7.04	0.93

#Level of factors D and E were determined by the levels of A*B and A*C, respectively.

Figure 4-26 shows the effect of the aliased and significant variables Current Density and Guar on surface roughness. It can be seen that increasing Guar concentration *increases* surface roughness at lower current densities than about 300A/m^2, a surprising result for an organic additive dosed to control dendrite formation. Moreover, it indicates that the surface roughness increases more steeply with an increment of the current density than with the increment of Guar concentration.

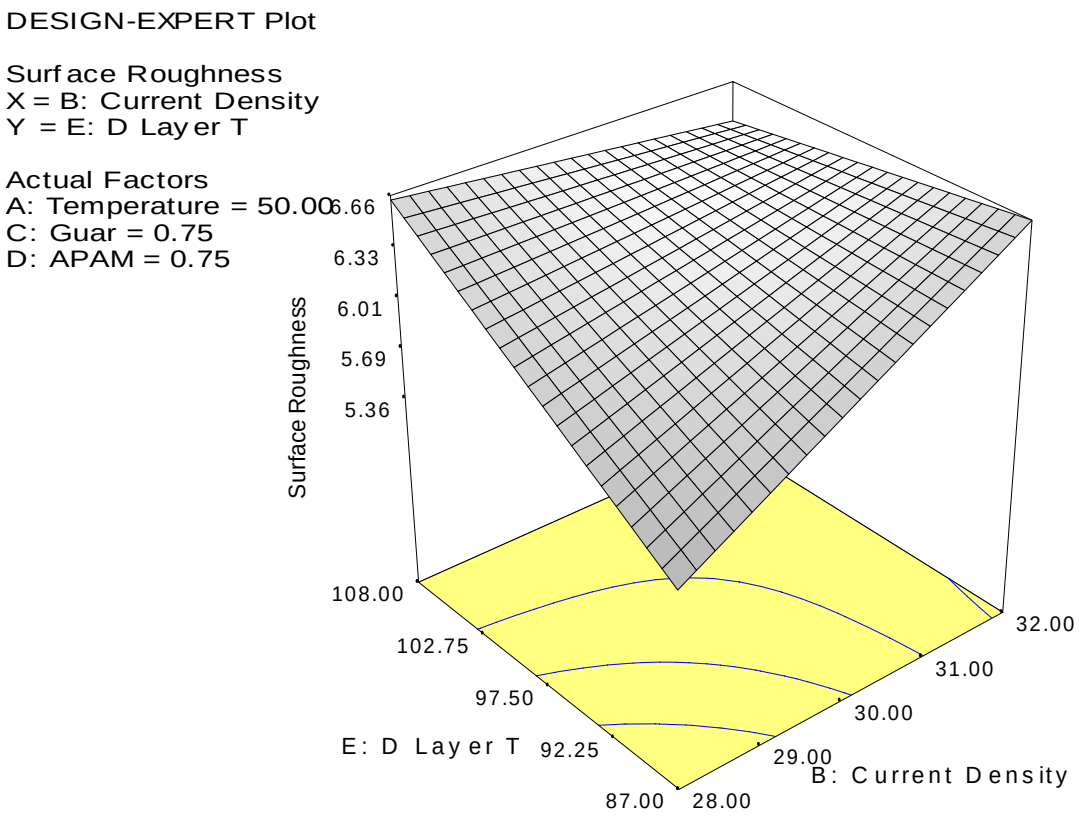

Figure 4-25: Effect of Diffusion Layer Thickness and Current Density on Surface Roughness

A: Temperature, ^{o}C; B: Current Density, mA/cm^2; C: Guar, mg/L; D: APAM, mg/L; E: D Layer Thickness, µm and Surface Roughness, µm

The adequacy of the model was tested graphically as shown in Figures 4-27, 4-28 and 4-29. An adequate model should show an almost straight line around the central values of the plot in Fig. 4-27, should show virtually all points in Figs. 4-28 and 4-29 within ± 3, and Fig. 4-29 should show a random distribution of the residual points[3, 5]. Based on these Figures, it is concluded that the model was adequate.

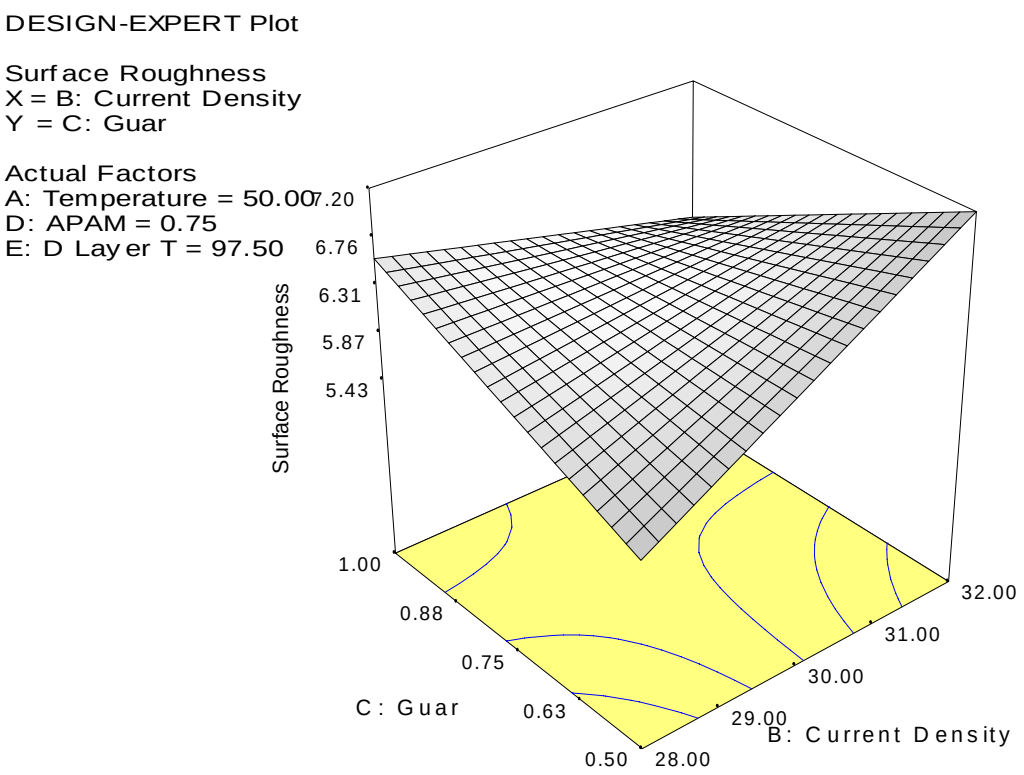

Figure 4-26: Effect of Current Density and Guar on Surface Roughness

A: Temperature, ^{o}C; B: Current Density, mA/cm^2; C: Guar, mg/L; D: APAM, mg/L; E: D Layer Thickness, µm and Surface Roughness, µm

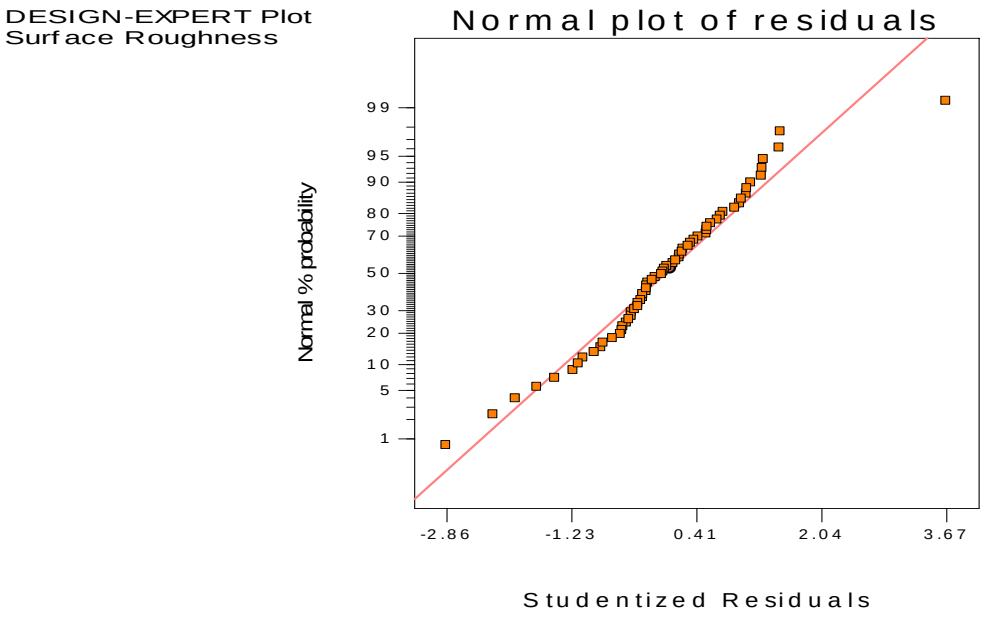

Figure 4- 27: Studentized Residuals Plot

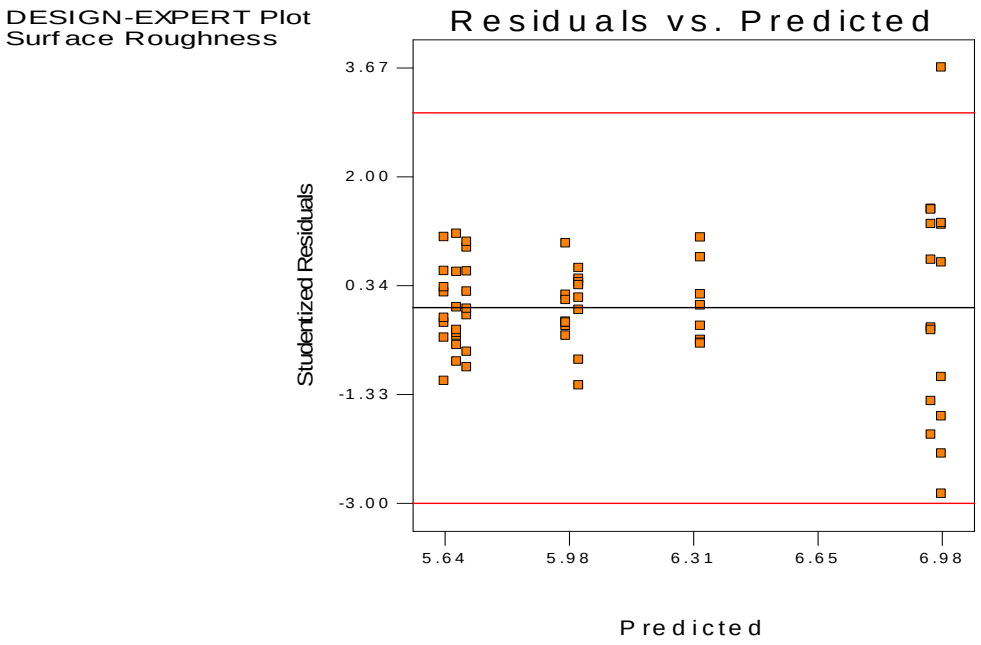

Figure 4-28: Residuals vs. Predicted Plot

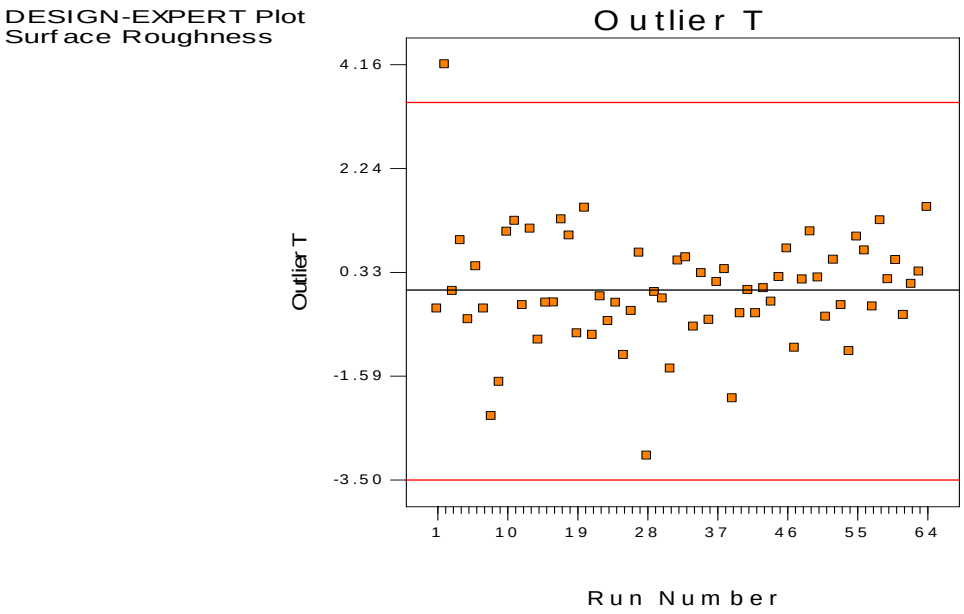

Figure 4-29: Outlier T Diagnostic Plot

The effect of APAM was insignificant in this temperature range possibly due to the kinetics of its ageing in the electrolyte. The rationale for this conclusion is as

follows. Cyclic Voltammetry tests indicate (Chapter 5 – Sections 5.4 and 5.5) that at 45°C, a maximum polarization of APAM was obtained at about 3 hours residence time in the electrolyte and at 65°C it was obtained at about 1hour residence time. EIS tests (Sections 5.7 and 5.9) at 45°C also indicates that the charge-transfer resistance steadily increases up 3-5 hours but at 65°C (Section 5.10) it sharply increases up to 2 hours then it decreases. It is therefore inferred that the first 2-3 hours of the EW tests at this temperature range (45°C - 55°C) carried out for 4.35 and 4.97 hours (14,000 Coulombs) took place under suboptimal adsorption conditions of APAM.

4.3.2 2^{5-2} Experimental Design Results at 45°C - 65°C

As before, it is noted that Guar was dosed *twice* in this testwork and APAM was prepared in 16-fold diluted electrolyte at 50°C for 2 hours and dosed once. Table 4-15 presents the results for this experimental design.

Table 4-15: 2^{5-2} Fractional Factorial Experimental Results–Temperature Levels 45°C-65°C

	A	B	C	D=A*B	E=A*C	Mean Surface	
Run	Temp.,	C. Density	Guar	PAM	D Layer T	Roughness,	Std.
Std	°C	mA/cm^2	mg/L	mg/L	µm	Ra, µm	Dev.
1	45	28	0.50	1.00	110	5.95	0.47
2	65	28	0.50	0.50	87	6.36	0.64
3	45	32	0.50	0.50	110	7.08	1.38
4	65	32	0.50	1.00	87	5.56	0.67
5	45	28	1.00	1.00	87	5.83	0.72
6	65	28	1.00	0.50	110	6.86	2.28
7	45	32	1.00	0.50	87	5.99	0.66
8	65	32	1.00	1.00	110	5.66	0.69

The model obtained from this testwork is shown in Equation 4-20. An F-value of 2.06 implies that the model is significant. There is a 6.30% chance that the model F-value this large could occur due to noise.

Surface Roughness (µm) =

$$+6.16-0.051*A-0.089*B-0.075*C-0.41*D+0.23*E-0.17*B*C \quad (4\text{-}20)$$

It can be seen from this model that APAM D, (α=0.0041) has the most significant effect on reducing surface roughness. Diffusion layer thickness E, (α=0.1004) has the next largest effect and it increases surface roughness as expected. The effect of current density (B) and Guar (C) are insignificant (B*C, α=0.2185). Current Density B (α=0.5192), Guar C, (α=0.5855) and Temperature A, (α=0.7129) are also insignificant. The model term temperature (A) was included in the above model for completeness only; otherwise there is only 4.04% chance that the model F-value of 2.38 could occur due to noise and the probability value, α for the other model terms decrease very slightly. The regression analysis also indicates again that APAM and Guar are not aliased, APAM appears to act truly independent of Guar to reduce surface roughness[3].

The model adequacy indicated the absence of abnormalities using the graphical tests as shown previously in Section 5.3.1. Figure 4-30 shows the significant effect of APAM on surface roughness.

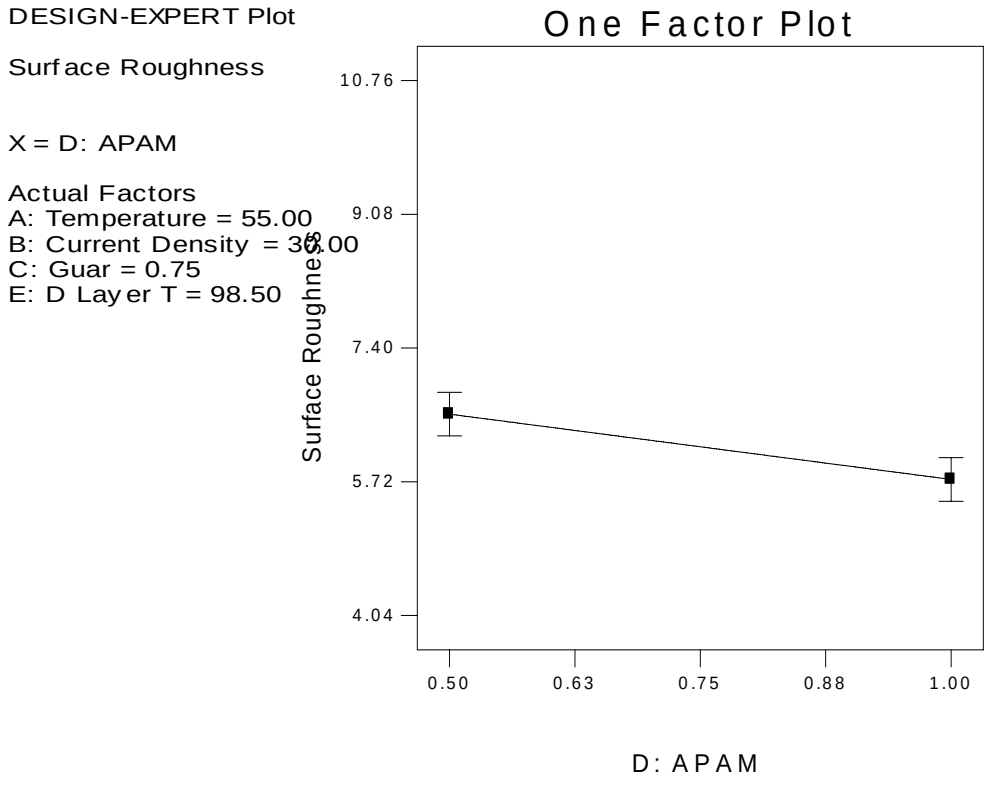

Figure 4-30: Significant Effect of APAM Concentration on Surface Roughness

It can be seen that the interaction significance of current density (B)*Guar(C) decreases from <0.0001 in the first model at 45°C-55°C to 0.2185 in the second model at 45°C-65°C. This reduction indicates that the second model is not significantly confounded in contrast to the first model. This difference is probably due to the faster degradation of Guar at 65°C than at 45°C at the same current density. This degradation process is probably true for APAM as well but if cleavage of the polyacrylamide backbone had taken place, it enhanced the reduction of surface roughness. This finding correlates with Grchev et al's.[9-11] studies on the adsorption of polyacrylamide on gold and mild steel in strong acidified solutions as follows: polyacrylamide with lower molecular weight confers higher surface coverage than polyacrylamide with high molecular weight.

4.3.3 Scanning Electron Microscopy of Electrowon Copper Deposits

Figure 4-31 – 4-38 show the Scanning Electron Micrographs (SEM) of the cross sections of the copper cathodes obtained in this test work and indicate the presence of columnar growth with small column widths of approximately 3 microns. Figure 4-32 from Run 2 at 65°C, 28mA/cm^2 current density, 0.5mg/L Guar, 0.5mg/L APAM and 87μm δ indicates the presence of voids as well as the columnar growth. Figure 4-33 from Run 3 at 45°C, 32mA/cm^2 current density, 0.5mg/L Guar, 0.5mg/L APAM and 110μm δ appears also to present some voids but its higher current density compared with Run 2 may have assisted the formation of greater number of nucleation sites.

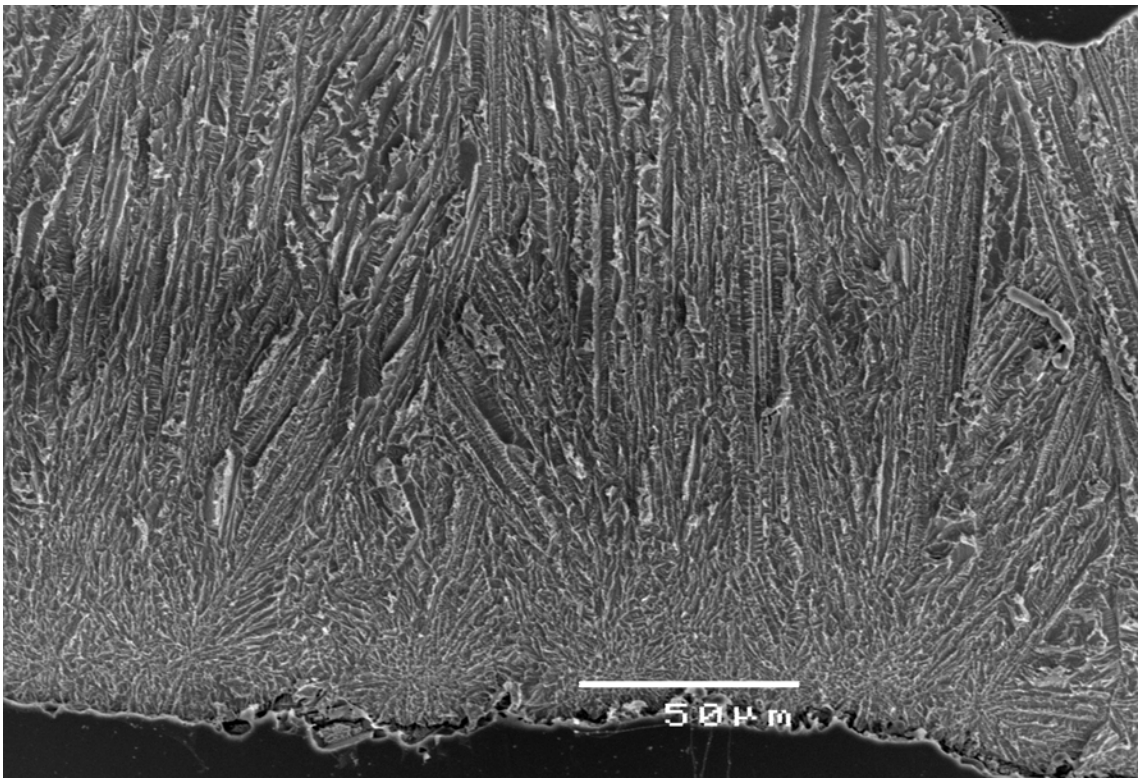

Figure 4-31: Run 1- Cross section of copper cathode obtained at 45°C, 28mA/cm2, 0.5mg/L Guar, 1mg/L APAM and 110µm δ. Surface Roughness, Ra = 5.95±0.47 microns.

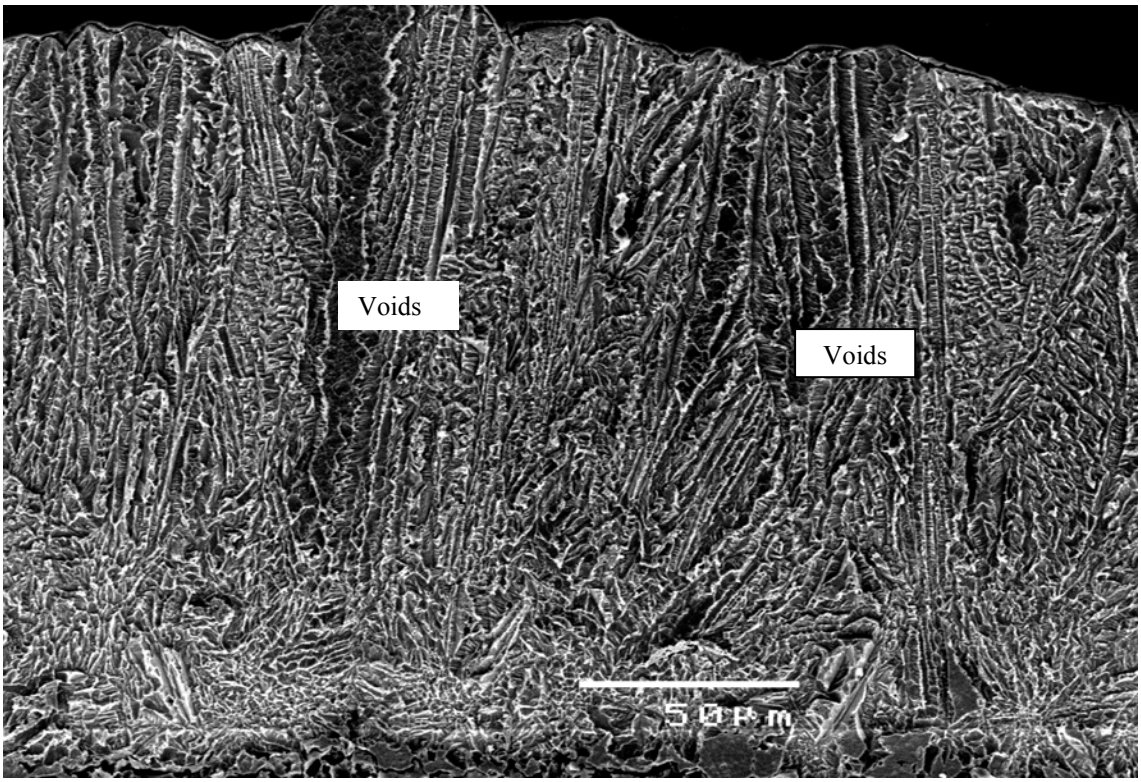

Figure 4-32: Run2 - Cross section of copper cathode obtained at 65°C, 28mA/cm2, 0.5mg/L Guar, 0.5mg/L APAM and 87µm δ. Surface Roughness, Ra = 6.36±0.64 microns.

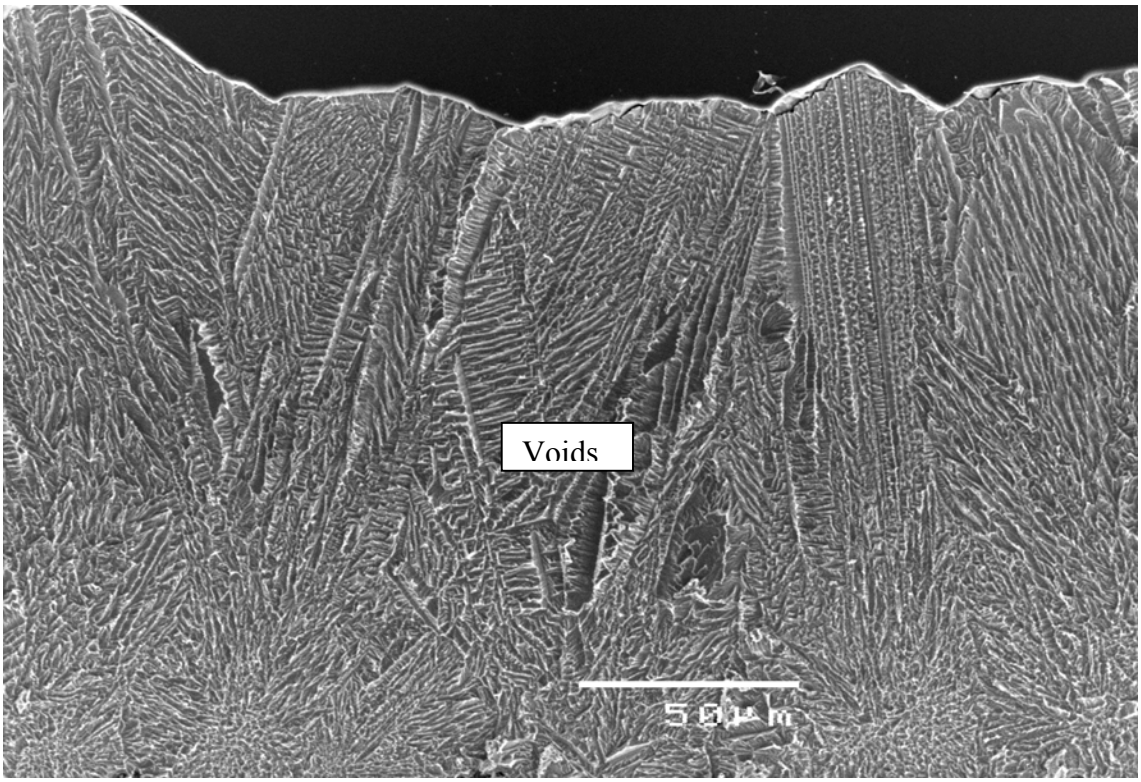

Figure 4-33: Run 3 - Cross section of copper cathode obtained at 45°C, 32mA/cm2, 0.5mg/L Guar, 0.5mg/L APAM and 110µm δ. Surface Roughness, Ra = 7.08±1.38 microns.

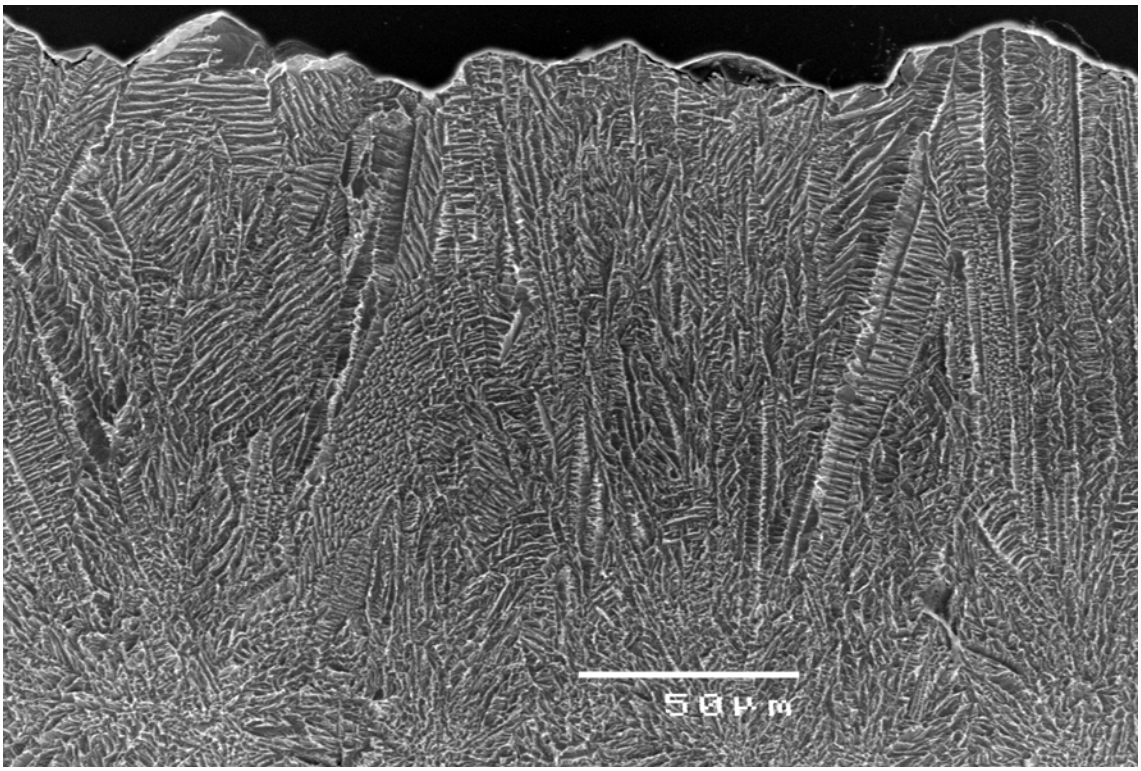

Figure 4-34: Run 4 – Cross section of copper cathode obtained at 65°C, 32mA/cm2, 0.5mg/L Guar, 1mg/L APAM and 87µm δ. Surface Roughness, Ra = 5.56±0.67 microns.

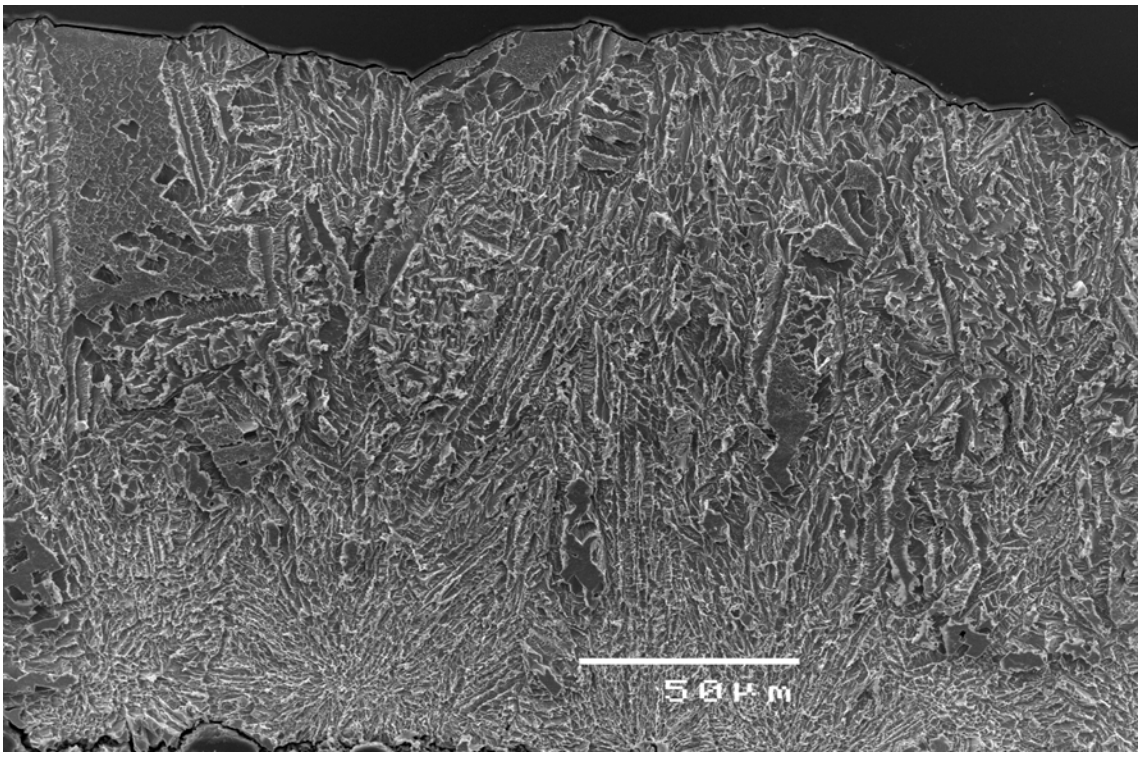

Figure 4-35: Run 5- Cross section of copper cathode obtained at 45°C, 28mA/cm2, 1mg/L Guar, 1mg/L APAM and 87µm δ. Surface Roughness, Ra = 5.83±0.72 microns.

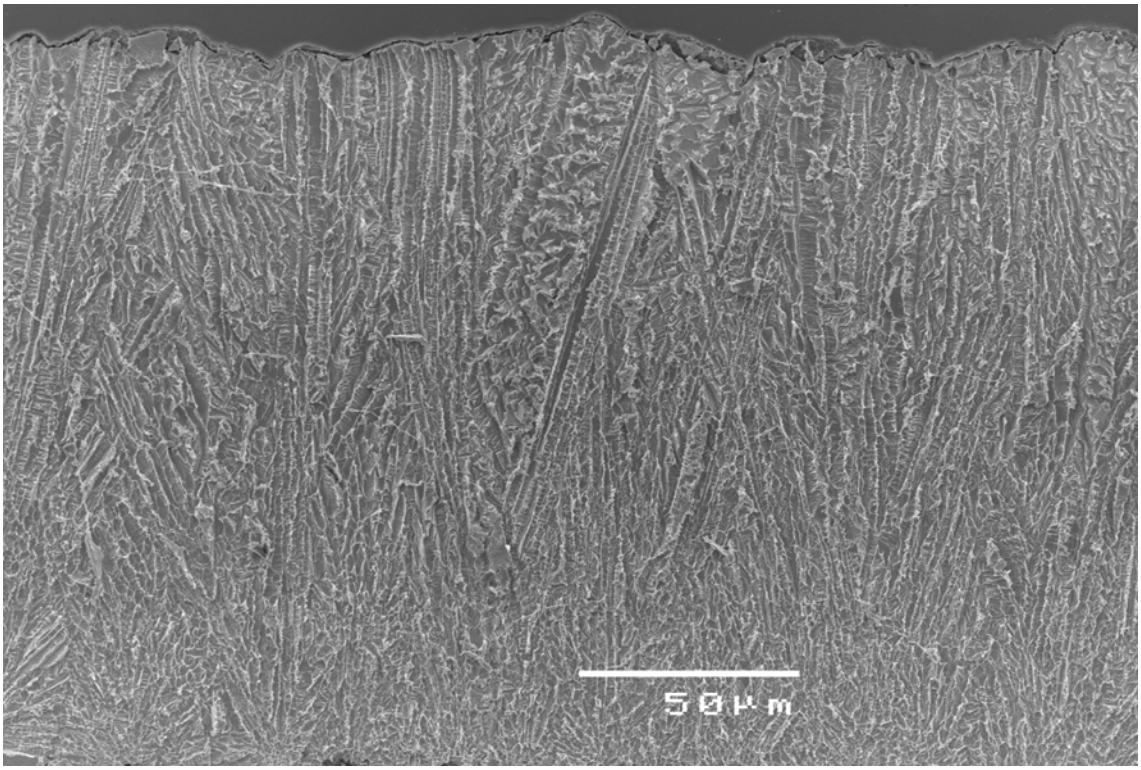

Figure 4-36: Run 6 – Cross section of copper cathode obtained at 65°C, 28mA/cm2, 1mg/L Guar, 0.5mg/L APAM and 110µm δ. Surface Roughness, Ra = 6.86±2.28 microns.

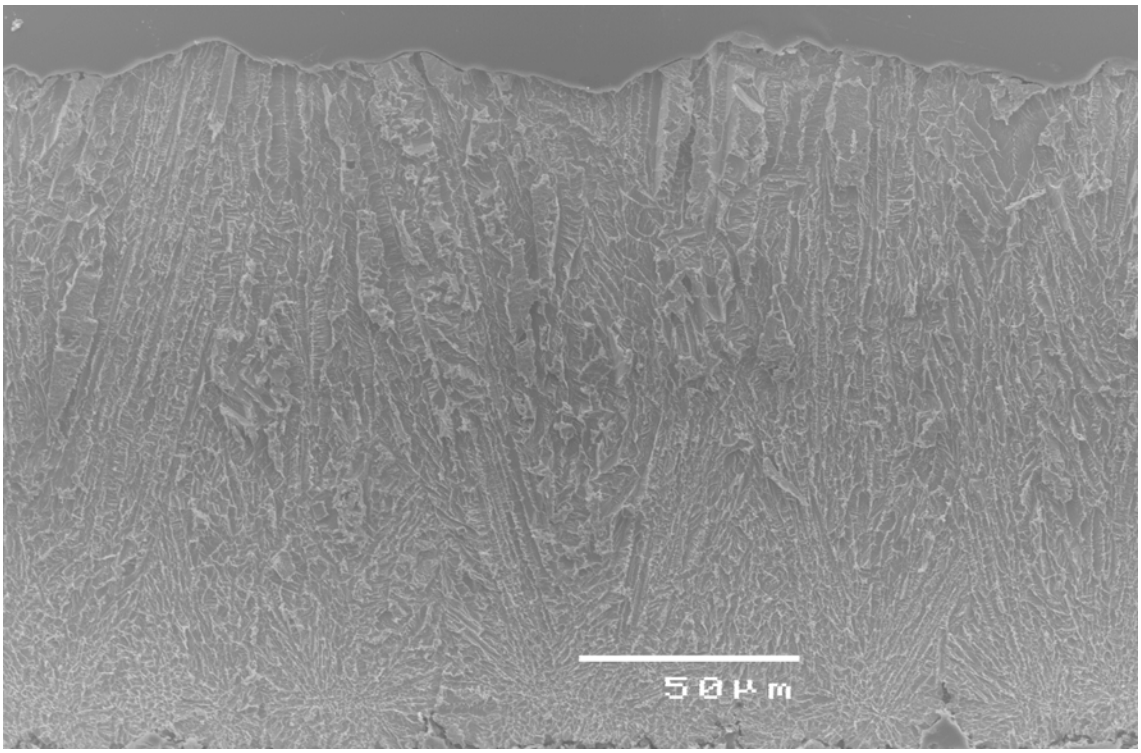

Figure 4-37: Run 7 – Cross section of copper cathode obtained at 45°C, 32mA/cm2, 1mg/L Guar, 0.5mg/L APAM and 87µm δ. Surface Roughness, Ra, = 5.99±0.66 microns.

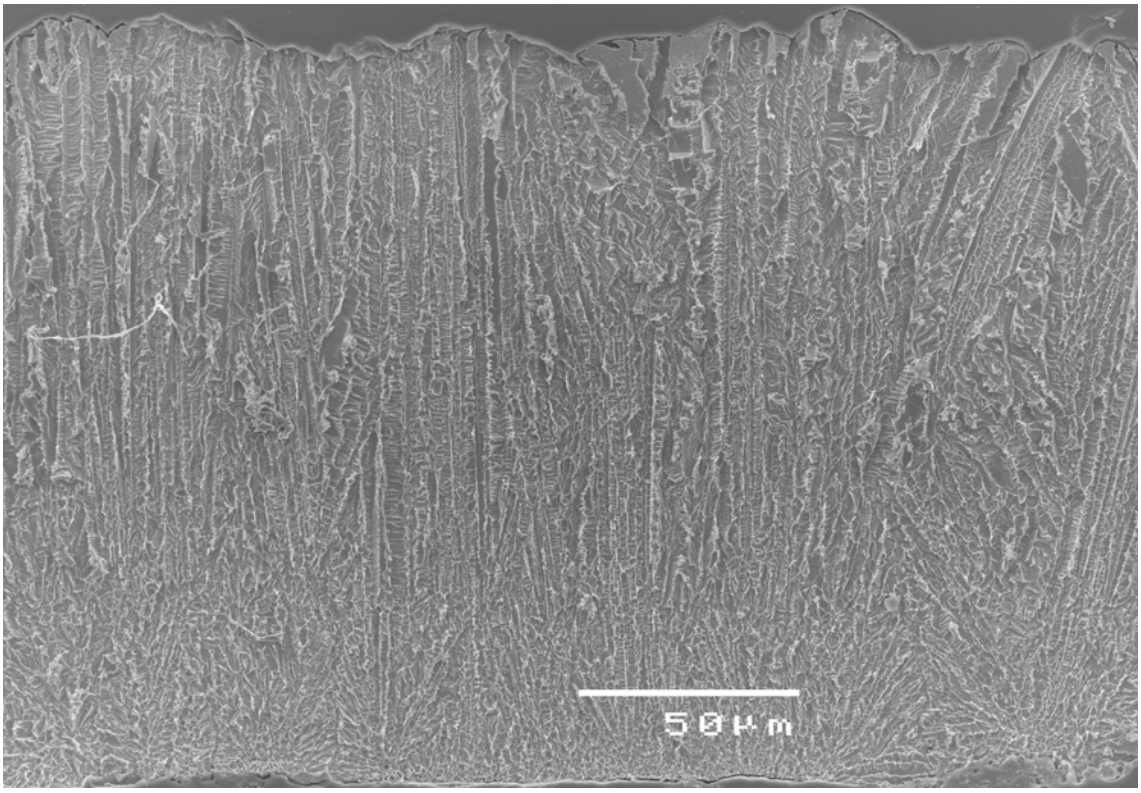

Figure 4-38: Run 8 – Cross section of copper cathode obtained at 65°C, 32mA/cm2, 1mg/L Guar, 1mg/L APAM and 110µm δ. Surface Roughness, Ra, = 5.66±069 microns.

4.3.4 Summary from Fractional Factorial Experimental Design

In conclusion, it was found that when 14,000 Coulombs were applied at 45^{o}C APAM has an insignificant effect on surface roughness, but at 65^{o}C, APAM has a significant effect in reducing surface roughness. This effect is interpreted to mean that APAM possibly achieves higher surface coverage at 65^{o}C than at 45^{o}C due to faster 'activation' and cleavage of its backbone at 65^{o}C than at 45^{o}C and therefore producing smaller molecular weights of APAM. The second conclusion drawn from these experiments is that APAM and Guar are not aliased; APAM appears to act truly independent of Guar to reduce surface roughness. Thus, APAM does not require the presence of Guar to reduce surface roughness in the concentration range 0.5 to 1 mg/L. This conclusion is further explored in the next Section.

The experiments, described in Sections 4.3.1 to 4.3.3, indicate that APAM is more effective in minimising surface roughness than Guar. A series of full factorial (2^2) experimental designs were undertaken to confirm and quantify the relative performance of APAM and Guar in controlling surface roughness.

In the following Section the effect of APAM and Guar on surface roughness, alone or in combination were studied under constant conditions of temperature, current density and RCE speed of rotation. Specifically the experiments were undertaken to.

(i) Confirm the independence of APAM and Guar by varying the the Guar to APAM systematically over 6-hours EW (Section 4.3.5),

(ii) Evaluate APAM and Guar independence using a Guar or APAM experimental design in 4.64 hours EW time (Section 4.3.6),

(iii) Re-evaluate APAM and Guar independence using Guar or APAM experimental design in 6 hours EW time (Section 4.3.7),

(iv) Confirm APAM and Guar independence using Guar or APAM in 12 hours EW time (Section 4.3.8).

4.3.5 2^2 Experimental Design – APAM *to* Guar Ratio at 50°C and 6-Hours EW Time

It was concluded in Section 4.3.4 that Guar and APAM act independently of ane another in affecting surface roughness. To confirm the independence of APAM and Guar on surface roughness the Guar to APAM ratio was expanded under fixed conditions of current density, temperature and diffusion layer thickness. A statistically significantly different surface roughness given by a specific ratio would indicate their dependence; otherwise, their independence indicated in the previous Sections will be confirmed.

Guar was dosed *twice* and APAM was dosed *only once*. The first dose of Guar was 20 minutes before EW time and the second dose at 2-hours and 50 minutes (or half of the total residence time of Guar in the electrolyte) after the EW cell was powered. The other EW conditions are in Table 4-16.

Table 4-16: Electrowinning Conditions for APAM-to-Guar Ratio

Current Density, A/m^2	300
Electrolyte Temperature, °C	50
Diffusion Layer Thickness, μm (10rpm)	109
Electrowinning Time, Hrs	6
Number of Coulombs per cm^2	650

A 2^2 full factorial design was used to expand the APAM to Guar concentration ratio from Sections 4.3.1 and 4.3.2. Therefore while the APAM/Guar low and high level ratios were set at 0.5 and 1.5; the low and high levels for Guar concentration were set at 0.25 and 1mg/L. This experimental design systematically increases the APAM concentration as shown in Table 4-17. The conditions were selected to clarify further whether an increased proportion of either Guar to APAM and APAM to Guar, i.e., 1.5/1, can reduce effectively surface roughness in an extended electrowinning time. The 2^2 experimental design and results for the Guar to APAM ratio are shown in Table 4-17 and Figure 4-39.

Table 4-17: 2^2 Experimental Design and Results for APAM-to-Guar Ratio

	Factors		Calculated Concentration	Surface Roughness, Ra, µm		Number Peaks-per-Centimeter	
Run	A=APAM/Guar	B=Guar,mg/L	APAM, mg/L	Mean	Std. Dev.	Mean	Std. Dev.
1	0.5	0.25	0.125	6.05	0.48	86	7.80
2	1.5	0.25	0.375	6.62	0.51	83	10.14
3	0.50	1	0.5	6.54	0.29	83.88	8.84
4	1.5	1	1.5	6.28	0.44	84.50	5.96

A model shown below as Equation (4-21) was obtained from this testwork with an F-value of 2.79 that implies that the model is significant. There is only a 5.91% chance that the model F-value this large could occur due to noise.

$$\text{Surface Roughness } (\mu\text{m}) = 6.37 - 0.21 * A * B \qquad (4\text{-}21)$$

The model indicates that A (APAM/Guar) and B (Guar) are confounded and significantly (α=0.0123) reduce the surface roughness. However, it could be deduced that APAM causes this effect since [(APAM/Guar)*Guar = APAM].

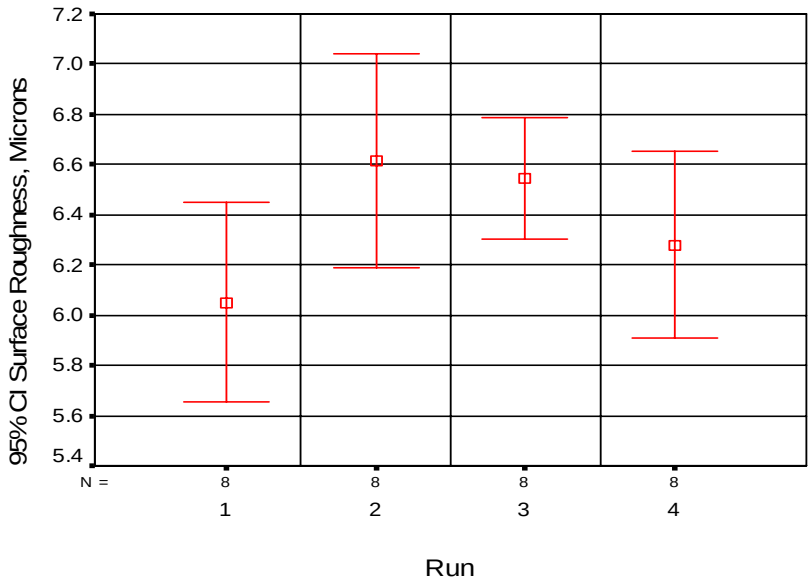

Figure 4-39: Error Box Plot of the Effect of APAM-to-Guar Ratio on Surface Roughness. Run 1 – Guar 0.25mg/L and APAM 0.125mg/L, Run 2 – Guar 0.25mg/L and APAM 0.375mg/L, Run 3 – Guar 1mg/L and APAM 0.5mg/L and Run 4 – Guar 1mg/L and APAM 1.5mg/L

Figure 4-40 shows the confounded and significant factors A (APAM/Guar) and B (Guar) indicating the effect of the APAM/Guar ratio and the Guar concentration on

the surface roughness. Low APAM/Guar ratio and low Guar concentration gave lower surface roughness values although their mean values are not significantly different. Figures 4-42, 4-43, and 4-44 show the diagnostic graphs validating the model.

Figure 4-40 shows the significant aliased term and indicates that an increase in Guar concentration increases surface roughness. The surprising and detrimental effect of Guar concentration on surface roughness noted in Figure 4-26 – Section 4.3.1 was replicated in these tests. Figure 4-40 also indicates that an increase of the APAM to Guar ratio appears to increase the surface roughness. As this last result is apparently contradictory with Section 4.3.2 – Figure 4-30, it is inferred that the presence of Guar in the electrolyte bath is altering the effect of APAM on surface roughness. In summary it has been shown that the overall results of this Section agree with those of Sections 4.3.1 and 4.3.2 in that Guar appears to increase surface roughness and, in contrast, APAM appears to decrease it. Therefore the effect of Guar and APAM on surface roughness should be investigated *separately*, as described in the following Sections.

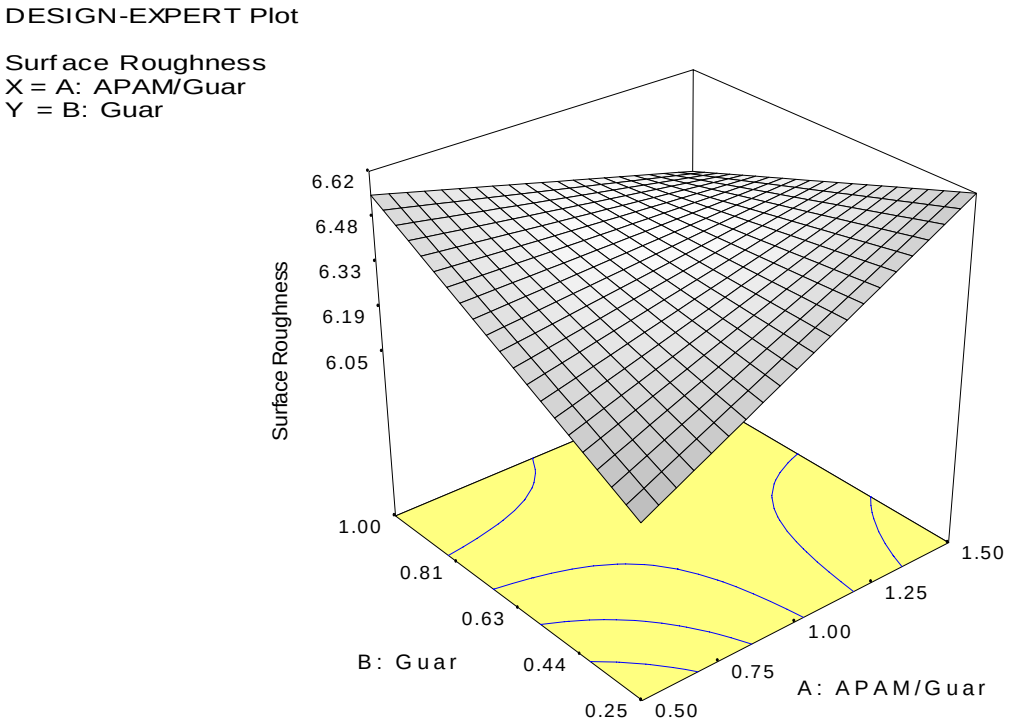

Figure 4-40: Significant Effect of APAM/Guar Ratio and Guar on Surface Roughness
A: [APAM/Guar], B: Guar, mg/L and Surface Roughness, µm

The concept of Peaks-per-Centimeter (PPC) is introduced to evaluate more closely the surface profile in the presence and absence of APAM and Guar. PPC is defined as the number of roughness profile elements per centimeter which consecutively intersect a specified upper profile section level and a lower profile section. The Mahr M1 Perthometer gives the surface roughness and PPC readings simultaneously. Figure 4-41 shows that for these experiments none of the PPC is significantly different.

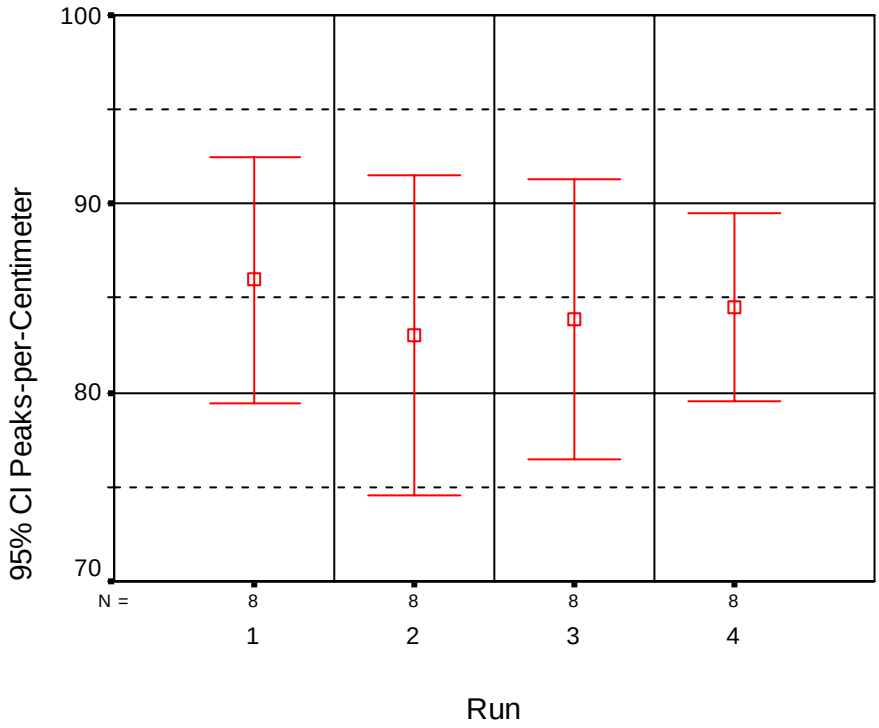

Figure 4-41: Error Box Plot of the Effect of APAM-to-Guar Ratio on PPC. Run 1 – Guar 0.25mg/L and APAM 0.125mg/L, Run 2 – Guar 0.25mg/L and APAM 0.375mg/L, Run 3 – Guar 1mg/L and APAM 0.5mg/L and Run 4 – Guar 1mg/L and APAM 1.5mg/L.

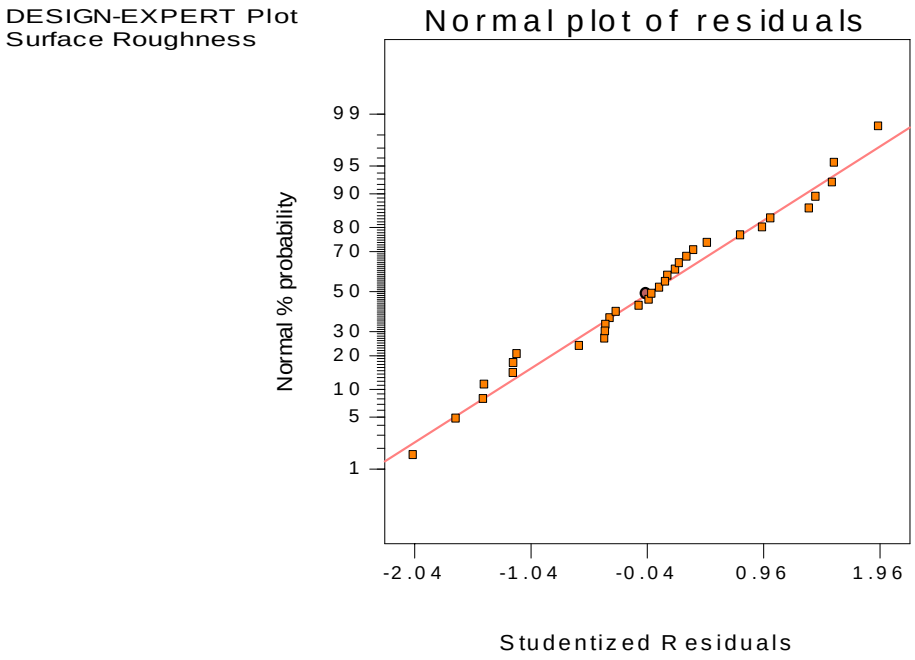

Figure 4-42: Studentized Residuals Plot

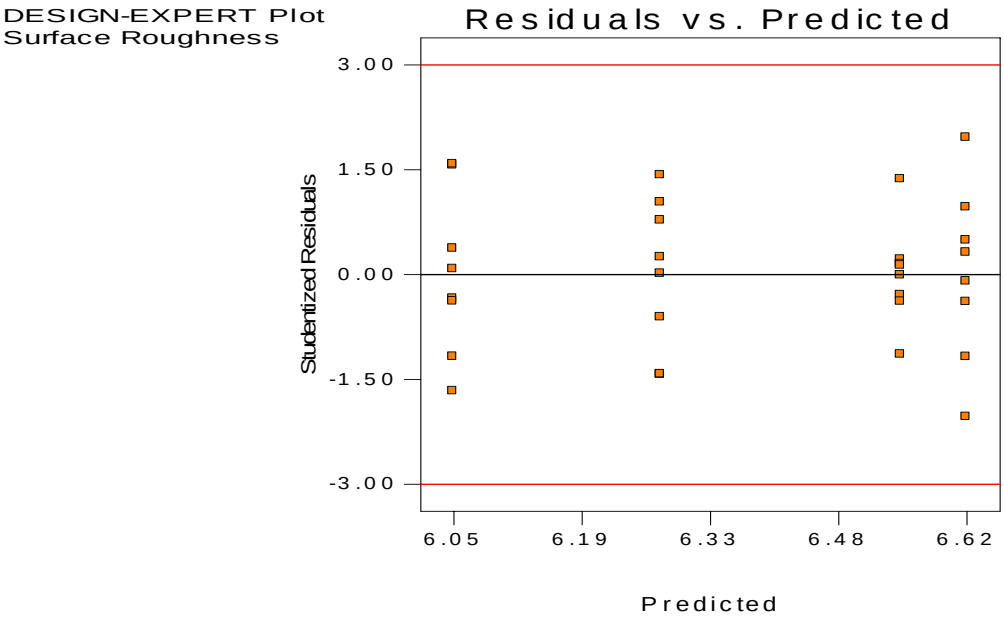

Figure 4-43: Residuals vs. Predicted Plot

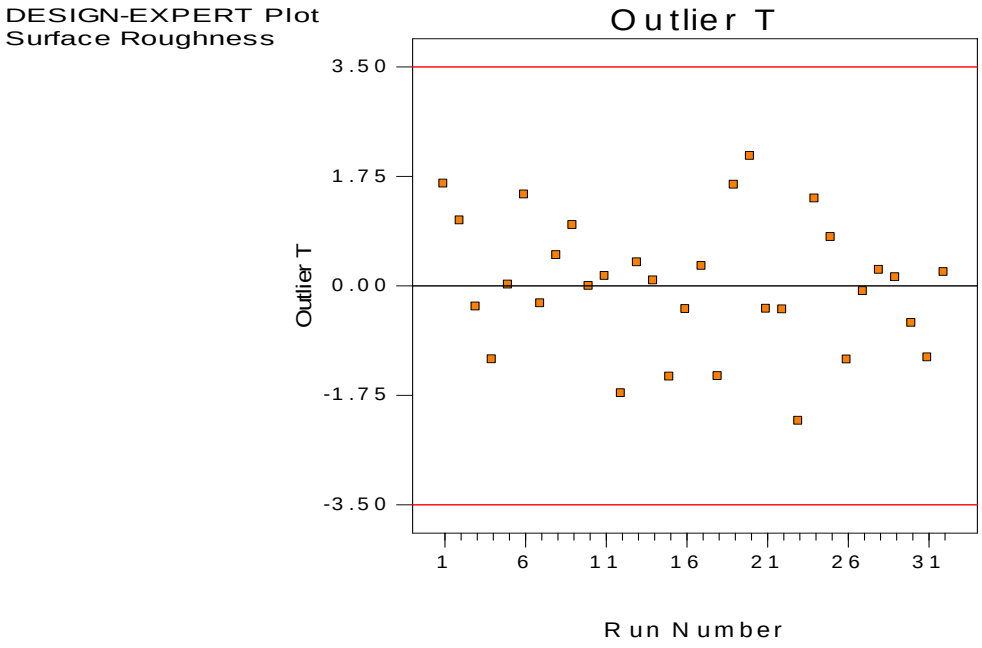

Figure 4-44: Outlier T Diagnostic Plot

4.3.6 2^2 Experimental Design APAM or Guar at 50°C and 4.6 Hours EW Time

A 2^2 full factorial design was used to evaluate the whether Guar *or* APAM is the most effective additive to control surface roughness. The temperature (50°C), current density (300A/m^2), RCE speed of rotation (17.5rpm) and the EW time were selected to be close of the mid-point of those used in Section 4.2. (Table 4-18). Both Guar and APAM were dosed *only once* at the beginning of each test.

Table 4-18: Electrowinning Conditions for APAM or Guar

Current Density, A/m^2	300
Electrolyte Temperature, °C	50
Diffusion Layer Thickness, µm	97.5
Electrowinning Time, Hrs	4.64
Number of Coulombs per cm^2	500

Table 4-19 present the 2^2 experimental design and their results in terms of surface roughness and Peaks-per-Centimeter (PPC). Figures 4-45 and 4-46 depict the surface roughness and PPC shown in Table 4-19.

Table 4-19: 2^2 Guar-or-APAM Experimental Design and Results

	Factors		Surface Roughness, Ra, μm		No. Peaks-per-Cm.	
Run	Guar,mg/L	APAM,mg/L	Mean	Std. Dev.	Mean	Std. Dev.
1	0.50	0.50	5.19	0.47	101.13	10.26
2	0.00	0.00	4.70	0.36	104.13	7.59
3	0.00	1.00	5.33	0.48	94.38	8.72
4	1.00	0.00	5.08	1.10	95.88	20.65
5	1.00	1.00	5.01	0.16	103	8.62

In this Section, PPC assists more clearly than surface roughness to explain the initial stages of dendrite formation in the absence of additives. The result on surface roughness in the *absence* of Guar or APAM is inconsistent with the general effect of an organic additive on nucleation and growth determining the smoothness of the deposit.

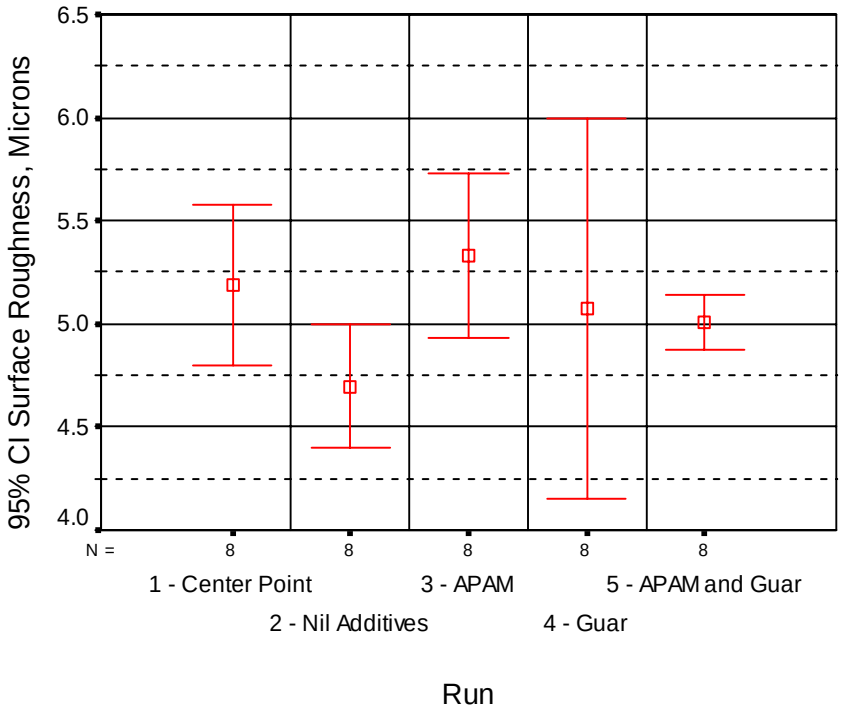

Figure 4-45: Error Bar Plot of Surface Roughness, Ra, μm after 4.64-Hours EW Time. Run 1 - Center Point, 0.5mg/L APAM and 0.5mg/L Guar; Run 2 – Nil additives; Run 3 – 1mg/L APAM; Run 4 – 1mg/L Guar and Run 5 – 1mg/L both APAM and Guar.

This finding appears to be due to the initial formation of dendrites, very fine needles, since two deposits can be obtained with the same surface roughness but with different numbers of PPC.

Table 4-19 and Figures 4-45 and 4-46 indicate that Run 2 in the absence of additives gave the lowest surface roughness and highest PPC value after 4.64-hours EW time or 500 Coulombs per square centimeter.

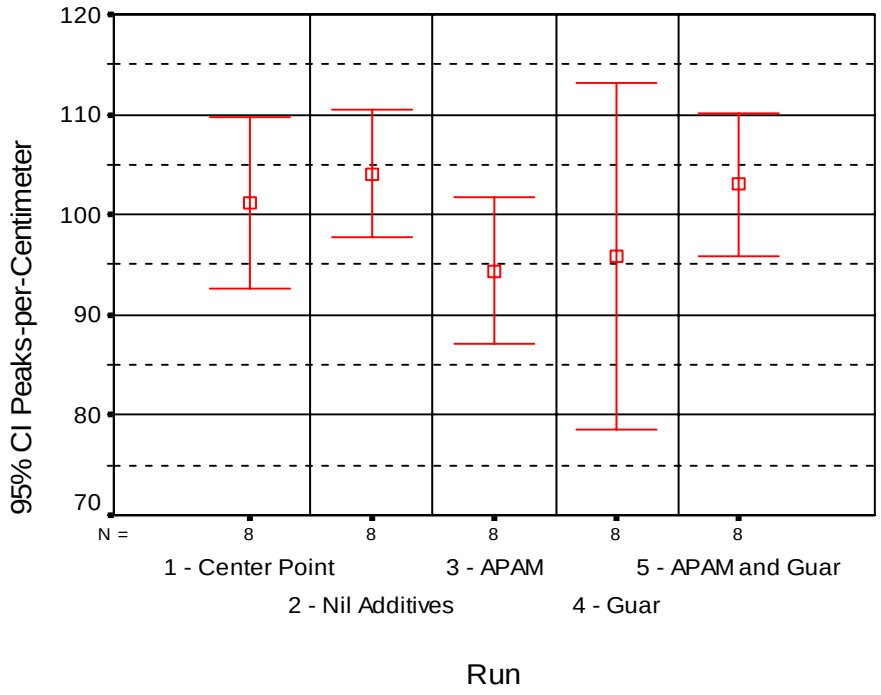

Figure 4-46: Error Bar Plot of PPC after 4.64-Hours EW Time. Run 1 - Center Point, 0.5mg/L APAM and 0.5mg/L Guar; Run 2 – Nil additives; Run 3 – 1mg/L APAM; Run 4 – 1mg/L Guar and Run 5 – 1mg/L both APAM and Guar.

The finding in this thesis is similar to that of Szymanski et al.[12] who studied the copper morphology in the absence of additives using Atomic Force Microscopy (AFM) mimicking industrial electrorefining conditions in terms of temperature (65^{o}C), current densities (21.3 and 25.3mA/cm^2), copper concentration (40g/L) but the concentration of sulphuric acid was not reported. It was concluded that in the early stages of electrodeposition, the *surface roughness was smalle*r when 25.3mA/cm^2 was used than when 21.3mA/cm^2 was used. However, the surface roughness increased faster with time at 25.3mA/cm^2 current density than at 21.3mA/cm^2 and hence time-scaling

modelling indicated that rougher copper deposit will be produced at the high current density than those at the low current density for 7 days plating.

It can be seen also from Figure 4-46 that the standard deviation for Guar alone experiments (Run 4) is markedly greater than those observed in the presence of APAM (Run 3). This result indicates the non-uniformity of the surface roughness in the presence of Guar alone. In contrast, APAM produced a more uniform copper deposit than Guar. This result indicates that Guar reacts faster and loses its levelling efficacy faster than APAM. Therefore, Guar needs to be dosed at least twice for every five hours of EW time or constantly to maintain efficacy. The physical appearance of the copper deposit obtained from this EW test with Guar and APAM at 1mg/L concentration was smooth and uniform. However, when Guar alone was present in the electrolyte, some convective lines on the copper deposit and some holes in the coper deposits (~3 spots of ~1x~1mm) were observed.

It is therefore concluded that EW time is critical to the evaluation of surface roughness. A regression model for the conditions stated in this section can be misleading due to the complex behaviour of the surface roughness and PPC at early stages of electrodeposition in the absence of additives. Therefore such a model was not presented. Nevertheless, the 2^2 experimental testwork at conditions of temperature (50^oC), current density ($300A/m^2$), 17.5rpm speed of rotation and 4 hours 38 minutes qualitatively indicated that APAM produces a more uniform surface roughness than Guar when both were *dosed once* only since APAM shows lower surface roughness standard deviation than Guar.

At the early stages of EW and in the absence of additives (i) the number of PPC was higher than in the presence of Guar and APAM and (ii) surface roughness at early stages can be smaller at higher current density, e.g., 25-30 mA/cm^2 than at lower current density, e.g., 20-25mA/cm^2 current densities. In Section 4.3.7 below it will be shown that the smaller surface roughness and high PPC and in the absence of additives is in a transition stage for the deterioration of the surface profile at 6-hours EW time.

4.3.7 2^2 Experimental Design – APAM or Guar at 50°C and 6 Hours EW Time

This test was conducted to continue evaluating the effectiveness of the additives Guar or APAM, either alone or in combination, on surface roughness and PPC over 6-hours of EW time. Guar was dosed *twice* and APAM *once.* The electrolyte temperature, current density and rotational speed of the electrode were 50°C, 300A/m^2 as in the previous Section and the RCE had a rotation of speed of 10 rpm. The experimental design and results are shown in Table 4-20.

Table 4-20: 2^2 Experimental Design APAM-or-Guar at 10 RPM - 50°C - 6 Hours EW

	Factors, mg/L		Surface Roughness, Ra, μm		No. Peaks per Centimeter		Observations
Run	APAM	Guar	Mean	Std. Dev	Mean	Std.Dev	Small Needles
1	0	0	7.68	2.16	65.13	13.95	Numerous
2	0	1	5.85	0.52	94.38	12.32	1big+Many
3	1	0	6.42	0.27	82.75	8.24	None
4	1	1	6.71	0.36	83.38	7.46	None
2R	0	1	6.48	0.70	87.63	8.35	Numerous nascents

The Model F-value of 9.96 for the number of PPC implies the model is significant. There is only a 0.01% chance that a "Model F-Value" this large could occur due to noise. In this case A and A*B are significant model terms as shown in Equation 4-22.

$$\text{Number of Peaks-per-Centimeter} = 81.41 + 7.47 * A + 1.66 * B - 7.16 * A * B \quad (4\text{-}22)$$

This model predicts that Guar (A, $\alpha<0.0006$) has a most significant effect to increase the number of PPC than APAM (B, $\alpha = 0.3948$). Guar*APAM (A*B, $\alpha = 0.0009$) has a significant effect to reduce PPC. Figure 4-47 shows these effects in an error box plot with 95% CI and Figure 4-48 in a 3D plot. The highest number of PPC shown in Figure 4-46 in the absence of additives decrease to the lowest number of PPC in Figure 4-47. This result confirms the conclusions made in Section 4.3.6.

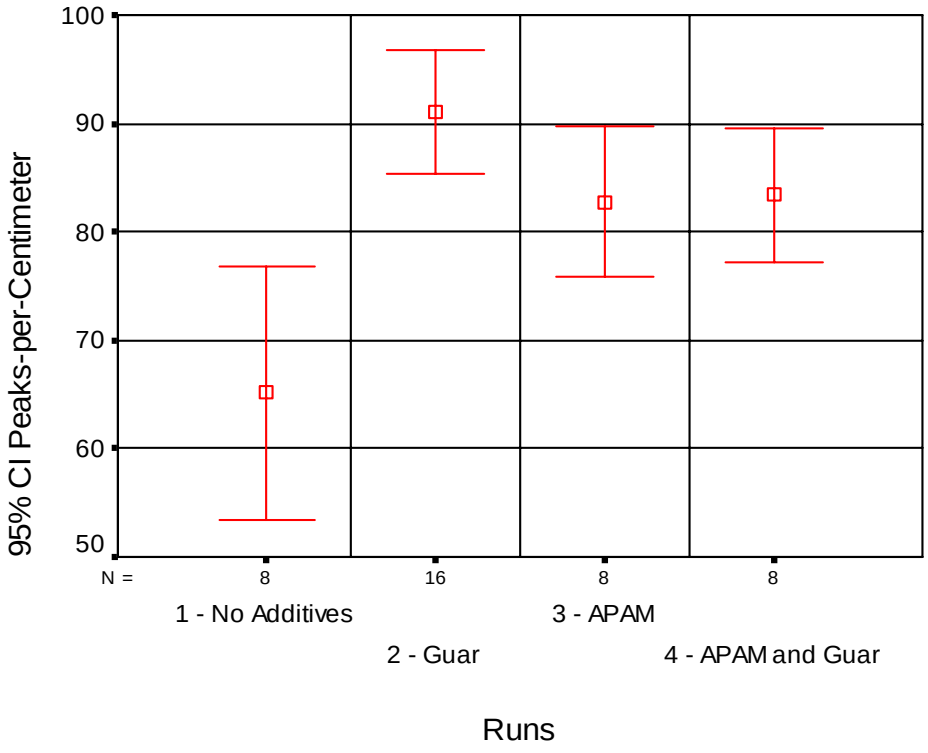

Figure 4-47: Effect of Guar or APAM on PPC after 6-Hours. EW Time

Table 4-20 shows that dendrite formation is uncontrollable from Run 2 and its replicate (2R) with Guar only. It indicates that the PPC for nil additives is statistically lower compared with those for Guar or APAM, alone or in combination. It also appears that the number of PPC for Guar is higher compared with those for Guar and APAM, and APAM alone. This observation implies that at longer EW time than 6-hours, the surface roughness with Guar should be deteriorated further.

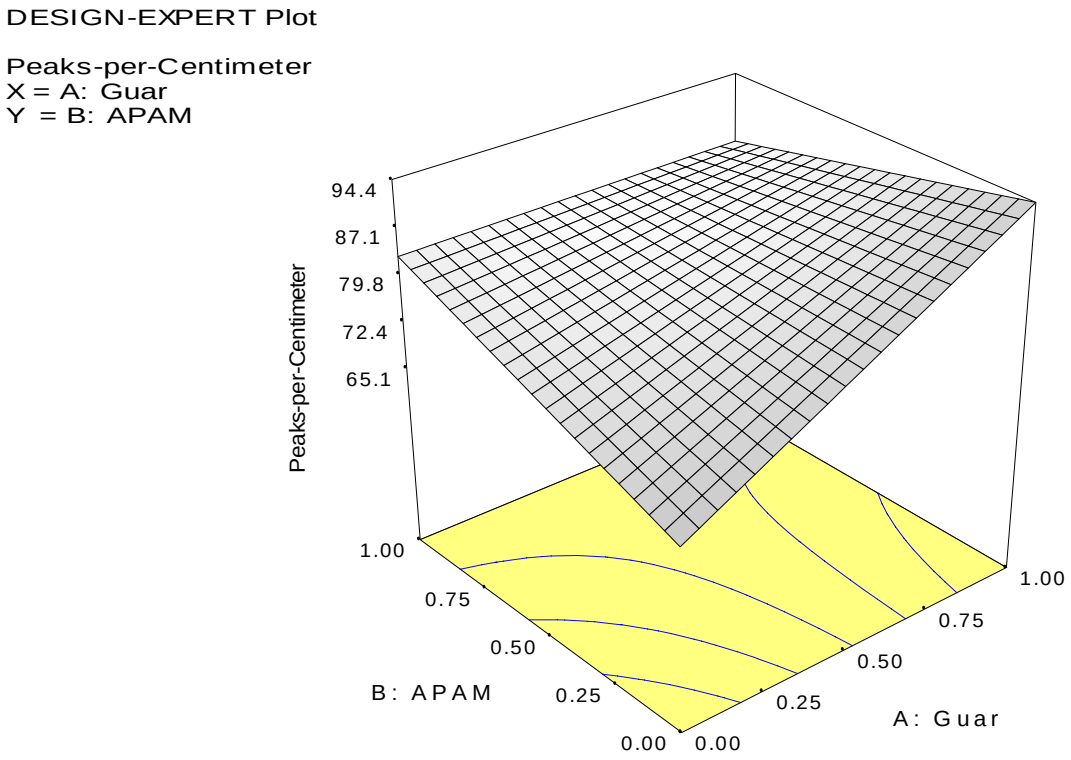

Figure 4-48: The Significant Effect of Guar and APAM on PPC after 6-Hours EW Time

Equation 4-23 shows the surface roughness model for this testwork.

$$\text{Surface Roughness } (\mu\text{m}) = 6.66 - 0.38 * A - 0.098 * B + 0.53 * A * B \quad (4\text{-}23)$$

The Model F-value of 3.64 for surface roughness implies the model shown in Equation 4-23 is significant. There is only a 2.48% chance that a "Model F-Value" this large could occur due to noise. The aliased term (Guar*APAM, $\alpha = 0.0134$) has the most significant effect on increasing surface roughness. Guar, (A, $\alpha = 0.0648$) has a weak effect on reducing surface roughness. APAM (B, $\alpha=0.6271$) has an insignificant effect on reducing surface roughness.

This surface roughness model indicating that Guar (A) has stronger effect than APAM (B) on reducing surface roughness may be misleading. Such a statistical model does not incorporate the complex mechanism of the early stages of dendrite formation in which initially passes through a period of smoother surface roughness and higher

number of PPC in the absence of both Guar and APAM which is followed by high surface roughness and dendrite formation quantitatively. Guar leads to dendrite formation as shown in Table 4-20. Moreover, no dendrites were observed from runs 3 and 4 in which APAM were present.

The PPC model, Equation 4-23, however, appears to predict that Guar produces higher PPC than APAM. It is therefore concluded that high number of PPC leads to the deterioration of the surface roughness profile as shown with nil additives at 4.64-hours EW time (Figure 4-46) and with Guar at 6-hours EW time (Figure 4-47). It is therefore inferred that the PPC obtained with Guar at longer EW time greater than 6-hours, must decrease. In other terms the surface roughness must become dendritic at 12-hours EW time. This behaviour will be shown in the next Section 4.3.8.

Figure 4-49 to 4-53 show the Scanning Electron Microscopy (SEM) micrographs of the copper cathodes. These micrographs show the electrolyte face for all runs. The line-scale is 50μm except Run 2 for which line-scale is 100μm. All micrographs show angled pyramidal crystal growth as reported in the recent literature[13-15] in the presence of animal glue and chloride ions. It is seen that the nucleation and growth is different in the presence and absence of organic additives. Figure 4-49 shows the presence of very small crystallites in the absence of additives but these crystallites are not observed in the presence of additives. The presence of small crystallites in the absence of additives agrees with the findings from recent studies using in-situ AFM on copper electrodeposition indicating that in the absence of PEG, chloride ions and Janus Green B (JGB) and bis(3-sulphopropyl) disulphide (SPS) copper deposition follows a progressive nucleation and 3D diffusion-limited growth[16]. Moreover, the nucleus density for solutions in the absence of additives were about an order of magnitude larger than those containing additives at any given potential, illustrating that the additives influence the nucleation rate.

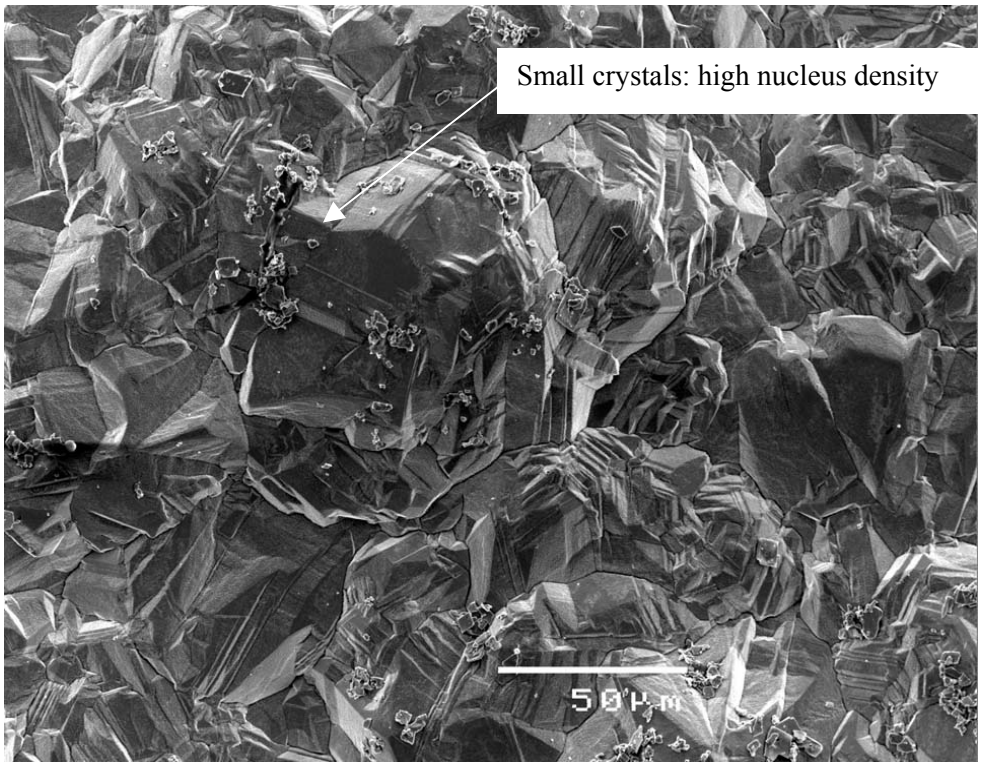

Figure 4-49: Run 1 - No Additives

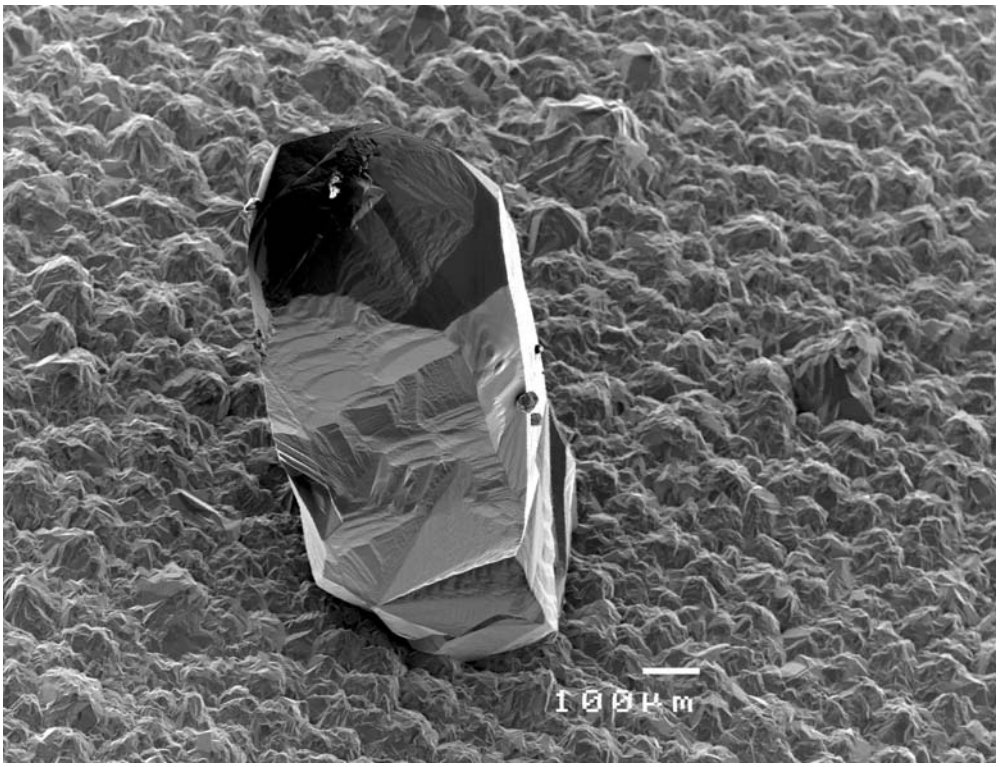

Figure 4-50: Run 2 – Guar Only

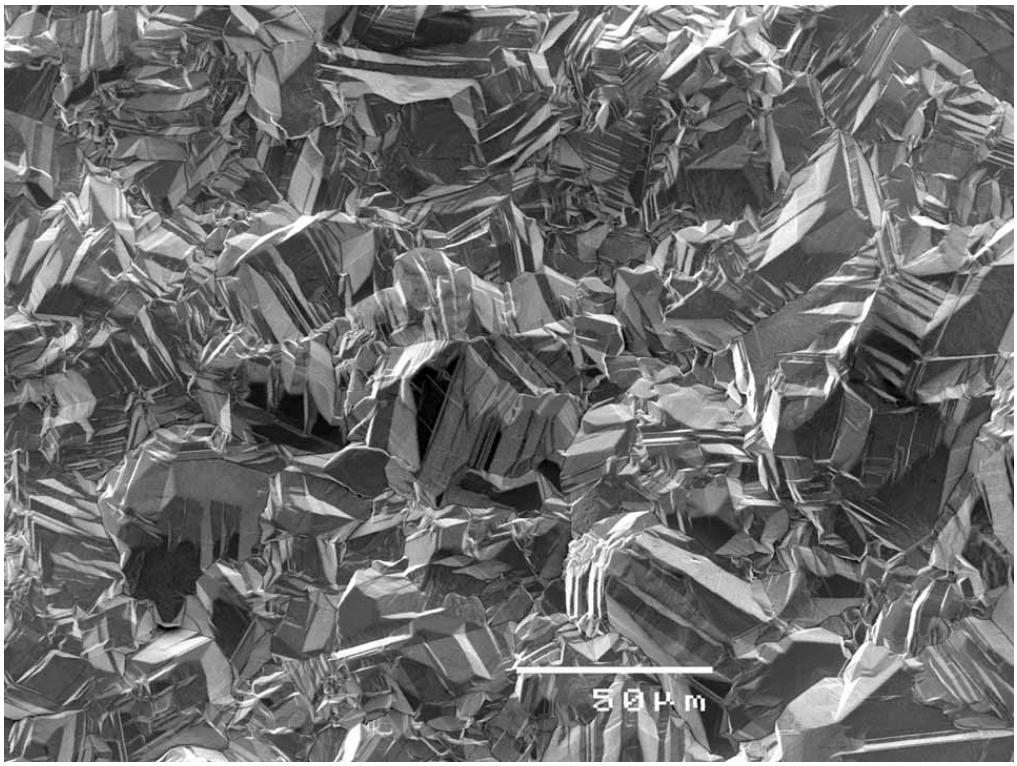

Figure 4-51: Run 2R – Guar Only

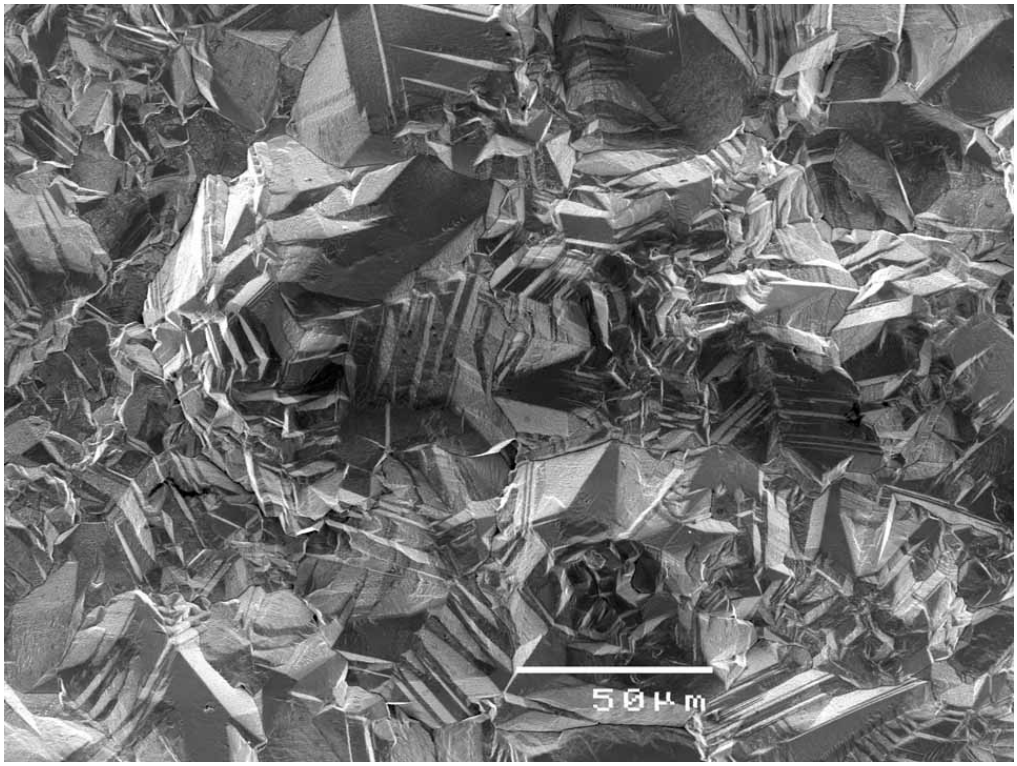

Figure 4-52: Run 3 – APAM Only

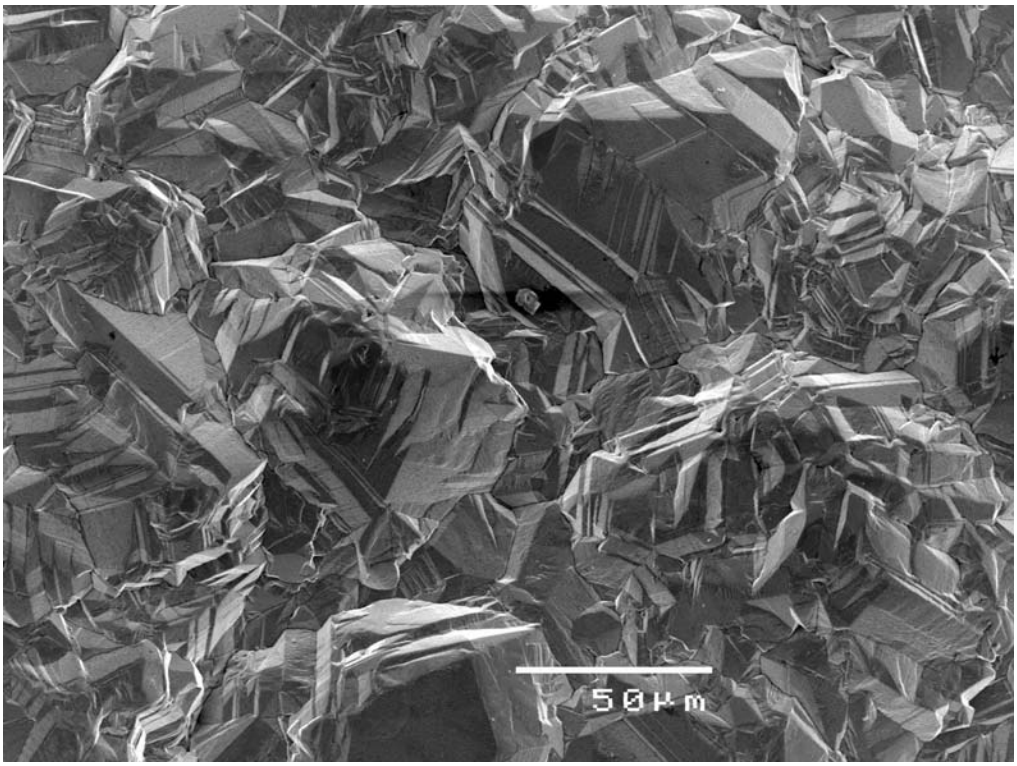

Figure 4-53: Run 4 – APAM and Guar

4.3.8 APAM or Guar at 50°C for 12 Hours EW Time

This test was conducted to compare APAM with Guar over 12 hours EW time to clearly resolve whether APAM produces smoother surface roughness than Guar as demonstrated in previous Section over 6 hours EW time. One mg/L Guar was dosed at 0 (20 minutes before the current was applied to the EW cell), 3, 6 and 9 hours giving a total cumulative concentration of 4 mg/L over 12 hours EW time. In Test 132 APAM was dosed o*nly once* at 20 minutes before the EW was powered, in Test 133, APAM was *dosed twice* at 0 and 6 hours over 12 hours EW time.

The experimental conditions and results are shown in Table 4-21 and Figures 4-54 and 4-55 and clearly reconfirm *all* previous tests that APAM is the most effective organic additive to control dendrite growth than Guar, the industry-standard additive.

Table 4-21: Effectiveness of Guar and APAM to Control Dendrite Growth

ADDITIVE	**Guar**	**APAM**	
RCE Test No.	128	132	133
PAM Prep. Residence Time, Hrs	2	2	2
Guar or PAM Preparation Media	water	16-fold DE	16-fold DE
Guar or PAM Preparation Temp., ^{o}C	25	50	50
Guar or APAM Initial Conc., mg/L	1	1	1
Guar or APAM Dosed, mg/L	1	1	1
Guar or APAM Dosing Frequency, Hrs	3	0	6
Guar or APAM Total Dosed, mg/L	4	1	2
Diffusion layer Thickness, µm (10rpm)	92	92	92
Electrowinning Time, Hrs	12	12	12
Current Density, Amp/m^2	300	300	300
Electrolyte Temperature, ^{o}C	50	50	50
No. Coulombs/cm^2	1300	1300	1300
Surface Roughness, Ra, µm	*Unmeasurable*	12.79	11.71
Surface Roughness Std. Dev., µm	*NA*	1.07	1.28
Number of Dendrites > 0.1mm	12	*Nil*	*Nil*

The surface roughness of the copper deposit obtained from the testwork with Guar was not able to be determined since the stylus gets stuck on the dendrites. In contrast, the surface roughness of the copper cathodes produced with APAM was still measurable even though only one and two mg/L were dosed for 12-hours EW time. This finding confirms that the ageing products of APAM are more effective than those of Guar and therefore it is consistent with the hypothesis that the APAM surface coverage is much higher than the Guar surface coverage.

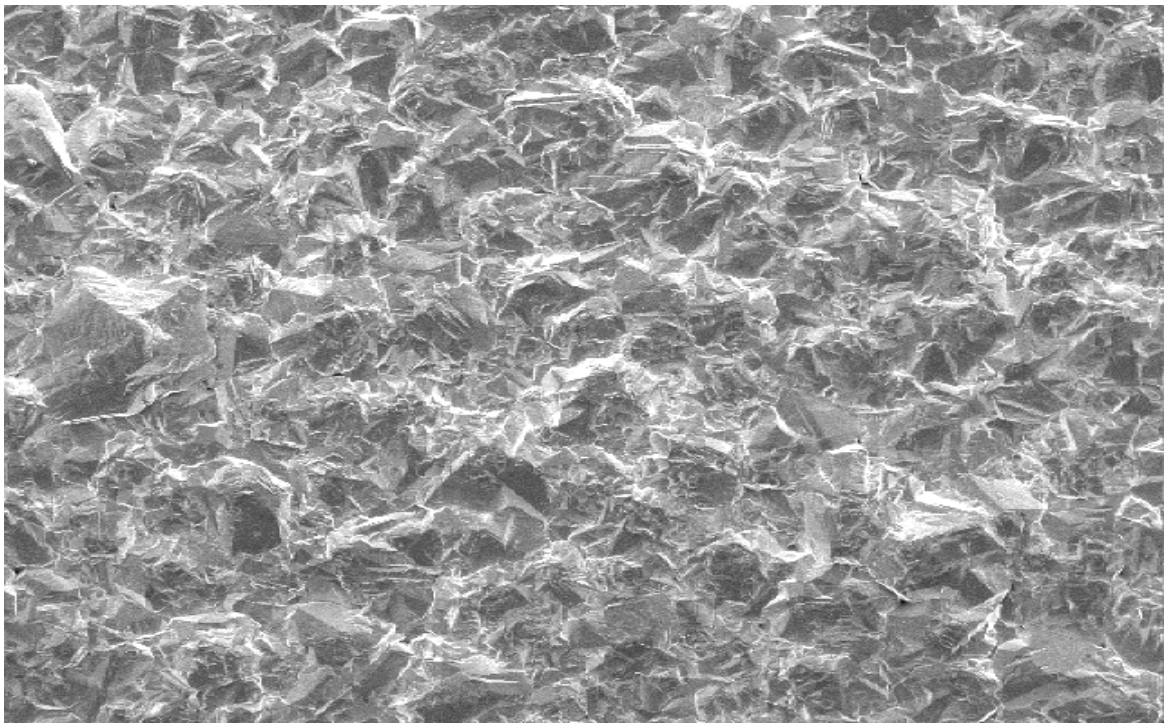

Figure 4-54: SEM Micrograph of the Copper Cathode obtained using APAM after 12 Hours EW time (75X Mag)

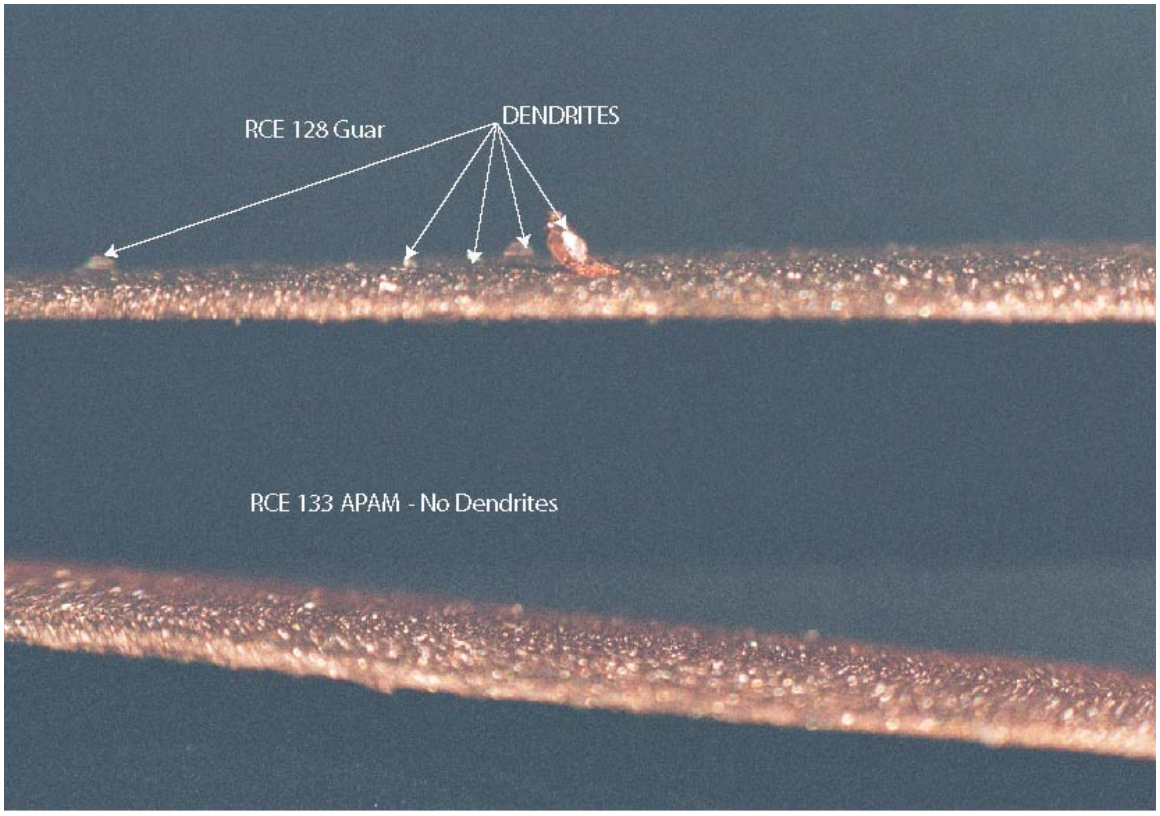

Figure 4-55: Photograph Comparing Guar and APAM after 12 Hours EW Time.

The Copper deposit obtained with Guar shows the presence of dendrites but when APAM was used no dendrites were obtained and its surface roughness was still measurable.

4.4. Discussion and Conclusions

At a 95% confidence interval the model derived from the fractional factorial experimental design in the temperature range of 45-55^{o}C was:

Surface Roughness (μm) =

$$+6.26+0.27*B-0.053*C-0.056*D+0.25*E-0.62*B*C-0.38*B*E$$

The model for the temperature range of 45-65^{o}C was:

Surface Roughness (μm) =

$$+6.16-0.051*A-0.089*B-0.075*C-0.41*D+0.23*E-0.17*B*C$$

where A is temperature; B, current density; C, Guar; D, APAM and E, diffusion layer thickness.

It was deduced that the aliased effect of current density(B)*Guar(C) decreases from significant ($\alpha<0.0001$) in the first model at 45-55^{o}C to insignificant ($\alpha = 0.2120$) in the second model at 45^{o}C-65^{o}C. This reduction in significance is probably due to the faster degradation of Guar at 65^{o}C than at 45^{o}C at the same current density. It can be seen that the effect of APAM is significant in the 45^{o}C-65^{o}C range than in the 45^{o}C-55^{o}C. This significance is probably also due to the faster degradation of APAM at 65^{o}C than at 45^{o}C. This indicates that degraded APAM is more effective at reducing surface roughness than fresh APAM a result which contrasts with that for Guar.

An optimal proportion of Guar to APAM to significantly reduce surface roughness was not determined. Therefore, the role of Guar and APAM was deduced to be independent and therefore Guar and APAM were compared independently as levelling agents.

The evolution of surface roughness/dendrites in copper electrodeposition occurs simultaneously with smaller surface roughness and higher number of PPC where EW time plays an important role as well as the effectiveness of an organic additive, if present, to control the uniformity of the surface profile. In the absence of additives, a

lower surface roughness and a higher PPC was observed than when Guar and/or APAM were present at 30mA/cm^2 and 4.64 hours EW time. This is consistent with AFM studies recently reported [12, 19]. The PPC model for 6-hours EW time indicates that Guar produces higher PPC than APAM. The surface roughness of the copper deposit with Guar was unmeasurable roughness after 12-hours EW time even though 1mg/L Guar was dosed every 3hours (4mg/L Guar total dosage). In contrast, the surface roughness of the copper deposits with APAM was 12.79 and 11.71μm after 12-hours EW time even though a total of 1 and 2mg/L APAM were dosed, respectively. It was therefore shown that the evolution of surface roughness/dendrites up to 12-hours of EW time follows: Nil additives>Guar>APAM.

The results obtained from Tests 3 and 8 in Section 3.4 where polyacrylmide was prepared in water and full-strength electrolyte are similar to the conditions under which Pye and Schurz[17], and Vereecken ad Winand[18] studied nonionic and cationic polyacrylamides and indicated that Guar controlled the surface roughness of electrowon copper more effectively than polyacrylamides. The results of this *Chapter* indicate the opposite of the above publications when PAM was prepared in 16-fold diluted electrolyte at 50^{o}C, for 2-hours under stirring. The preparation of APAM is the major difference between this work and any previous work and it is critical to its levelling effect. APAM is a more effective organic additive to reduce surface roughness than Guar, the industry-standard additive.

4.5 References

1. Paunovic M, Schlesinger M. *Fundamentals of Electrochemical Deposition*: John Wiley & Sons, Inc.; 1998.

2. Schmickler W. *Interfacial Electrochemistry*. New York: Oxford University Press; 1996.

3. Montgomery DC. *Design and Analysis of Experiments*. 5th ed: John Wiley & Sons; 2001.

4. Mahr. *M1 Mahr Perthometer Operating Manual*. 2002.

5. Stat-Ease SME. Design-Expert Software. In. 6.1.10 ed: John Wiley & Sons, Inc; 2003.

6. Arvia AJ, Carrozza JSW. *Mass Transfer in the Electrolysis of Cuso4-H2so4 in Aqueous Solutions under Limiting Current and Forced Convection Employing a Cylindrical Cell with Rotating Electrodes*. Electrochimica Acta 1962;7:65-78.

7. Newman J, Thomas-Alyea KE. *Electrochemical Systems*. Third ed. Hoboken, New Jersey: John Wiley & Sons, Inc.; 2004.

8. MathSoft Engineering & Education I. Mathcad. In. 12 ed; 2004.

9. Grchev T, Cvetkovska M. *Electrochemically Initiated (Co)Polymerization of Acrylamide and Acrylonitrile on a Steel Cathode - Electrochemical and Impedance Study*. Journal of Applied Electrochemistry 1989;19(3):434-42.

10. Grchev T, Cvetkovska M, Stafilov T, Schultze J. *Adsorption of Polyacrylamide on Gold and Iron from Acidic Aqueous Solutions*. Electrochimica Acta 1991;36(8):1315-1323.

11. Grchev T, Cvetkovska M, Schultze JW. *The Electrochemical Testing of Polyacrylic Acid and Its Derivatives as Inhibitors of Corrosion*. Corrosion Science 1991;32(1):103-12.

12. Szymanski G, Dymarska M, Zhao T, Lipkowski J. *Atomic Force Microscopy Study of the Morphology of Electrodeposited Nickel and Copper at Conditions Mimicking Industrial Nickel and Copper Electrorefining*. Electrometallurgy 2001, Proceedings of Annual Hydrometallurgy Meeting, 31st, Toronto, ON, Canada, Aug. 26-29, 2001 2001:375-387.

13. Damajanovic A, Setty THV, Bockris J. *Effect of Crystal Plane on the Mechanism and the Kinetics of Copper Electrocrystallization*. J. Electrochem. Soc. 1966;113(5):429-435.

14. Veilleux B, Lafront A, Ghali E. *Influence of Gelatin on Deposit Morphology During Copper Electrorefining Using Scaled Industrial Cells*. Canadian Metallurgical Quarterly 2002 Jan;41(1):47-61.

15. Kondo K, Murakami H. *Crystal Growth of Electrolytic Cu Foil*. J. Electrochem. Soc. 2004;151(7):C514-C518.

16. Radisic A, West A, Searson P. *Influence of Additives on Nucleation and Growth of Copper on N-Si(111) from Acidic Sulfate Solutions*. Journal of the Electrochemical Society 2002;149(2):C94-C99.

17. Pye D, Schurz G; inventors. The Dow Chemical Company, assignee. Electrowinning of Metals. United States patent 2,798,040. 1957 July 2, 1957.

18. Vereecken J, Winand R. *Influence of Polyacrylamides on the Quality of Copper Deposits from Acidic Copper Sulphate Solutions*. Surface Technology 1976; 4:227-235.

19. Schmidt W, Alkire R, Gewirth A. *Mechanic Study of Copper Deposition onto Gold Surfaces by Scaling and Spectral Analysis of in-Situ Atomic Force Microscopic Images*. J. Electrochem. Soc. 1996(10):3122-3132.

CHAPTER 5

KINETICS OF COPPER DEPOSITION IN THE PRESENCE OF GUAR AND ACTIVATED POLYACRYLAMIDE USING CYCLIC VOLTAMMETRY AND ELECTROCHEMICAL IMPEDANCE SPECTROSCOPY

5.1 Introduction

The previous two Chapters have shown that polyacrylamide prepared in 16-fold diluted electrolyte at 50^{o}C for two hours under stirring most likely forms a block copolymer with up to 10% hydrolysis and a molecular weight less than 15 million Dalton. This polyacrylamide structure was named "activated polyacrylamide" (APAM). It has also been shown in the previous Chapters that APAM produces copper deposits with a lower surface roughness than polyacrylamide prepared in water or full-strength electrolyte. Moreover, APAM produced smoother copper deposits than either Guarfloc66 (Guar) the 40-year-old industry-standard organic additive or polyacrylic acid. The aim in this section is to investigate the interface between either stainless steel or copper metal and copper electrolyte in the presence and absence of both Guar and APAM using both Cyclic Voltammetry (CV) and Electrochemical Impedance Spectroscopy (EIS).

Electrochemical techniques are unique for in-situ investigation of electrochemical interfaces during deposition or dissolution of metals. The electrical quantities measured permit kinetic studies of elementary phenomena such as single-electron steps of the reaction mechanism and the presence of intermediates, often

unstable, may therefore also be inferred[1-4]. Cyclic Voltammetry and Electrochemical Impedance Spectroscopy were selected to extract kinetic parameters for copper electrodeposition in the presence of a mass transport rate-determining step and organic additives.

The interest in Electrochemical Impedance Spectroscopy to determine the double-layer capacitance, to characterize the electrode processes and to unravel the kinetics of electrochemical systems has enormously increased in recent years[5, 6]. The application of this technique in metals electrodeposition in the presence of additives has also increased in recent years since adsorption phenomena strongly influence the electrochemical impedance structure[7].

The principle of EIS is to measure the impedance, usually at fixed potential during a frequency scan, to study the kinetics of processes at the metal electrolyte interface and to distinguish between the various mechanisms that regulate charge-transfer. EIS involves high-precision measurements over wide time ranges (10^4 to 10^{-6} s or 10^{-4} to 10^6 Hz), which makes it suitable for the study of two one-electron steps with the stabilization of the intermediate step in copper deposition discussed in Section 2.4. This method analyses the response of the electrochemical system to a small-amplitude alternating current signal perturbation.

The results of EIS testwork can be interpreted using either or both the complex-plane plot, also known as the Nyquist plot, and Bode plot. The complex-plane plot presents the real and imaginary impedances as a function of frequency and the Bode plot presents the dependence of the phase angle on frequency. Analysis of the system response therefore may contain information about the chemical and electronic structure of the metal electrode/cupric ions-sulfuric acid electrolyte with either APAM or Guar at the interface as the impedance is measured as a function of the frequency of the AC source.

A number of studies have been recently conducted to understand the effect of organic additives on copper deposition. The effect of chloride ions on the current-voltage polarization behaviour of polyethylene glycol [PEG: $(CH_2\text{-}O\text{-}CH_2)_n$] indicates that, in the presence of either cupric ions (0.3M) or sulfuric acid (2.2M), PEG polarizes

or inhibits the electrode more strongly in the presence of chloride ions than in its absence[8, 9]. In separate studies, Moffat et al.[8, 10-12] presented the effect of the competitive interaction of 3-mercapto-1-propane-sulfonic acid (MPSA) with PEG and chloride ions in the copper electrolyte bath on the current voltage polarization as well as on the superconformal deposition of a smooth and "bright" copper deposit. While PEG and chloride ions reduce the deposition rate or provide the inhibition/polarization process, MPSA or some derivative thereof is associated with acceleration/depolarization processes.

A surface-enhanced Raman (SERS) study on the polarization effect of PEG during copper deposition indicates that the presence of chloride ions enhance the *adsorption* of PEG to the copper electrode surface[13]. It suggests the formation of PEG-Cu-Cl complex in which there are only two possible types of oxygen atoms the Cu(I) could bind with (i) an ether O in the CH_2-O-CH_2 chain and (ii) a hydroxyl oxygen O at the CH_2-O-H end. Therefore, Feng et al.[13] suggested two structural models involving a Cu atom with two oxygen atoms of PEG and one chloride ligand and (ii) with one ether oxygen and one hydroxyl oxygen atom of PEG and one chloride ligand.

The kinetics of copper electrodeposition from an acidified copper sulphate (0.25M) – sulfuric acid (1.8M) electrolyte containing PEG, bis(3-sulfo-propyl) disulfide (SPS: $Na_2[SO_3(CH_2)_3S]_2$) and chloride ions also indicated that there is a competitive interaction between PEG and SPS using EIS[8, 14]. PEG and chloride ions interact with cuprous ions to form a passivating film inhibiting the metal deposition[15]. SPS accelerates the formation of cuprous complexes near the surface of the electrode such as cuprous thiolate $[Cu(I)(S(CH_2)_3SO_3H_{ad}]$ as reported from current-potential curves using a rotating Pt-disk-glassy carbon (GC)-ring electrode[15].

The effect of glue, thiourea and chloride ions on copper electrodeposition was also studied using EIS at a copper-metal rotating disk electrode (RDE)[16, 17]. It was concluded that thiourea decreases the charge-transfer resistance that was increased by the presence of glue and chloride ions.

In summary, the presence of PEG and chloride ions or glue and chloride ions in a sulfuric acid – cupric ion electrolyte polarizes the current-potential relationship. In other words, these additives increase the charge-transfer resistance. The addition to the electrolyte of MPSA, SPS or thiourea, all of which contain the thiol group, depolarizes the electrode thus compensating from the inhibition processes caused by PEG and chloride ions or glue and chloride ions. The formation of PEG-cuprous ion and MPSA- or SPS-cuprous ion complexes are proposed for surface coverage purposes[8, 14] but the actual adsorption mechanisms of these organic additives have not been discussed in detail. Despite the variety of mechanisms proposed for the smoothening effect of additives[18], a consensus exists that adsorption of the additive near the surface of the substrate plays the determining role[19, 20].

5.1.1 Equivalent Circuit for Electrochemical Systems – Copper Deposition

An electrochemical cell can be considered as an impedance to the passage of a small sinusoidal amplitude current at the exact amplitude and phase angle as the source and therefore its performance can be represented by an equivalent circuit of resistors and capacitors in parallel[1, 3]. The main objective of EIS studies is to find the frequency dependencies of resistances and pseudo-capacitances in the equivalent circuit and to transform these functions into an improved knowledge of the chemical data.

Bard et al.[1] states that it is highly unlikely the faradaic process can be represented by a simple circuit in series comprising a single resistor, R and a single capacitor, C_d, whose values are independent of frequency, but as a general impedance, Z_f. Therefore parallel elements were introduced into the equivalent circuit to account for the total current through the working electrode as the sum of the distinct contributions from the faradaic processes, i_f, and double layer charging, i_c. The double-layer capacitance, sometimes referred to as constant phase element (CPE), represented in equivalent circuits by C_{dl} or C_d, is nearly a pure capacitance[1] and is generally associated with space charge polarization regions, specific adsorption[1], surface coverages[21] and electrocrystallization[4].

As the current passes through the electrolyte, a resistance, Rs, is inserted into the equivalent circuit as a series element. In contrast to Rs and C_d, which are nearly ideal circuit elements independent of frequency, the components of the faradaic impedance are non-ideal or dependent on the frequency (ω). As a result, the faradaic impedance consists of a pure resistance, R_{ct}, the charge-transfer resistance, also known as polarization resistance, and the Warburg impedance, Z_W, described by Bard et al.[1] as "the kind of resistance to mass transfer" or diffusion impedance.

The equivalent circuit most often referred to in the literature for electrochemical interfaces is depicted in Figure 5-56[4, 22-27]. This equivalent circuit that consists *only* of resistors and capacitors is used to describe the two single-electron transfer steps[21]. This selection appears to be valid for Langmuir isotherms and other similar isotherms such as the Frumkin isotherm. This equivalent circuit was also used for copper deposition in the presence[24] and absence[25] of organic additives.

Diffusion creates impedance in the low frequency range, known as the Warburg impedance. This impedance depends on the frequency of the potential perturbation. At high frequencies, the Warburg impedance drops out because the time scale is so short that diffusion cannot manifest itself as a factor affecting the current.

At very high frequencies, the equivalent circuit is represented by Figure 5.56 - R1, R2 and C2 only since R2 and C2 lead to a time constant, τ_D=R2*C2, the dielectric relaxation time of the electrode material. The value of τ_D gives the smallest time constant of interest in EIS experiments. The condition $\omega_{max}*\tau_D \ll 1$ is satisfied for the highest angular frequency applied, ω_{max}; since τ_D is often so small, e.g., 10^{-7}s. Therefore, the impedance plane curve is not observed. As the peak frequency, ω_p conforms in the vicinity of $\omega_p*\tau_D=1$ and therefore $\omega_{max}*\tau_D \gg 1$ it is only then that almost the full curve of the impedance plane can be observed[4].

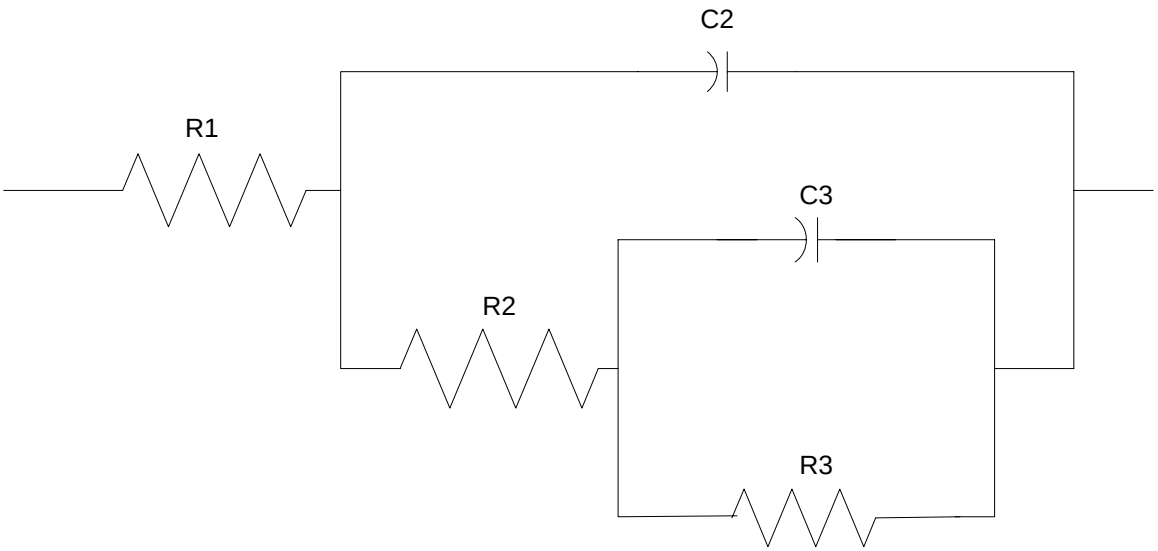

Figure 5-56: Parameters Definition in LEVM Equivalent Circuit B[28]
Legend: R1 = P(1), Electrolyte Resistance; R2 = P(4), Charge-Transfer Resistance; C3 = P(5), Double-Layer Capacitance and R3 = P(26) and C3 = P(27) are part of the Diffusion-Related Elements, the Warburg Impedance[4]. P(i) represents the parameters selected in LEVM.

The results of EIS testwork will be presented in the complex-plane plot, also known the Nyquist plot, where the imaginary and real impedance are depicted as a function of frequency. A plot of Z_{Im} vs. Z_{Re} should give a circular plot centered at Z_{Re} = R1+R2/2 and Z_{Im}=0 having a radius of R2/2 where R2 is the charge-transfer resistance, R_{ct}. The imaginary component to the impedance plotted from Figure 5-56 comes solely from the double-layer capacitance.

Figure 5-57 shows the complex-plane plot for an electrochemical system[1, 29]. The regions of kinetic and mass-transfer control are found at high and low frequencies, respectively.

The sine-wave for parallel circuits is described using the complex plane for an electrochemical cell. The total impedance characterizing the linear response of the system as a function of the oscillation frequency is given by[3, 14, 29, 30]

$$Z(\omega) = Rs + \frac{1}{\frac{1}{Z_F(\omega)} + j\omega C_{dl}} \qquad (5\text{-}24)$$

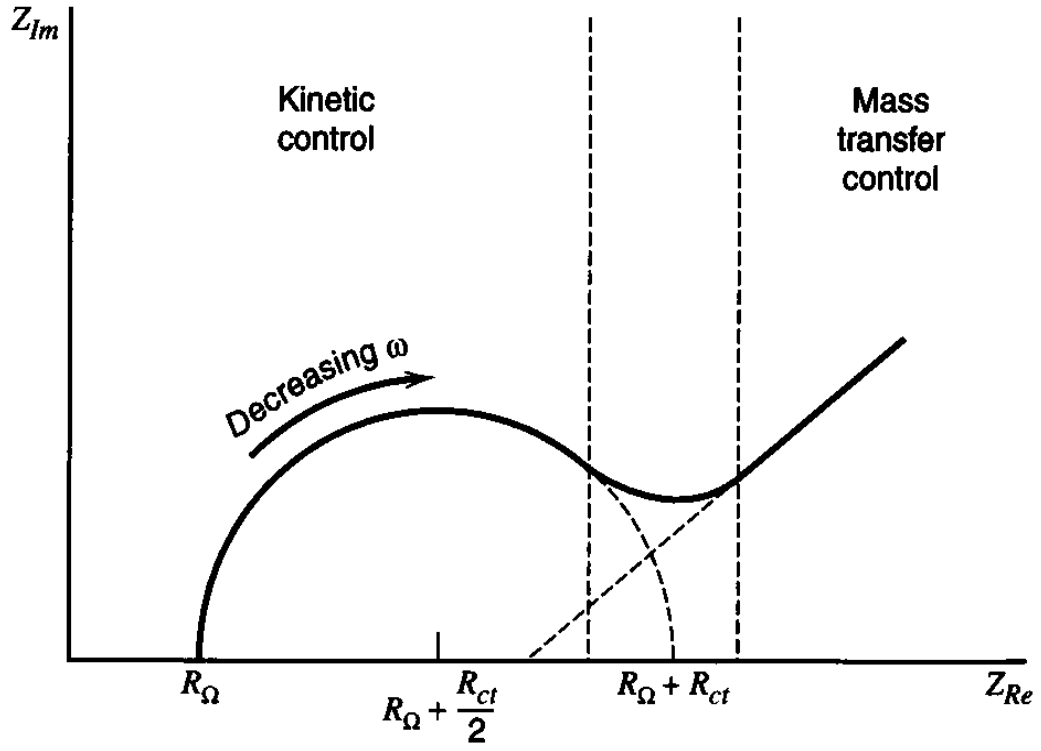

Figure 5-57: Complex-Plane Plot for an Electrochemical System

Z_{Re}, real impedance; **Z_{Im}**, imaginary impedance; **R_Ω,** electrolyte resistance (**R_s**); **R_{ct}**, charge-transfer resistance or polarization resistance and **ω**, frequency.

where Rs (or RΩ in Figure 5-57) represents the ohmic resistance of the electrolyte between the electrode surface and the reference electrode, and C_{dl} the double-layer capacitance and

$$Z_F(\omega) = \frac{\Delta V}{\Delta i_F} \qquad (5\text{-}25)$$

represents the complex faradaic impedance and it is often replaced by the charge-transfer resistance, R_{ct} for the high frequency region depicted in Figure 5-57. It is widely known that the current that flows is partly due to charging the double-layer capacity and to the faradaic reaction when the potential of the electrode is varied.

The equivalent circuit presented in Figure 5-56 will be used to conduct measurement modelling[31-34] of *all* experimental data in the presence and absence of

Guar and APAM using the commercially available software LEVM[28] and ZSimpWin™[35, 36]. LEVM and ZSimpWin™ (Princeton Applied Research) use the Levenberg-Marquardt algorithm to conduct the minimization procedure to find the set of parameters in the equivalent circuit.

5.1.2 Measurement Modelling of Electrochemical Impedance Spectroscopy Data

It is often suggested to derive the impedance as a function of the kinetic parameters for a given mechanism, and therefore data analysis should proceed from the measured impedance spectrum directly to the kinetic parameters of the postulated mechanism[21, 31]. The mechanism for copper deposition was given in Section 2.4.

The impedance measurement is valid provided that the criteria of linearity, causality, stability and finiteness are satisfied[3, 4]:

(i) The linearity of the system is defined when sum of individual input signals is equal to the sum of individual responses. Linearization of differential equations determines the impedance since electrochemical systems are usually highly nonlinear. This criteria holds with the application of a small AC amplitude such as $\Delta E < 8/n$ mV[3] peak-to-peak, where n is the number of electrons exchanged in the reaction.

(ii) A system is causal if the response of the system is entirely due to the applied perturbation,

(iii) A stable system remains invariant unless it is excited by an external source.

(iv) Finally, the real and imaginary components of the impedance must be finite valued over the entire frequency range $0 < \omega < \infty$.

Once the data is obtained, a measurement model can be conducted in which a complex nonlinear least-squares (CNLS) program is used to fit the real and imaginary parts, or the magnitude and phase angle of the experimental data to a given model. In general, the sum of squares is minimized using the following equation:

$$S(P) = \sum_{i=1}^{N} \left[w_i' \left(Z_i' - Z_{i,calc}' \right)^2 + w_i'' \left(Z_i'' - Z_{i,calc}'' \right)^2 \right] \qquad (5\text{-}26)$$

Where Z_i' and Z_i'' are the real and imaginary parts of the experimental impedances, respectively at frequency ω_i; $Z_{i,calc}'$ and $Z_{i,calc}''$ are the values calculated from the given model and w_i' and w_i'' are the statistical weights of the data. (P) represents the parameters selected in LEVM. The minimization is carried out using the iterative Marquardt-Levenberg algorithm[3, 4]. Thus the electrochemical impedance data can be directly correlated with an idealized model circuit of discrete electrical components[1, 4, 31, 37].

The EIS data in this thesis were obtained using a rotating cylinder electrode. However, a small number of tests were also conducted using a RDE to validate the RCE results. The non-uniformity of current distribution for the rotating disk electrode for finite values of the dimensionless exchange current density is widely known as is the uniformity of the current distribution for the rotating cylinder electrode[38]. Numerical calculations presented by Durbha et al.[39] demonstrated that the non-uniform current distribution observed below the mass-transfer-limited current has a significant effect on the impedance response of the rotating disc electrode when the electrode kinetics are fast and therefore the physical parameters obtained by regression models will be incorrect[39, 40].

The hydrodynamics for the RDE are well understood and hence surface concentration can be computed. The surface concentration of cupric ions on the RCE can also be calculated as described by Newman[38] and elsewhere[3, 41] and in Equation 2-11. Since planar electrodes, used in copper electrowinning and electrorefining, also have uniform current distribution[38], and since RCE's also show uniform current distribution, RCE was also used for the work described in this Chapter.

The effect of Guar and APAM will be compared in the high frequency loop only since the high frequency loop reflects the kinetic control region of a process[1]. The commercial software packages LEVM and ZSimpWin™ were used to the EIS modelling. ZSimpWin™ is often also known as the Boukamp software package in

honour of its author[35]. The statistical analysis presented in this work was conducted using LEVM. However, if poor fitting was obtained with LEVM; ZsimpWin™ was used to obtain the initial parameter values. These initial values were then used in LEVM for further iteration. ZSimpWin™ was easier to use than LEVM but the documentation for LEVM appears to be more comprehensive[4, 28].

5.2 Experimental

The electrochemical cell was a 500 mL long-necked glass beaker with a four-port lid made of Perspex depicted in Figure 5-58. A circular retaining wall, made also of Perspex, with an internal diameter similar to the external to the mouth of the beaker diameter was sealed on the bottom face of this four-port lid to immobilize it from any lateral movement. A PVC bush centred the working electrode within the electrochemical cell. This bush had an external diameter similar to the central-port diameter and internal diameter similar to the diameter of the shaft. Therefore the beaker was always centralized through the shaft and the distance between the electrodes were always kept constant.

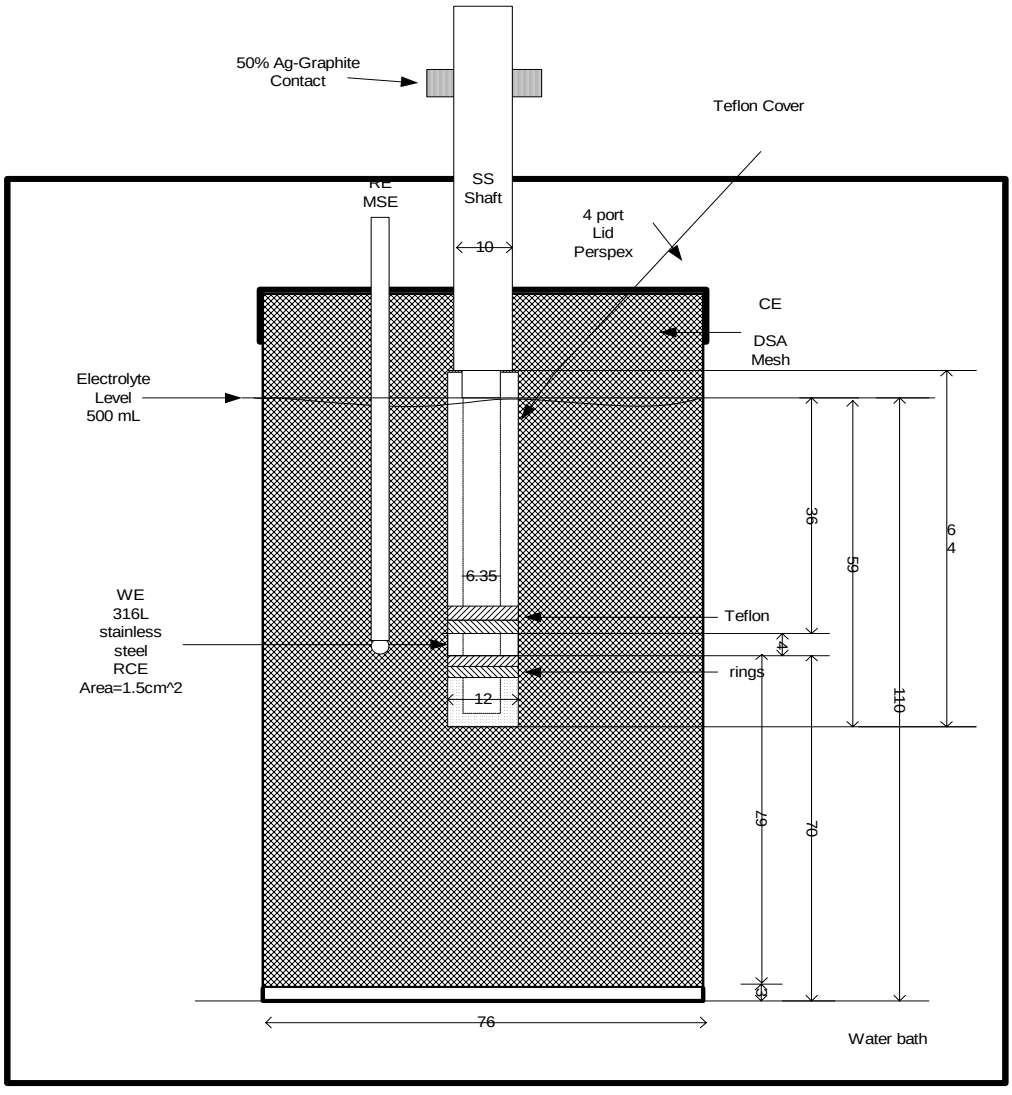

Figure 5-58: Rotating Cylinder Electrode Configuration used for CV and EIS

The cell was immersed in a water bath at either 45°C±0.5°C or 65±0.5°C. Evaporation was made up with water at about 1.4mL (45°C) and 7mL (65°C) per hour, respectively. The working electrode (WE) was a 316L stainless steel rotating cylinder electrode (RCE) sourced from Pine Instruments (QC3 series – ACQ012CY316). However, the original WE surface area was reduced to a $2cm^2$ surface area to conduct CV tests and to $1.5cm^2$ to conduct EIS tests. The smaller surface area produced less induction at the high frequency end where the frequency count starts. A mercurous-mercuric sulfate electrode (MSE, 651 mV vs. NHE) in saturated potassium sulfate from Radiometer Analytical was used as a reference electrode.

The counter electrode was prepared from dimensionally stable anode (DSA, a titanium-based substrate coated with ruthenium dioxide or iridium dioxide), sourced from Eltech Systems Corp. DSA is the standard anode for generating chlorine in the chlor-alkali, chlorate and hypochlorite industries where it has very long lifetimes. The DSA surrounded the internal wall of the 500mL long-necked beaker. The working electrode was initially polished with 1μm and 0.25μm diamond paste (Struers). After every test it was polished with the latter only, washed with distilled water and acetone, rinsed in an electrolyte solution and rinsed again with distilled water. Table 5-22 shows the experimental conditions for CV and EIS experiments.

The aim of the experimental design was to approximate the diffusion layer thickness of a commercial scale electrowinning plant as suggested in a computational fluid dynamic study by Filzwierser et al.[42]. The rotation speed of the RCE at 25rpm and at temperatures from 25°C to 65°C gives a Reynolds number ($Re=\omega d^2/2\nu$) from 48 to 527. At this rpm and temperature range the Taylor (Ta) number varies from 932 to 1804. It is reported that the critical Reynolds number is 200 for the RCE[43] and therefore radial and axial motion is superimposed on the tangential flow across the electrolyte[38, 44]. This can been seen in Figure 5-59. The Reynolds and Taylor numbers therefore appear to indicate that the flow regime at 25 rpm and 45°C - 65°C is laminar with vortexes. Deposition conditions such as electrolyte composition, temperature and current density also simulate commercial scale conditions.

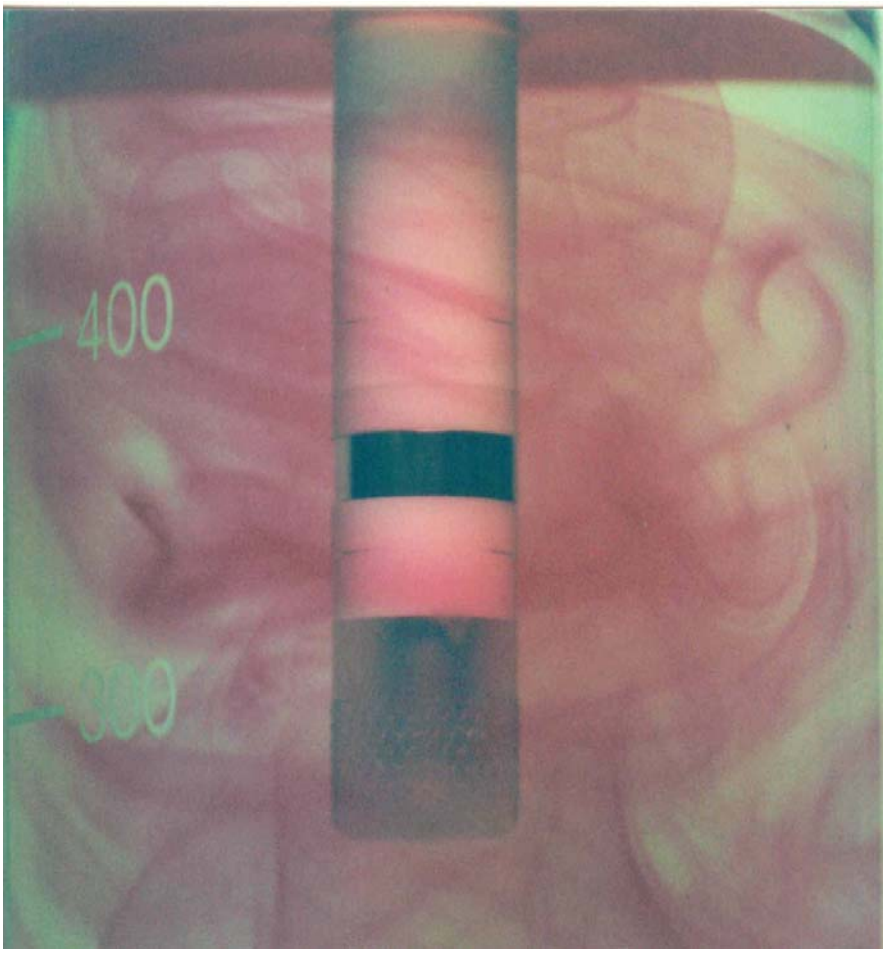

Figure 5-59: Fluid Flow Produced by the RCE at 25rpm and 25°C in Water

The critical Reynolds number ($Re = \omega * d^2/2\nu$) at 25°C is 200[43]. The Reynolds number for the copper electrolyte at 45°C and 25rpm is 204.

The experimental conditions for the CV tests are summarized in Table 5-22. These tests were conducted to determine the polarization behaviour of Guar and APAM on 316L stainless steel and on copper pre-plated onto 316L stainless steel at 10mA/cm^2 for 225 seconds.

The EIS tests were conducted in potentiostatic mode. The EIS tests were always conducted on pre-plated copper[8] formed as follows: chronopotentiometry for 360 seconds at 10mA/cm^2 current density to pre-plate copper, followed by automatic stabilization for 15 seconds at the potential to be applied during the EIS experiment followed by the EIS test itself. The EIS tests were run using 6mV AC over the

frequency range from 30kHz to 0.2Hz using the RCE and 50kHz – 0.2Hz using the RDE. Preliminary tests were run using 8mV AC and the impedance data obtained were similar to those observed using 6mV AC. Therefore, it was confirmed that the system was linear[3].

Table 5-22: Experimental Conditions for CV and EIS Experiments

Copper, g/L	36
Sulfuric acid, g/L	160
Chloride ions, mg/L	25
Guar Preparation Media	Water at 25°C
APAM Preparation Media	16-fold DE
APAM Preparation Media Temperature, °C	50
Electrolyte Volume, mL	500
APAM Concentration in Electrolyte, mg/L	2
RCE rpm	10 and 25
Copper Pre-plating Time for CV and EIS, respectively, sec	225 and 360
Current Density during Pre-plating, mA/cm^2	10
Electrolyte Temperature, °C	45 and 65
Sweep rate, mV/sec	1
Diffusion Layer Thickness for ***CV*** using RCE, at ***10 rpm***, μm*	90 (110)
Diffusion Layer Thickness for ***EIS*** using RCE, at ***25rpm***, μm*	87 (99)
Outer Cylinder Diameter, cm	7.6
Inner (rotating) Cylinder Diameter, cm	1.2
WE (316L Stainless Steel) surface area for CV, cm^2 [Set up: Potential 0 = -370 mV, Potentials 1 and 2 = -725mV vs. MSE]	2
WE surface area for EIS using RCE and RDE, respectively, cm^2	1.5 and 0.178
Schmidt Number (ν/D) for EIS at 45°C and 65°C, respectively	1005 and 435

*Diffusion layer thickness at 45°C and 65°C in brackets.

The pre-plating process of copper onto the stainless steel at 10mA/cm^2 was done to obtain a smooth deposit and to plateau the surface overpotential. The potential of the working electrode was fixed at -470 mV vs. MSE or 300 A/m^2 (30mA/cm^2) and -490mV vs. MSE 340 A/m^2 (34mA/cm^2) current density at steady-state conditions in the absence of APAM and Guar. All tests were replicated at least twice. The reference electrode was located about 1.5cm away from the WE to maintain a uniform velocity of the electrolyte around the electrode. This experimental configuration was similar to that reported by Kelly[8].

5.3 Cyclic Voltammetry in the Presence of Guar at 45°C

These tests were conducted to determine the polarization behaviour of Guar during copper electrodeposition on bare 316L stainless steel and on pre-plated copper at 10mA/cm^2 for 225 seconds. The pre-plating process achieves a constant overpotential over this period. These tests determined how the polarization behaviour varied when Guar was aged in the electrolyte heated at 45°C over a 5-hour period.

The initial cathodic scan of the cyclic voltammetry curves are presented in Figure 5-60. The left and right-sets of curves were obtained on stainless steel (SS) and on pre-plated copper (Cu), respectively. Each curve was sequentially obtained every hour starting with the bare stainless steel electrode after about 20minutes once Guar was dosed and followed with the pre-plated copper electrode and so on up to five hours. Therefore, CVs on stainless steel were conducted at 0.3, 2, and 4-hours and on pre-plated copper at 1, 3, and 5-hours.

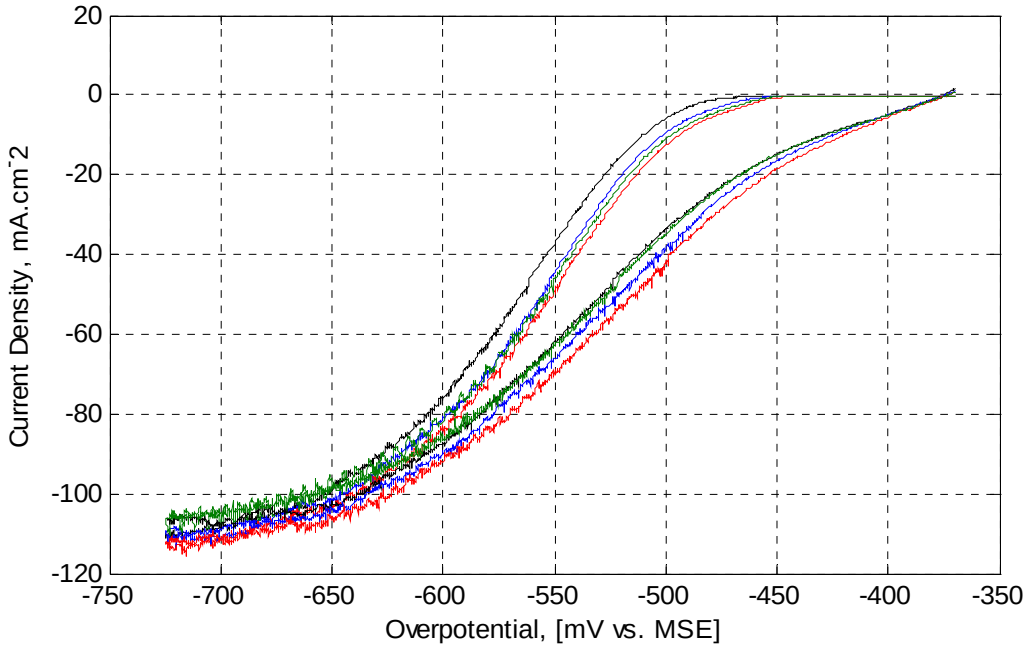

Figure 5-60: Effect of Guar Residence Time on Depolarization at 45°C.

Legend: Left-Set of Curves on Stainless Steel and Right-Set of Curves on Pre-plated Copper: Control (without Guar) – Black; 0.3 (SS) and 1Hr (Cu) – Blue; 2 (SS) and 3Hrs (Cu). – Red; and 4 (SS) and 5Hrs (Cu) – Green.

It can be seen that Guar de-polarized the electrode on both stainless steel and pre-plated-copper. This is based on the observation that the electrode potential in the presence of an additive is less negative than the potential without the additive at a determined current density. It can also be seen that there is a trend in the depolarization behaviour. Polarization increases from the 0.3-1hr to a maximum in 2-3hours and then its depolarizing activity decayed such that within 4-5hours an insignificant effect can be observed on pre-plated copper.

The limiting current density remains about constant in the presence and absence of Guar as others have observed in the presence of PEG and chloride ions[9, 11]. Figure 5-60 also indicates that less energy is required to plate on fresh copper-metal formed than on the stainless steel substrate. The same preferential deposition was obtained with PEG and chloride ions when the working electrode was made of copper metal[9]. This preferential deposition is probably due to the reduced activation energy required to nucleate on fresh copper-metal and the growth may also follow the Stranski-Krastanov mode where 3D copper metal islands form on top of the pre-deposited 2D copper overlayers[45] described in Chapter 2 – Section 2.5.1.

CV and EIS tests were found to be more reproducible on pre-plated stainless steel than on bare-stainless steel. Kelly et al.[8] also reported that EIS tests on pre-plated copper metal WE for 3minutes were more reproducible than on unpre-plated WE. This effect is probably due to the crystallographic misfit between 316L stainless steel and the freshly plated copper metal. This pre-plating process would simulate commercial electrowinning and electrorefining operations on 316L stainless steel since traces of copper are always left behind after the copper plate is stripped off.

Table 5-23 presents the depolarization data at 30mA/cm^2 (300Amp/m^2) current density extracted from Figure 5-60. Figure 5-61 depicts the extracted data and indicates that a maximum depolarization of approximately 14mV was obtained at 2-3 hours residence time whether on stainless steel or copper metal.

The polarization curves in the presence and absence of Guar were also used to calculate the potential at zero current (Ei=0), the (cathodic) Tafel slope (b) and the transfer coefficient (α). These values are shown in Table 5-24 for pre-plated copper

only. It can be seen that the potential at zero current appears to follow the overall polarization pattern of the aging of Guar in the electrolyte. The most important result in Table 5-24 is the transfer coefficient value of 0.50 in the absence of Guar. This agrees with that given by Wu and Barkey[46] and Mattson and Bockris[47].

Table 5-23: De-polarization Behaviour of Guar at 45°C

On Stainless Steel		On Pre-plated Copper	
Residence Time, Hrs	Potential, mV vs. MSE at 30 mA/cm^2 Current Density,	Residence Time, Hrs	Potential, mV vs. MSE at 30 mA/cm^2 Current Density,
0(Nil Guar)	-541	0(Nil Guar)	-493
0.3	-533	1	-484
2	-527	3	-478
4	-530	5	-491

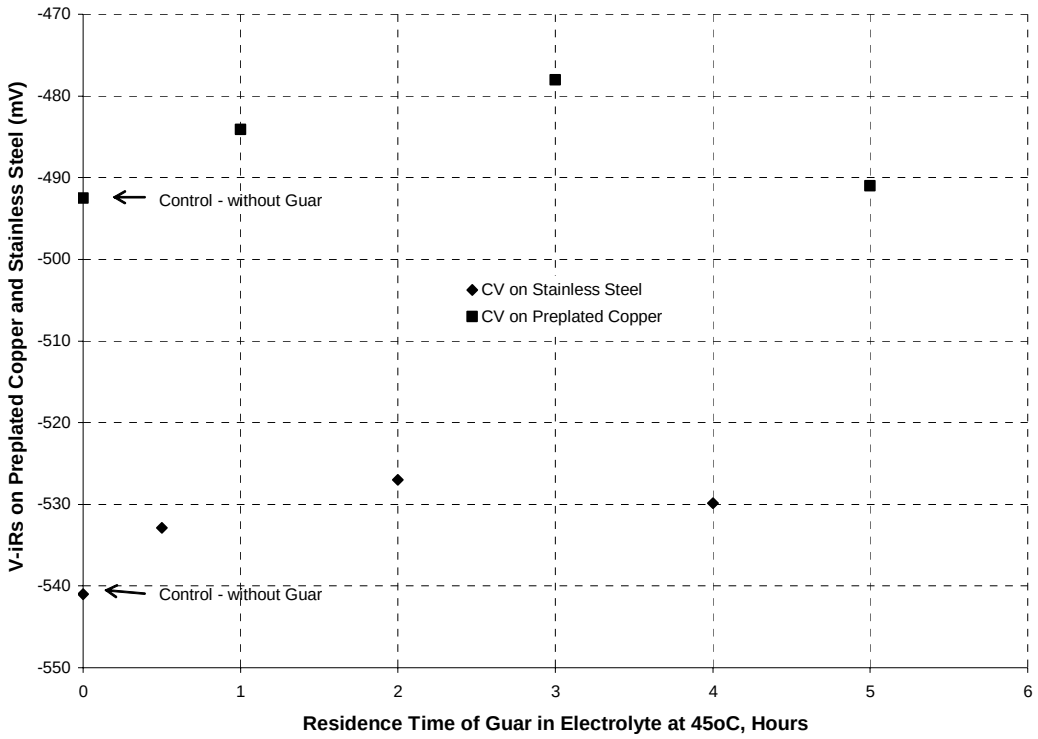

Figure 5-61: Effect of Time on the De-polarization Behaviour of Guar at 45°C at 300A/m^2 Current Density.

Table 5-24: Kinetic Parameters for Copper Deposition in the Presence of Guar at 45°C

Residence Time, Hours	E(i=0) mV vs. MSE	Tafel Slope, mV b	Transfer Coefficient α [=2.3R*T/(b*F)]
0 (Nil Guar)	-375.3	-127.1	0.50
1	-374.4	-122.6	0.52
3	-373.0	-123.6	0.51
5	-373.2	-125.9	0.50
Wu and Barkey[46]		-122	0.5 ± 0.05

5.4 Cyclic Voltammetry in the Presence of Activated Polyacrylamide at 45°C

These tests were conducted to determine the polarization behaviour of APAM during copper electrodeposition on bare 316L stainless steel and on pre-plated copper at 10mA/cm^2 for 225 seconds.

Figure 5-62 shows the results obtained at 45°C in the presence and absence of APAM. It indicates that APAM polarizes or inhibits the working electrode whether it is stainless steel or pre-plated copper. It can also be seen that APAM appears to confer higher adsorption on pre-plated copper electrode than on stainless steel since the polarization values are higher for pre-plated copper than that for the stainless steel electrode. This result contrasts with those of Vereecken and Winand[48] who found that polyacrylamide did not polarize the electrode when it was prepared in water and in full-strength electrolyte. It is therefore concluded that the preparation of APAM, i.e., the formation of block copolymers, confers an increase of the adsorption and therefore the polarization of the working electrode.

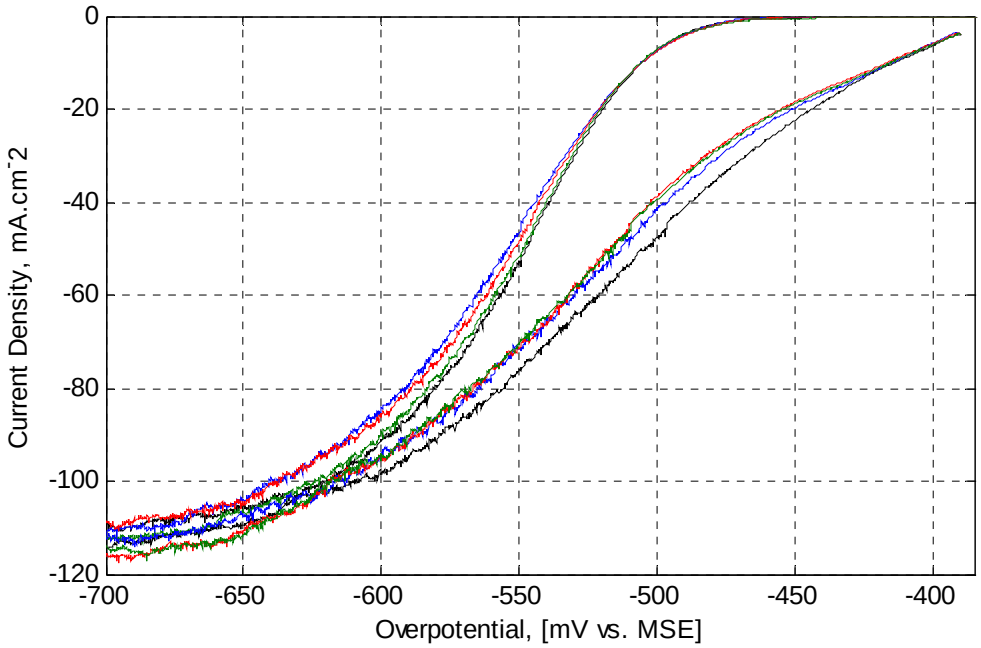

Figure 5-62: Effect APAM Residence Time on Polarization at 45°C.

Legend: Left-Set of Curves on Stainless Steel and Right-Set of Curves on Pre-plated Copper: Control (without APAM) – Black; 0.3 (SS) and 1 Hr. (Cu) – Blue; 2 (SS) and 3 Hrs. (Cu) – Red; and 4 (SS) and 5 Hrs. (Cu) – Green.

Table 5-25 shows the data extracted from Figure 5-62 for stainless steel and pre-plated copper at 300 and 400A/m^2. Figure 5-63 depicts the data from Table 5-25 for pre-plated copper only since it closely reflects a commercial application as discussed previously. A maximum polarization of 14mV is observed at 3 hours residence time.

Table 5-25: Polarization in the Presence of APAM at 45°C

On Stainless Steel			On Pre-plated Copper		
Residence Time, Hours	Potential, mV vs. MSE Current Density, mA/cm^2		Residence Time, Hours	Potential, mV vs. MSE Current Density, mA/cm^2	
	30	**40**		**30**	**40**
0 (No APAM)	-529	-538	0 (No APAM)	-468	-489
0.3	-533	-544	1	-477	-497
2	-532	-543	3	-482	-503
4	-531	-540	5	-481	-502

Figure 5-63 shows that the presence of APAM results in a significant polarization of the electrode over the 5-hour experimental period. These results are consistent with APAM acting as a surfactant/levelling agent and doing so for extended

period of time, which is consistent with the results described in Chapters 3 where 1mg/L APAM was dosed once for 6 hours electrowinning time.

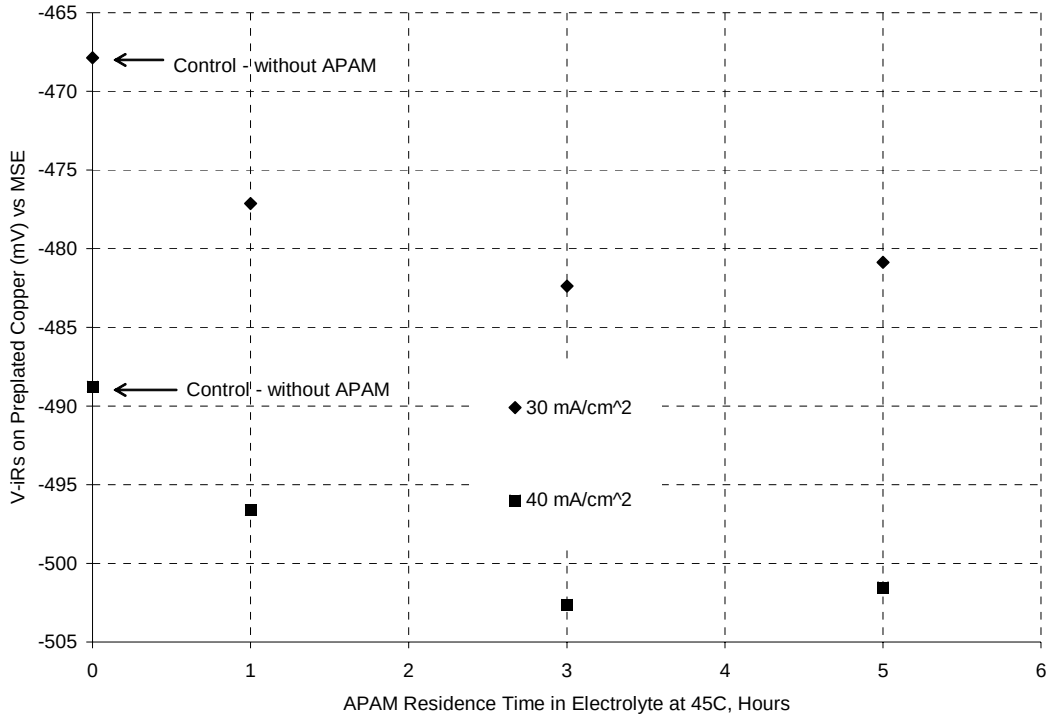

Figure 5-63: Effect of APAM Ageing on Polarization on Pre-plated Copper at 45^{o}C

5.5 Cyclic Voltammetry in the Presence of Activated Polyacrylamide at 65^{o}C

These tests were conducted at the temperature used in copper electrorefining[49]. Figure 5-64 shows the results in the presence of APAM at 65^{o}C. It can be seen clearly that the polarization behaviour of APAM increases with time giving a maximum polarization in the first hour (blue colour). Table 5-26 shows the potentials at 300 and 400 A/m^2 extracted from Figure 5-64. Figure 5-65 depicts these values.

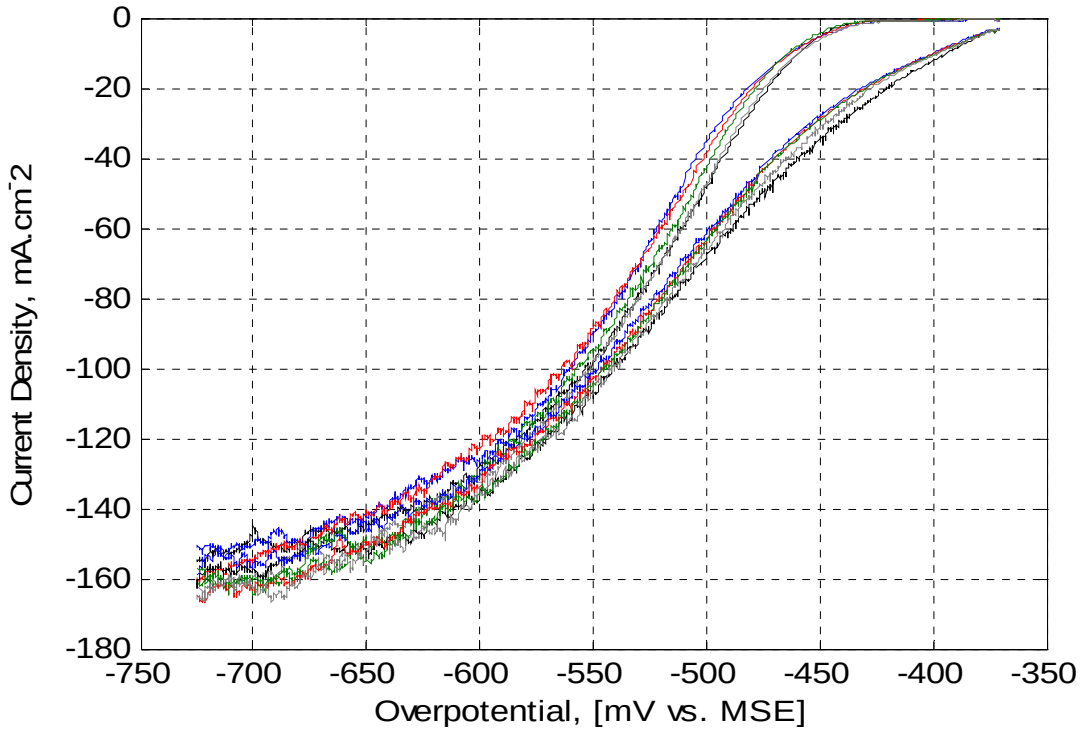

Figure 5-64: Effect of APAM Residence Time on Polarization at 65°C and 10rpm.

Legend: Left Set of Curves on Stainless Steel and Right Set of Curves on Pre-plated Copper: Control (without APAM) – Black; 0.3 (SS) and 1 Hr (Cu) – Blue; 2 (SS) and 3 Hrs.(Cu) – Red; 4 (SS) and 5 Hrs.(Cu) – Green; 6 (SS) and 7 Hrs.(Cu) – Grey.

Figure 5-64 shows that the presence of APAM results in a significant polarization of the electrode over a 7-hour period, with the polarization reaching a maximum of 13mV at 1hr residence time at 300A/m^2. It can also be noted that APAM appears to confer higher adsorption on pre-plated copper than on stainless steel since the net polarization values are higher for pre-plated copper than for stainless steel. This preferential adsorption on pre-plated copper was also observed at 45°C. Once again, these results indicate that APAM acts as a levelling agent for extended periods of time. The effectiveness of APAM is also dependent on the temperature. It has been shown in Sections 4.3.1 and 4.3.2 that APAM in the temperature range of 45°C- 65°C had the highest significant effect on reducing surface roughness than in the temperature range of 45°C-55°C. This result is also consistent with those described in Chapter 4 where APAM was dosed once for 6 hours electrowinning time and produced smoother copper deposits than Guar.

Table 5-26: Polarization in the Presence of APAM at 65°C

On Stainless Steel			On Pre-plated Copper		
Residence Time, Hours	Potential, mV vs. MSE Current Density, mA/cm2		Residence Time, Hours	Potential, mV vs. MSE Current Density, mA/cm2	
	30	40		30	40
(0) No APAM	-484	-493	(0) No APAM	-441	-459
0.3	-494	-505	1	-454	-472
2	-492	-501	3	-453	-470
4	-489	-499	5	-452	-470
6	-485	-494	7	-448	-464

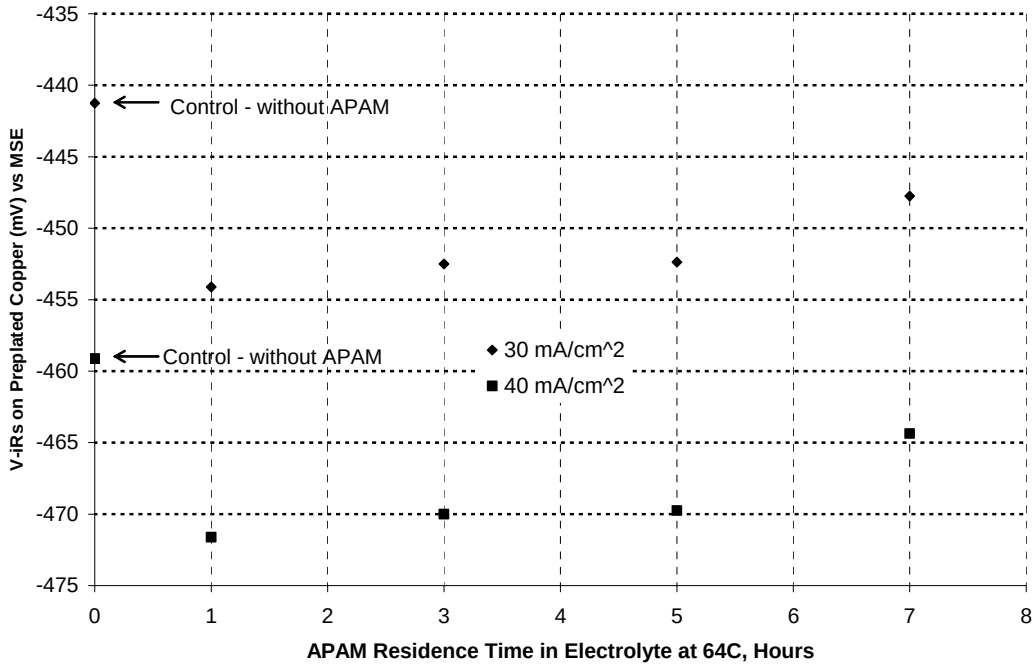

Figure 5-65: Polarization of APAM on Pre-plated Copper at 65°C

The maximum polarization at 45°C and 65°C is approximately 14mV but the time to attain this maximum value is about 3.5 hours at 45°C and 1.5 hours at 65°C as shown in Figure 5-66.

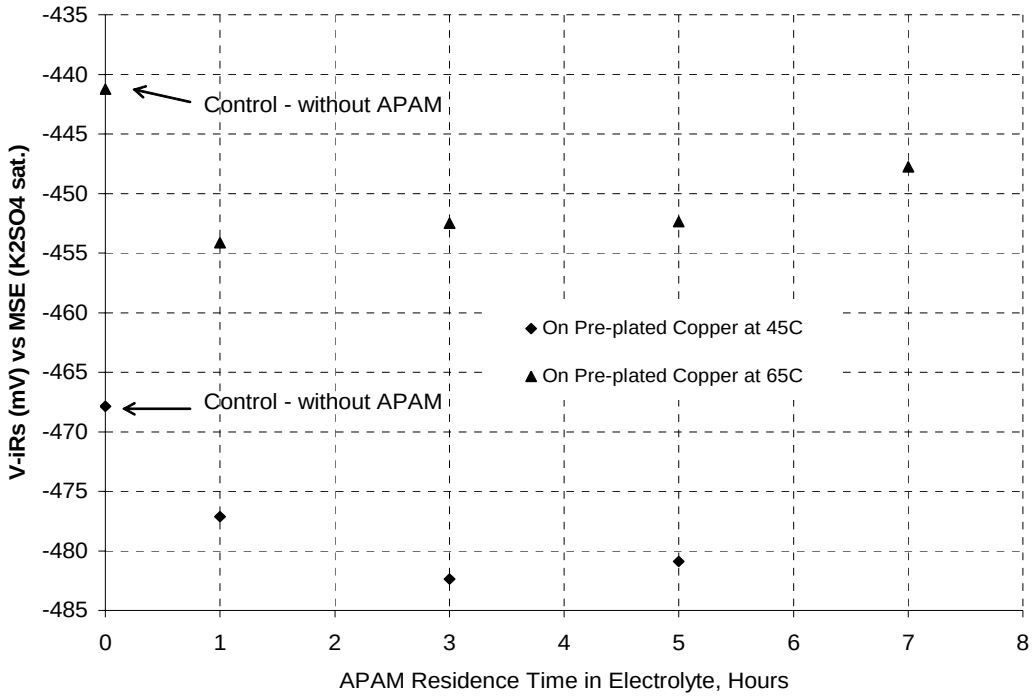

Figure 5-66: Effect of Temperature on APAM Polarization at 300 A/m^2 and 45^{o}C and 65^{o}C

5.6 Electrochemical Impedance Spectroscopy Results in the Absence of Additives

Preliminary tests were conducted to compare the results of this work with those presented in the literature in the absence of organic additives[8]. Figure 5-67 shows experimental data at two potentials (-470 and -490mV versus MSE) as open symbols and data fitted to the equivalent circuit shown in Figure 5-56 produced by LEVM as solid lines.

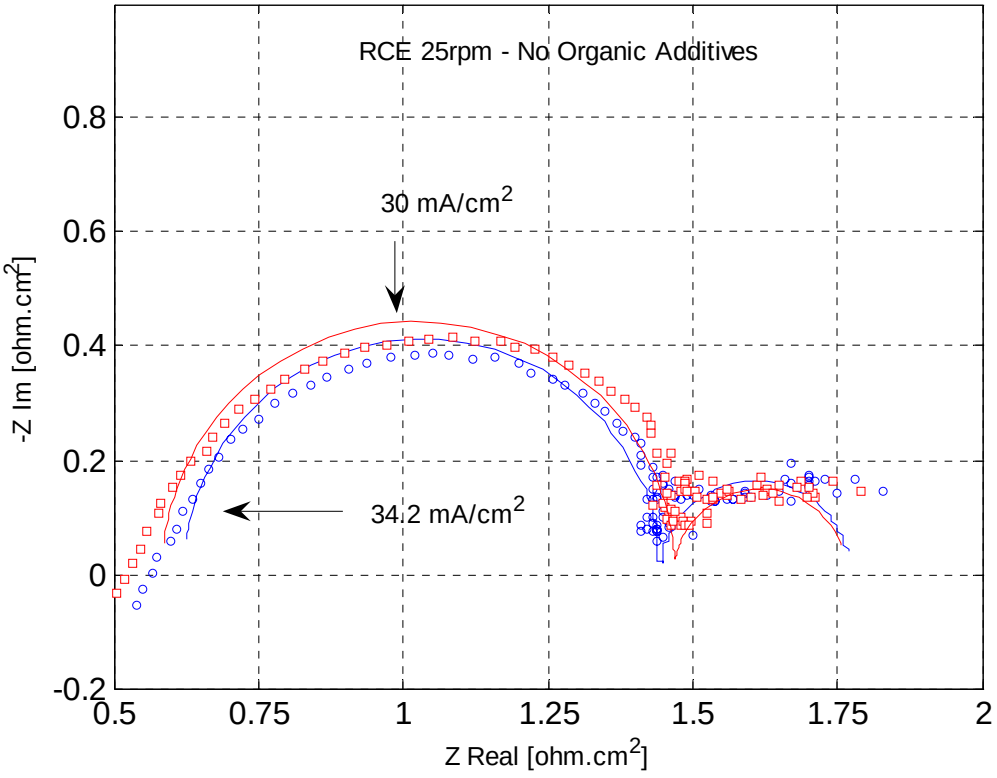

Figure 5-67: Complex-Plane Plot of Experimental and Simulated EIS data at -470 (30mA/cm^2 - red) and -490mV (34.2mA/cm^2 - blue) vs. MSE and 45^{o}C in the Absence of Organic Additives. Charge-Transfer Resistance, R_{ct} in the High Frequency loop, at 25 rpm and 30mA/cm^2 = 1.45ohm.cm^2 and at 25rpm and 34.2mA.cm^2 = 1.4ohm.cm^2.

It can be seen that the data can be reasonably interpreted in terms of an equivalent circuit as shown in Figure 5-56 which results in the prediction of two loops. The predicted two loops are the results of resistors and capacitors in parallel.

The results shown in Figure 5-67 are in agreement with studies of adsorbed species undergoing a single electron transfer step. Such reaction have been shown to have equivalent circuits that consist only of capacitors and resistors and exclude inductive behaviour[21]. This conclusion is valid for the Langmuir isotherm[21] and possibly for the Frumkin isotherm. The capacitor is often known as the constant phase element (CPE) to describe different electrochemical phenomena such as double-layer capacitance, adsorption and surface coverage[21]. The adsorption of polyacrylamide in acid solutions follows the Frumkin isotherm slightly better than the Langmuir isotherm according to Grchev et al.[50].

Figure 5-67 correlates with the experimental work in the published literature[8, 14, 17, 51-53] where RDEs were used in terms of the electrolyte resistance and the charge-transfer resistance, Rct, in the high frequency loop. However, measurement modelling or regression analysis was absent from the above published literature, except from the work of Fabricus et al.[17]and Chassaing et al.[52]. It has been recently stated that the inherent non-uniform primary current distribution of the rotating disc electrode precludes measurement modelling[40].

The results presented in Figure 5-67 will be compared with those in the literature to confirm the validity of EIS spectra recorded with the RCE. However, since there are no RCE data in the literature except the data from Nava et al.[25] who used 15.7mM cupric ions in 1M H_2SO_4; this comparison will be made with data recorded with RDE's in the literature.

It can be seen in Figure 5-67 that the electrolyte (0.567M $CuSO_4$, 1.6M H_2SO_4 and 25mg/L chloride ions at 45^oC) resistance is about 0.6ohm.cm^2 where the curve crosses the imaginary impedance (See Figure 5-57). This result correlates well with that of Kelly et al.[8] who reported 0.5ohm.cm^2 for 0.25M $CuSO_4$, 1.8M H_2SO_4 and 50mg/L chloride ions using a RDE at 25^oC.

Figure 5-67 indicates that at 45^oC the R_{ct} from the simulated data at 25 rpm and 30mA/cm^2 is equal to 1.45ohm.cm^2 and at 25rpm and 34.2mA/cm^2 is equal to 1.4ohm.cm^2. It would be expected that the R_{ct} would decrease at the higher current density, as is observed.

The charge-transfer resistance, Rct, for the high frequency loop can also be obtained from the studies of Kelly et al.[8] and Gabrielli et al.[14] Kelly et al.[8] obtained R_{ct} values of about 1.97ohm.cm^2 at 400rpm and 36mA/cm^2 and 1.47ohm.cm^2 at 2500 rpm and 43mA/cm^2. These values do not exactly correlate with the data produced by Gabrielli et al.[14] who obtained 1.7ohm.cm^2 at 100 rpm and 25mA/cm^2 using also a RDE at 25^{o}C for the same cupric ions and sulfuric acid concentrations as used by Kelly et al.[8] but with a concentration of chloride ions of 35mg/L.

The R_{ct} results presented in this section with the RCE broadly correlate with the Rct data reported in the preceding paragraph where RDEs were used. The RCE results at 25rpm (laminar flow with 2-3 vortexes)[54] and with 0.567M $CuS0_4$ in 1.6M H_2SO_4 at 45^{o}C gave faster copper deposition kinetics (lower R_{ct} value) than the RDE (laminar flow) data obtained from 0.25M $CuSO_4$ in 1.8M H_2SO_4 at 25^{o}C as would be expected given the lower concentration of cupric ions and temperature in the latter study.

The low frequency loop is more complex and less understood in terms of the number and nature of the parameter values. It depends on the surface preparation of the substrate, growth mode[55] of the deposit including its crystallographic orientation, hydrodynamic conditions and current density[56]. The cylindrical diffusion produced by the rotating cylinder electrode results in the relatively constant imaginary impedance component[3, 41] and therefore the RCE appears highly sensitive to surface roughness in the low frequency range as will be shown in the next Sections. It is stated by Macdonald[4] that the roughness of an electrode may lead to a frequency dispersion of the interface, the lines of electric force do not converge evenly on that surface and therefore the double-layer will be charged unevenly.

The simulated data of the low frequency range in Figure 5-67 also shows the difference between the diffusion of cupric ions across the concentration boundary layer: more cupric ions at 30mA/cm^2 yields a reduced amount of charge-transfer resistance than that at 34.2 mA/cm^2. This observation is similar to that presented by Kelly[8].

It is therefore concluded that EIS data presented in this thesis using the RCE are valid. The results are in agreement with mechanistic studies for single electron transfer

steps that have equivalent circuits that consist only of capacitors and resistors and exclude an inductive loop. The charge-transfer resistance values for the high frequency loop are consistent with the rate of copper deposition at different current densities.

The noise level predominantly observed in the low frequency region in the present study appears be inherent to deposition processes since the nucleation and growth of the deposit is different in the presence and absence of organic additives. This hypothesis will be shown in the following Sections where the presence and absence of both Guar and APAM are evaluated.

5.7 Electrochemical Impedance Spectroscopy Results in the Presence of Activated Polyacrylamide at -470mV vs. MSE and 45°C

These tests were conducted to determine the effect of APAM ageing on the kinetics of copper deposition. The EIS tests on freshly plated copper were carried out every hour for 7-hours.

Figure 5-68 presents the EIS response over the 7-hour period and shows a sequential increase of the charge-transfer resistance in the high frequency ranges. The monotonic increase in the high frequency range is possibly due to the ageing process of APAM in the cupric ion-sulfuric acid electrolyte at 45°C, i.e., additional hydrolysis of the block copolymer backbone and reduction of its molecular weight. Grchev et al.[50] found the surface coverage at 2-3ppm polyacrylamide concentration decreased from about 0.52, 0.3, 0.2 to 0.02 as the polyacrylamide molecular weight increased from $5x10^3$, $2.2x10^4$, $2.25x10^5$ and $1.5x10^6$, respectively. (see also Section 2.6.3 – Polyacrylamide Adsorption Mechanism). It was also found by Radeva et al.[57] that the adsorbed layer thickness of 4% and 12% hydrolysed polyacrylamide has a *flatter* conformation than that of nonionic or neutral polyacrylamide.

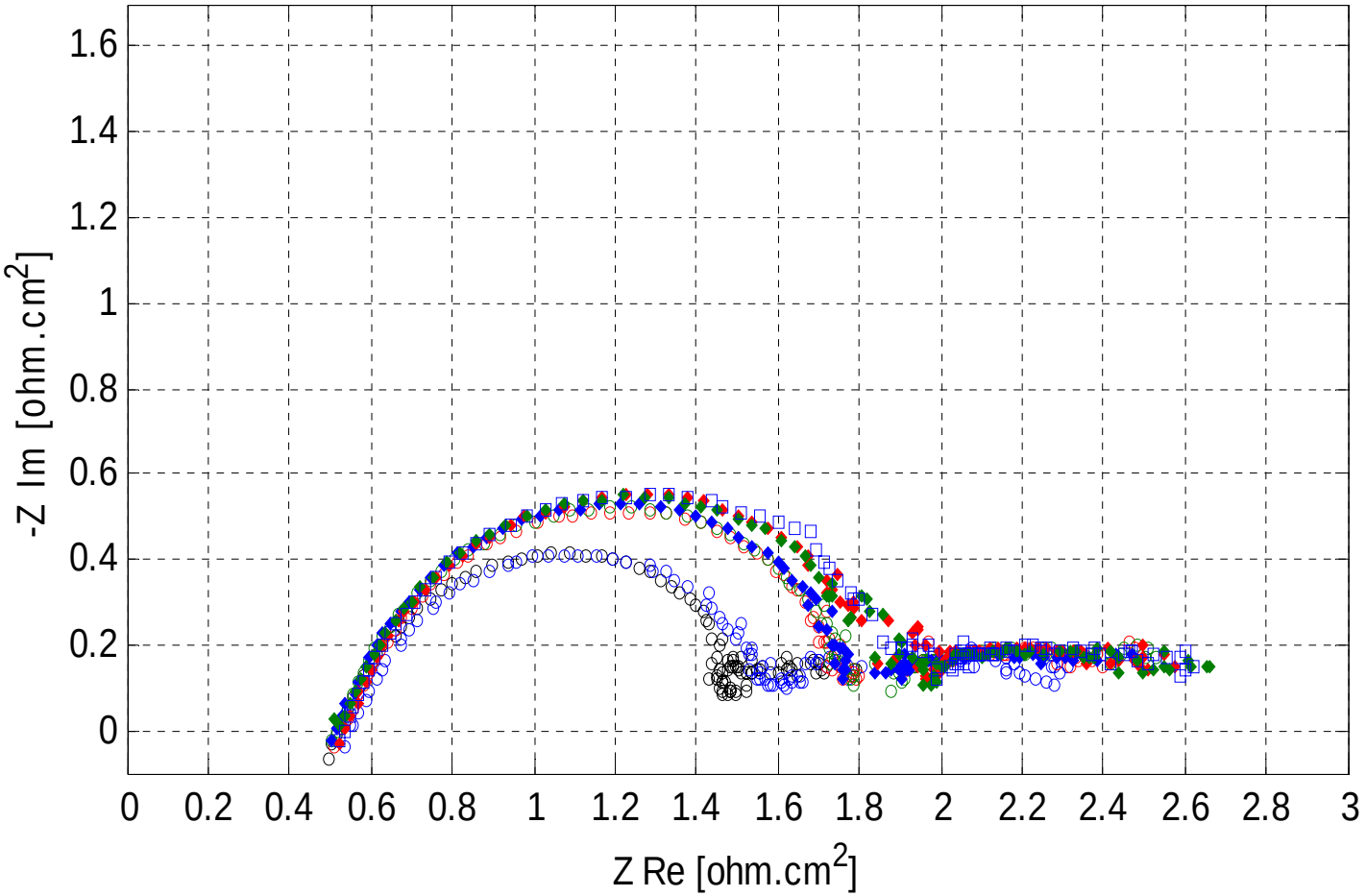

Figure 5-68: Complex-Plane Plots of Experimental EIS in the Presence and Absence of APAM at -470mV vs. MSE and 45°C
Legend: o - Black – Control – without APAM; o blue, 0.5 Hrs; o red, 1Hr; o green, 2Hrs; ♦ blue, 3Hrs; ♦ red, 5 Hrs; ♦ green, 6 Hrs and □ blue, 7 Hrs Residence Time of APAM in Electrolyte at 45oC. Overpotential: 93mV vs. SHE.

Figure 5-68 also shows that in the low frequency range, Z_{Im} is approximately constant or changes very slowly. This is consistent with the work of Lasia[3] and Jacobsen[41] who solved the cylindrical diffusion equations and concluded that cylindrical diffusion gives an almost constant imaginary impedance component in the low frequency range.

Figure 5-69 shows a subset of the experimental data (dots) from Figure 5-69 and simulated data (line) at -470mV versus SME (93mV vs. SHE) which corresponds to about 30mA/cm^2 in the absence of APAM. Two data sets are presented; one in the absence of APAM and the other is for the experiment after 2 hours residence time of APAM in the electrolyte.

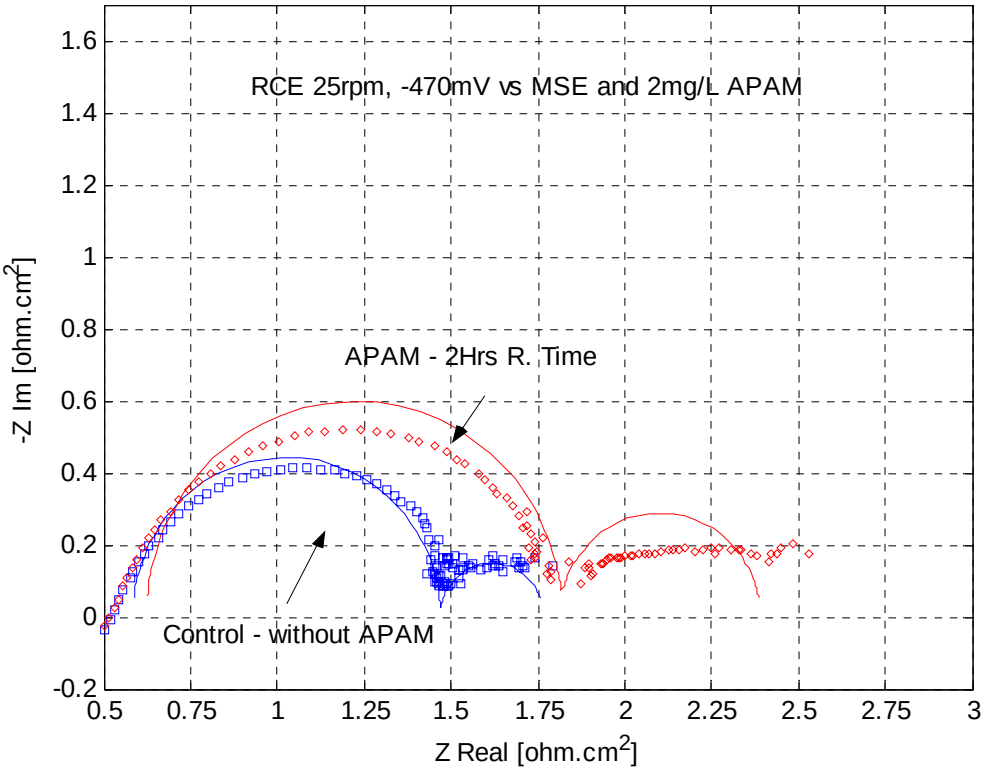

Figure 5-69: Complex-Plane Plot of Experimental and Simulated Impedance Spectra in the Presence and Absence of APAM at -470mV versus MSE and 45°C. Overpotential: 93mV vs. SHE.

Table 5-27 shows the variation of the calculated charge-transfer resistance, double-layer capacitance and current density in the presence and absence of APAM for

periods up to seven hours residence time of APAM in the electrolyte. Table 5-27 also shows that the current density decreased in the presence of APAM. Figures 5-70 and 5-71 depict the effect of time on the value of these parameters. LEVM[28], ZSipmWin™[36] and Voltamaster4[58] give approximately the same parameter values for the high frequency loop. The low frequency loop is more complex and less understood since the fitting process fails to simulate the cylindrical diffusion produced by the rotating cylinder electrode. However the difference between the presence and absence of APAM can be assessed qualitatively in the low frequency loop: APAM also increases diffusion impedance, "the kind of resistance to mass transfer"[1].

Table 5-27: Results for APAM at 45°C and -470mV CD versus MSE

	Charge-Transfer Resistance (P4)		Double-Layer Capacitance (P5)		C. Density
Hours	Ohm.cm^2	Std. Dev.	μF/cm^2	Std. Dev.	mA/cm^2
0(Nil)	0.89	1.43E-02	1.04E-04	3.80E-07	30
0.5	0.96	1.98E-02	1.01E-04	5.23E-07	27
1	1.16	1.47E-02	9.57E-05	3.87E-07	27
2	1.20	1.46E-02	9.57E-05	3.84E-07	25
3	1.20	1.39E-02	8.98E-05	3.64E-07	26
5	1.26	1.41E-02	9.52E-05	3.74E-07	25
6	1.27	1.44E-02	9.37E-05	3.80E-07	25
7	1.31	1.35E-02	9.51E-05	3.56E-07	25

The main elementary phenomena which take place at the electrode interface are the heterogeneous kinetics of the two one-electron steps reactions, mass transport and above all diffusion. It is not clear whether species adsorbed on the surface including APAM are located on macroscopic areas where the reactant species diffuse through the Nernst layer or that the species including APAM are adsorbed on active sites, i.e., the protruding sites.

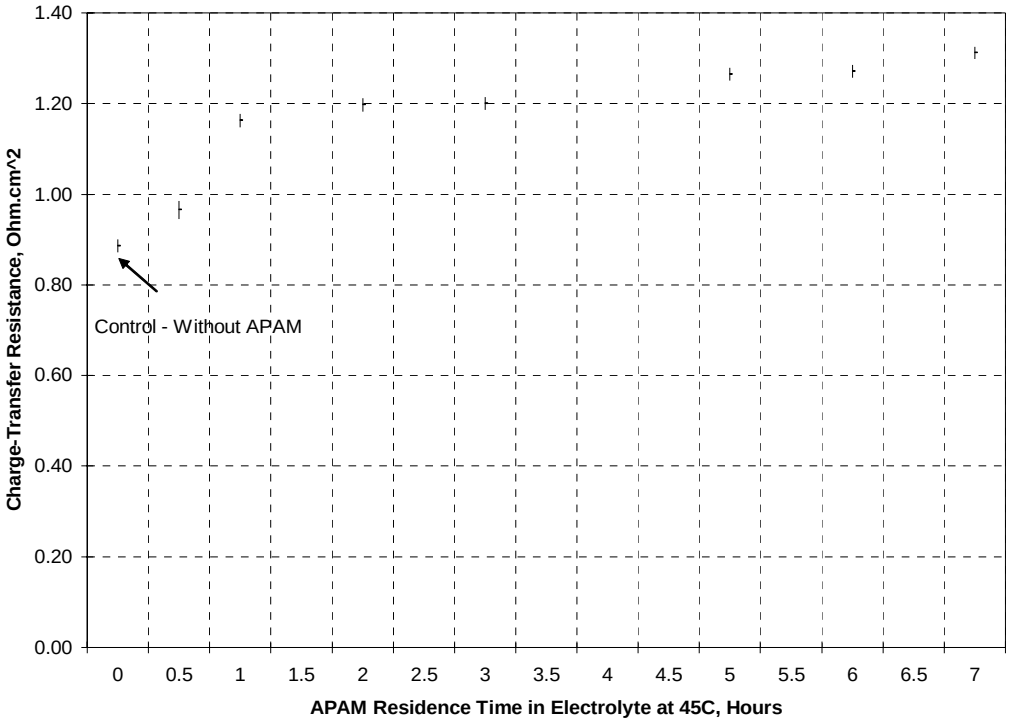

Figure 5-70: Effect of Time on Simulated Charge-Transfer Resistance (P4) in the Presence of APAM at -470mV DC versus MSE at 45°C.

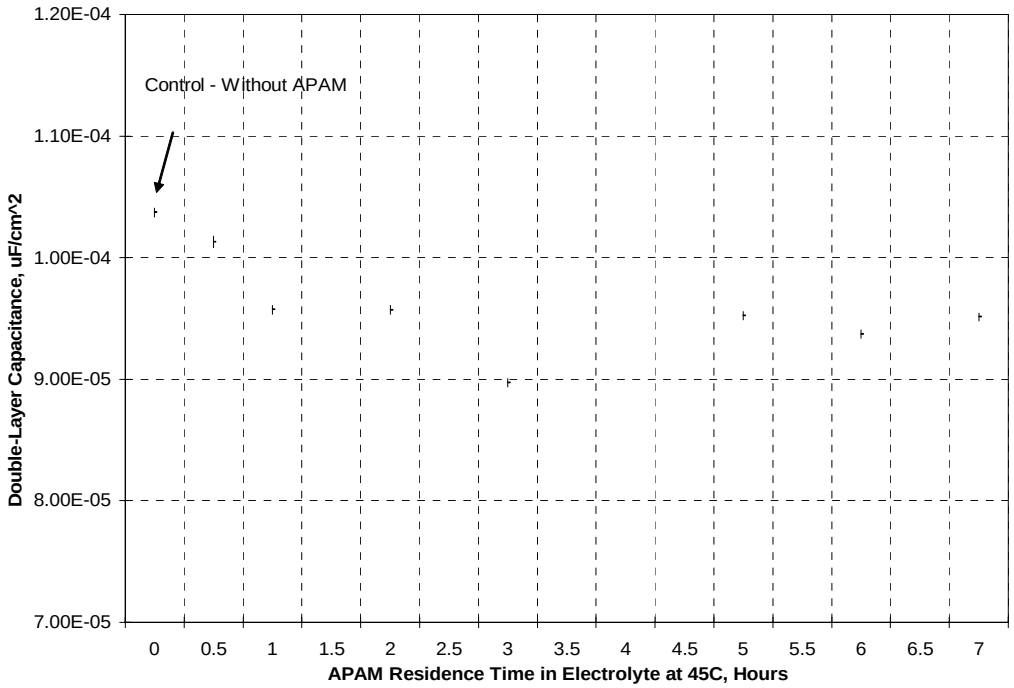

Figure 5-71: Effect of Time on the Simulated Double-Layer Capacitance (P5) in the Presence of APAM at -470mV DC vs. MSE and 45°C

The ageing trend clearly indicates that APAM increased charge-transfer resistance and decreased the double-layer capacitance and that this effect persisted over 7 hours at 45°C. This result is consistent with electrowinning results where 1mg/L APAM was dosed once for 6 and 12 hours at 45°C where smoother deposits were obtained with APAM than with Guar (Chapter 4).

The results presented above with APAM will be compared with similar studies recently published in the literature. These studies often refer to the effect of polyethylene glycol (PEG), an inhibitor/surfactant, on copper deposition for the damascene process. Gabrielli et al.[14] studied the effect of PEG and chloride ions on the deposition of copper using a RDE and obtained about 1.7ohm.cm^2 as the charge-transfer resistance in the high frequency loop at 100rpm, at a current density of 25mA/cm^2 at 25°C using 0.25M $CuSO_4$, 1.8M H_2SO_4 and 60mg/L chloride ions in the absence of PEG. When 300mg/L PEG was added to the system, this charge-transfer resistance decreased from 1.7 to about 1.2ohm.cm^2. These EIS results are inconsistent with Cyclic Voltammetry tests that indicate that PEG polarizes the elecrode[10-12, 24, 59, 60] and hence the reduction of the R_{ct}.

In contrast, Figure 5-68 shows the increase in the charge-transfer resistance in the high frequency loop on addition of 2mg/L APAM. It is widely known that the high frequency loop represents the region of kinetic control[1] and PEG did not show this inhibition/levelling behaviour in this loop. It is thought that EIS tests with PEG at an RDE should also indicate an increase in the charge-transfer resistance in the high frequency loop.

The effect of PEG and APAM on the low frequency loop is similar. The charge-transfer resistance may also be deduced from the low frequency loops (2 loops) as described qualitatively by Gabrielli et al.[14]. Their induction loop[14] is not considered since theoretical studies of two single-electron transfer steps do not include its presence[21]. Gabrielli et al.[14] showed that the charge-transfer resistance increased from about 1.2ohm.cm^2 in the absence of PEG to 2ohm.cm^2 in its presence. This increase of the charge-transfer resistance in the low frequency loops is consistent with the results for APAM described above.

5.8 Electrochemical Impedance Spectroscopy Results in the Presence of Guar at -490mV vs. MSE and 45°C

In this Section, the effect of the ageing process of Guar in the electrolyte at 45°C on the parameter values of the equivalent circuit is presented. Appendix C shows all the experimental data and measurement models for the ageing process of Guar in the electrolyte determined every hour for up to 5hours. Figure 5-72 shows the complex-plane plot after 2-hours residence time of Guar in the electrolyte and in its absence.

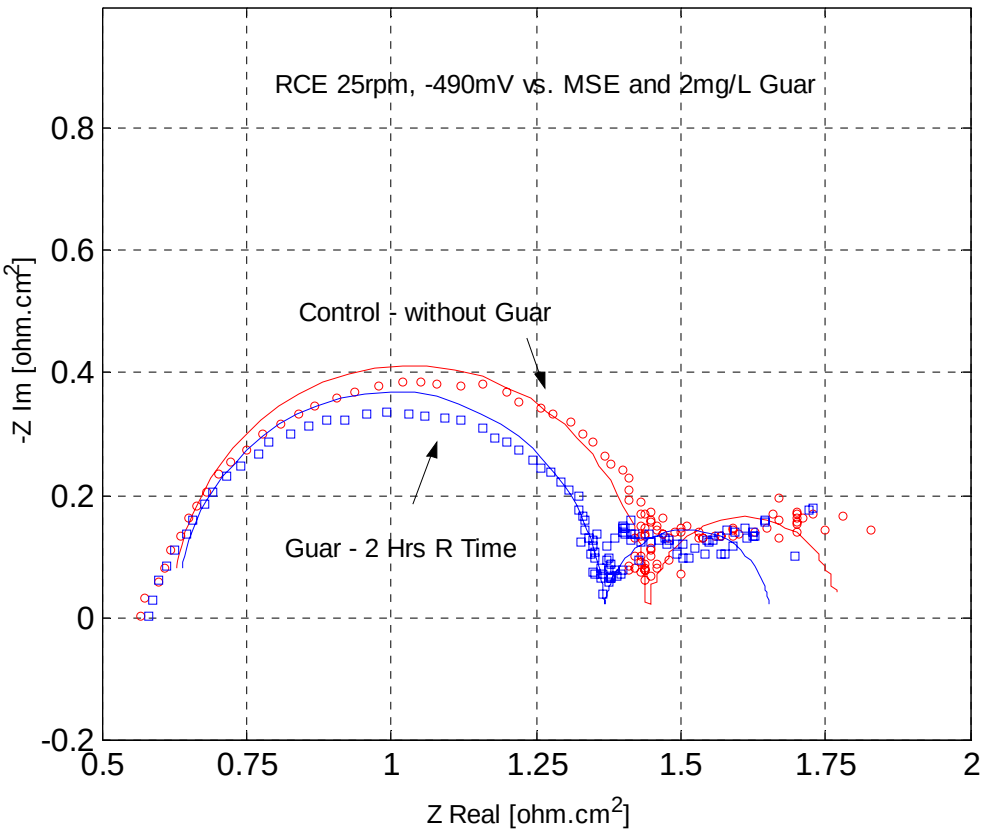

Figure 5-72: Complex-Plane Plot of Experimental and Simulated Impedance Spectra at 45°C in the Presence and Absence of Guar. Overpotential: 113mV vs. SHE

Table 5-28 shows the charge-transfer resistance (P4) and double-layer capacitance (P5) values and their relative standard deviation for the *high frequency loop only* calculated by LEVM[28].

The EIS experiments were measured potentiostatically and therefore the current density varied slightly between tests. Table 5-28 also shows that the current density (34mA/cm^2) obtained in the absence of Guar slightly increased in its presence. The

mechanism for this increase is not understood but it indicates that Guar does not behave as a levelling agent since a levelling agent polarizes the electrode and therefore at constant potential should decrease the current density. This result is consistent with the de-polarization behaviour of Guar observed from Cyclic Voltammetry tests.

Figures 5-73, 5-74 and Table 5-28 summarize the effect of the ageing process of Guar in the electrolyte in terms of its change on charge-transfer resistance and double-layer capacitance over 5-hours.

Table 5-28: Simulation Results for Guar at 45°C and -490 mV DC versus MSE

	Charge-Transfer Resistance (P4)		Double-Layer Capacitance (P5)		C. Density
Hours	Ohm.cm^2	Std. Dev	µF/cm2	Std. Dev.	mA/cm^2
Nil	0.83	0.50E-02	8.93E-05	2.05E-07	34
0.5	0.83	1.59E-02	8.47E-05	4.21E-07	35
1	0.75	1.67E-02	8.59E-05	4.34E-07	39
2	0.74	1.66E-02	8.62E-05	4.35E-07	40
3	0.75	2.03E-02	8.74E-05	5.36E-07	40
4	0.79	1.67E-02	8.79E-05	4.41E-07	38
5	0.79	1.66E-02	8.78E-05	4.38E-07	38

Figure 5-73 shows that the effect of Guar on charge-transfer resistance is relatively small, but a reduction in charge-transfer resistance is apparent after 1-hour. Therefore Guar confers little or no effect on the charge-transfer resistance. The scale used for the charge-transfer resistance shown in Figure 5-73 is the same as used for APAM to allow a direct comparison.

Figure 5-74 shows that Guar reduces the double-layer capacitance. As the residence time increases, this effect becomes progressively less pronounced. The reduction of the double-layer capacitance in the presence of additives is consistent with the literature[61, 62].

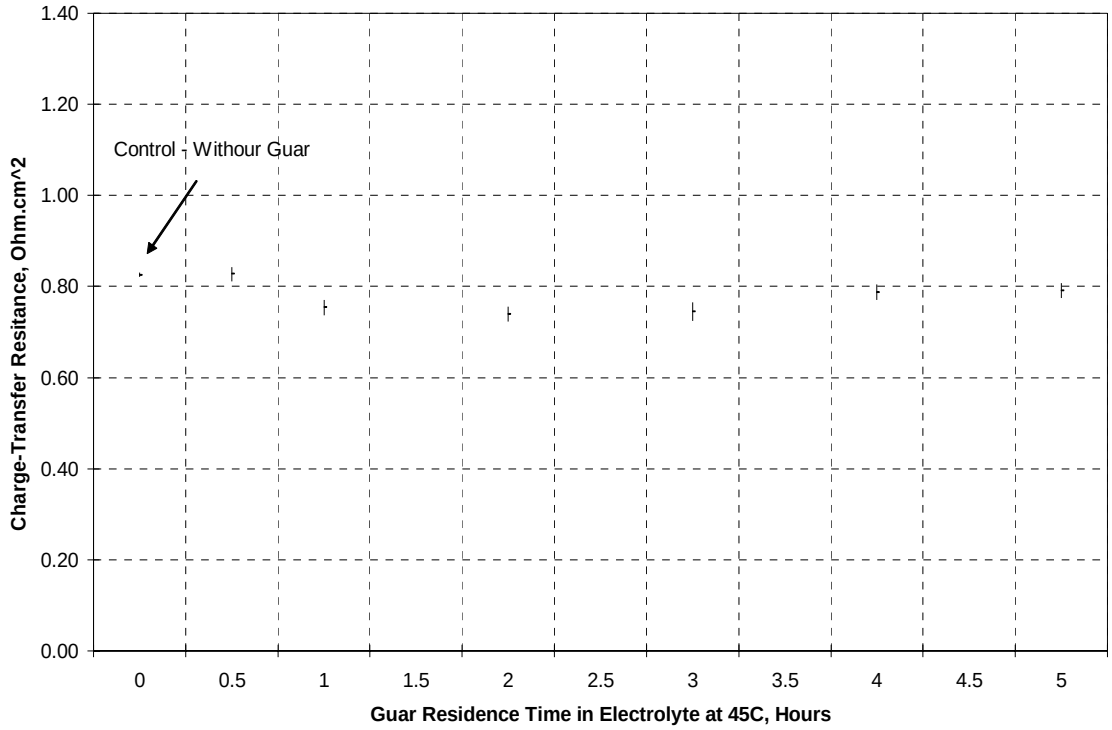

Figure 5-73: Effect of Time on Charge-Transfer Resistance in the Presence of Guar at 45^{o}C

It has been shown from CV tests (Section 5.3) that Guar depolarizes the electrode and from EIS tests it slightly decreases the charge-transfer resistance or polarization resistance. This result will be discussed by comparison with the effect of chloride ions on copper deposition. Sulfate ions, SO_4^{2-} rather than bisulfate ions, HSO_4^- are adsorbed on copper even though the latter is the predominant species in a cupric ion-sulfuric acid electrolyte[63, 64]. However, chloride ions are more strongly adsorbed on the surface of the cathode than sulfate ions causing the reduction of Cu^+ to Cu to become the rate limiting step instead of Cu^{2+} to Cu^{+}[46, 56] and therefore sulfate ions are displaced by chloride ions[63]. Gabrielli et al.[53] in a very recent study also indicated that chloride ion is a depolarizer. It is then concluded from the literature that chloride ions depolarize the electrode.

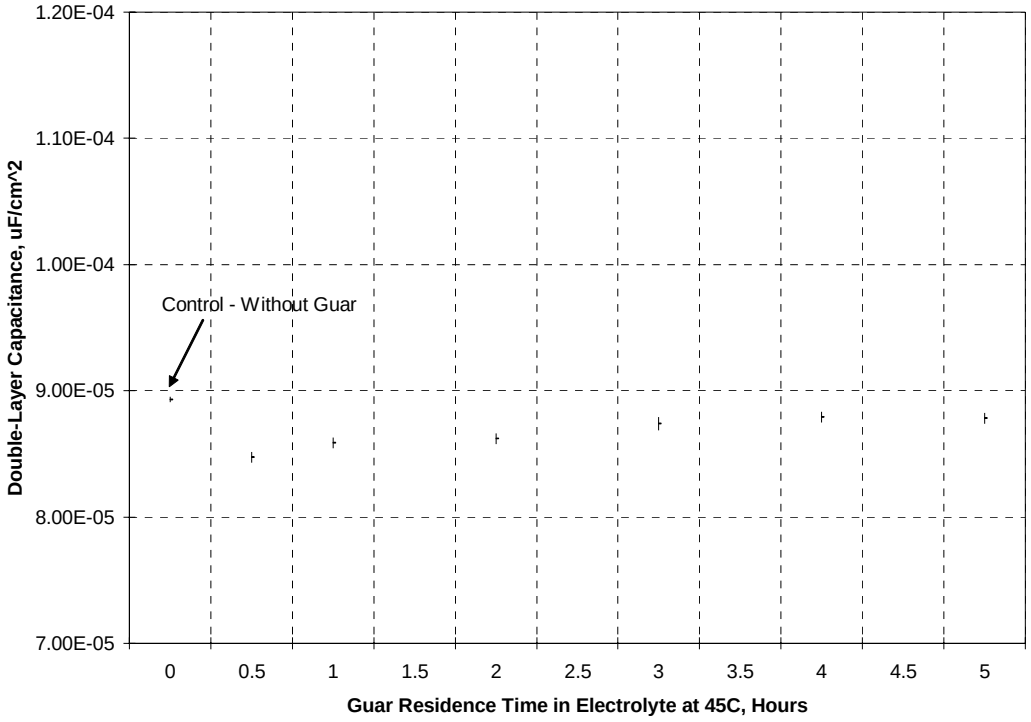

Figure 5-74: Effect of Time on the Double-Layer Capacitance in the Presence of Guar

It was shown in Chapter 4 that Guar increases surface roughness and Ilgar and O'Keefe[65] also have shown that chloride ions also increases surface roughness. It is widely known that the competition between nucleation and growth controls the smoothness of the deposit: the higher the nucleation rate; the finer the crystal size[45]. It can be therefore concluded that the presence of Guar and chloride ions increase the growth rate of copper rather the nucleation rate. In contrast, the form of the growing crystals determines the physical appearance and structure: for a higher growth rate of the crystal size normal to the substrate, a more *fibrous* structure is obtained. It will be shown in Chapter 6 that the cross-section of a copper deposit produced with Guar possesses a porous structure. The experimental Cyclic Voltammetry and EIS results correlate and indicate that Guar further depolarizes the electrode beyond that caused by chloride ions.

5.9 Electrochemical Impedance Spectroscopy Results in the Presence of Activated Polyacrylamide at -490mV vs. MSE and 45°C

These tests were conducted to determine the effect of APAM on the kinetics of copper deposition at potentials more cathodic than -470mV versus MSE (93mV vs.

SHE). This testwork at -490mV vs. MSE was conducted to compare APAM with Guar under the same experimental conditions. Separate EIS testwork was also conducted using a rotating disc electrode (RDE) to determine the behaviour of the charge-transfer resistance in the high frequency loop.

Figure 5-75 shows the complex-plane plot at -490mV versus MSE (113mV vs. SHE) which corresponds to about 34mA/cm^2 with and without APAM using the RCE. The EIS results obtained every hour are shown in Appendix B. Figure 5-75 also shows a constant imaginary impedance component at low frequencies as described in Section 5.7. The gap observed in the low frequency range was attributed to 50Hz mains power noise. Table 5-29 presents the values of the charge-transfer resistance and the double-layer capacitance up to four hours. Figures 6-76 and 6-77 depict the effect of time on the value of these parameters.

Table 5-29: Results for APAM at -490mV CD versus MSE and 45^{o}C

	Charge-Transfer Resistance (P4)		Double-Layer Capacitance (P5)		C. Density
Hours	Ohm.cm^2	Std. Dev.	Hours	μF/cm^2	mA/cm^2
0(Nil)	0.79	1.64E-02	1.046E-04	4.35E-07	34
0.5	0.96	1.98E-02	1.01E-04	5.23E-06	31
1	0.96	1.92E-02	9.78E-05	5.09E-07	30
2	0.99	1.76E-02	9.55E-05	4.66E-07	30
3	1.02	1.62E-02	9.30E-05	4.29E-07	29
4	1.01	1.63E-02	9.29E-05	4.28E-07	29

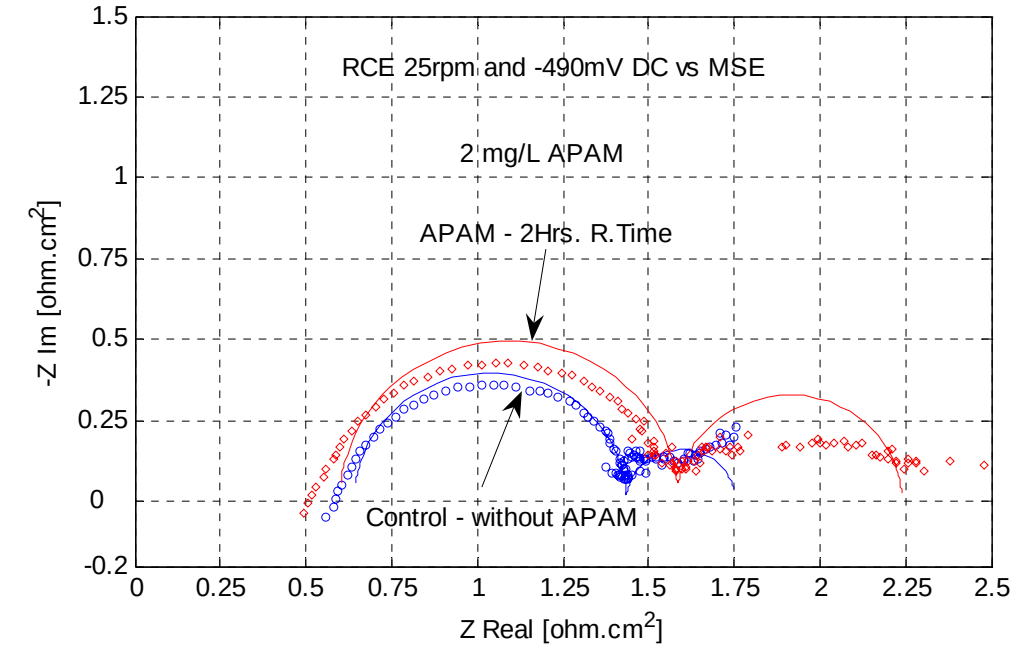

Figure 5-75: Complex-Plane Plot of Experimental and CNLS Simulated Impedance Spectra in the Presence and Absence of APAM at -490mV versus MSE and 45°C. Overpotential: 113 vs. SHE.

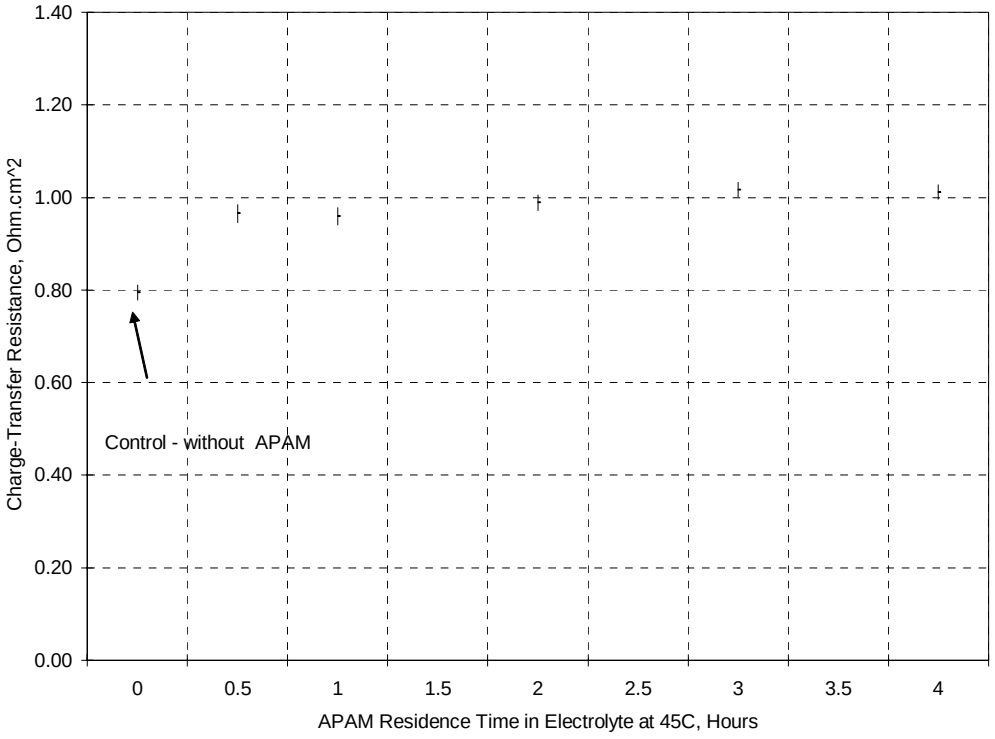

Figure 5-76: Effect of Time on the Simulated Charge-Transfer Resistance in the Presence of APAM at -490mV DC versus MSE and 45°C.

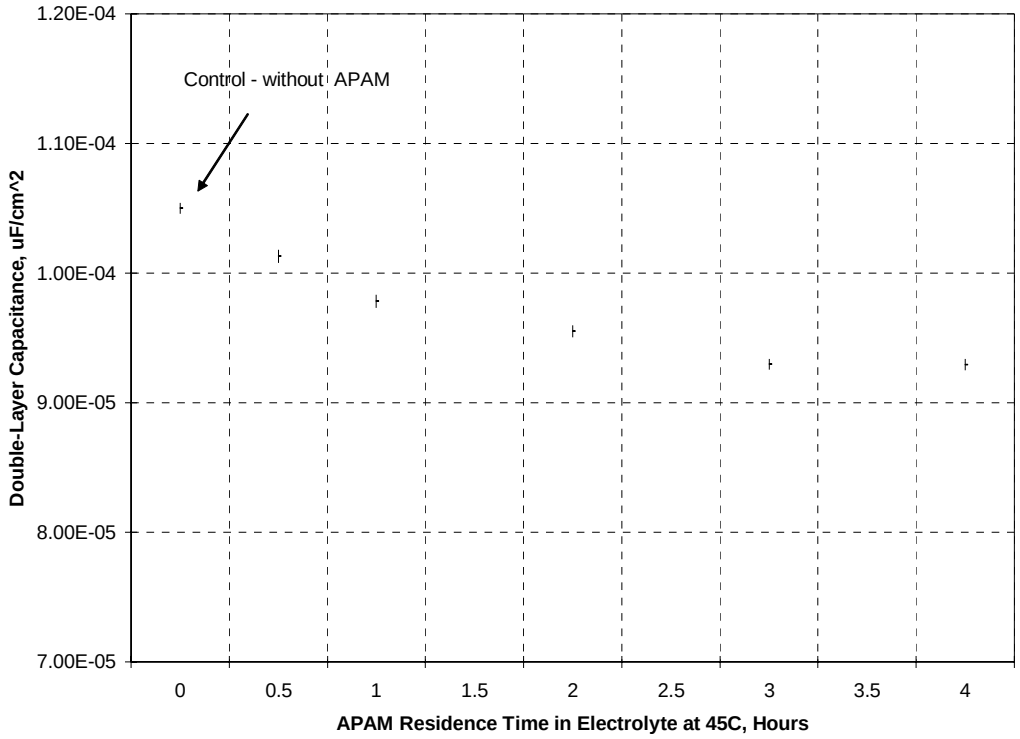

Figure 5-77: Simulated Double-Layer Capacitance versus Time in the Presence of APAM at -490mV DC versus MSE and 45^{o}C.

The increase in the charge-transfer resistance in the high frequency range is possibly due to the ageing process of APAM in the cupric ion-sulfuric acid electrolyte at 45^{o}C through additional hydrolysis of the block copolymer backbone and reduction of its molecular weight. Figure 5-77 indicates also that the double-layer capacitance steadily decreases up to 3 hours then it levels off at about 4 hours. This trend was also observed at -470mV vs. MSE overpotential where tests where conducted up to 7 hours and fully described in Section 5-7.

Figure 5-78 compares the complex-plane plots for 2-hours aged APAM and 2-hours aged Guar, and Nil additives at -490 mV vs. MSE at 45^{o}C using the RCE. It can be seen that the charge-transfer resistance is greatest in the presence of APAM and least in the presence of Guar.

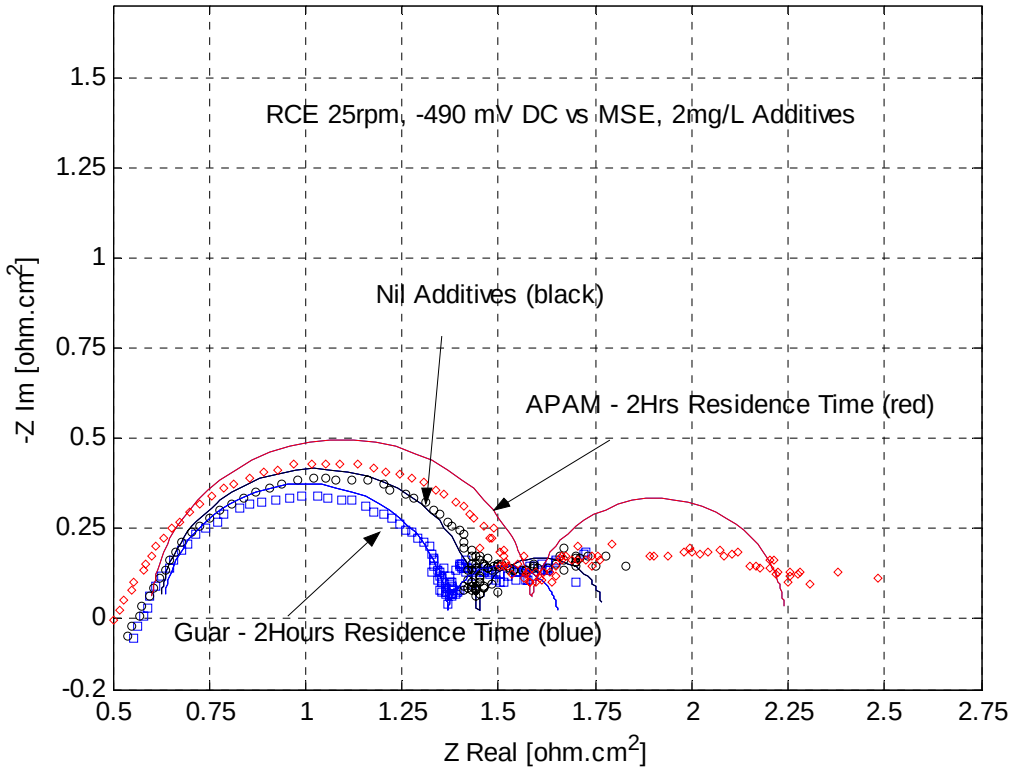

Figure 5-78: Comparison of Complex-Plane Plot of Experimental and Simulated Impedance Spectra in the Presence of both APAM and Guar at -490mV DC and at 45°C.
Legend: Black – 340A/m^2 CD in the Absence of APAM and Guar. APAM (red dots and line) increases the charge-transfer resistance and Guar (blue dots and line) decreases the charge-transfer resistance.

A short set of EIS experiments were undertaken on an RDE to compare with the results on a RCE. The rationale for doing this was the fact that no published EIS data have been collected on both electrodes.

Figure 5-79 shows the EIS results using the rotating disc electrode (RDE). The EIS testwork with the RDE started at 50kHz as in the experiments conducted by Kelly et al.[8] and with the RCE at 30kHz.

Figure 5-79 shows the ageing of APAM in the electrolyte also increases the charge-transfer resistance in the high frequency loop up to six hours. The other important findings from Figure 5-79 are: (i) the electrolyte resistance, Rs, is constant with and without the presence of APAM and (ii) The Rs value with the RDE is about one-half of that obtained with the RCE (Figure 5-76). The reasons for this difference are unclear but the electrolyte/electrode interface must be at steady-state during the

presence and absence of additive. Therefore, a difference can be expected in the presence and presence of additives due to inhibition (surface coverage). However, there is a clear difference for the RDE with APAM at 45°C and with PEG at 25°C. The presence of PEG at 25°C reduced the charge-transfer resistance as discussed in Section 5.7 but the presence of APAM at 45°C increased the charge-transfer resistance at the RDE and RCE.

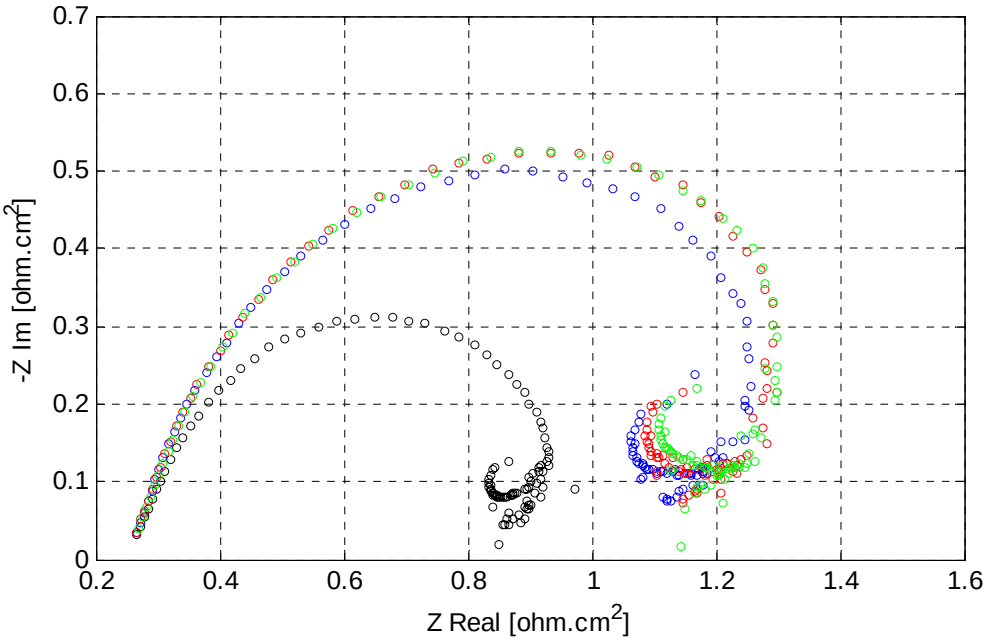

Figure 5-79: Complex-Plane Plot using RDE at -490mV vs. MSE, 25rpm and 45°C (50^3Hz-0.2Hz).
Legend: Black – Control without APAM, Blue – 1 Hrs, Red – 3Hrs. and Green – 6Hrs.

The EIS response presented in Figure 5-79 cannot be simulated using the equivalent circuit presented in Figure 5-56 possibly due to convection and low stirring affecting the diffusion in the low frequency range. Moreover, the non-uniform current distribution inherent to the RDE may also influence the formation of the inductive type EIS data in the low frequency loop. The Ohmic resistance in solution determines the primary current distribution, which then becomes a unique function of cell geometry[38]. It has been also observed in Sections 5.4 and 5.5 that the electrode kinetics of copper electrodeposition is faster on pre-plated copper than on bare stainless steel. Therefore, the problem of the non-uniform primary current distribution inherent to the RDE may have become more serious due to the faster reaction, large current density and large disc ($0.178cm^2$)[38]. In contrast, the motivation to use the RCE was to achieve a uniform

metal distribution during the electrodeposition process. Nevertheless, it has been shown that APAM increased the charge-transfer resistance in the high frequency loop whether RCE or RDE was used.

5.10 Electrochemical Impedance Spectroscopy Results in the Presence of Activated Polyacrylamide at -445mV vs. MSE at 65°C

These EIS tests were run using RCE and RDE at 65°C, the copper electrorefining electrolyte temperature. The RCE was used for nil APAM and at 0.5, 2 and 5hours APAM residence time in the electrolyte. The RDE was used for nil APAM and at 1, 3 and 6hours APAM residence time in the electrolyte. The speed of rotation of both electrodes were 25rpm. These runs were carried out by simply replacing the RCE shown in Figure 5-59 by an RDE of the same height. Figure 5-80 shows the complex-plane plot at -445mV vs. SME which corresponds to about 50mA/cm^2 in the absence of APAM at 65°C for the RCE. The EIS spectra obtained for 0.5 and 5 hours are also presented in Appendix B.

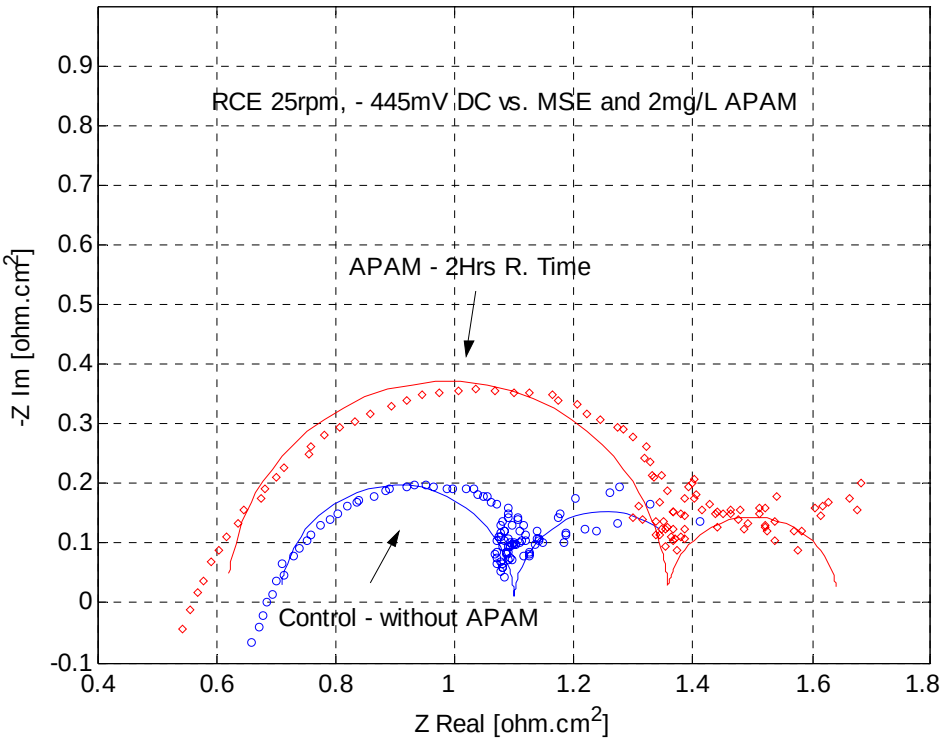

Figure 5-80: Complex-Plane Plot of Experimental and CNLS Simulated Impedance Spectra in the Presence and Absence of APAM at -445mV versus MSE and 65°C. Overpotential: 90mV vs. SHE.

Figure 5-80 clearly shows that the presence of APAM at 2-hours residence time in the electrolyte increases the charge-transfer resistance in the high frequency loop as also found in Sections 5.7 and 5.9. Table 5-30 presents the charge-transfer resistance and double-layer capacitance for this testwork. Figures 5-81 and 5-82 depict the data presented in Table 5-30.

Table 5-30: Results for APAM at 65°C and -445mV CD versus MSE

	Charge-Transfer Resistance (P4)		Double-Layer Capacitance (P5)		C. Density
Hours	Ohm.cm^2	Std. Dev.	μF/cm^2	Std. Dev.	mA/cm^2
Nil APAM	0.39	2.91E-02	1.84E-04	7.76E-06	50
0.5	0.73	2.08E-02	1.16E-04	5.53E-06	34
2	0.74	2.02E-02	1.13E-04	5.32E-06	33
5	0.69	2.12E-02	1.16E-04	5.60E-06	34

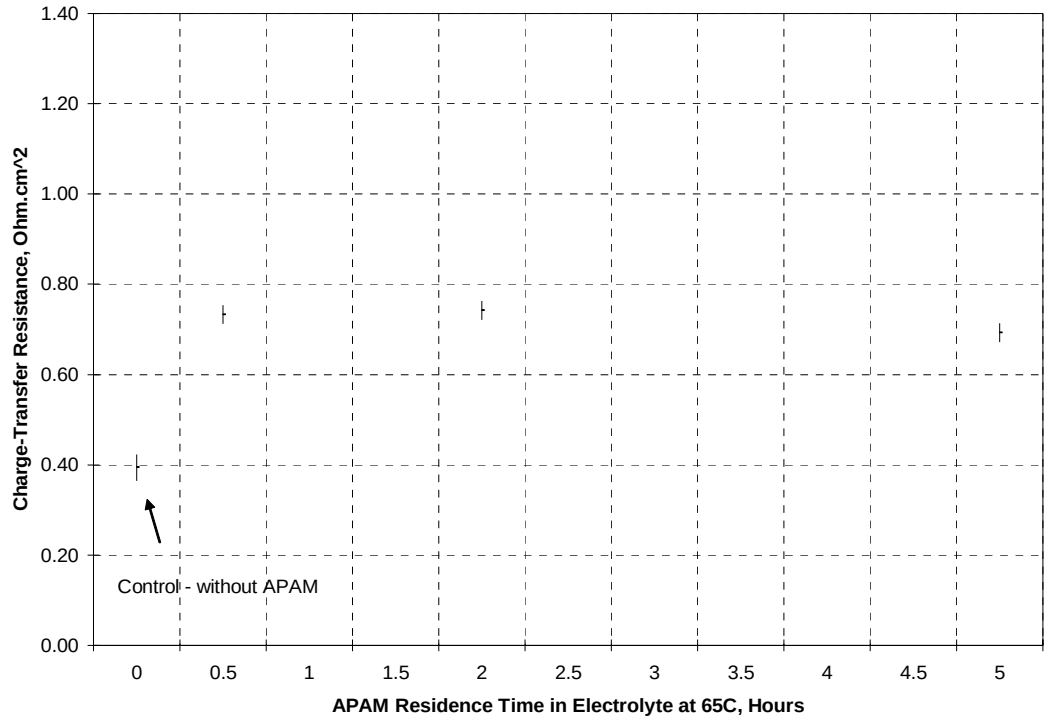

Figure 5-81: Effect of Time on the Simulated Charge-Transfer Resistance (P4) in the Presence of 2mg/L APAM at 65°C and -445mV DC vs. MSE

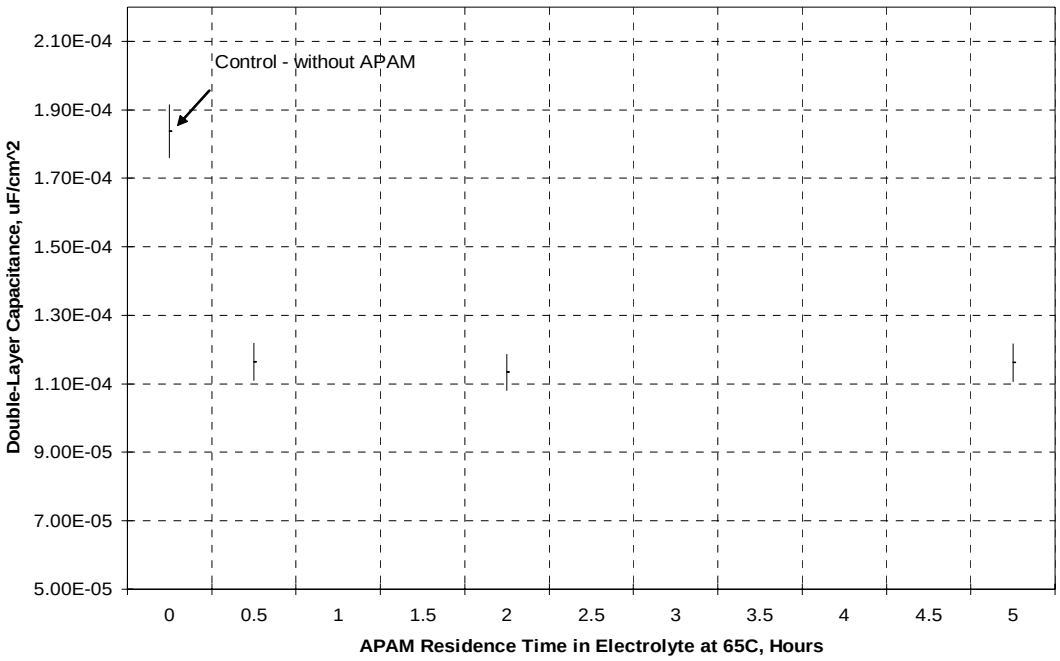

Figure 5-82: Effect of Time of the Simulated Double-Layer Capacitance (P5) in the Presence of 2mg/L APAM at 65°C and -445mV DC vs. MSE.

The noise in the low frequency loop is not clearly understood. It may be due to non-steady state conditions of the electrochemical crystal growth process and surface topography[45] and to the fluid flow of the system. Different impedance features can be observed on single crystals with and without screw dislocations[45]. It will be recalled (Sections 3.2.3 and 3.2.4) that at Reynolds number of approximately 200, a transition from laminar to laminar with vortexes occurs. Accordingly, since Reynolds number increases from 204 at 45°C to 293 at 65°C, a significant change in the fluid flow is likely which may account for the increased noise at 65°C due to the unstable and superimposed Taylor vortices.

Figure 5-83 shows the EIS results using the rotating disc electrode (RDE). It can be seen than the ageing of APAM in the electrolyte occurs more rapidly and increased the charge-transfer resistance in the high frequency loop from the first hour to 3-4hours and then decreases at 6-hours residence time. This trend of APAM was also observed from the CV results at 65°C, Figure 5-65 and the EIS results using the RCE at 65°C, Figure 5-81. However, these curves also cannot be simulated using the equivalent circuit presented in Figure 5-56. However, Figure 5-83 shows that APAM

increases the charge-transfer resistance in the high frequency loop whether RCE or RDE is used at 45°C and 65°C and the electrolyte resistance, Rs is constant with and without APAM.

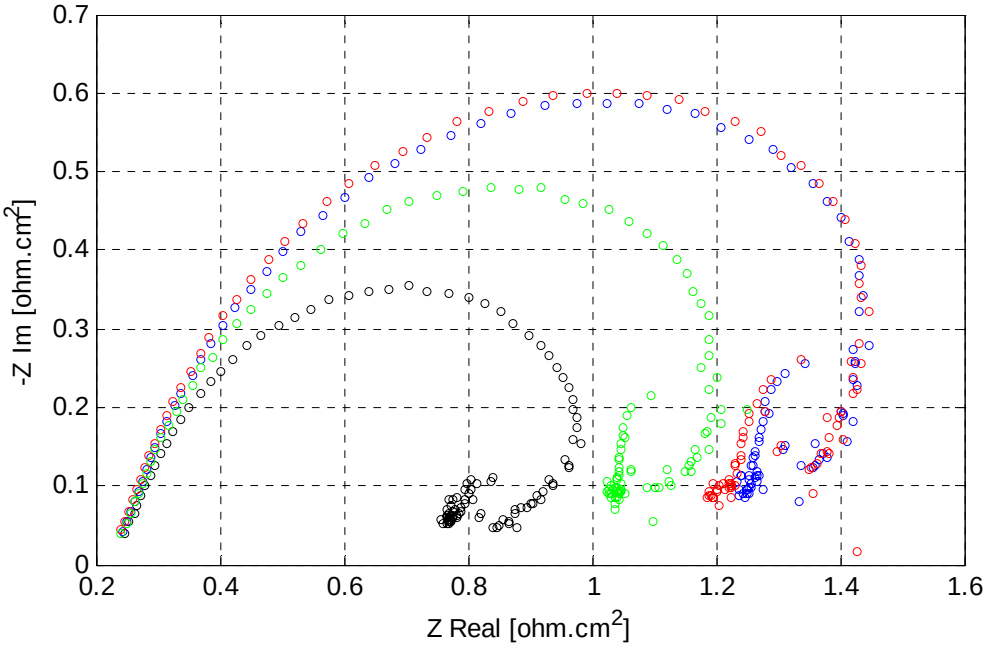

Figure 5-83: Complex-Plane Plot using RDE at -445mV vs. MSE, 25 rpm and 65°C (50^3 Hz-0.2Hz).
Black – Control without APAM, Blue – 1 Hrs, Red – 3Hrs. and Green – 6Hrs.

5.11 Discussion and Conclusions

It was seen by Cyclic Voltammetry that Guar de-polarized the electrode on both stainless steel and pre-plated-copper (Section 6-3). It was also seen that there was a trend in depolarization behaviour as measured by Cyclic Voltammetry. It increases from 0.3-1hour to a maximum at 2-3hours and then its depolarizing activity decayed such that within 4-5hours an insignificant effect was observed on pre-plated copper. The transfer coefficient value of 0.50 in the absence of Guar agrees with that given by Wu and Barkey[46] and Mattson and Bockris[47]. The charge-transfer resistance determined by EIS for Guar also follows the overall trend of the *depolarization* behaviour of Guar from Cyclic Voltammetry tests.

In contrast, cyclic voltammetry tests indicate that APAM *polarizes* the electrode. The maximum polarization at 45°C and 65°C was approximately 14mV but the time to attain this maximum value was about 3.5 hours at 45°C and 1.5 hours at 65°C as shown in Figure 5-66. These results correlate with the fractional factorial experimental results in which it was demonstrated that APAM had a more significant effect on reducing surface roughness at 65°C than at 45°C (See Chapter 4). These results indicate that APAM at 45°C requires about 3.5 hours ageing to produce the smoothest deposit while at 65°C it requires about 1hour.

APAM also appeared to confer higher adsorption on pre-plated copper than on stainless steel since the net polarization values are higher for pre-plated copper than for stainless steel at 45° and 65°C. These results are consistent with both APAM acting as a surfactant/levelling agent and doing so for extended periods of time, which is consistent with the results described in Chapter 3 where APAM was dosed once for 6 hours electrowinning time.

The complex-plane plots presented in this thesis using a RCE agree with the theoretical work for single-electron step reactions requiring only the presence of resistors and capacitors in the equivalent circuit[21]. It also agrees with experimental work in the published literature[8, 14, 17, 51-53] where RDEs were used in terms of the electrolyte resistance and the charge-transfer resistance, Rct, in the high frequency loop. However, measurement modelling or regression analysis were absent from the above published literature, except from the work of Fabricius et al.[17]and Chassaing et al.[52]. It has been recently stated that the inherent non-uniform primary current distribution of the rotating disc electrode precludes measurement modelling[40]. In contrast, the uniform current distribution produced by the RCE is widely documented[38].

The low frequency loop is more complex and less understood in terms of the number and nature of the parameter values. It depends on the surface preparation of the substrate, growth mode[55] of the deposit including its crystallographic orientation, hydrodynamic conditions and current density[56]. The cylindrical diffusion produced by the rotating cylinder electrode results in the relatively constant imaginary impedance component[3, 41]. Comparison of Figures 5-69 (-470mV vs. MSE, 30mA/cm^2 and 45°C), 5-75 (-490mV, 34mA/cm^2, 45°C) and 5-80 (-445mV, 50mA/cm^2, 65°C) show that the

noise level in the low frequency loop increases as the current density increases. This indicates that the RCE is highly sensitive to surface roughness in the low frequency range. It is known that the roughness of an electrode may lead to a frequency dispersion of the interfacial impedance[4] and the lines of electric force do not converge evenly on the surface. The double layer will therefore be charged unevenly[4]. This behaviour was more apparent in the presence and absence of Guar than in the presence of APAM.

Table 5-31 summarizes the maximum change in the charge-transfer resistance and double-layer capacitance produced by APAM and Guar at 45°C and 65°C. APAM increased the charge-transfer resistance throughout the testwork while Guar reduced it. APAM reduced the double-layer capacitance more than Guar at 45°C. This reduction of the double-layer capacitance increased when the temperature was increased from 45°C to 65°C. These results indicate that *APAM is more specifically* adsorbed than Guar.

Table 5-31: Maximum Change in Charge-Transfer Resistance and Double-Layer Capacitance Relative to the Presence and Absence of Guar and APAM

Additive	mV vs. MSE	Max. Change in C-T Resistance, R_{ct}, ohm.cm^2	Max. Change in D-L Capacitance, x 10^{-5}, C_{dl}, µF/cm^2	Guar/APAM Residence Time in Electrolyte, Hrs.*
Guar	-490mV and 45°C	-0.086	-0.46	2-3
APAM	-470 mV and 45°C	+0.42	-1.2	3-5
APAM	-490mV and 45°C	+0.23	-1.2	3-5
APAM	-445mV and 65°C	+0.34	-6.8	2

*Maximum change determined at these residence times.

It was also shown that the effect of temperature on the ageing sequence is consistent with reaction kinetics for polyacrylamide hydrolysis and cleavage, i.e., it is faster at 65°C than at 45°C as would be expected. The EIS data at 65°C and 45°C are consistent with the CV data whether the RCE or RDE was used but the EIS data with the RDE was not amenable to be modelled using the equivalent circuit presented in Figure 5-56.

The CV results at 45°C area consistent with the EIS results at 45°C in that Guar depolarizes the electrode or decreases the charge-transfer resistance. In other terms Guar increases the rate of growth rather than the rate of nucleation. In contrast, APAM polarizes the electrode or increases the charge-transfer resistence, promotes nucleation

rate rather than growth rate. These results for APAM were replicated at 65^{o}C. Overall electrowinning tests, crystallite size measurements, Cyclic Voltammetry and Electrochemical Impedance Spectroscopy indicated that Guar depolarises the electrode and, in contrast, APAM polarizes the electrode. Therefore, APAM behaves as a true levelling agent and does so for extended periods of time, which is consistent with the results described in Chapter 3 where APAM was dosed 1mg/L once for 6 hours electrowinning time.

5.12 References

1. Bard AJ, Faulkner L. *Electrochemical Methods, Fundamentals and Applications*. Second ed. Brisbane: John Wiley & Sons, Inc.; 2001.

2. Calvo EJ. The Current-Potential Relationship. In: Bard AJ, Stratmann M, editors. *Encyclopedia of Electrochemistry, Volume 2: Interfacial Kinetics and Mass Transport*: Wiley-VCH; 2003. p. 3-30.

3. Lasia A. Electrochemical Impedance Spectroscopy and Its Applications. In: Conway B, Bockris J, White R, editors. *Modern Aspects of Electrochemistry*: Kluwer Academic / Plenum; 1999. p. 143-245.

4. Macdonald JR, editor. *Impedance Spectroscopy Emphasizing Solid Materials and Systems*. Brisbane: John Wiley & Sons; 1987.

5. Conway B, Bockris J, White R, editors. *Electrochemical Impedance Spectroscopy and Its Applications in Modern Aspects of Electrochemistry*: Kluwer Academic / Plenum; 1999.

6. Macdonald D. *Transient Techniques in Electrochemistry*: Plenum Press; 1977.

7. Grafov BM, Damaskin BB. *Theory of Electrochemical Faradaic Impedance for Mixed Electrolyte Solutions*. Electrochimica Acta 1996;41(17):2707-2714.

8. Kelly J. Copper Deposition in the Presence of Mixed Surfactants [PhD]: Columbia University; 1999.

9. Bonou L, Eyraud M, Denoyel R, Massiani Y. *Influence of Additives on Cu Electrodeposition Mechanisms in Acid Solution: Direct Current Study*

Supported by Non-Electrochemical Measurements. Electrochimica Acta 2002;47(26):4139-4148.

10. Moffat T, Bonevich J, Huber W, Stanishevsky A, Kelly D, Stafford G, Josell D. *Superconformal Electrodeposition of Copper in 500-90 Nm Features*. J. Electrochem. Soc. 2000;147(12):4524-4535.

11. Moffat TP, Wheeler D, Josell D. *Electrodeposition of Copper in the Sps-Peg-Cl Additive System*. Journal of the Electrochemical Society 2004;151(4):C262-C271.

12. Moffat T, Baker B, Wheeler D, Josell D. *Accelerator Aging Effects During Copper Electrodeposition*. Electrochemical and Solid-State Letters 2003;6(4):C59-C62.

13. Feng ZV, Li X, Gewirth A. *Inhibition Due to the Interaction of Polyethylene Glycol , Chloride and Copper in Plating Baths: A Surface-Enhanced Raman Study*. J. Phys. Chem. B 2003;107:9415-9423.

14. Gabrielli C, Kittel J, Mocoteguy P, Perrot H, Zdunek A, Bouard P, Haddix M, Doyen L, Clech MC. *A Model of Copper Deposition for the Damascene Process*. Proceedings - Electrochemical Society 2003;2003-13(Thin Film Materials, Processes, and Reliability):100-109.

15. Vereecken PM, Binstead RA, Deligianni H, Andricacos PC. *The Chemistry of Additives in Damascene Copper Plating*. IBM Journal of Research and Development 2005;49(1):3-19.

16. Fabricius G, Sundholm G. *The Effect of Additives on the Electrodeposition of Copper Studied by the Impedance Technique*. Journal of Applied Electrochemistry 1984;14:797-801.

17. Fabricius G. The Electrochemistry of Copper in Sulfuric Acid in the Presence of Additives [Doctor of Technology Thesis]. Espoo: Helsinki University of Technology; 1995.

18. Onicio L, Muresan L. *Some Fundamental Aspects of Levelling and Brightening in Metal Electrodeposition*. Journal of Applied Electrochemistry 1991;21:565-574.

19. Jordan K, Tobias C. *The Effect of Inhibitor Transport on Leveling in Electrodeposition*. J. Electrochem. Soc. 1991;138(5):1251-1259.

20. Chung D. Localized Adsorption of Organic Additives During Copper Electrodeposition [Ph.D.]. Urbana-Champaign: University of Illinois; 1996.

21. Harrington DA, van den Driessche P. *Equivalent Circuits for Some Surface Electrochemical Mechanisms*. Journal of Electroanalytical Chemistry 2004;567(2):153-166.

22. Franceschetti DR, Macdonald JR. *Diffusion of Neutral and Charged Species under Small-Signal A.C. Conditions*. J. Electroanal. Chem. 1979;101:307-316.

23. Mansfeld F, Shih H, Greene H, Tsai C. Analysis of Eis Data for Common Corrosion Processes. In: Scully JR, Silverman DC, Kending MW, editors. *Electrochemical Impedance: Analysis and Interpretation*; 1993; 1993. p. 37-53.

24. Jovic VD, Jovic BM. *Copper Electrodepositon from Copper Acid Baths in the Presence of Polyethylene Glycol and Sodium Chloride*. J. Serb. Chem. Soc. 2001;66(11-12):935-952.

25. Nava de Oca J, Sosa E, Ponce de Leon C, Oropeza M. *Effectiveness Factors in an Electrochemical Reactor with Rotating Cylinder Electrode for the Acid-Cupric/Copper Cathode Interface Process*. Chemical Engineering Science 2001;56(8):2695-2702.

26. Diard JP, Montella C. *Diffusion-Trapping Impedance under Restricted Linear Diffusion Conditions*. Journal of Electroanalytical Chemistry 2003;557:19-36.

27. Brett CMA, Brett AMO. *Electrochemistry, Principles, Methods and Applications*. New York; 1993.

28. Macdonald J. Levm Manual - Complex Nonlinear Least Squares (Cnls). In. 8.0 ed; 2003.

29. Gabrielli C. Electrochemcial Impedance Spectroscopy: Principles, Instrumentation and Applications. In: Rubinstein I, editor. *Physical Electrochemistry*. New York: Marcel Dekker, Inc; 1995. p. 243-292.

30. Madore C, Agarwal P, Landolt D. *Blocking Inhibitors in Cathodic Leveling Iii. Electrochemical Impedance Spectroscopy Study*. J. Electrochem. Soc. 1998;145(5):1561-1565.

31. Agarwal P, Orazem ME, Garcia-Rubio L. *Measurement Models for Electrochemical Impedance Spectroscopy I. Demonstration and Applicability*. J. Electrochem. Soc. 1992;139(7):1917-1927.

32. Agarwal P, Moghissi O, Orazem M, Garcia-Rubio L. *Application of Measurement Models for Analysis of Impedance Spectra*. Corrosion 1993;49(4):278-89.

33. Agarwal P, Orazem ME, Garcia-Rubio LH. *Application of Measurement Models to Impedance Spectroscopy. Iii. Evaluation of Consistency with the Kramers-Kronig Relations*. Journal of the Electrochemical Society 1995;142(12):4159-68.

34. Orazem ME, Wojcik PT, Durbha M, Frateur I, Garcia-Rubio LH. *Application of Measurement Models for Interpretation of Impedance Spectra for Corrosion*. Materials Science Forum 1998;289-292(Pt. 2):813-828.

35. Boukamp BA. *A Package for Impedance/Admittance Data Analysis*. Solid State Ionics 1986;18-19(1):136-40.

36. Princeton-Applied-Research. Zsimpwin Electrochemical Spectroscopy Analysis Software V3.1. In; 2003.

37. Orazem ME, Agarwal P, Jansen AN, Wojcik PT, Garcia-Rubio LH. *Development of Physico-Chemical Models for Electrochemical Impedance Spectroscopy*. Electrochimica Acta 1993;38(14):1903-11.

38. Newman J, Thomas-Alyea KE. *Electrochemical Systems*. Third ed. Hoboken, New Jersey: John Wiley & Sons, Inc.; 2004.

39. Durbha M, Orazem ME, Tribollet B. *A Mathematical Model for the Radially Dependent Impedance of a Rotating Disk Electrode*. J. Electrochem. Soc. 1999;146(6):2199-2208.

40. Shukla PV, Orazem ME. *Hydrodynamics and Mass-Transfer-Limited Current Distribution for a Submerged Stationary Hemispherical Electrode under Jet Impingement*. Electrochimica Acta 2004;49:2901-2908.

41. Jacobsen T, West K. *Diffusion Impedance in Planar, Cylindrical and Spherical Symmetry*. Electrochimica Acta 1995;40(2):255-262.

42. Filzwieser A, Hein K, Hanko G. Application of Two Phase Hydrodynamic Modeling to an Electrowinning Cell. In: Dutrizac JE, Ji J, Ramachandran V, editors. *Copper 99 - Cobre 99 International Conference*; 1999: The Minerals, Metals & Materials Society; 1999.

43. Gabe D. *Rotating Electrodes for Use in Electrodeposition Process Control*. Plating & Surface Finishing 1995;9:69-76.

44. Schlichting H. *Boundary-Layer Theory*. Sydney: McGraw-Hill; 1968.

45. Budevski E, Staikov G, Lorenz W. *Electrochemical Phase Formation and Growth, an Introduction to the Initial Stages of Metal Deposition*. New York: VCH; 1996.

46. Wu Q, Barkey D. *Faceting and Roughening Transitions on Copper Single Crystals in Acid Sulfate Plating Baths with Chloride*. Journal of the Electrochemical Society 2000 Mar;147(3):1038-1045.

47. Mattsson E, Bockris JOM. *Galvanostatic Studies of the Kinetics of Deposition and Dissolution in the Copper+Copper Sulphate System*. Transaction Faraday Soc. 1959;55:1586-1601.

48. Vereecken J, Winand R. *Influence of Polyacrylamides on the Quality of Copper Deposits from Acidic Copper Sulphate Solutions*. Surface Technology 1976; 4:227-235.

49. Robinson T, Davenport WG, Quinn J, Karkas G. Electrolytic Copper Refining - 2003 World Tankhouse Operating Data. In: Dutrizac JE, Clement CG, editors. *Copper 2003 - Cobre 2003*; 2003; Santiago, Chile: Canadian Institute of Mining, Metallurgy and Petroleum; 2003. p. 3-66.

50. Grchev T, Cvetkovska M, Stafilov T, Schultze J. *Adsorption of Polyacrylamide on Gold and Iron from Acidic Aqueous Solutions*. Electrochimica Acta 1991;36(8):1315-1323.

51. Reid J, David A. *Effects of Polyethylene Glycol on the Electrochemical Characteristics of Copper Cathodes in an Acid Copper Medium*. Plating & Surface Finishing 1987;74(1):66-70.

52. Chassaing E. *Effect of Organic Additives on the Electrocrystallization and the Magnetoresistance of Cu-Co Multilayers*. Journal of the Electrochemical Society 2001;148(10):C690-C694.

53. Gabrielli C, Mocoteguy P, Perrot H, Wiart R. *Mechanism of Copper Deposition in a Sulfate Bath Containing Chlorides*. Journal of Electroanalytical Chemistry 2004;572(2):367-375.

54. Mandin P, Fabian C, Lincot D, Ridd M. *In Preparation*.

55. Gabrielli C, Mocoteguy P, Perrot H, Zdunek A, Bouard P, Haddix M. *Electrochemical Impedance Spectroscopy Investigation of Bath Ageing in Damascene Process Chemistries*. Electrochemical & Solid-State Letters 2004;7(3):C31-C34.

56. Chassaing E, Wiart R. *Epitaxial Growth and Electrode Impedance of Copper Electrodeposits*. Electrochimica Acta 1984;29(5):649-660.

57. Radeva T, Petkanchin I. *Electro-Optic Study of Oxide Particles in Hydrolyzed Polyacrylamide Solutions*. Journal of Colloid and Interface Science 1995;182:1-5.

58. Radiometer-Analytical. Voltamaster 4.0. In; 2003.

59. Kelly J, Tian C, West A. *Leveling and Microstructural Effects of Additives for Copper Electrodeposition*. Journal of the Electrochemical Society 1999;146(7):2540-2545.

60. Moffat T, Wheeler D, Huber W, Josell D. *Superconformal Electrodeposition of Copper*. Electrochemical & Solid-State Letters 2001;4(4):C26-C29.

61. Tsai W-C, Wan C-C, Wang Y-Y. *Pulsed Current and Potential Response of Acid Copper System with Additives and the Double Layer Effect*. J. Electrochem. Soc. 2002;149(5):C229-C236.

62. Petri M, Kolb D, Memmert U, Meyer H. *Adsorption of Polyethylene Glycol on Au(111) Single-Crystal Electrodes and Its Influence on Copper Deposition*. J. Electrochem. Soc. 2004;151(12):C793-C797.

63. Hope GA, Woods R. *Transient Adsorption of Sulfate Ions During Copper Electrodeposition*. J. Electrochem. Soc. 2004;151(9):C550-553.

64. Lipkowski J. *1998 Alcan Award Lecture - Surface Electrochemistry - Surface Science with a Joy Stick*. Canadian Journal of Chemistry 1999;77(7):1163-1176.

65. Ilgar E, O'Keefe T. Surface Roughening of Electrowon Copper in the Presence of Chloride Ions. In: Dreisinger D, editor. *Aqueous Electrotechnologies: Progress in Theory and Practice*; 1997: The Minerals Metals and Materials Society; 1997. p. 51-62.

CHAPTER 6

BENCH SCALE COPPER ELECTROWINNING TESTS

6.1 Introduction

This testwork was aimed at investigating the effectiveness of Guarfloc 66 (Guar) and activated polyacrylamide (APAM) in controlling dendrite growth in a *continuous* copper electrowinning system using *parallel plate* electrodes. These tests were also conducted for longer EW times than previously described.

In metal deposition, nucleation is a very important process. The first step of metal deposition is the formation of nuclei of the depositing metal on a foreign substrate and on a substrate of the same metal. The competition between nucleation and growth determines the smoothness of the deposit: the higher the nucleation rate; the finer the crystal size[1]. Moreover, the forms of the growing crystals determine the physical appearance and structure. A higher crystal size growth rate normal to the substrate leads to a more fibrous structure. A brightening effect can be achieved when large developed crystal faces grow parallel to the substrate.

The formation of coherent deposit can take place by a layer growth mechanism or 3D crystallite growth (or nucleation-coalescence growth)[2]. The layer growth mechanism is indicated by lateral spreading of discrete layers, one after another across

the surface. The 3D crystallite growth mechanism forms a coherent deposit by coalescence of these crystallites. Three-dimensional (3D) epitaxial crystallites have been observed in the first stages of copper electrodeposition[2]. The coherent deposit was formed by growth and coalescence of the three dimensional epitaxial crystallites.

6.2 Experimental

The comparison between Guar and APAM was carried out using the current-industry standard copper electrowinning operating conditions except for current density which was increased to 340A/m^2 from the industry standard[3] of 280-300 A/m^2. Additionally, Guar and APAM concentrations were also increased from about 175 grams/tonne copper cathode or 0.25-0.50 mg/L in the electrolyte as it was dosed at Mount Gordon Operations to 200grams/tonne or 0.68 mg/L.

The electrolyte was prepared using AR grade copper sulphate and AR grade sulphuric acid. Figure 6-84 shows the EW cell design in detail and Figure 6-85 shows the overall bench scale design. Figure 6-86 shows a photograph of the equipment.

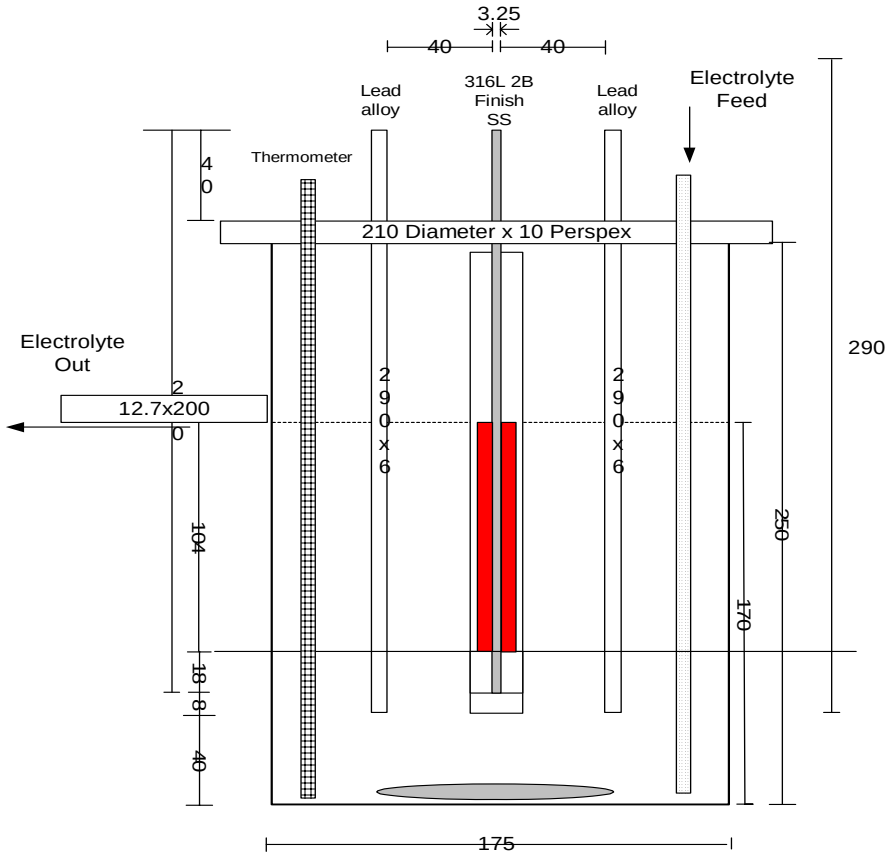

Figure 6-84: EW cell design – parallel plate electrodes

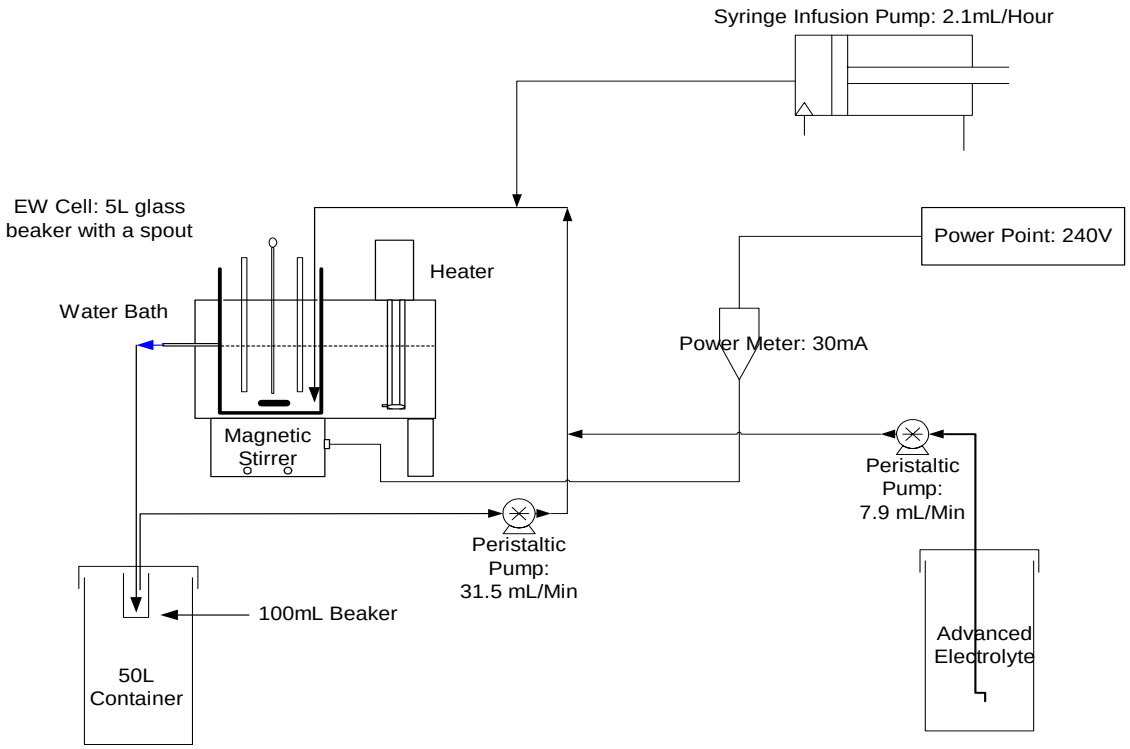

Figure 6-85: Bench Scale Process

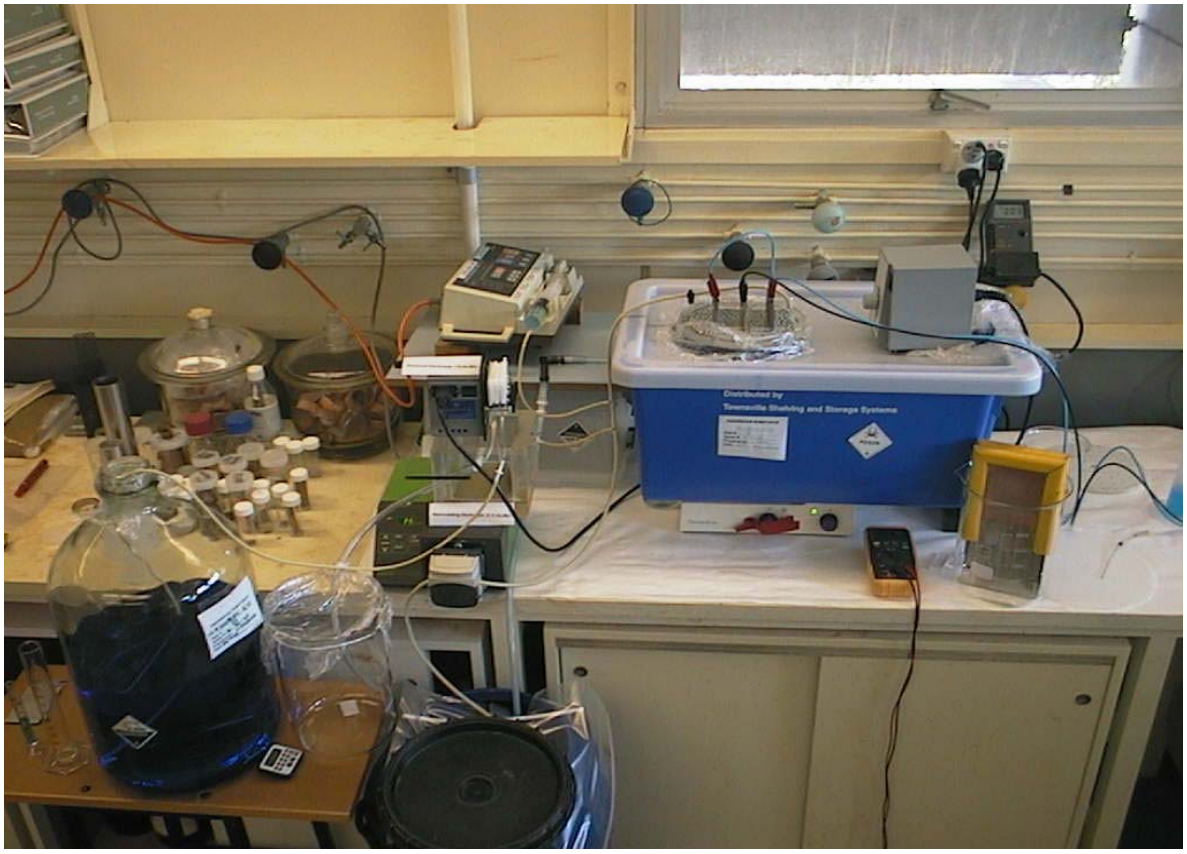

Figure 6-86: Photograph of Bench Scale Equipment

Table 6-32 shows the details of the operating conditions. The net electrolyte volume in the EW cell was 3.9L (without electrodes) and the flow rates of the re-circulating and advanced electrolyte were maintained constant at 31.5 and 7.9 mL/Min, respectively. Eighty percent of the total electrolyte flow rate was re-circulated to the EW cell using a Watson Marlow 505S peristaltic pump to simulate the commercial operation at Mt. Gordon. This recirculation maintains the activity of Guar or APAM constant in the EW cell and also possibly controls their ageing process. The organic additives were dosed constantly at 2.1 mL/hour using a syringe infusion pump. The concentration of the organic additive in the aliquot was 0.68 mg/mL. The electrolyte in the EW cell was stirred using a magnetic stirrer at 30 mA measured with a power meter. This low current induced a minimum agitation to improve the diffusion of the organic additive. The electrolyte temperature was kept at 50.5±0.5^{o}C in a water bath.

Table 6-32: Experimental Conditions

Current Density, A/m^2	340
Voltage Drop, V	2.15
EW Time	44 hours 35 Minutes
Deposition Area (85.5x103.5mm), cm^2	88.5
Average Copper Concentration, g/L	35±1
Sulphuric Acid Concentration, g/L	160
Chloride ions Concentration mg/L	25
Electrolyte Net Volume, L	3.9
Electrolyte Temperature, ^{o}C	50.5 ± 0.5
Guar or APAM, g/tonne Copper Cathode	200
Guar or APAM Conc. in Electrolyte, mg/L	0.68
Advanced Electrolyte, mL/Min	31.5
Recirculating Electrolyte, mL/Min	7.9
Syringe Pump - Dosing Guar or APAM, mL/Hour	2.1
Power to Stir Solution, (30 mA), Watts	7-8
Copper Conc. in Advanced Electrolyte, g/L	50
Sulphuric Conc. in Advanced Electrolyte, g/L	142
Chloride Conc. in Advanced Electrolyte, mg/L	30

The cathode substrate was a 316L 2B finish stainless steel procured from Townsville Refinery Operations, Xstrata and the anodes were prepared from a lead alloy anode received from Mt. Gordon. Current industry-standard ABS edge strips were inserted on the stainless steel and the corners were joined at 45^{o} with Araldite

K138 and hardener K138 Part B, an acid resistant and thermally stable epoxy resin. The stainless steel substrates (3 cathodes) were thoroughly washed with acetone and water, soaked in an electrolyte solution for 24 hours and washed again with distilled water. The distance between the electrodes was 40mm which is similar to the industry standard of copper electrowinning.

Guar was dissolved in water at room temperature, under stirring, for two hours and APAM in 16-fold diluted electrolyte at 50^{o}C also under stirring for two hours.

X-Ray diffraction data was collected using a Siemens/Bruker General Area Detector Diffraction Solution, GADDS diffractometer at the Advanced Analytical Center of James Cook University. The instrumental parameters such as collimator size, detector resolution and beam divergence critically affect the determination of peak broadening[4]. The description of the instrumental parameters used to determine the peak broadening and the electrowinning conditions are presented elsewhere[5] as Appendix C. The GADDS diffractometer was set up to automatically map out a 2cm^2 surface area from the 88.5 cm^2 copper deposits obtained from these electrowinning tests. Preparation of the copper cathode samples for SEM analysis was described in Section 4.2.

6.3 Experimental Results

Three EW tests were conducted (i) with nil additives for 10 hours; (ii) with Guar 44 hours 35 minutes and (iii) and with APAM 44 hours 35 minutes. The copper deposits obtained from the three tests showed no dendrites greater than 1-2mm. The surface roughness of the copper deposits was unable to be measured since it surpassed the specifications of the M1 Perthometer (10nm-100μm). Photographs of the electrowon copper deposits in the presence of Guar are shown in Figures 6-87 and 6-88 and in the presence of APAM are shown in Figures 6-89 and 6-90. It can be seen that the physical appearance of copper deposit obtained with Guar was rougher than that obtained with APAM. Both sides of the deposit produced with Guar have a needle-like, granular appearance throughout the plate. In contrast, the deposit produced with APAM is smoother, brighter and more compact than the copper deposit produced with Guar. Moreover, the copper deposits obtained with Guar possess three areas where copper

deposition has not taken place. This is described as “lacy copper” and was also reported by Sun and O’Keefe[6] in the absence of additives. This kind of deposit is often found at commercial scale electrowinning operations but not at electrorefining operations where animal glue and thiourea are used as organic additives.

These results are consistent with previous EW tests conducted with a rotating cylinder electrode and with CV and EIS tests on the RCE. CV tests indicate that Guar predominantly behaves as a depolarizer on bare stainless steel and on pre-plated copper stainless steel substrates. EIS on pre-plated copper also indicates that Guar reduces the charge-transfer resistance which is consistent with depolarization behaviour. The stainless steel substrate with pre-plated copper at 10 mA/cm^2 for 6 minutes simulates a stainless steel mother plate *in-use* since copper is always present after a stripping operation. In contrast, CV with APAM indicates that under the same conditions it polarizes the electrode and EIS with APAM indicates that it increases the charge-transfer resistance. The polarization behaviour of APAM is similar to a typical levelling agent/surfactant, i.e., glue and polyethylene glycol (PEG).

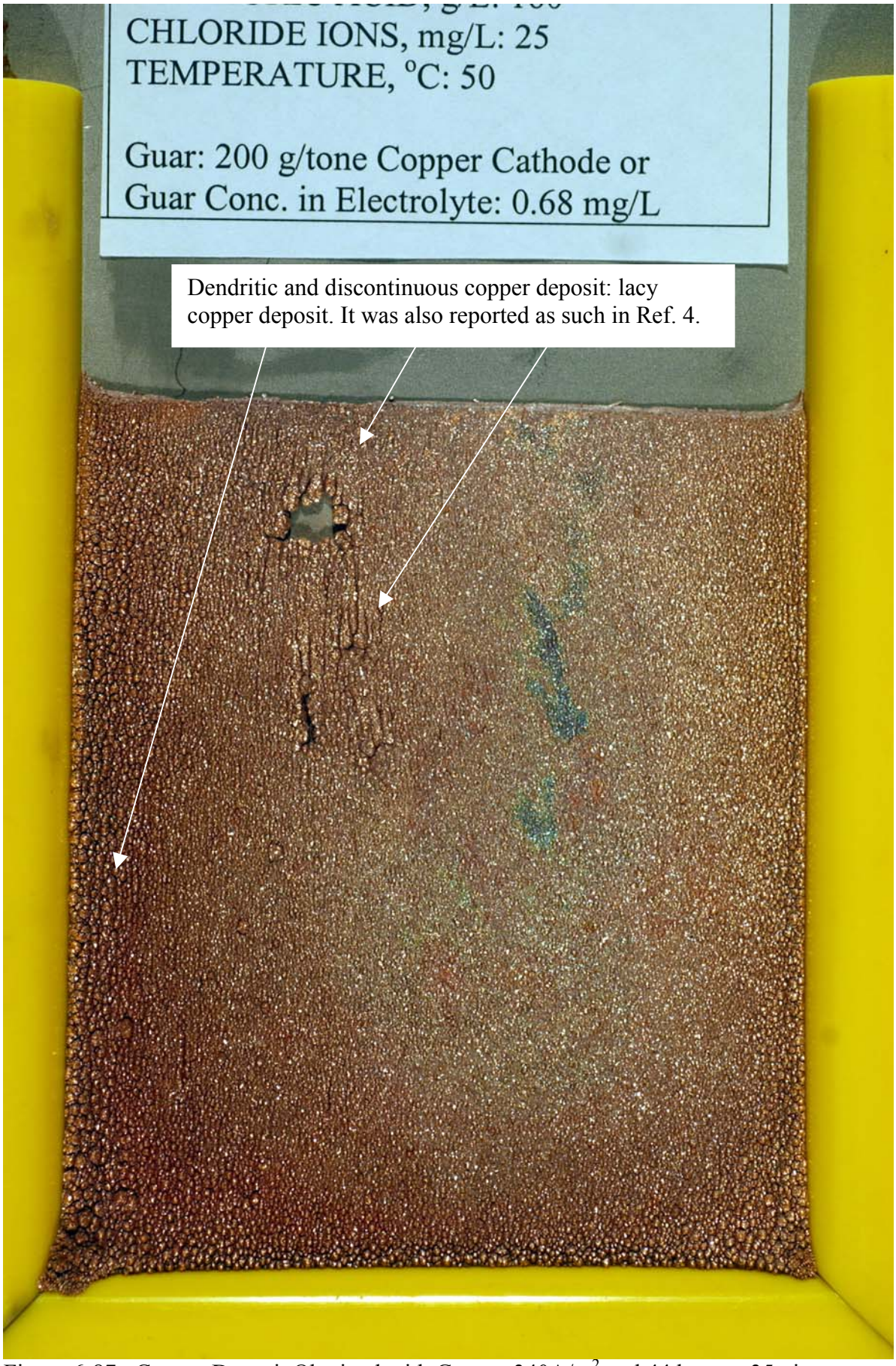

Figure 6-87: Copper Deposit Obtained with Guar at 340A/m^2 and 44 hours - 35minutes

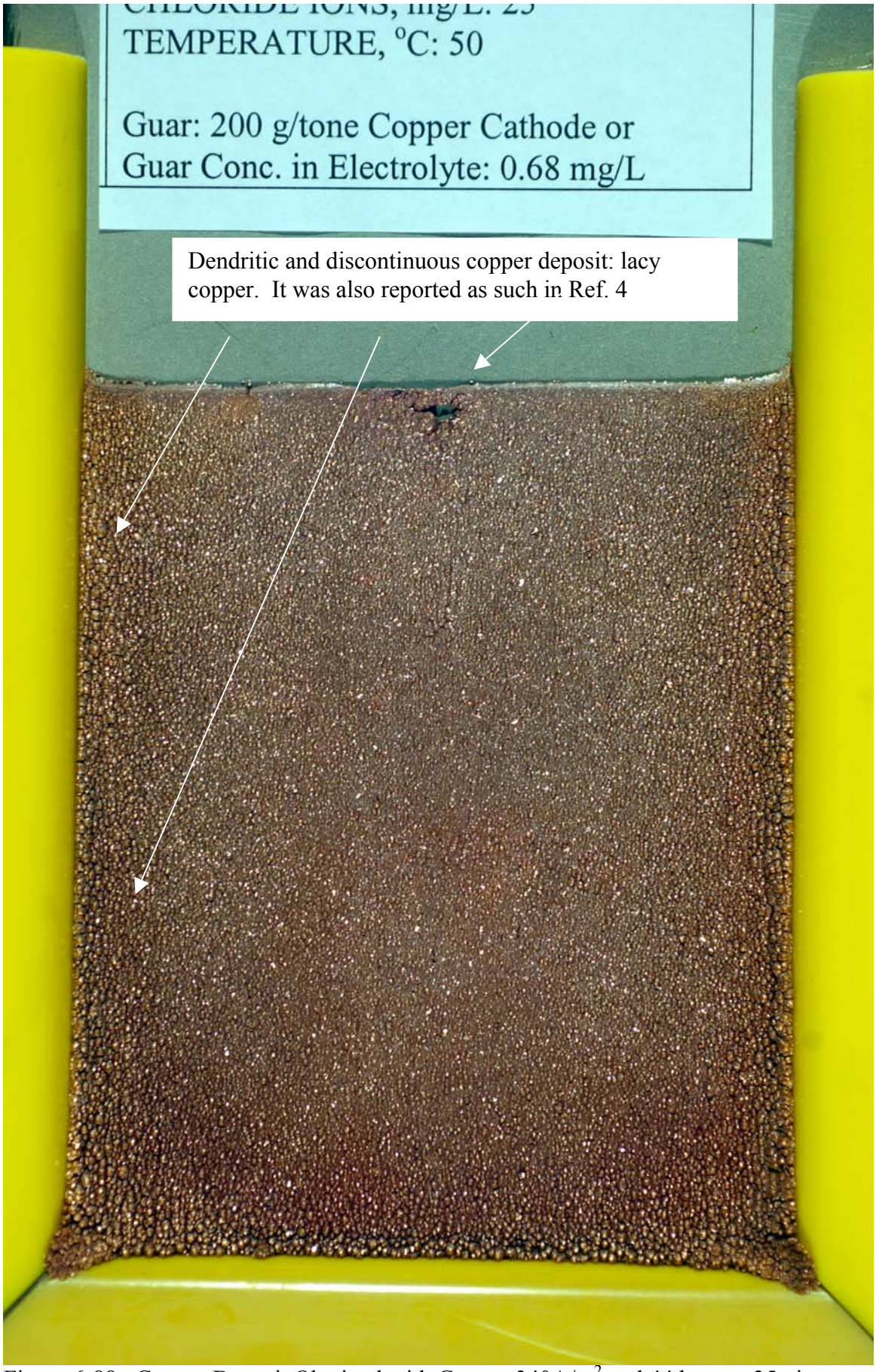

Figure 6-88: Copper Deposit Obtained with Guar at 340A/m^2 and 44 hours - 35minutes

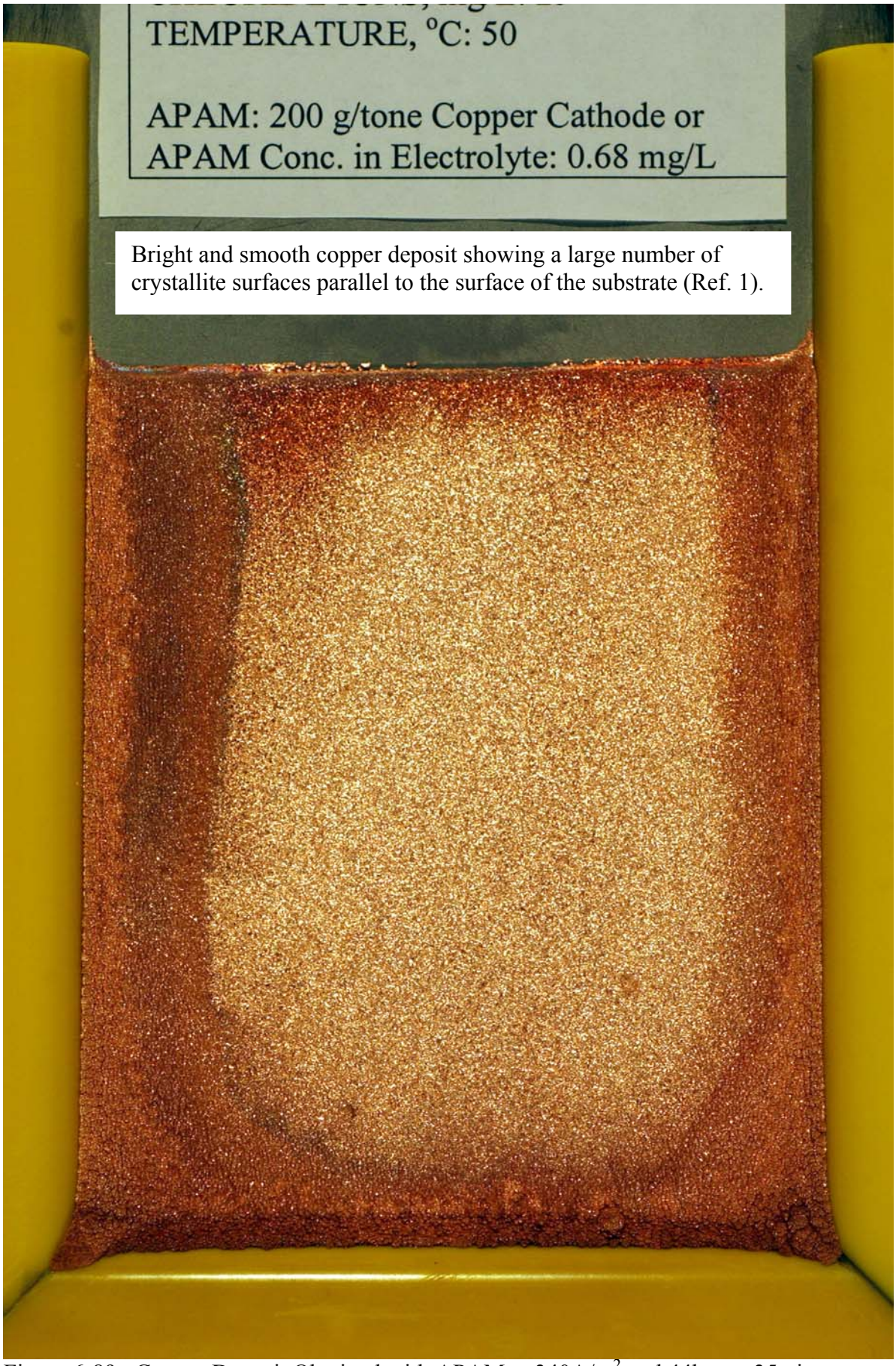

Figure 6-89: Copper Deposit Obtained with APAM at 340A/m^2 and 44hours-35minutes

Figure 6-90: Copper Deposit Obtained with APAM at 340A/m^2 and 44hours-35minutes

6.4 Scanning Electron Microscopy of Copper Cathode Cross-Sections

Figures 6-91 and 6-92 show the scanning electron microscopy (SEM) micrographs of the cross-sectioned copper cathodes obtained from this test work. It can be seen in Figure 6-91 that the cross section of the copper cathode obtained with APAM is slightly columnar growth. It has been reported that this type of growth may be improved into an equiaxial microstructure by adding a sulfur bearing organic additive into the electrolyte bath[7].

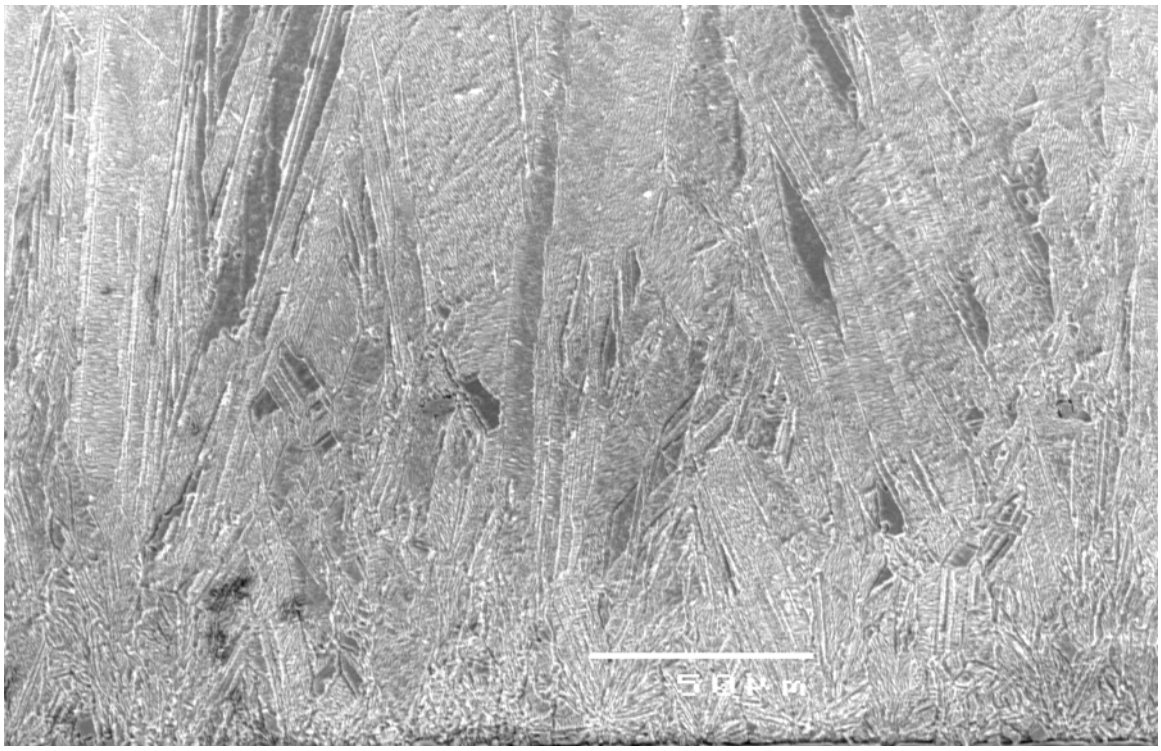

Figure 6-91: SEM micrograph of the copper deposit obtained using 0.68mg/L APAM (200 g/tonne Copper Cathode) at 340 A/m^2 current density. Note the slightly fibrous or columnar structure.

In the presence of Guar (Figure 6-92) the microstructure of the copper deposit is *porous*. This porosity appears to be consistent with the reduction in the charge-transfer resistance that Guar imparts during the deposition process and the inferred predominance of crystal growth over crystal nucleation as discussed in Section 5.8.

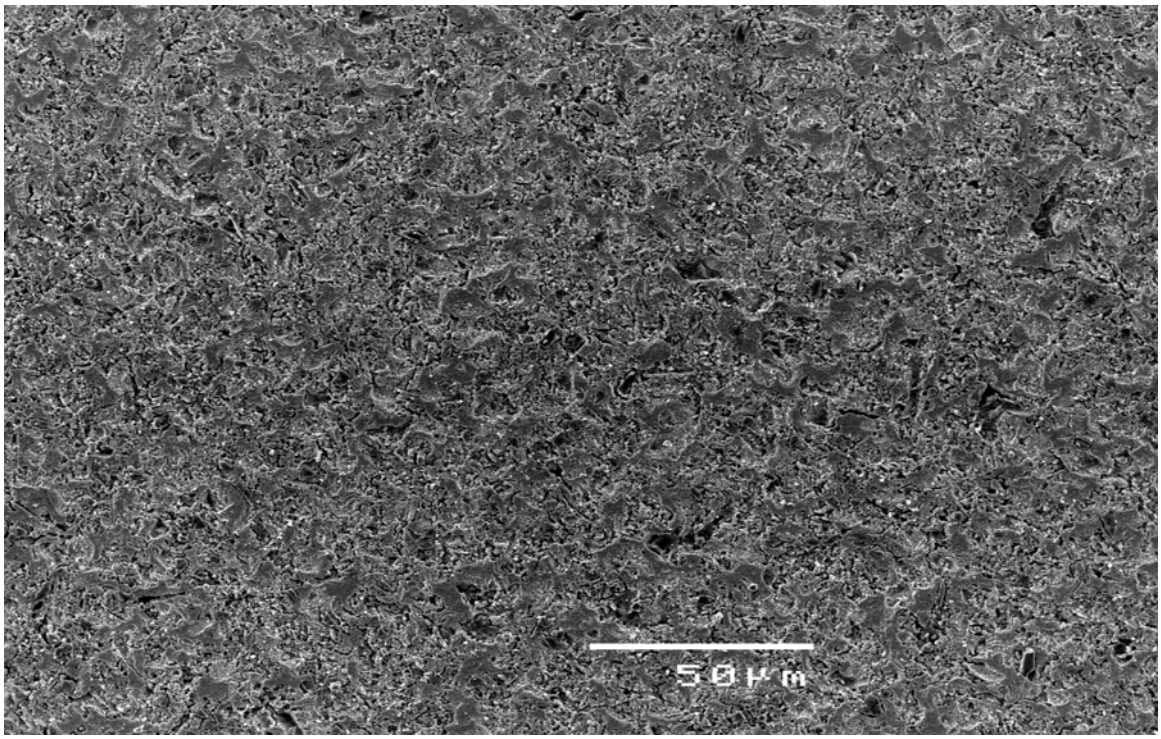

Figure 6-92: SEM micrograph of the copper deposit obtained using 0.68mg/L Guar (200 g/tonne Copper Cathode) at 340 A/m^2 current density. *Note a porous copper cathode.*

6.5 Determination of Crystallite Size

Crystallite size was measured using the General Area Diffraction Detector Solution (GADDS) as described in the paper Fabian et al[5] and reproduced in Appendix C. In summary, GADDS is an x-ray diffraction technique by which the breadth β of the pure diffraction profile commonly also known as the full-width at half-maximum (FWHM) is determined. The crystallite size can then be estimated using the Sherrer Equation as described in Equation 6-27[4,8]:

$$L = \frac{K.\lambda}{\beta.\cos\theta} \qquad (6\text{-}27)$$

where θ and λ are the Bragg angle and x-ray diffraction wavelength in Ansgtroms (Å), respectively. β is the line breadth intensity of the peak in radians. The line breadth is corrected using a Gaussian profile fit ($\beta^2 = U^2\text{-}S^2$; U= copper cathode sample, S= standard). K, λ and θ are 0.9, 1.54184 and 15 degrees, respectively. Lanthanum hexaboride (LaB_6, 660a) procured from National Institute of Standards and

Technology (NIST) was the standard reference material. The GADDS Diffractometer Parameters are shown in Table 6-33.

Table 6-33: GADDS Diffractometer Parameters

Radiation	Cu
Sample-detector distance, cm	30
Collimator, μm	500
kV, mA	40,52
Data Collection time/reading, sec	60
2θ, ω	70, 30
Step size, mm	0.5
Copper plate mapped area, cm^2	~2

The crystallite size was determined to assess whether the presence of APAM or Guar results in different have higher nucleation rates during EW under otherwise constant conditions. These tests may also be important to determine coalescence of small crystallite sizes to form larger crystal sizes according to the mechanism of 3D crystallite size growth.

Table 6-34 and Figure 6-93, reproduced from Fabian et al[5], presented as Appendix C, show the Kruskal-Wallis test results for the effect of the ageing of APAM on crystallite size. The typical preferred orientation profile was [110]>>[111]>[100] for all samples. The copper cathode samples for this analysis were obtained using the *RCE* described in Section 3.2.1. The data was analysed using SPSS program version 11. It indicates that the mean crystallite size differs significantly between the four tests at the 99% confidence level. It can be concluded that at least one of the four samples differs from the others. Inspection of Table 6-34 shows that the crystallite size mean rank and the median crystallite size decreased in the presence of fresh APAM (364 Å) and degraded APAM (398 Å). These values increase in old APAM (438 Å) when APAM had undergone further degradation at 50^oC from 18 to 22 hours by which time it had possibly become inactive. The crystallite size with old APAM (436 Å) is similar to nil APAM (426 Å). Thus:

$$FreshAPAM < DegradedAPAM < OLDAPAM \cong NILAPAM$$

Table 6-34 also shows that the proportion of crystallites larger than 4500Å varied between the 4 Tests. Fresh APAM produced the lowest proportion of crystallite size greater than 4500 Å (15%). Degraded APAM produced greater proportion of crystallites greater than 4500 Å (38%) compared with old APAM (26%) and nil organic additive (27%). Test 3 shows a maximum number of large crystallites and an intermediate median crystallite size. This must mean that there are large numbers of smaller crystallites as well as large crystallites. This is consistent with the formation of a relatively large proportion of small crystallites formed on top of large crystals and their subsequent 3D coalescence.

Table 6-34: Kruskal-Wallis Test Results for APAM Crystallite Size

Test No.	1	2	3	4
Presence/Age of APAM	Nil	Fresh	Degraded	Old
Electrowinning Time, Hours	4	4	4	4
APAM Ageing in Electrolyte at 50°C, Hours		0-4	8-12	18-22
FWHM* Number of Readings, N	1428	156	1479	1493
Crystallite Size Data Processed, N	1040	133	913	1102
Crystallites Size > 4500 Å, %	27	15	38	26
Kruskal-Wallis Crystallite Size Mean Rank	1657	1333	1414	1716
Asymptotic. Sig., Monte Carlo Sig., 99% CI, lower and upper bounds	p = .0000			
Median Crystallite Size, Å	426	364	398	438

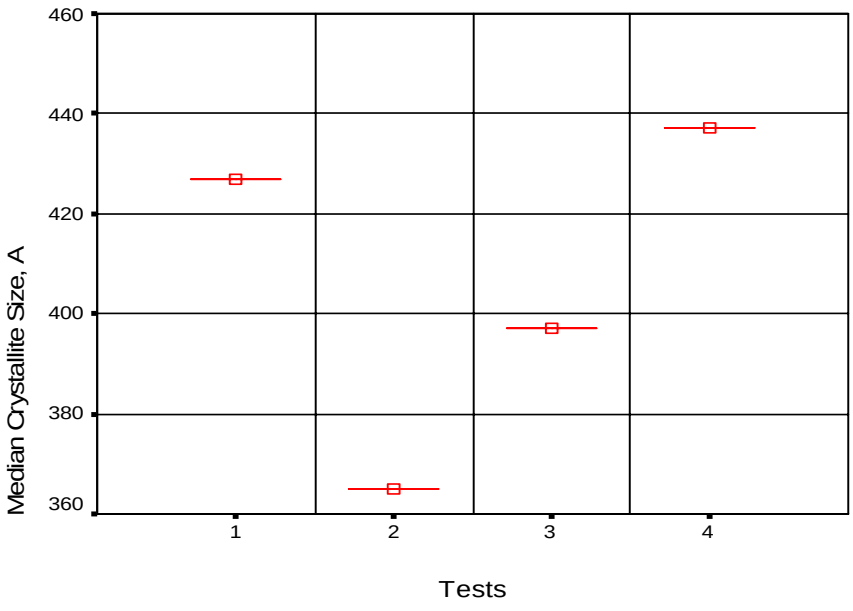

Figure 6-93: Median of Crystallite Size

Table 6-35 shows the Kruskal-Wallis test results for APAM and Guar crystallite size obtained from the bench scale testwork using *parallel plate electrode*. Due to the experimental design, fresh, degraded and old APAM are simultaneously present in the electrowinning cell as would be the case in commercial plants for any additive. It can be seen that the median crystallite size for APAM is smaller than that for Guar. Therefore, APAM appears to favour a higher nucleation rate than Guar. The other important results are the percentage of crystallite size greater than 1800 Å: 41% and 24% for APAM and Guar, respectively. It appears that 3D crystallite growth and coalescence is higher with APAM than that with Guar. This behaviour is probably acceptable as long as the copper deposit is smooth as it is the case with APAM compared with the copper deposit produced with Guar.

Finally, Table 6-34 shows that for degraded APAM (Test 3) 38% of crystallites were larger than 4500Å and 41% (Table 6-35) were larger than 1800Å. It appears from both results that fresh and degraded APAM, also produced in the continuous electrowinning process, favours smoother, brighter with greater proportions of large and small crystallite sizes. The median crystallite size with APAM (405Å) is smaller than with Guar (427Å). Therefore must be a larger number of smaller crystallites with APAM than Guar.

Table 6-35: Kruskal-Wallis Test Results for APAM and Guar Crystallite Size

Test No.	APAM	Guar
Electrowinning Time, Hrs	44.60	44.60
FWHM Number of Readings, N	338	440
Crystallite Size Data Processed, N	198	335
Crystallites Size > 1800 Å, %	41	24
Kruskal-Wallis Crystallite Size Mean Rank	220	295
Asymptotic Significance	0.000	
Median Crystallite Size, Å	405	427

6.6 Conclusions

The rate of nucleation and growth play a dominant role in determining the overall deposition kinetics, as well as the appearance, structure and properties of the

deposit. The copper deposit with APAM is brighter and does have greater amounts of smaller and larger crystallite sizes than those with Guar. It can therefore be inferred that the presence of APAM favours higher nucleation rates and greater 3D crystallite growth and coalescence than those in the presence of Guar (see Table 6-35). APAM is a levelling agent and therefore polarizes the electrode and thus assists the nucleation rate which in turn produces purer copper deposits since voids and porosity are reduced by smaller crystallites. APAM possibly covers the active surface areas (peaks) and therefore deposition has to restart from less active areas (valleys) by forming new nucleates. The brightening effect of the copper deposit in the presence of APAM was probably achieved through large crystal faces that are parallel to the substrate[1].

The quality of the copper deposits in terms of smoothness obtained with APAM are greater than those with Guar. This result is consistent with previous EW tests conducted on a rotating cylinder electrode and CV and EIS tests.

6.7 References

1. Budevski E, Staikov G, Lorenz W. *Electrochemical Phase Formation and Growth, an Introduction to the Initial Stages of Metal Deposition*. New York: VCH; 1996.

2. Paunovic M, Schlesinger M. *Fundamentals of Electrochemical Deposition*: John Wiley & Sons, Inc.; 1998.

3. Robinson T, Rasmussen S, Davenport WG, Jenkings J, King M. Copper Electrowinning - 2003 World Tankhouse Operating Data. In: Dutrizac JE, Clement CG, editors. *Copper 2003 - Cobre 2003 Copper Electrorefining and Electrowinning*; 2003; Santiago, Chile; 2003. p. 421-472.

4. Klug H, Alexander L. *X-Ray Diffraction Procedures for Polycrystalline and Amorphous Materials*. Second ed. Sydney: John Willey & Sons; 1974.

5. Fabian C, Ridd M, Ness S, Lancaster T, Griffin G. Determination of Crystallite Size and Surface Roughness of Copper Deposits for Electrowinning in the Presence of an Organic Additive. In: CA Young AA, CG Anderson, DB Dreisinger, B Harris and A James, editor. *Hydrometallurgy 2003*; 2003; Vancouver, BC Canada: TMS; 2003. p. 1233-1245.

6. Sun M, O'Keefe T. *The Effect of Additives on the Nucleation and Growth onto Stainless Steel Cathodes*. Metallurgical Transaction B 1992;23B:591-599.

7. Plieth W. *Additives in the Electrocrystallization Process*. Electrochimica Acta 1992;37(12):2115-2121.

8. Siemens, Bruker. GADDS Introduction Manual; 2001.

CHAPTER 7

SUMMARY AND CONCLUSIONS

7.1 Introduction

The aim of this thesis was to investigate the role of polyacrylamide as an organic additive in copper electrodeposition. Despite the variety of mechanisms proposed for the smoothening effect of additives[1], a consensus exists that adsorption of the additive on the substrate plays the determining role[2, 3]. The polarizer/inhibitor/leveller controls the vertical growth to produce smooth deposits by conferring preferential adsorption on the peaks or active sites. The grain refiner/accelerator may predominantly control the nucleation process by promoting the formation of new nuclei to form new crystallites at the recesses. There is a synergy between the action of the inhibitor that reduces the rate of vertical growth and the grain refiner that accelerates the formation of nuclei in the recesses of the surface. This synergistic process between the leveller/inhibitor and grain refiner is aimed at improving the overall quality of the copper deposit in terms of purity, smoothness and plant productivity by for example elimination/reduction of short-circuits caused by dendrites in copper electrometallurgy and superconformal growth in the damascene process.

The mechanism and electrochemical action of both Guar and chloride ions have been poorly documented in the literature for copper electrowinning compared with those of glue, thiourea and chloride ions for copper electrorefining.

A better understanding of the role of polyacrylamide and Guar, alone and combined, on copper deposition is particularly important since Mount Gordon Operations of Western Metals Copper Limited, Australia occasionally produced the smoothest copper cathode ever known in the industry. At the commencement of the work described in this thesis, it was not known whether polyacrylamide behaved as a levelling agent or grain refiner or both. The industry-standard additives for copper deposition are shown in Table 7-36. While a levelling agent, grain refiner and chloride ions are dosed in copper electrorefining and in the microelectronics industry, only Guarfloc (Guar) and chloride ions are dosed for copper electrowinning. Guar in copper electrowinning is known as "weak levelling/polarizer" but it has been found throughout this study that Guar is a depolarizer.

Table 7-36: Industry-Standard Additives Used in Copper Electrodeposition

Role of the Additive	Electrorefining		Electrowinning		Microelectronics, PCB and IC	
	Additive	mg/L	Additive	mg/L	Additive	mg/L
Leveller	glue	1	Nil	Nil	PEG*	100-300
Brightener**			Guar	0.25-5		
Grain refiner	thiourea	2	Nil	Nil	SPS&JGB/MPSA*	1&1/1,respectively
Depolarizer	Cl^-	50-60	Cl^-	20-25	Chloride ions	40-60

*PEG, polyethylene glycol; SPS, bis(3-sulfo-propyl) disulfide; JGB, Janus Green B (safranine dye); MPSA, 3-mercapto-1-propanesulfinate. Cl^- = chloride ions, **Guar is also known as weak polarizer in the industry.

It is widely known in the copper deposition industry that chloride ions depolarize the electrode or in other words increases the rate of charge-transfer and consequently increases surface roughness since it enhances growth rate rather than nucleation rate[4-6].

7.2 Hydrolysis and Adsorption of Polyacrylamide

(v)

(vi) Polyacrylamide hydrolysis increases the number of carboxyl functional groups in the polymer chain and the initial hydrolysis reaction is faster than the remainder. Hydrolysis in water at room temperature is

negligible (<2 percent)[7]. Hydrolysis of non-anionic polyacrylamide in strong acid solutions can also lead to the formation polyacrylimide.

(vii)

(viii) It is stated by Halverson et al.[8] and Panzer et al.[9, 10] that hydrolysis at pH 2 predominantly produced *blocks of continuous acrylic acid* or acrylamide segments, i.e., AAA (acrylamide segments) and BBB (acrylic acid segments) functional groups but alkaline hydrolysis contains ABB, BAB, ABA triads. The B-segments from alkaline hydrolysis indicate that it are well distributed along the polymer chain or recently known as *random copolymer*. This average sequence length of carboxyl groups from pH 2 acid hydrolysis was about ten-fold greater[10] than that from alkaline hydrolysis at 110°C after 24-hours. The presence of polyacrylimide was insignificant at pH 2 and alkaline hydrolysis.

(ix)

(x) Literature on the adsorption of PAM on copper metal and 316L stainless steel appears to be nonexistent. The adsorption of polyacrylamide depends on the solution pH, chemical nature of the surface, the presence of solutes and functional groups in the polymer chain. The reaction pathway and therefore product from alkaline hydrolysis is different to that from acid hydrolysis. In general, polyacrylamide adsorption onto solid surfaces may involve both chemical and physical adsorption. Nonionic polyacrylamide in a strong acid medium is attached to the surface through hydrogen bonding as shown in Figure 7-94.

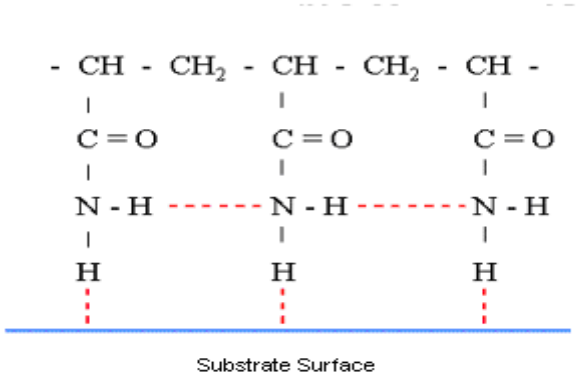

Figure 7-94: Hydrogen Bonding of Non-ionic Polyacrylamide

B*lock copolymers*, Figure 7-95, obtained at pH 2 acid hydrolysis appear to exhibit adsorption by covalent bonding or "salt linkage" where electrons are transferred from the acrylate group to multivalent cations like calcium and iron present in or on the mineral surface[8, 10]. Moreover, light scattering data indicates that under slightly acidic conditions the molecular weight of the polymer remained relatively "static" during the hydrolysis process[11].

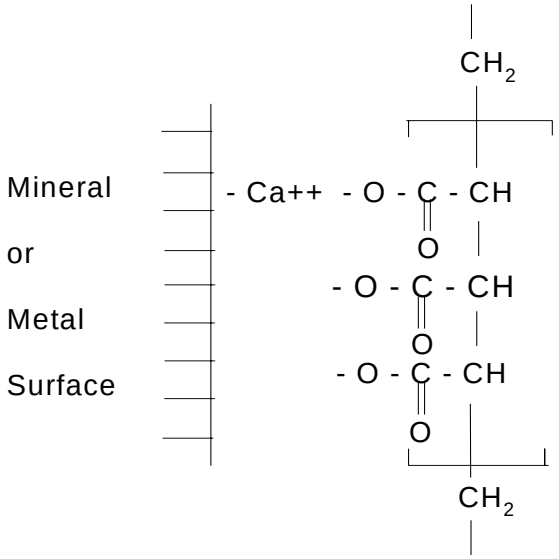

Figure 7-95: Blocky polyacrylamide may exhibit covalent bonding with divalent ions such as calcium and iron [64]

Grchev et al.[12] showed that the surface coverage of 2-3ppm polyacrylamide concentration under strong acid conditions decreased from about 0.52 to 0.02 as the polyacrylamide molecular weight increased from $5x10^3$ to $1.5x10^6$.

7.3 Rotating Cylinder Electrodes

Two rotating cylinder electrodes were built as part of the investigations for this thesis. The diffusion layer thickness (δ) obtained by using the equation developed by Arvia et al.[13] more closely replicate the experimental data than those obtained by using the equation developed by Eisenberg et al.[14]. Moreover, the equation developed by Arvia et al.[13] gives similar δ for the small and large RCE used in this thesis. Therefore diffusion layer thicknesses obtained using Arvia et al.'s[14] equation were compared with

the experimental data produced for this thesis. The results were shown in Chapter 3-Section 3.2.3.

It was shown that the average of surface roughness measurements obtained in this testwork is consistent with those results obtained with Ilgar and O'Keefe[4] who used parallel plate electrodes. However, the δ of 175μm (30°C-40°C) reported by Ilgar and O'Keefe[4] for natural convection, is higher than 97μm at 45°C and 115μm at 65°C δ obtained for this thesis at 0rpm. Nevertheless, these experimental δ values obtained for natural convection for this thesis more closely agrees to 78μm at 25°C which was recently used by Drews et al.[15] but reported elsewhere[16] to conduct Monte Carlo simulation for an electrolyte composition of 18g/L cupric ions and 180g/L sulfuric acid. It has been therefore shown that the fluid flow produced for the RCE built for this thesis is within the published data[4 16] and therefore the fluid flow data produced by the RCE build for this thesis are validated. Moreover, the fluid flow shown produced by the small RCE is *laminar with vortices* and by the large RCE is turbulent with vortices according to Reynolds and Taylor numbers.

7.4 Effect of Polyacrylamide Preparation Media on Surface Roughness

It was shown that when 15 million Dalton Ciba Magnafloc® 800HP nonionic polyacrylamide was prepared in 16-fold diluted electrolyte (sulfuric acid, 10 g/L; copper, 2.25g/L; pH 1.5) at 50°C for 2 hours the under stirring produced a surface with a statistically significantly lower roughness than PAM prepared in water, full-strength electrolyte and alkaline hydrolysis (3hours preparation time). In acid solutions, the surface roughness decreases as the concentration of sulfuric acid decreases indicating its effect on the hydrolysis of polyacrylamide and hence on surface roughness. Based on the material presented in Section 7.2 that showed the formation of block copolymers due to acid hydrolysis of PAM, it is inferred that the reaction product from the 16-fold DE at 50°C for 2 hours under stirring is a block copolymer[8], depicted below, which may also confer covalent bonding with divalent metals as stated by Halverson et al.[8] and Panzer et al.[9, 10]. This reaction product from 16-fold diluted electrolyte is named activated polyacrylamide (APAM) throughout the thesis.

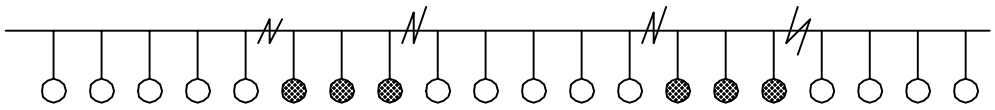

OR

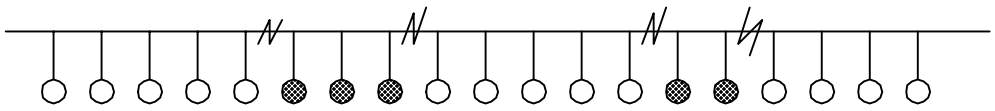

In contrast, it has also been shown that a random copolymer, depicted below, produced from alkaline hydrolysis[8-10], is less effective in controlling the surface roughness than APAM. Based on these results it is also inferred that the adsorption of a random copolymer is less effective than that produced by a block copolymer during copper deposition.

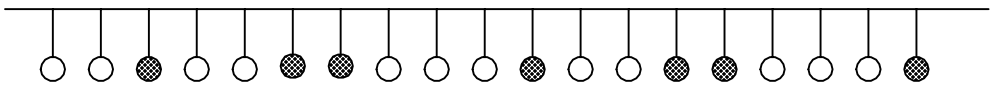

Nonionic polyacrylamide prepared in water, where hydrolysis is insignificant, and in full-strength electrolyte produces similar hydrolysis reactions and products. These hydrolysis products may also adsorb statistically significantly less possibly due to polyacrylimide formation discussed in Chapter 3.

Light scattering data indicated that under slightly acidic condition the molecular weight of the polymer remained relatively "static" during the hydrolysis process[17]. The structure of APAM was confirmed using ^{13}C NMR analysis which indicates the predominance of amide carbonyl carbon with less than 10% hydrolysis. This result is consistent with the experimental hydrolysis of 57% obtained at pH 2, 110^{o}C after 24-hours[8].

APAM is more effective at eliminating dendrite formations than polyacrylic acid up to 12-hours electrowinning. APAM can be maintained in 16-fold diluted electrolyte for about 24 hours without significantly affecting surface roughness.

The APAM degradation process consists of cleavage of the polyacrylamide backbone and this process may enhance the surface coverage and appears to be most likely beneficial to the reduction of surface roughness. This process correlates with the studies of Grchev et al.[12, 18, 19] on the adsorption of polyacrylamide on gold and mild steel in strongly acidified solutions. Polyacrylamide with low molecular weight confers higher surface coverage than polyacrylamide with high molecular weight.

The less optimal results obtained when polyacrylmide was prepared in water and full-strength electrolyte are similar to the experimental conditions conducted by of Pye and Schurz[23] and Vereecken ad Winand[24] who indicated that polyacrylamide controlled the surface roughness of electrowon copper less effectively than Guar. The results obtained with APAM are clearly the opposite than the findings of Pye et al.[23] and Vereecken et al.[24] and this difference is most probably due to the preparation media. APAM is a more effective organic additive to reduce surface roughness than Guar, the industry-standard additive.

7.5 Comparison of Activated Polyacrylamide with Guar

It is shown in the following Section that initially Guar and APAM were studied combined since at the beginning of this project it was not known whether their role were as levelling agent and/or grain refiner. As the results of the initial testwork indicate that APAM and Guar combined were unable to effectively control the surface roughness of the copper cathode due to the presence of Guar; the following testwork were conducted using Guar or APAM alone.

7.5.1 Effect of Guar and APAM on Surface Roughness of Copper Deposits

Two 2^{5-2} fractional factorial experimental designs were conducted as shown Table 7-37. The factors at low level are common for both designs and at high level differ in temperature only.

Table 7-37: Two 2^{5-2} Fractional Factorial Experimental Designs

Factors		Factor Level		
		Low	High	
A	T (Temperature, ^{o}C)	45	55	65
B	i (Current Density, A.m^{-2})	280	320	320
C	L (Guar, mg/L)	0.5	1	1
D	S (APAM, mg/L)	0.5	1	1
E	δ (Diffusion Layer Thickness, μm)	87 (25rpm)	108 (10rpm)	110 (10rpm)

At a 95% confidence interval the models derived from the fractional factorial experimental designs in the temperature range of 45^{o}C-55^{o}C was:

Surface Roughness (μm) =

$$+6.26+0.27*B-0.053*C-0.056*D+0.25*E-0.62*B*C-0.38*B*E \quad (7\text{-}28)$$

where A is temperature; B, current density; C, Guar; D, APAM and E, diffusion layer thickness (δ).

It can be seen from this model that the surface roughness is strongly influenced by an increment of the current density B, (α=0.0180) and diffusion layer thickness E, (α=0.0247). In addition, it is evident that there are two strong interacting terms involving B*C (Current Density*Guar, α<0.0001) and B*E (Current Density*Diffusion Layer Thickness, α=0.0009) which decreases the surface roughness. APAM (D, α=0.6098) and Guar (C, α=0.6316) have an insignificant effect on reducing surface roughness in this temperature range.

At a 95% confidence interval the model derived from the fractional factorial experimental designs in the temperature range of 45^{o}C-65^{o}C was:

Surface Roughness (μm) =

$$+6.16-0.051*A-0.089*B-0.075*C-0.41*D+0.23*E-0.17*B*C \quad (7\text{-}29)$$

It can be seen from this model that APAM D, (α=0.0041) has the most significant effect to reduce surface roughness and APAM is truly independent from Guar (C). Diffusion layer thickness E, (α=0.1004) has the next largest effect and it increases surface roughness as expected. The effect of current density (B) and Guar (C) are insignificant (B*C, α=0.2185). Current Density B (α=0.5192), Guar C, (α=0.5855) and Temperature A, (α=0.7129) follow the sequence and are also insignificant.

It can be seen that the aliased effect of current density (B)*Guar(C) decreases from significant (α<0.0001) in the first model at 45-55^{o}C to insignificant (α = 0.2120) in the second model at 45^{o}C-65^{o}C. This reduction in significance is probably due to the faster degradation of Guar at 65^{o}C than at 45^{o}C at the same current density. It was also shown that the effect of APAM on reducing surface roughness is greater in the 45^{o}C-65^{o}C range than in the 45^{o}C-55^{o}C. This may indicate that the rate of degradation of APAM at 65^{o}C is faster and more effective in reducing surface roughness from the start-up of the EW process than that at 45^{o}C. This is opposite to the effect of Guar.

An experimental design to investigate the effect of an optimal proportion of Guar to APAM on the reduction of surface roughness indicates that this ratio is nonexistent. Overall, Guar alone results in a surface roughness and standard deviation that is higher than for APAM alone or for APAM/Guar combination. This result indicates that Guar reacts faster and loses its levelling efficacy faster than APAM even when it was dosed twice for 6 hours EW time. As Guar quickly looses it levelling effect at 50^{o}C, its degradation process is probably faster at higher temperatures. Therefore, the role of Guar and APAM in copper deposition is independent.

The early stages of dendrite formation in copper electrodeposition occur simultaneously with lower surface roughness and higher number of Peaks-per-Centimeter in the absence of additives, i.e., 30mA/cm^2 and 4.64 hours deposition time. This result agrees with in-situ AFM studies[21, 22].

The peaks-per-Centimeter model for 6 hours electrowinning time accurately predicts that Guar produces higher Peaks-per-Centimeter than APAM. This correlation was clearly demonstrated when electrowinning was conducted for 12 hours where the surface roughness was unmeasurable from the copper cathode produced with Guar dosed for every three hours. In contrast, the surface roughness produced with one and two mg/L of APAM was still measurable (12.79 and 11.71μm) after 12-hours electrowinning time.

It appears that the use of surface roughness measurements to study the effect of organic additives under simulated commercial electrowinning and electrorefining conditions presented in this thesis is the first of its kind.

7.5.2 Physical Appearance, Scanning Electron Microscopy and General Area Detection Diffraction Solutions (GADDS) Results

The effect of the ageing of APAM in the electrolyte was examined using the crystallite size of copper cathodes produced from laboratory scale using a rotating cylinder electrode and bench scale using parallel plate electrodes where Guar or APAM were dosed continuously. An 80% of the spent electrolyte was recycled and mixed with the advanced electrolyte to simulate a commercial EW plant.

Inspection of the results indicate that the median crystallite size decreased in the presence of fresh APAM (364 Å) and degraded APAM (398 Å). These values increase in the presence of old APAM (438 Å) when fresh APAM had undergone further degradation at 50^{o}C from 18 to 22 hours by which time it had possibly become inactive. The crystallite size with old APAM (436 Å) is similar to nil APAM (426 Å).

It has also been shown that degraded APAM (8-12 hours in the electrolyte) has 38% of crystallite size greater than 4500Å and bench scale EW tests with parallel plate electrodes and continuous dosage of APAM shows 41% of crystallite size greater than 1800Å. Moreover, the bench scale copper deposits also indicate to have a median crystallite size of 405Å and 427Å with APAM and Guar, respectively. As the median

crystallite size with APAM is smaller than with Guar, there must be a larger number of smaller crystallites with APAM than Guar.

The rate of nucleation and growth play a dominant role in determining the overall deposition kinetics, as well as the appearance, structure and properties of the deposit. The copper deposit with APAM is brighter and does have greater amounts of smaller and larger crystallite sizes than those with Guar. It can therefore be inferred that the presence of APAM favours higher nucleation rates and greater 3D crystallite growth and coalescence than those in the presence of Guar. APAM possibly covers the active surface areas (peaks) and therefore deposition has to restart from less active areas (valleys) by forming new nucleates. The brightening effect of the copper deposit in the presence of APAM was probably achieved through large crystal faces that are parallel to the substrate[25].

7.5.3 Cyclic Voltammetry and Electrochemical Impedance Spectroscopy Results

Cyclic voltammetry and Electrochemical Impedance Spectroscopy experiments were conducted to investigate the effect of Guar and APAM on the metal electrode (stainless steel and pre-plated copper on stainless steel)/electrolyte interface.

Figure 7-96 depicts the depolarization behaviour of Guar extracted from CV testwork and indicates that about 15mV maximum depolarization was obtained at 2-3 hours residence time whether the metal electrode was stainless steel or copper metal.

In contrast, the maximum polarization on pre-plated copper at with APAM at 45^{o}C and 65^{o}C is approximately 13mV ± 1 but the time to attain this maximum value is about 3.5 hours at 45^{o}C and 1.5 hours at 65^{o}C as shown in Figure 7-97. These results correlate with the fractional factorial experimental results (Section 4.3.2) in which it was demonstrated that APAM had a more significant effect on reducing surface roughness at 65^{o}C than at 45^{o}C.

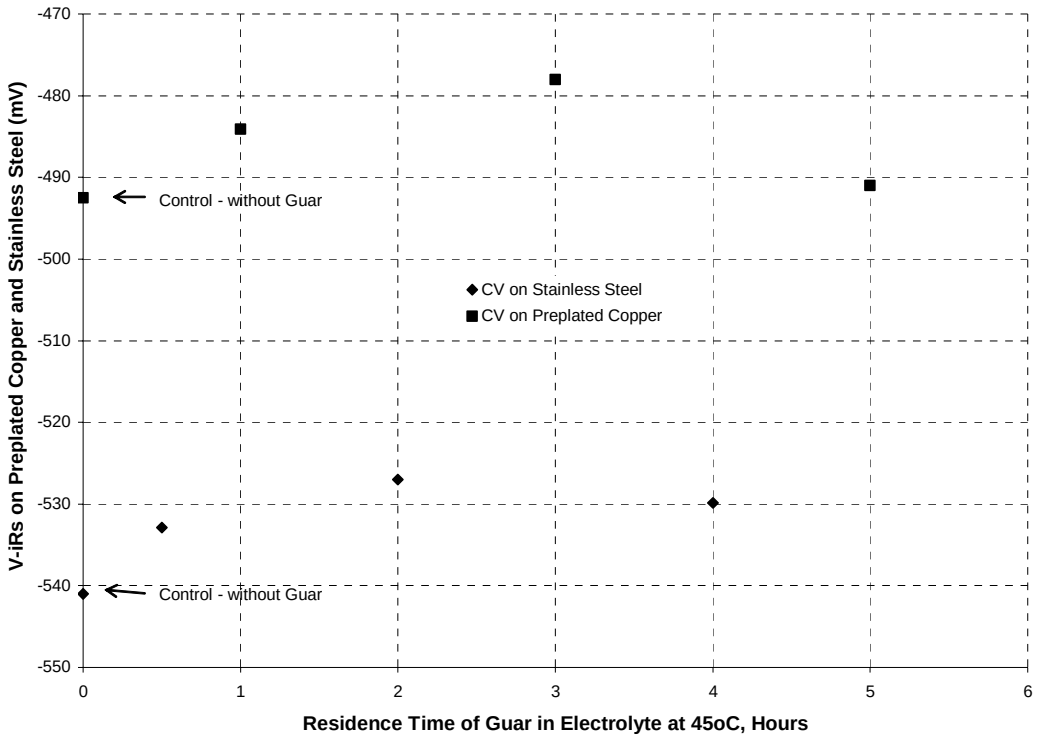

Figure 7-96: Effect of Time on the De-polarization Behaviour of Guar at 45°C at 300A/m^2 Current Density.

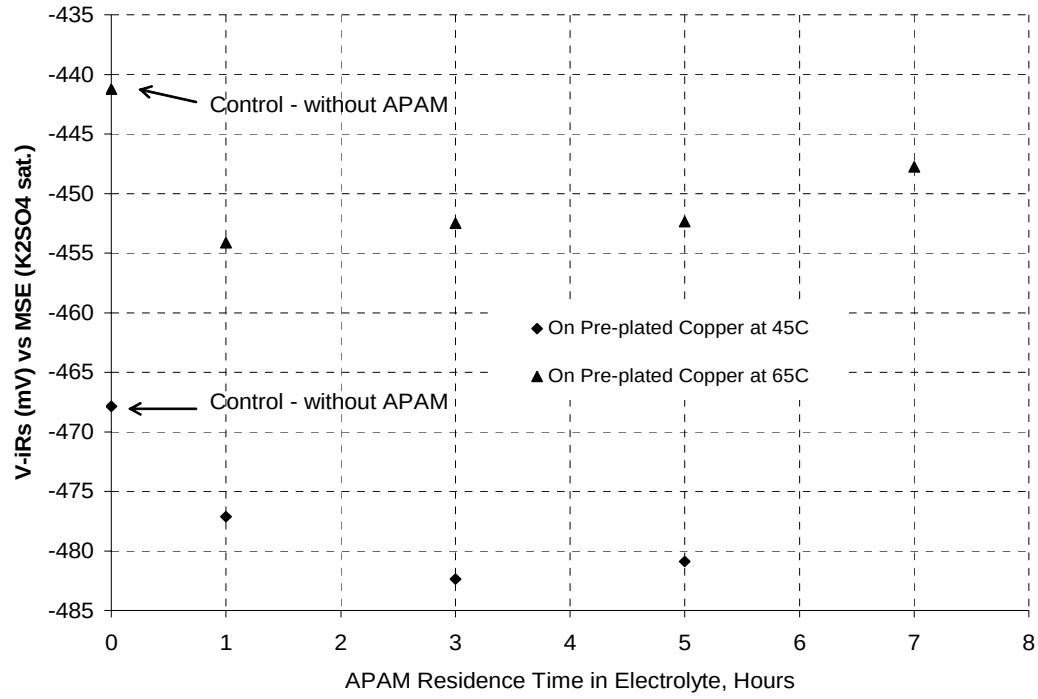

Figure 7-97: Effect of Temperature on APAM Polarization at 300 A/m^2 and 45°C and 65°C

The EIS experimental results were simulated using the equivalent circuit most often referred to in the literature for electrochemical interfaces as depicted in Figure 7-98[26-32] and the LEVM program[27, 33]. This equivalent circuit that consists *only* of resistors and capacitors is used to describe the two single-electron transfer steps[34]. This selection appears to be valid for Langmuir isotherms and other similar isotherms, i.e., Frumkin isotherm. This equivalent circuit was also used for copper deposition in the presence[29] and absence[30] of organic additives.

Table 7-38 summarizes the maximum change in the charge-transfer resistance and double-layer capacitance produced by Guar at 45°C and APAM at 45°C and 65°C. APAM increased the charge-transfer resistance throughout the testwork; in contrast, Guar reduced it. At 45°C, APAM reduced the double-layer capacitance more than Guar at 45°C. This reduction of the double-layer capacitance by APAM was increased when the temperature was increased from 45°C to 65°C. These results indicate that *APAM is more specifically* adsorbed than Guar.

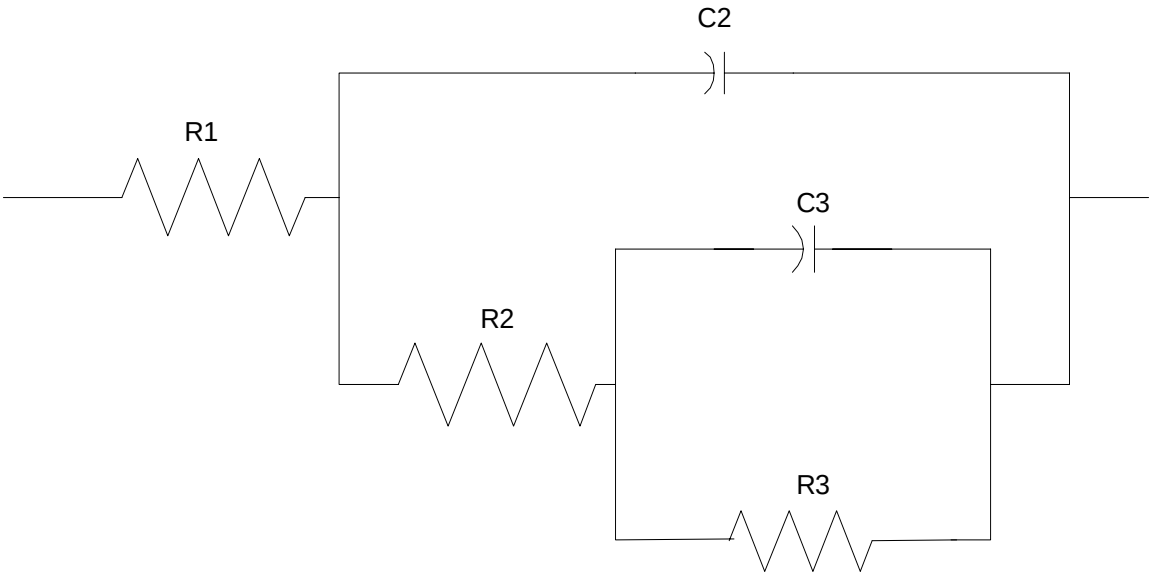

Figure 7-98: Parameters Definition in Equivalent Circuit B[33]

Table 7-38: Charge-Transfer Resistance and Double-Layer Capacitance Differences due to the Presence of Guar and APAM

Additive	EIS Conditions mV vs. MSE	Charge-Transfer Resistance, ohm.cm^2	D-L Capacitance, x 10^{-5}, μF/cm^2	Res. Time in Elec., Hrs.*
Guar	-490mV and 45^{o}C	-0.086	-0.46	2-3
APAM	-470 mV and 45^{o}C	+0.42	-1.2	3-5
APAM	-490mV and 45^{o}C	+0.23	-1.2	3-5
APAM	-445mV and 65^{o}C	+0.34	-6.8	2

*Maximum change determined at these residence times.

The CV results at 45^{o}C is consistent with the EIS results at 45^{o}C in terms that Guar depolarizes the electrode or decreases the charge-transfer resistance and APAM polarized the electrode or increases the charge-transfer resistance. These results for APAM were replicated at 65^{o}C. The EIS data were simulated using the most often referred to equivalent circuit for electrochemical interfaces depicted in Figure 7-98 and LEVM[27, 33]. Moreover, the EIS data with an RDE was not amenable to being modelled using the equivalent circuit presented in Figure 7-98. Overall Cyclic Voltammetry and Electrochemical Impedance Spectroscopy indicated that Guar depolarises the electrode and in contrast APAM polarizes the electrode. Therefore, APAM behaves as a true levelling agent and does so for extended periods of time.

The quality of the copper deposits in terms of smoothness obtained with APAM is greater than those with Guar. This result is consistent with previous EW tests conducted on a rotating cylinder electrode and CV and EIS tests. It is widely recognized in the copper electrometallurgy industry that a smoother copper deposit entrains less impurities. Therefore, APAM is a new levelling agent for copper deposition and may assist the production of copper cathodes with less than 10 ppm total impurities excluding oxygen and will attract a premium price since APAM produces more compacted copper deposits than Guar.

Further investigations to eliminate/reduce the slightly columnar copper deposit obtained with APAM needs to be undertaken. It has been shown that in copper electrorefining the additive system used for about 100 years consists of a levelling agent- glue; grain refiner-thiourea and chloride ions. Similarly, in copper deposition for the fabrication of printed circuit boards and interconnects the additive system consists of a levelling agent and an accelerator/grain refiner. It is therefore hypothesised that

APAM also requires the presence of an accelerator/grain refiner in the electrolyte bath to obtain further improvements of the copper deposits physical and chemical properties. The optimal concentrations of APAM and accelerator/grain in the electrolyte bath (tune up) could be determined using AFM.

(xi) The second research activity is the characterization of the chemical structure of APAM using surface –enhanced Raman spectroscopy (SERS). This study would assist to understand the adsorption mechanism of APAM at the electrode interface. It appears that two contiguous carboxyl oxygens in the block copolymer complex with cuprous or cupric ions. This hypothesis is drawn in accordance with a recently published SERS study on PEG[38].

7.6 References

1. Onicio L, Muresan L. *Some Fundamental Aspects of Levelling and Brightening in Metal Electrodeposition*. Journal of Applied Electrochemistry 1991;21:565-574.

2. Jordan K, Tobias C. *The Effect of Inhibitor Transport on Leveling in Electrodeposition*. J. Electrochem. Soc. 1991;138(5):1251-1259.

3. Chung D. Localized Adsorption of Organic Additives During Copper Electrodeposition [Ph.D.]. Urbana-Champaign: University of Illinois; 1996.

4. Ilgar E, O'Keefe T. Surface Roughening of Electrowon Copper in the Presence of Chloride Ions. In: Dreisinger D, editor. *Aqueous Electrotechnologies: Progress in Theory and Practice*; 1997: The Minerals Metals and Materials Society; 1997. p. 51-62.

5. Wu Q, Barkey D. *Faceting and Roughening Transitions on Copper Single Crystals in Acid Sulfate Plating Baths with Chloride*. Journal of the Electrochemical Society 2000 Mar;147(3):1038-1045.

6. Gabrielli C, Mocoteguy P, Perrot H, Wiart R. *Mechanism of Copper Deposition in a Sulfate Bath Containing Chlorides*. Journal of Electroanalytical Chemistry 2004;572(2):367-375.

7. Tackett J; inventor. Marathon Oil Company, assignee. A Method for Inhibiting Hydrolysis of Polyacrylamide patent WO 92/07881. 1992.

8. Halverson F, Lancaster J, O'Connor M. *Sequence Distribution of Carboxyl Groups in Hydrolyzed Polyacrylamide*. Macromolecules 1985;18(6):1139-44.

9. Panzer H, Halverson F, Lancaster J. *Carboxyl Sequence Distribution in Hydrolyzed Polyacrylamide*. Polymeric Materials Science and Engineering 1984;51:268-71.

10. Panzer H, Halverson F. Blockiness in Hydrolyzed Polyacrylamide. In: Moudgil B, Scheiner B, editors. *Flocculation Dewatering, Proc. Eng. Found. Conf.*; 1988; Palm Coast Florida, USA; 1988. p. 239-49.

11. Muller G, Fenyo J, Selegny E. *High Molecular Weight Hydrolyzed Polyacrylamides. Iii. Effect of Temperature on Chemical Stability*. Journal of Applied Polymer Science 1980;25:627.

12. Grchev T, Cvetkovska M, Stafilov T, Schultze J. *Adsorption of Polyacrylamide on Gold and Iron from Acidic Aqueous Solutions*. Electrochimica Acta 1991;36(8):1315-1323.

13. Arvia AJ, Carrozza JSW. *Mass Transfer in the Electrolysis of Cuso4-H2so4 in Aqueous Solutions under Limiting Current and Forced Convection Employing a Cylindrical Cell with Rotating Electrodes*. Electrochimica Acta 1962;7:65-78.

14. Eisenberg M, Tobias C, Wilke C. *Ionic Mass Transfer and Concentration Polarization at Rotating Electrodes*. Journal of the Electrochemical Society 1954;101(6):306-319.

15. Drews T, Ganley J, Alkire R. *Evolution of Surface Roughness During Copper Electrodepositon in the Presence of Additives*. J. Electrochem. Soc. 2003;150(5):C325-C334.

16. Wilke C, Eisenberg M, Tobias C. *Correlation of Limiting Currents under Free Convection Conditions*. J. Electrochem. Soc. 1953;100(11):513-523.

17. Radeva T, Petkanchin I. *Electro-Optic Study of Oxide Particles in Hydrolyzed Polyacrylamide Solutions*. Journal of Colloid and Interface Science 1995;182:1-5.

18. Grchev T, Cvetkovska M. *Electrochemically Initiated (Co)Polymerization of Acrylamide and Acrylonitrile on a Steel Cathode - Electrochemical and Impedance Study*. Journal of Applied Electrochemistry 1989;19(3):434-42.

19. Grchev T, Cvetkovska M, Schultze JW. *The Electrochemical Testing of Polyacrylic Acid and Its Derivatives as Inhibitors of Corrosion*. Corrosion Science 1991;32(1):103-12.

20. Haschke H, Miles MJ, Koutsos V. *Conformation of a Single Polyacrylamide Molecule Adsorbed onto a Mica Surface Studied with Atomic Force Microscopy*. Macromolecules 2004;37(10):3799-3803.

21. Szymanski G, Dymarska M, Zhao T, Lipkowski J. *Atomic Force Microscopy Study of the Morphology of Electrodeposited Nickel and Copper at Conditions Mimicking Industrial Nickel and Copper Electrorefining*. Electrometallurgy 2001, Proceedings of Annual Hydrometallurgy Meeting, 31st, Toronto, ON, Canada, Aug. 26-29, 2001 2001:375-387.

22. Schmidt W, Alkire R, Gewirth A. *Mechanic Study of Copper Deposition onto Gold Surfaces by Scaling and Spectral Analysis of in-Situ Atomic Force Microscopic Images*. J. Electrochem. Soc. 1996(10):3122-3132.

23. Pye D, Schurz G; inventors. The Dow Chemical Company, assignee. Electrowinning of Metals. United States patent 2,798,040. 1957 July 2, 1957.

24. Vereecken J, Winand R. *Influence of Polyacrylamides on the Quality of Copper Deposits from Acidic Copper Sulphate Solutions*. Surface Technology 1976; 4:227-235.

25. Budevski E, Staikov G, Lorenz W. *Electrochemical Phase Formation and Growth, an Introduction to the Initial Stages of Metal Deposition*. New York: VCH; 1996.

26. Franceschetti DR, Macdonald JR. *Diffusion of Neutral and Charged Species under Small-Signal A.C. Conditions*. J. Electroanal. Chem. 1979;101:307-316.

27. Macdonald JR, editor. *Impedance Spectroscopy Emphasizing Solid Materials and Systems*. Brisbane: John Wiley & Sons; 1987.

28. Mansfeld F, Shih H, Greene H, Tsai C. Analysis of Eis Data for Common Corrosion Processes. In: Scully JR, Silverman DC, Kending MW, editors. *Electrochemical Impedance: Analysis and Interpretation*; 1993; 1993. p. 37-53.

29. Jovic VD, Jovic BM. *Copper Electrodepositon from Copper Acid Baths in the Presence of Polyethylene Glycol and Sodium Chloride*. J. Serb. Chem. Soc. 2001;66(11-12):935-952.

30. Nava de Oca J, Sosa E, Ponce de Leon C, Oropeza M. *Effectiveness Factors in an Electrochemical Reactor with Rotating Cylinder Electrode for the Acid-Cupric/Copper Cathode Interface Process*. Chemical Engineering Science 2001;56(8):2695-2702.

31. Diard JP, Montella C. *Diffusion-Trapping Impedance under Restricted Linear Diffusion Conditions*. Journal of Electroanalytical Chemistry 2003;557:19-36.

32. Brett CMA, Brett AMO. *Electrochemistry, Principles, Methods and Applications*. New York; 1993.

33. Macdonald J. Levm Manual - Complex Nonlinear Least Squares (Cnls). In. 8.0 ed; 2003.

34. Harrington DA, van den Driessche P. *Equivalent Circuits for Some Surface Electrochemical Mechanisms*. Journal of Electroanalytical Chemistry 2004;567(2):153-166.

35. Chibowski S, Wisniewska M. *Study of Electrokinetic Properties and Structure of Adsorbed Layers of Polyacrylic Acid and Polyacrylamide at Ferric Oxide-Polymer Solution Interface*. Colloids and Surfaces A: Physicochemical and Engineering Aspects 2002;208(1-3):131-145.

36. Mark H, Gaylord N, Bikales N. *Encyclopedia of Polymer Science and Technology*; 1969.

37. Petri M, Kolb D, Memmert U, Meyer H. *Adsorption of Polyethylene Glycol on Au(111) Single-Crystal Electrodes and Its Influence on Copper Deposition*. J. Electrochem. Soc. 2004;151(12):C793-C797.

38. Feng ZV, Li X and Gewirth AA, *Inhibition due to the Interaction of Polyethylene Glycol, Chloride and Copper in Plating Baths: A Surface-Enhanced Raman Study*. J. Phys. Chem. B 107, 2003, 9415-9423.

APPENDIX A - PART 1
FLUID FLOW AT SMALL ROTATING CYLINDER ELECTRODE

Mathcad 12 (2005) was used to undertake all the calculations shown in this Appendix. This program firstly calculates the kinematic viscosity and diffusion coefficient of cupric ions at different temperatures from the raw data collected from the literature (Ref. 1-4). It then derives the Reynolds and Taylor numbers to charaterize the fluid flow at the small and large RCE. Finally it uses these numbers to calculate the limiting current density and diffusion layer thickness, δ. The calculated limiting current density and δ are then compared with the experimental data.

The following table provides the raw data from the literature. An exponential curve was fitted to the raw data to obtain the absolute viscosity and diffusion of cupric ions data at the temperatures of interest.

TABLE 1

Temperature C	Fitted-Data Absolute Viscosity μ $\frac{g}{cm\cdot s}$*	Original Density Data(1)*, ρ $\frac{g}{cm^3}$*	Fitted-Data Diffusion Coefficient Cupric Ions, D $\frac{cm^2}{s}$*	RPM*	Original Data (1)* Absolute Viscosity μodata $\frac{g}{cm\cdot s}$*	Original Data (2-4)* Diffusion Coefficient Cupric Ions DO $\frac{cm^2}{s}$*
data :=						
0	20	0.019	1.186	$6\cdot10^{-6}$	10	0.019	$5\cdot10^{-6}$
1	25	0.017	1.183	$7\cdot10^{-6}$	10	0	$4.81\cdot10^{-6}$
2	30	0.015	1.18	$8\cdot10^{-6}$	15	0.015	$7.8\cdot10^{-6}$
3	40	0.012	1.174	$1\cdot10^{-5}$	20	0.012	$9.5\cdot10^{-6}$
4	45	0.011	1.173	$1.1\cdot10^{-5}$	25	0	$9.16\cdot10^{-6}$
5	50	$9.8\cdot10^{-3}$	1.168	$1.2\cdot10^{-5}$	30	$9.79\cdot10^{-3}$	0
6	55	$9.05\cdot10^{-3}$	1.165	$1.3\cdot10^{-5}$	35	0	$1\cdot10^{-5}$
7	60	$8.3\cdot10^{-3}$	1.161	$1.4\cdot10^{-5}$	40	$8.27\cdot10^{-3}$	0
8	65	$7.5\cdot10^{-3}$	1.15	$1.5\cdot10^{-5}$	45	0	$1.62\cdot10^{-5}$

$i := 0..8$*

$T := data^{\langle 0 \rangle}$* $\quad \mu := \left(data \cdot \frac{g}{cm\cdot s}\right)^{\langle 1 \rangle}$* $\quad RPM := data^{\langle 4 \rangle}$*

$D := \left(data \cdot \frac{cm^2}{s}\right)^{\langle 3 \rangle}$* $\quad DO := \left(data \cdot \frac{cm^2}{s}\right)^{\langle 6 \rangle}$*

$\rho := \left(data \cdot \frac{g}{cm^3}\right)^{\langle 2 \rangle}$* $\quad \mu odata := \left(data \cdot \frac{g}{cm\cdot s}\right)^{\langle 5 \rangle}$*

* References in brackets. The ZERO value in the Table 1 means NOT AVAILABLE data.

CALCULATION OF KINEMATIC VISCOSITY, μ/ρ (cm^2/s)

ν = kinematic viscosity - fitted data $\quad$ ν = kinematic viscosity - original data

$$\nu_i := \frac{\mu_i}{\rho_i} *$$

$$N_i := \frac{\mu odata_i}{\rho_i} *$$

$\nu_i =$ *

$1.573 \cdot 10^{-6}$	$m^2 \cdot s^{-1}$
$1.41 \cdot 10^{-6}$	
$1.246 \cdot 10^{-6}$	
$1.005 \cdot 10^{-6}$	
$9.207 \cdot 10^{-7}$	
$8.39 \cdot 10^{-7}$	
$7.772 \cdot 10^{-7}$	
$7.149 \cdot 10^{-7}$	
$6.522 \cdot 10^{-7}$	

$T_i =$

20
25
30
40
45
50
55
60
65

$N_i =$ *

0.01573	stokes
0	
0.01242	
0.01005	
0	
$8.38185 \cdot 10^{-3}$	
0	
$7.12317 \cdot 10^{-3}$	
0	

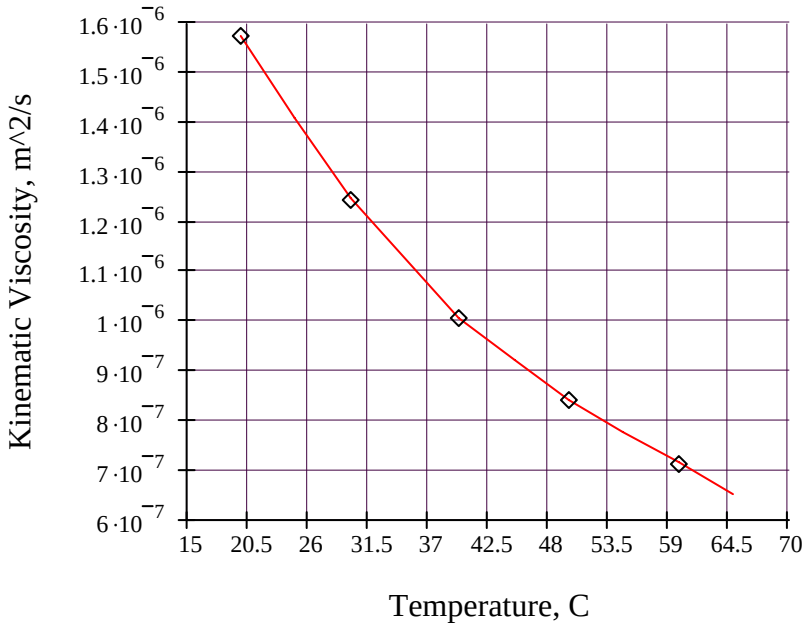

Figure 1. Plot of the Effect of Temperature on Kinematic Viscosity
Original Data (point) and Fitted Data (line)

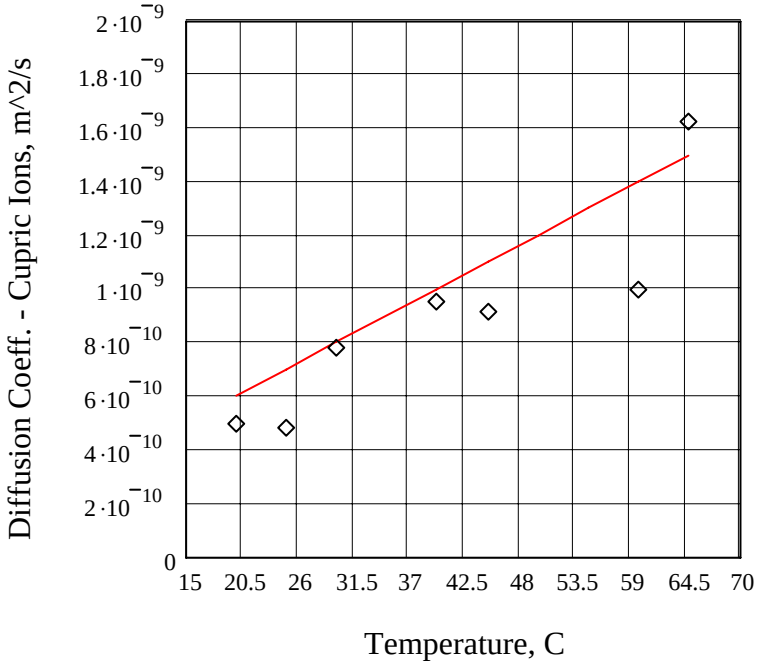

Figure 2. Plot on the Effect of Temperature on the Diffusion Coefficient of Cupric Ions
Original Data (point) and Fitted Data (line)

CALCULATION OF DIFFUSION LAYER THICKNESS USING THE NERNST EQUATION FOR THE SMALL RCE

$$Co := \frac{36\cdot 10^{-3}\ \frac{mol}{cm^3}}{63.546}$$ *

$n := 2$ *

$$F \equiv \frac{96485.3A\cdot s}{mol}$$ *

$di := 1.2cm$ * di is the diameter of the inner RCE, the rotating electrode.

$do := 7.6cm$ * do is the diameter of the outer RCE, stationary electrode.

$ri := \frac{di}{2}$ * $ro := \frac{do}{2}$ * $d := ro - ri$ d is the annulus, interelectrode distance

1. CALCULATION OF SCHMIDT NUMBERS, Sc

Sc numbers at their corresponding temperatures

$$Sc_i := \frac{\nu_i}{D_i}$$ *

$$Sc = \begin{pmatrix} 2622 \\ 2014 \\ 1557 \\ 1005 \\ 837 \\ 699 \\ 598 \\ 511 \\ 435 \end{pmatrix}$$ * $$T = \begin{pmatrix} 20 \\ 25 \\ 30 \\ 40 \\ 45 \\ 50 \\ 55 \\ 60 \\ 65 \end{pmatrix}$$

The Schmidt number varies from 435 at 65 degree C to 2736 at 20 degreeC.

2. CALCULATION OF REYNOLDS NUMBERS, Re

2.1 Calculation of Angular Velocity and Peripheral Velocity

Angular Velocity, ω

$$\omega_i := 2\pi \cdot \frac{RPM_i}{60 \cdot s}*$$

$$\omega = \begin{pmatrix} 1.047 \\ 1.047 \\ 1.571 \\ 2.094 \\ 2.618 \\ 3.142 \\ 3.665 \\ 4.189 \\ 4.712 \end{pmatrix} \frac{1}{sec}*$$

Peripheral Velocity, U

$$U_i := RPM_i \cdot \pi \cdot \frac{di}{60s}*$$

$$U = \begin{pmatrix} 0.628 \\ 0.628 \\ 0.942 \\ 1.257 \\ 1.571 \\ 1.885 \\ 2.199 \\ 2.513 \\ 2.827 \end{pmatrix} \frac{cm}{s}*$$

2.2 Calculation of Reynolds number according to J. Newman, Electrochemical Systems, **2004**, pp. 399: Re=d^2*ω/2ν ; DR Gabe and FC Walsh, J. App. Electrochemistry, 14, **1984**, pp. 555-564: Re=U*d/ν and Eisenberg, M, Tobias, and Wilke, C., J. Electrochem. Soc., **1954**, 101, 6, 306-319.

$$ReNewman_i := \frac{\omega_i \, di^2}{2 \nu_i}*$$

$$ReNewman = \begin{pmatrix} 48 \\ 53 \\ 91 \\ 150 \\ 205 \\ 270 \\ 340 \\ 422 \\ 520 \end{pmatrix}* \qquad RPM = \begin{pmatrix} 10 \\ 10 \\ 15 \\ 20 \\ 25 \\ 30 \\ 35 \\ 40 \\ 45 \end{pmatrix} \qquad T = \begin{pmatrix} 20 \\ 25 \\ 30 \\ 40 \\ 45 \\ 50 \\ 55 \\ 60 \\ 65 \end{pmatrix}$$

$$ReGabe_i := U_i \cdot \frac{di}{\nu_i}*$$

$$ReGabe = \begin{pmatrix} 48 \\ 53 \\ 91 \\ 150 \\ 205 \\ 270 \\ 340 \\ 422 \\ 520 \end{pmatrix}* \qquad RPM = \begin{pmatrix} 10 \\ 10 \\ 15 \\ 20 \\ 25 \\ 30 \\ 35 \\ 40 \\ 45 \end{pmatrix} \qquad T = \begin{pmatrix} 20 \\ 25 \\ 30 \\ 40 \\ 45 \\ 50 \\ 55 \\ 60 \\ 65 \end{pmatrix}$$

2.3 Calculation of Reynolds numbers according to AJ Arvia and JSW Carrozza, Mass Transfer in the Electrolysis of CuSO4-H2SO4 in Aqueous Solutions under Limiting Current Density and Forced Convection Employing a Cylindrical Cell with Rotating Electrodes, Electrochimica Acta, **1962**, pp. 65-78

The anode is the *inner* and *rotating* electrode. Therefore the chatacteristic length is D2 in Arvia et al.'s study and D2 is equal to "di" in this thesis. Arvia et al's. electrolyte composition: CuSO4, 1.5 - 3.5g/L; H2SO4, 147 g/L; Temperature 18C and RPM from 0 - 300.

$$ReArvia_i := \frac{U_i \cdot di}{\nu_i}$$

$$ReArvia = \begin{pmatrix} 48 \\ 53 \\ 91 \\ 150 \\ 205 \\ 270 \\ 340 \\ 422 \\ 520 \end{pmatrix} \quad RPM = \begin{pmatrix} 10 \\ 10 \\ 15 \\ 20 \\ 25 \\ 30 \\ 35 \\ 40 \\ 45 \end{pmatrix} \quad T = \begin{pmatrix} 20 \\ 25 \\ 30 \\ 40 \\ 45 \\ 50 \\ 55 \\ 60 \\ 65 \end{pmatrix}$$

2.4 Calculation of Reynolds numbers according to Barkey et al., J. Electrochem. Soc., Vol. 136, 8, **1989**, 2199-2207 and Silverman DC. *The Rotating Cylinder Electrode for Examining Velocity-Sensitive Corrosion - a Review*. Corrosion **2004**;60(11):1003-1022: Re=w*d^2/ν

$$ReSilverman_i := \frac{\omega_i \, di^2}{\nu_i} *$$

$$ReSilverman = \begin{pmatrix} 96 \\ 107 \\ 182 \\ 300 \\ 409 \\ 539 \\ 679 \\ 844 \\ 1040 \end{pmatrix} * \quad RPM = \begin{pmatrix} 10 \\ 10 \\ 15 \\ 20 \\ 25 \\ 30 \\ 35 \\ 40 \\ 45 \end{pmatrix} \quad T = \begin{pmatrix} 20 \\ 25 \\ 30 \\ 40 \\ 45 \\ 50 \\ 55 \\ 60 \\ 65 \end{pmatrix}$$

2.5 Calculation of Reynolds numbers according to H. Schlichting, Boundary-Layer Theory, **1968**, pp. 500-503.

$$ReSchlichting_i := U_i \cdot \frac{ro - ri}{\nu_i}$$

$$ro - ri = 0.032000m$$

$$ReSchlichting = \begin{pmatrix} 128 \\ 143 \\ 242 \\ 400 \\ 546 \\ 719 \\ 906 \\ 1125 \\ 1387 \end{pmatrix} \quad RPM = \begin{pmatrix} 10 \\ 10 \\ 15 \\ 20 \\ 25 \\ 30 \\ 35 \\ 40 \\ 45 \end{pmatrix} \quad T = \begin{pmatrix} 20 \\ 25 \\ 30 \\ 40 \\ 45 \\ 50 \\ 55 \\ 60 \\ 65 \end{pmatrix}$$

2.6 Calculation of Reynolds numbers according to Wang, L., et al., Chemical Engineering Science, 60, **2005**, 5555-5568 in Reapperance of Azimuthal Waves in Turbulent Taylor-Couette Flow at Large Aspect Ratio. Re=w*ri*d/ν

$$ReWang_i := \frac{\omega_i \cdot ri \cdot d}{\nu_i}$$

$$ReWang = \begin{pmatrix} 128 \\ 143 \\ 242 \\ 400 \\ 546 \\ 719 \\ 906 \\ 1125 \\ 1387 \end{pmatrix} \quad RPM = \begin{pmatrix} 10 \\ 10 \\ 15 \\ 20 \\ 25 \\ 30 \\ 35 \\ 40 \\ 45 \end{pmatrix} \quad T = \begin{pmatrix} 20 \\ 25 \\ 30 \\ 40 \\ 45 \\ 50 \\ 55 \\ 60 \\ 65 \end{pmatrix}$$

2.7 Comparison of Reynolds numbers for the RCE

It has been shown that:

ReNewman = ReGabe = ReEisenberg = ReArvia
ReSilverman = Re Barkey, and
ReSchilichting = ReWang

It appears that the equation for the Reynolds number used by Newman, Gabe, Eisenberg and Arvia is more often quoted in the literature than those used by Barkey, Silverman and Schlichting. Therefore the Reynolds equation used by Newman (Re=ω*d/2ν), Gabe, Eisenberg and Arvia will be used in this thesis.

$$Reynolds_i := ReNewman_i$$

2.8 Calculation of Reynolds numbers at Electrowinning and Electrorefining Temperatures and at Different Speeds fo Rotation

Reynolds Number at 25 C

$$Reynolds25 := \frac{\omega di^2}{(2\nu)_1} *$$

$$Reynolds25 = \begin{pmatrix} 53 \\ 53 \\ 80 \\ 107 \\ 134 \\ 160 \\ 187 \\ 214 \\ 241 \end{pmatrix} * \quad RPM = \begin{pmatrix} 10 \\ 10 \\ 15 \\ 20 \\ 25 \\ 30 \\ 35 \\ 40 \\ 45 \end{pmatrix}$$

Reynolds number at 45 C

$$Reynolds45 := \frac{\omega di^2}{(2\nu)_4} *$$

$$Reynolds45 = \begin{pmatrix} 82 \\ 82 \\ 123 \\ 164 \\ 205 \\ 246 \\ 287 \\ 328 \\ 369 \end{pmatrix} *$$

Reynolds Number at 50 C

$$\text{Reynolds50} := \frac{\omega \text{di}^2}{(2\nu)_5} *$$

$$\text{Reynolds50} = \begin{pmatrix} 90 \\ 90 \\ 135 \\ 180 \\ 225 \\ 270 \\ 315 \\ 359 \\ 404 \end{pmatrix} * \qquad \text{RPM} = \begin{pmatrix} 10 \\ 10 \\ 15 \\ 20 \\ 25 \\ 30 \\ 35 \\ 40 \\ 45 \end{pmatrix}$$

Reynolds Number at 65 C

$$\text{Reynolds65} := \frac{\omega \text{di}^2}{(2\nu)_8} *$$

$$\text{Reynolds65} = \begin{pmatrix} 116 \\ 116 \\ 173 \\ 231 \\ 289 \\ 347 \\ 405 \\ 462 \\ 520 \end{pmatrix} *$$

The Reynolds numbers at 25 rpm increases from Re= 134 at 25C to 205 at 45C, to 225 at 50C and to 289 at 65C. According to DR Gabe, Rotating Electrodes for Use in Electrodeposition Process Control, Plating and Surface Finishing, V 9, 1995, pp. 69-76, the critical Reynolds number for a RCE is 200.

2.8 Calculation of Taylor numbers According to J.Newman, Electrochemical Systems, 1991.

J. Newman (cited above) stated that turbulent flow prevails for Reynolds numbers greater than 3960 or Taylor numbers greater than about 3 x 10^6.

$$\text{TaNewman}_i := \left(\text{Reynolds}_i\right)^2 \cdot \frac{\text{ro} - \text{ri}}{\text{ri}}$$

$$\text{TaNewman} = \begin{pmatrix} 12248 \\ 15251 \\ 43972 \\ 120007 \\ 223537 \\ 387612 \\ 614949 \\ 949181 \\ 1443508 \end{pmatrix} \qquad \text{RPM} = \begin{pmatrix} 10 \\ 10 \\ 15 \\ 20 \\ 25 \\ 30 \\ 35 \\ 40 \\ 45 \end{pmatrix} \qquad \text{T} = \begin{pmatrix} 20 \\ 25 \\ 30 \\ 40 \\ 45 \\ 50 \\ 55 \\ 60 \\ 65 \end{pmatrix}$$

Taylor numbers at 25 rpm and 45C and 65C TaNewmanXXYY: XX=rpm and YY=temperature

$$TaNewman2545C := \left(\frac{\omega_4 \cdot di^2}{2\nu_4}\right)^2 \cdot \frac{ro - ri}{ri} \qquad TaNewman2545C = 224 \times 10^3$$

$$TaNewman2565C := \left(\frac{\omega_4 \cdot di^2}{\nu_8}\right)^2 \cdot \frac{ro - ri}{ri} \qquad TaNewman2565C = 2 \times 10^6$$

2.9 Calculation of Taylor number according to H. Schlichting, Boundary-Layer Theory, 1968, pp. 500-503.

H. Schlichting stated that for 41.3 < Ta < 400 Taylor vortices prevails between 41.3 and 400. Ta > 400 is turbulent.

$$TaSchlichting_i := U_i \frac{ro - ri}{\nu_i} \cdot \sqrt{\frac{ro - ri}{ri}} *$$

$$TaSchlichting = \begin{pmatrix} 295 \\ 329 \\ 559 \\ 924 \\ 1261 \\ 1660 \\ 2091 \\ 2598 \\ 3204 \end{pmatrix} * \qquad RPM = \begin{pmatrix} 10 \\ 10 \\ 15 \\ 20 \\ 25 \\ 30 \\ 35 \\ 40 \\ 45 \end{pmatrix} \qquad T = \begin{pmatrix} 20 \\ 25 \\ 30 \\ 40 \\ 45 \\ 50 \\ 55 \\ 60 \\ 65 \end{pmatrix}$$

Taylor number at 25rpm and 45 C TaSchlichtingXXYY: XX=rpm and YY=temperature

$$TaSchlichting2545 := U_4 \frac{ro - ri}{\nu_4} \cdot \sqrt{\frac{ro - ri}{ri}} * \qquad TaSchlichting2545 = 1.261 \times 10^3 *$$

Taylor number at 25rpm and 65 C

$$TaSchlichting2565 := U_4 \frac{ro - ri}{\nu_8} \cdot \sqrt{\frac{ro - ri}{ri}} * \qquad TaSchlichting2565 = 1.780 \times 10^3 *$$

ν with the subscripts of 4 and 8 indicate the kinematic viscosity at 45C and 65C, respectively.

2.10 SUMMARY

Schlichting (10) indicates that at Re = 94.5 and Ta 41.3 the flow is laminar and at the onset of vortex formation. It remains laminar up to ReSchlichting = 868 and TaSchlichting = 387. Since ReSchlichting and TaSchlichting at 25rpm and 45C and 65C are greater than 868 and 387, respectively; it has then been shown that the fluid flow for the RCE used in this thesis is turbulent according to Schlichting. However, Silverman (cited in Section 2.4 above) states that the Taylor number defined by Schlichting appears to be valid for narrow distances between the concentric cylinders (annular gap) only, i.e., 0.588mm.

The fluid flow for wider annular gaps such as used in this work (d=3.2cm) appears to be better described by Reynolds and Taylor numbers described by J. Newman, Electrochemical Systems, 1991. Newmand states that the fluid flow becomes instable at Re and Ta greater than 200 and 1708, respectively. It is therefore concluded that the fluid flow at the RCE is laminar with vortices since ReNewman at 25 rpm and 45C and 65C are 205 and 289, respectively. The TaylorNewman at 45C and 65C are 223,537 and 1.78 x 10^6, respectively. The onset of turbulence is at Ta 3 x 10^6 according to J. Newman.

3. CALCULATION OF THE LIMITING CURRENT DENSITY (iL) ACCORDING TO M. EISENBERG ET AL. AND J. NEWMAN CITED ABOVE.

3.1 Calculation of the Limiting Current Density According to J. Newman (Electrochemical Systems, 2004, pp. 398) when dR (rotating) = di (limiting CD electrode). The original equation was derived by Eisenberg et al. cited above.

$$iL_i := 0.0791 \cdot \left[n \cdot F \cdot D_i \frac{Co}{di} \cdot \left(\frac{\omega_i \cdot di^2}{2 \nu_i} \right)^{0.7} \left(Sc_i \right)^{0.356} \right] *$$

$$iL = \begin{pmatrix} 11 \\ 12 \\ 19 \\ 28 \\ 36 \\ 45 \\ 54 \\ 64 \\ 75 \end{pmatrix} \frac{mA}{cm^2} * \qquad Reynolds = \begin{pmatrix} 48 \\ 53 \\ 91 \\ 150 \\ 205 \\ 270 \\ 340 \\ 422 \\ 520 \end{pmatrix} \qquad T = \begin{pmatrix} 20 \\ 25 \\ 30 \\ 40 \\ 45 \\ 50 \\ 55 \\ 60 \\ 65 \end{pmatrix}$$

The diffusion layer thickness, δ

$$\delta Newman_i := \frac{n \cdot F \cdot Co \cdot D_i}{iL_i} *$$

$$\delta Newman = \begin{pmatrix} 613 \\ 624 \\ 472 \\ 388 \\ 333 \\ 293 \\ 264 \\ 239 \\ 219 \end{pmatrix} \mu m *$$

3.4 Calculation of the Limiting Current Density and Diffusion Layer Thickness Using Arvia et al.'s Equation cited above

$$iLArvia_i := 0.0791\left(\frac{di}{\nu_i}\right)^{-0.30}\cdot\left(U_i\right)^{0.70}\cdot\left(\frac{do}{di}\right)\cdot\left(Sc_i\right)^{-0.644}\cdot n\cdot F\cdot Co$$

$$iLArvia = \begin{pmatrix}68\\78\\117\\178\\229\\284\\341\\405\\474\end{pmatrix}\frac{mA}{cm^2} \qquad Reynolds = \begin{pmatrix}48\\53\\91\\150\\205\\270\\340\\422\\520\end{pmatrix} \qquad RPM = \begin{pmatrix}10\\10\\15\\20\\25\\30\\35\\40\\45\end{pmatrix} \qquad T = \begin{pmatrix}20\\25\\30\\40\\45\\50\\55\\60\\65\end{pmatrix}$$

SUMMARY
The DLT obtained from Eisenberg's equation is relatively higher than that obtained from Arvia's Equation. The Eisenberg Eq. was determined using hexacyanoferrate (II) and hexacyanoferrate (III) in 2M NaOH as supporting electrolyte. Arvia et al. obtained it using 1.5-3.5g/L copper in 1.5M sulfuric acid and also worked with a fixed cathode as the outer cylinder and a *stirred anode as the inner cylinder*.

3.6 Calculation of the Diffusion Layer Thickness at 10 and 25RPM and 45C and 64C Using Arvia's LCD and Nernst Equation.

$$\delta Arvia_i := \frac{n\cdot F\cdot Co\cdot D_i}{iLArvia_i}*$$

$$\delta Arvia = \begin{pmatrix}97\\98\\75\\61\\53\\46\\42\\38\\35\end{pmatrix}\mu m \qquad RPM = \begin{pmatrix}10\\10\\15\\20\\25\\30\\35\\40\\45\end{pmatrix} \qquad T = \begin{pmatrix}20\\25\\30\\40\\45\\50\\55\\60\\65\end{pmatrix}$$

3.7 Calculation of Diffusion Layer Thickness at 10RPM AND 45C. The results of the LCD and δ are plotted in Figure 3.

$$iLArvia1045 := 0.0791\left(\frac{di}{\nu_4}\right)^{-0.30}\cdot\left(U_1\right)^{0.70}\cdot\left(\frac{do}{di}\right)\cdot\left(Sc_4\right)^{-0.644}\cdot n\cdot F\cdot Co \qquad iLArvia1045 = 1204\,\frac{A}{m^2}$$

$$\delta Arvia1045 := \frac{n\cdot F\cdot Co\cdot D_4}{iLArvia1045}* \qquad \delta Arvia1045 = 100\,\mu m$$

3.8 Calculation of Diffusion Layer Thickness at 10RPM and 65C

$$iLArvia1065 := 0.0791\left(\frac{di}{\nu_8}\right)^{-0.30}\cdot\left(U_1\right)^{0.70}\cdot\left(\frac{do}{di}\right)\cdot\left(Sc_8\right)^{-0.644}\cdot n\cdot F\cdot Co \qquad iLArvia1065 = 1655\,\frac{A}{m^2}$$

$$\delta Arvia1065 := \frac{n\cdot F\cdot Co\cdot D_8}{iLArvia1065}* \qquad \delta Arvia1065 = 99\,\mu m$$

3.9 Calculation of Diffusion Layer Thickness at 25RPM and 45C

$$iLArvia2545 := 0.0791\left(\frac{di}{\nu_4}\right)^{-0.30}\cdot\left(U_4\right)^{0.70}\cdot\left(\frac{do}{di}\right)\cdot\left(Sc_4\right)^{-0.644}\cdot n\cdot F\cdot Co \qquad iLArvia2545 = 2286\,\frac{A}{m^2}$$

$$\delta Arvia2545 := \frac{n\cdot F\cdot Co\cdot D_4}{iLArvia2545}* \qquad \delta Arvia2545 = 53\,\mu m \qquad iLArvia_4 = 2286\,\frac{A}{m^2}$$

3.10 Calculation of Diffusion Layer Thickness at 25RPM and 65C

$$iLArvia2564 := 0.0791\left(\frac{di}{\nu_8}\right)^{-0.30}\cdot\left(U_4\right)^{0.70}\cdot\left(\frac{do}{di}\right)\cdot\left(Sc_8\right)^{-0.644}\cdot n\cdot F\cdot Co \qquad iLArvia2564 = 3143\,\frac{A}{m^2}$$

$$\delta Arvia2564 := \frac{n\cdot F\cdot Co\cdot D_8}{iLArvia2564}* \qquad \delta Arvia2564 = 52\,\mu m$$

3.9 Comparison of Limiting Current Densities

iL = iLNewman = iLEisenberg = ILGabe

$$iL = \begin{pmatrix} 107 \\ 123 \\ 185 \\ 282 \\ 361 \\ 448 \\ 539 \\ 639 \\ 749 \end{pmatrix} \frac{A}{m^2} \qquad RPM = \begin{pmatrix} 10 \\ 10 \\ 15 \\ 20 \\ 25 \\ 30 \\ 35 \\ 40 \\ 45 \end{pmatrix} \qquad T = \begin{pmatrix} 20 \\ 25 \\ 30 \\ 40 \\ 45 \\ 50 \\ 55 \\ 60 \\ 65 \end{pmatrix} \qquad iLArvia = \begin{pmatrix} 677 \\ 777 \\ 1174 \\ 1784 \\ 2286 \\ 2836 \\ 3415 \\ 4047 \\ 4742 \end{pmatrix} \frac{A}{m^2}$$

SUMMARY
The LCD data obtained from the Eq. of Eisenberg et al. is lower than that obtained from the Arvia et al. Eq. The equation for the LCD (iL) was obtained using hexacyanoferrate (II) and hexacyanoferrate (III) in 2M NaOH at 25C. Howeve, LCD iLArvia was obtained using 1.5-3.5g/L cupric ions and 1.5M sulfuric acid at 18C and the *rotating* electrode was the *anode* operating as *inner electrode*. This electrode set up is opposite to that used for this thesis.

Moreover, the diffusion coeficient for cupric ions for Arvia's study was 5.22 x 10^-6 cm^2/s and the kinematic viscosity was 1.279 x 10^-2 cm^2/s at 18C. These overall conditions do not exactly replicate to the conditions under which the data for this thesis were obtained. Therefore, Arvia's data will be used as a reference only.

4.0 Experimental Limiting Current Density and Diffusion Layer Thickness at 0, 10 and 25rpm and 45C and 65C

This experimental LCD was sourced from Chapter 3 - Section 3.2.3 - Table 3.2 to calculate the experimental diffusion layer thickness. The LCD data and δ results are plotted in Figure 3.

4.1 DLT at Zero RPM (Free Convection) at 45C and 65C

iLXXYY, XX=RPM and YY=temperature.

$iL0045 := 1037 \frac{A}{m^2}$ $\qquad \delta 0045 := n \cdot F \cdot Co \cdot \frac{D_4}{iL004}$ $\qquad \delta 0045 = 116 micron$

$iL0065 := 1432 \frac{A}{m^2}$ $\qquad \delta 0065 := n \cdot F \cdot Co \cdot \frac{D_8}{iL006}$ $\qquad \delta 0065 = 115 \mu m$

4.2 DLT at 10 RPM at 45C and 65C

$iL1045 := 1118 \frac{A}{m^2}$ $\qquad \delta 1045 := n \cdot F \cdot Co \cdot \frac{D_4}{iL104}$ $\qquad \delta 1045 = 108 \mu m$

$iL1065 := 1497 \frac{A}{m^2}$ $\qquad \delta 1065 := n \cdot F \cdot Co \cdot \frac{D_8}{iL106}$

$\delta 1065 = 110\,\mu m$

4.3 DLT at 25 RPM at 45C and 65C

$iL2545 := 1150\frac{A}{m^2}$ $\quad \delta 2545 := n \cdot F \cdot Co \cdot \frac{D_4}{iL2545}$ $\quad \delta 2545 = 105\,micron$

$iL2565 := 1660\frac{A}{m^2}$ $\quad \delta 2565 := n \cdot F \cdot Co \cdot \frac{D_8}{iL2565}$ $\quad \delta 2565 = 99\,micron$

Table 2: summarizes the calculated (using Arvia et al.'s equation) and the experimental diffusion layer thickness

TABLE 2

Calculated and Experimental Diffusion Layer Thickness at 0, 10 and 25 RPM and 45C and 65C

			Calculated		Experimental	
	RPM	Temp. C	DiffLT, μm	LCD	DiffLT, μm	LCD
Result :=						

	0	1	2	3	4	5
0	0	45	0	0	97	$1.037 \cdot 10^3$
1	0	65	0	0	115	$1.432 \cdot 10^3$
2	10	45	94	$1.07 \cdot 10^3$	90	$1.118 \cdot 10^3$
3	10	65	99	$1.655 \cdot 10^3$	110	$1.497 \cdot 10^3$
4	25	45	49	$2.032 \cdot 10^3$	87	$1.15 \cdot 10^3$
5	25	65	52	$3.143 \cdot 10^3$	99	$1.66 \cdot 10^3$

$j := 0..5$ $\quad RPMData := Result^{\langle 0 \rangle}$ $\quad TempData := Result^{\langle 1 \rangle}$ $\quad ExpDiffLT := (Result \cdot micron)^{\langle 4 \rangle}$

$DiffLT := (Result \cdot micron)^{\langle 2 \rangle}$ $\quad LCD := \left(Result \cdot \frac{A}{m^2}\right)^{\langle 3 \rangle}$ $\quad ExpLCD := \left(Result \cdot \frac{A}{m^2}\right)^{\langle 5 \rangle}$

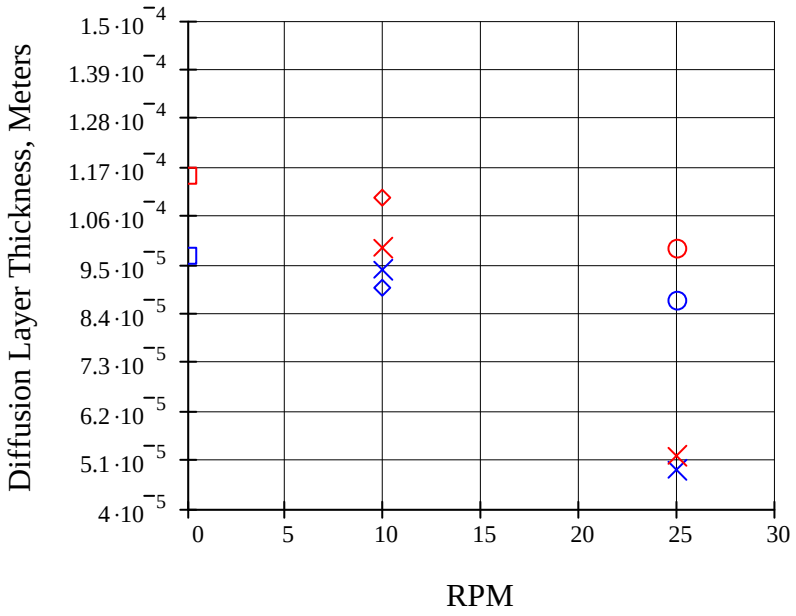

Figure 3: Calculated and Experimental Diffusion Layer Thickness at 0, 10 and 25 RPM and 45C and 65C

Legend: blue=45C; red=65C; squares=Free Convection; x = calculated using Arvia et al.'s LCD Eq. and Nernst Eq.

REFERENCES

1. Price D, Davenport W. *Physico-Chemical Properties of Copper Electrorefining and Electrowinning Electrolytes*. Metallurgical & Materials Transactions B-Process Metallurgy & Materials Processing Science 1981;12B:639-643.

2. Uceda D. Determination of Mass Transfer Characteristics in the Electrolysis of Copper [PhD Thesis]. Missouri-Rolla: University Missouri-Rolla; 1988.

3. Dutra A, O'Keefe T. *Copper Nucleation on Titanium for Thin Film Applications*. Journal of Applied Electrochemistry 1999;29:1217-1227.

4. Newman J, Thomas-Alyea KE. *Electrochemical Systems*. Third ed. Hoboken, New Jersey: John Wiley & Sons, Inc.; 2004.

5. Gabe D. *Rotating Electrodes for Use in Electrodeposition Process Control*. Plating & Surface Finishing 1995;9:69-76.

6. Eisenberg M, Tobias C, Wilke C. *Ionic Mass Transfer and Concentration Polarization at Rotating Electrodes*. Journal of the Electrochemical Society 1954;101(6):306-319.

7. Arvia AJ, Carrozza JSW. *Mass Transfer in the Electrolysis of Cuso4-H2so4 in Aqueous Solutions under Limiting Current and Forced Convection Employing a Cylindrical Cell with Rotating Electrodes*. Electrochimica Acta 1962;7:65-78.

8. Barkey D, Muller R, Tobias C. *Roughness Development in Metal Electrodeposition I. Experimental Results*. Journal of the Electrochemical Society 1989;138(8):2199-2207.

9. Silverman DC. *The Rotating Cylinder Electrode for Examining Velocity-Sensitive Corrosion - a Review*. Corrosion 2004;60(11):1003-1022.

10. Schlichting H. *Boundary-Layer Theory*. Sydney: McGraw-Hill; 1968.

11. Wang L, Olsen M, Vigil R. *Reappearance of Azimuthal Waves in Turbulent Taylor-Couette Flow at Large Aspect Ratio*. Chemical Engineering Science 2005;60:5555-5568.

12. Newman J. *Electrochemical Systems*. Second ed. London: Prentice-Hall International; 1991.

APPENDIX A - PART 2
FLUID FLOW AT LARGE ROTATING CYLINDER ELECTRODE

Mathcad 12 (2005) was used to undertake all the calculations shown in this Appendix. This program firstly calculates the kinematic viscosity and diffusion coefficient of cupric ions at different temperatures from the raw data collected from the literature (Ref. 1-4). It then derives the Reynolds and Taylor numbers to charaterize the fluid flow at the small and large RCE. Finally it uses these numbers to calculate the limiting current density and diffusion layer thickness, δ. The calculated limiting current density and δ are then compared with the experimental data.

The following table provides the raw data from the literature. An exponential curve was fitted to the raw data to obtain the absolute viscosity and diffusion of cupric ions data at the temperatures of interest.

TABLE 1

Temperature C	Fitted-Data Absolute Viscosity μ	Original Density Data(1)*, ρ	Fitted-Data Diffusion Coefficient Cupric Ions, D		Original Data (1)* Absolute Viscosity μodata	Original Data (2-4)* Diffusion Coefficient Cupric Ions DO
	$\frac{g}{cm\cdot s}$*	$\frac{g}{cm^3}$*	$\frac{cm^2}{s}$*	RPM*	$\frac{g}{cm\cdot s}$*	$\frac{cm^2}{s}$*

data :=

	0	1	2	3	4	5	6
0	20	0.019	1.186	$6\cdot10^{-6}$	10	0.019	$5\cdot10^{-6}$
1	25	0.017	1.183	$7\cdot10^{-6}$	10	0	$4.81\cdot10^{-6}$
2	30	0.015	1.18	$8\cdot10^{-6}$	15	0.015	$7.8\cdot10^{-6}$
3	40	0.012	1.174	$1\cdot10^{-5}$	20	0.012	$9.5\cdot10^{-6}$
4	45	0.011	1.173	$1.1\cdot10^{-5}$	25	0	$9.16\cdot10^{-6}$
5	50	$9.8\cdot10^{-3}$	1.168	$1.2\cdot10^{-5}$	30	$9.79\cdot10^{-3}$	0
6	55	$9.05\cdot10^{-3}$	1.165	$1.3\cdot10^{-5}$	35	0	$1\cdot10^{-5}$
7	60	$8.3\cdot10^{-3}$	1.161	$1.4\cdot10^{-5}$	40	$8.27\cdot10^{-3}$	0
8	65	$7.5\cdot10^{-3}$	1.15	$1.5\cdot10^{-5}$	45	0	$1.62\cdot10^{-5}$

$i := 0..8$*

$T := data^{\langle 0 \rangle}$*

$\mu := \left(data \cdot \frac{g}{cm\cdot s}\right)^{\langle 1 \rangle}$*

$\rho := \left(data \cdot \frac{g}{cm^3}\right)^{\langle 2 \rangle}$*

$D := \left(data \cdot \frac{cm^2}{s}\right)^{\langle 3 \rangle}$*

$RPM := data^{\langle 4 \rangle}$*

$\mu odata := \left(data \cdot \frac{g}{cm\cdot s}\right)^{\langle 5 \rangle}$*

$DO := \left(data \cdot \frac{cm^2}{s}\right)^{\langle 6 \rangle}$*

* References in brackets. The ZERO value in the Table 1 means NOT AVAILABLE data.

CALCULATION OF KINEMATIC VISCOSITY, μ/ρ (cm^2/s)

ν = kinematic viscosity - fitted data

$$\nu_i := \frac{\mu_i}{\rho_i} *$$

ν = kinematic viscosity - original data

$$N_i := \frac{\mu odata_i}{\rho_i} *$$

ν_i =

$1.573 \cdot 10^{-6}$	$m^2 \cdot s^{-1}$
$1.41 \cdot 10^{-6}$	
$1.246 \cdot 10^{-6}$	
$1.005 \cdot 10^{-6}$	
$9.207 \cdot 10^{-7}$	
$8.39 \cdot 10^{-7}$	
$7.772 \cdot 10^{-7}$	
$7.149 \cdot 10^{-7}$	
$6.522 \cdot 10^{-7}$	

T_i =

20
25
30
40
45
50
55
60
65

N_i =

0.01573	stokes
0	
0.01242	
0.01005	
0	
$8.38185 \cdot 10^{-3}$	
0	
$7.12317 \cdot 10^{-3}$	
0	

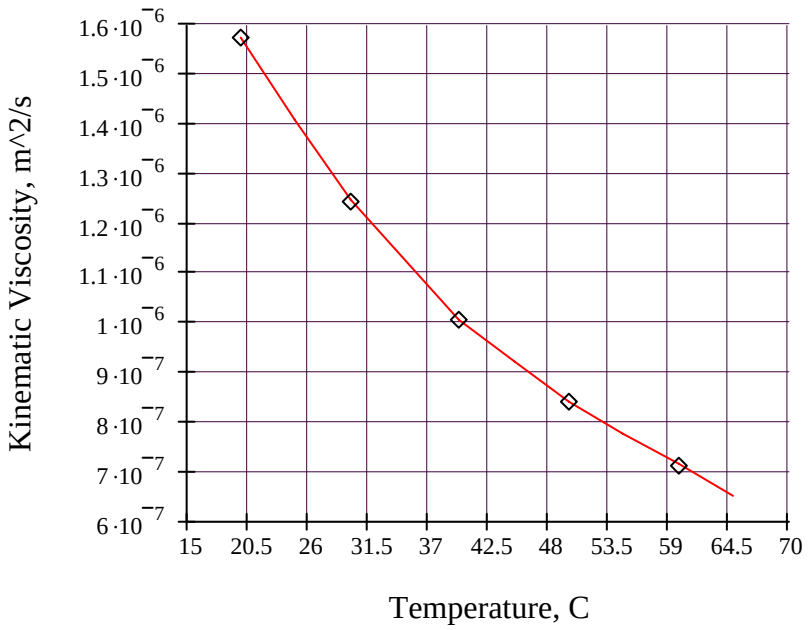

Figure 1. Plot of the Effect of Temperature on Kinematic Viscosity
Original Data (point) and Fitted Data (line)

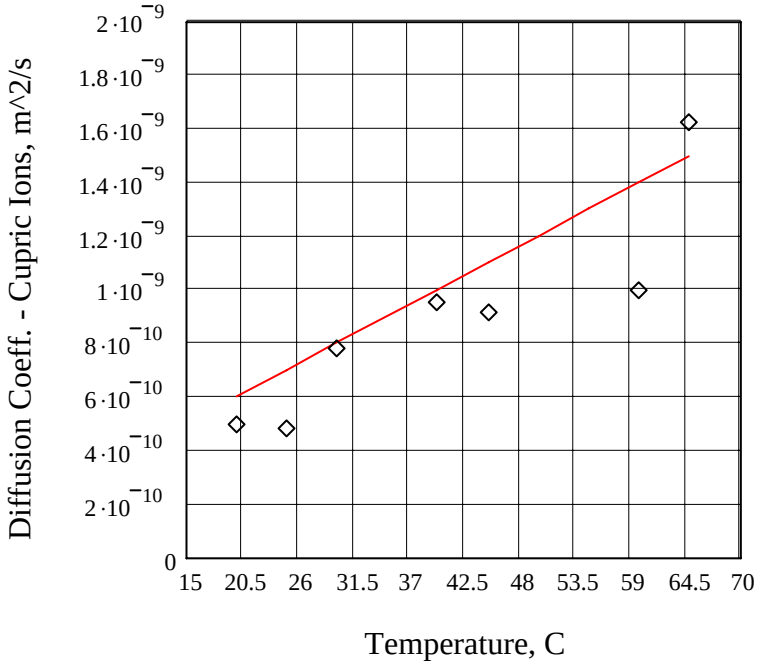

Figure 2. Plot on the Effect of Temperature on the Diffusion Coefficient of Cupric Ions
Original Data (point) and Fitted Data (line)

CALCULATION OF DIFFUSION LAYER THICKNESS USING THE NERNST EQUATION FOR THE SMALL RCE

$$Co := \frac{36 \cdot 10^{-3} \frac{mol}{cm^3}}{63.546} \quad n := 2 \quad F \equiv \frac{96485.3\,A \cdot s}{mol}$$

$di := 4.445\,cm$ di is the diameter of the inner RCE, the rotating electrode.

$do := 16.6\,cm$ do is the diameter of the outer RCE, stationary electrode.

$ri := \frac{di}{2}$ $ro := \frac{do}{2}$ $d := ro - ri$ d is the annulus, interelectrode distance

1. CALCULATION OF SCHMIDT NUMBERS, Sc

Sc numbers at their corresponding temperatures

$$Sc_i := \frac{\nu_i}{D_i}*$$

$$Sc = \begin{pmatrix} 2622 \\ 2014 \\ 1557 \\ 1005 \\ 837 \\ 699 \\ 598 \\ 511 \\ 435 \end{pmatrix} \quad T = \begin{pmatrix} 20 \\ 25 \\ 30 \\ 40 \\ 45 \\ 50 \\ 55 \\ 60 \\ 65 \end{pmatrix}$$

The Schmidt number varies from 435 at 65 degree C to 2736 at 20 degreeC.

2. CALCULATION OF REYNOLDS NUMBERS, Re

2.1 Calculation of Angular Velocity and Peripheral Velocity

Angular Velocity, ω

$$\omega_i := 2\pi \cdot \frac{RPM_i}{60 \cdot s}*$$

$$\omega = \begin{pmatrix} 1.047 \\ 1.047 \\ 1.571 \\ 2.094 \\ 2.618 \\ 3.142 \\ 3.665 \\ 4.189 \\ 4.712 \end{pmatrix} \frac{1}{sec}*$$

Peripheral Velocity, U

$$U_i := RPM_i \cdot \pi \cdot \frac{di}{60s}*$$

$$U = \begin{pmatrix} 2.327 \\ 2.327 \\ 3.491 \\ 4.655 \\ 5.818 \\ 6.982 \\ 8.146 \\ 9.31 \\ 10.473 \end{pmatrix} \frac{cm}{s}*$$

2.2 Calculation of Reynolds number according to J. Newman, Electrochemical Systems, **2004**, pp. 399: Re=d^2*ω/2ν ; DR Gabe and FC Walsh, J. App. Electrochemistry, 14, **1984**, pp. 555-564: Re=U*d/ν and Eisenberg, M, Tobias, and Wilke, C., J. Electrochem. Soc., **1954**, 101, 6, 306-319.

$$ReNewman_i := \frac{\omega_i \cdot di^2}{2 \cdot \nu_i} *$$

$$ReNewman = \begin{pmatrix} 658 \\ 734 \\ 1246 \\ 2058 \\ 2809 \\ 3699 \\ 4659 \\ 5788 \\ 7138 \end{pmatrix} * \quad RPM = \begin{pmatrix} 10 \\ 10 \\ 15 \\ 20 \\ 25 \\ 30 \\ 35 \\ 40 \\ 45 \end{pmatrix} \quad T = \begin{pmatrix} 20 \\ 25 \\ 30 \\ 40 \\ 45 \\ 50 \\ 55 \\ 60 \\ 65 \end{pmatrix}$$

$$ReGabe_i := U_i \cdot \frac{di}{\nu_i} *$$

$$ReGabe = \begin{pmatrix} 658 \\ 734 \\ 1246 \\ 2058 \\ 2809 \\ 3699 \\ 4659 \\ 5788 \\ 7138 \end{pmatrix} * \quad RPM = \begin{pmatrix} 10 \\ 10 \\ 15 \\ 20 \\ 25 \\ 30 \\ 35 \\ 40 \\ 45 \end{pmatrix} \quad T = \begin{pmatrix} 20 \\ 25 \\ 30 \\ 40 \\ 45 \\ 50 \\ 55 \\ 60 \\ 65 \end{pmatrix}$$

2.3 Calculation of Reynolds numbers according to AJ Arvia and JSW Carrozza, Mass Transfer in the Electrolysis of CuSO4-H2SO4 in Aqueous Solutions under Limiting Current Density and Forced Convection Employing a Cylindrical Cell with Rotating Electrodes, Electrochimica Acta, **1962**, pp. 65-78

The anode is the *inner* and *rotating* electrode. Therefore the chatacteristic length is D2 in Arvia et al.'s study and D2 is equal to "di" in this thesis. Arvia et al's. electrolyte composition: CuSO4, 1.5 - 3.5g/L; H2SO4, 147 g/L; Temperature 18C and RPM from 0 - 300.

$$ReArvia_i := \frac{U_i \cdot di}{\nu_i}$$

$$ReArvia = \begin{pmatrix} 658 \\ 734 \\ 1246 \\ 2058 \\ 2809 \\ 3699 \\ 4659 \\ 5788 \\ 7138 \end{pmatrix} \quad RPM = \begin{pmatrix} 10 \\ 10 \\ 15 \\ 20 \\ 25 \\ 30 \\ 35 \\ 40 \\ 45 \end{pmatrix} \quad T = \begin{pmatrix} 20 \\ 25 \\ 30 \\ 40 \\ 45 \\ 50 \\ 55 \\ 60 \\ 65 \end{pmatrix}$$

2.4 Calculation of Reynolds numbers according to Barkey et al., J. Electrochem. Soc., Vol. 136, 8, **1989**, 2199-2207 and Silverman DC. *The Rotating Cylinder Electrode for Examining Velocity-Sensitive Corrosion - a Review*. Corrosion **2004**;60(11):1003-1022: Re=w*d^2/ν

$$ReSilverman_i := \frac{\omega_i \cdot di^2}{\nu_i} *$$

$$ReSilverman = \begin{pmatrix} 1315 \\ 1467 \\ 2492 \\ 4116 \\ 5618 \\ 7398 \\ 9318 \\ 11577 \\ 14276 \end{pmatrix} * \quad RPM = \begin{pmatrix} 10 \\ 10 \\ 15 \\ 20 \\ 25 \\ 30 \\ 35 \\ 40 \\ 45 \end{pmatrix} \quad T = \begin{pmatrix} 20 \\ 25 \\ 30 \\ 40 \\ 45 \\ 50 \\ 55 \\ 60 \\ 65 \end{pmatrix}$$

2.5 Calculation of Reynolds numbers according to H. Schlichting, Boundary-Layer Theory, **1968**, pp. 500-503.

$$ReSchlichting_i := U_i \cdot \frac{ro - ri}{\nu_i}$$

$$ro - ri = 0.060775m$$

$$ReSchlichting = \begin{pmatrix} 899 \\ 1003 \\ 1703 \\ 2814 \\ 3841 \\ 5057 \\ 6370 \\ 7914 \\ 9760 \end{pmatrix} \quad RPM = \begin{pmatrix} 10 \\ 10 \\ 15 \\ 20 \\ 25 \\ 30 \\ 35 \\ 40 \\ 45 \end{pmatrix} \quad T = \begin{pmatrix} 20 \\ 25 \\ 30 \\ 40 \\ 45 \\ 50 \\ 55 \\ 60 \\ 65 \end{pmatrix}$$

2.6 Calculation of Reynolds numbers according to Wang, L., et al., Chemical Engineering Science, 60, **2005**, 5555-5568 in Reapperance of Azimuthal Waves in Turbulent Taylor-Couette Flow at Large Aspect Ratio. Re=w*ri*d/ν

$$ReWang_i := \frac{\omega_i \cdot ri \cdot d}{\nu_i}$$

$$ReWang = \begin{pmatrix} 899 \\ 1003 \\ 1703 \\ 2814 \\ 3841 \\ 5057 \\ 6370 \\ 7914 \\ 9760 \end{pmatrix} \quad RPM = \begin{pmatrix} 10 \\ 10 \\ 15 \\ 20 \\ 25 \\ 30 \\ 35 \\ 40 \\ 45 \end{pmatrix} \quad T = \begin{pmatrix} 20 \\ 25 \\ 30 \\ 40 \\ 45 \\ 50 \\ 55 \\ 60 \\ 65 \end{pmatrix}$$

2.7 Comparison of Reynolds numbers for the RCE

It has been shown that: ReNewman = ReGabe = ReEisenberg = ReArvia
ReSilverman = Re Barkey, and
ReSchilichting = ReWang

It appears that the equation for the Reynolds number used by Newman, Gabe, Eisenberg and Arvia is more often quoted in the literature than those used by Barkey, Silverman and Schlichting. Therefore the Reynolds equation used by Newman (Re=ω*d/2ν), Gabe, Eisenberg and Arvia will be used in this thesis.

$$Reynolds_i := ReNewman_i$$

2.8 Calculation of Reynolds numbers at Electrowinning and Electrorefining Temperatures and at Different Speeds fo Rotation

Reynolds Number at 25 C

$$Reynolds25 := \frac{\omega di^2}{(2\nu)_1} *$$

$$Reynolds25 = \begin{pmatrix} 734 \\ 734 \\ 1101 \\ 1467 \\ 1834 \\ 2201 \\ 2568 \\ 2935 \\ 3302 \end{pmatrix} * \qquad RPM = \begin{pmatrix} 10 \\ 10 \\ 15 \\ 20 \\ 25 \\ 30 \\ 35 \\ 40 \\ 45 \end{pmatrix}$$

Reynolds number at 45 C

$$Reynolds45 := \frac{\omega di^2}{(2\nu)_4} *$$

$$Reynolds45 = \begin{pmatrix} 1124 \\ 1124 \\ 1685 \\ 2247 \\ 2809 \\ 3371 \\ 3933 \\ 4494 \\ 5056 \end{pmatrix} *$$

Reynolds Number at 50 C

$$Reynolds50 := \frac{\omega di^2}{(2\nu)_5} *$$

$$Reynolds50 = \begin{pmatrix} 1233 \\ 1233 \\ 1849 \\ 2466 \\ 3082 \\ 3699 \\ 4315 \\ 4932 \\ 5548 \end{pmatrix} * \qquad RPM = \begin{pmatrix} 10 \\ 10 \\ 15 \\ 20 \\ 25 \\ 30 \\ 35 \\ 40 \\ 45 \end{pmatrix}$$

Reynolds Number at 65 C

$$Reynolds65 := \frac{\omega di^2}{(2\nu)_8} *$$

$$Reynolds65 = \begin{pmatrix} 1586 \\ 1586 \\ 2379 \\ 3173 \\ 3966 \\ 4759 \\ 5552 \\ 6345 \\ 7138 \end{pmatrix} *$$

The Reynolds numbers at 25 rpm increases from Re= 134 at 25C to 205 at 45C, to 225 at 50C and to 289 at 65C. According to DR Gabe, Rotating Electrodes for Use in Electrodeposition Process Control, Plating and Surface Finishing, V 9, 1995, pp. 69-76, the critical Reynolds number for a RCE is 200.

2.8 Calculation of Taylor numbers According to J.Newman, Electrochemical Systems, 1991.

J. Newman (cited above) stated that turbulent flow prevails for Reynolds numbers greater than 3960 or Taylor numbers greater than about 3 x 10^6.

$$TaNewman_i := \left(Reynolds_i\right)^2 \cdot \frac{ro - ri}{ri}$$

$$TaNewman = \begin{pmatrix} 1182262 \\ 1472126 \\ 4244500 \\ 11583817 \\ 21577247 \\ 37414810 \\ 59358842 \\ 91621151 \\ 139336753 \end{pmatrix} \qquad RPM = \begin{pmatrix} 10 \\ 10 \\ 15 \\ 20 \\ 25 \\ 30 \\ 35 \\ 40 \\ 45 \end{pmatrix} \qquad T = \begin{pmatrix} 20 \\ 25 \\ 30 \\ 40 \\ 45 \\ 50 \\ 55 \\ 60 \\ 65 \end{pmatrix}$$

Taylor numbers at 25 rpm and 45C and 65C TaNewmanXXYY: XX=rpm and YY=temperature

$$TaNewman2545C := \left(\frac{\omega_4 \cdot di^2}{2\nu_4}\right)^2 \cdot \frac{ro - ri}{ri} \qquad TaNewman2545C = 22 \times 10^6$$

$$TaNewman2565C := \left(\frac{\omega_4 \cdot di^2}{\nu_8}\right)^2 \cdot \frac{ro - ri}{ri} \qquad TaNewman2565C = 2 \times 10^8$$

2.9 Calculation of Taylor number according to H. Schlichting, Boundary-Layer Theory, 1968, pp. 500-503.

H. Schlichting stated that for 41.3 < Ta < 400 Taylor vortices prevails between 41.3 and 400. Ta > 400 is turbulent.

$$TaSchlichting_i := U_i \frac{ro - ri}{\nu_i} \cdot \sqrt{\frac{ro - ri}{ri}} *$$

$$TaSchlichting = \begin{pmatrix} 1487 \\ 1659 \\ 2817 \\ 4653 \\ 6351 \\ 8363 \\ 10534 \\ 13087 \\ 16139 \end{pmatrix} * \quad RPM = \begin{pmatrix} 10 \\ 10 \\ 15 \\ 20 \\ 25 \\ 30 \\ 35 \\ 40 \\ 45 \end{pmatrix} \quad T = \begin{pmatrix} 20 \\ 25 \\ 30 \\ 40 \\ 45 \\ 50 \\ 55 \\ 60 \\ 65 \end{pmatrix}$$

Taylor number at 25rpm and 45 C TaSchlichtingXXYY: XX=rpm and YY=temperature

$$TaSchlichting2545 := U_4 \frac{ro - ri}{\nu_4} \cdot \sqrt{\frac{ro - ri}{ri}} * \qquad TaSchlichting2545 = 6.351 \times 10^3 *$$

Taylor number at 25rpm and 65 C

$$TaSchlichting2565 := U_4 \frac{ro - ri}{\nu_8} \cdot \sqrt{\frac{ro - ri}{ri}} * \qquad TaSchlichting2565 = 8.966 \times 10^3 *$$

ν with the subscripts of 4 and 8 indicate the kinematic viscosity at 45C and 65C, respectively.

2.10 SUMMARY

Schlichting (10) indicates that at Re = 94.5 and Ta 41.3 the flow is laminar and at the onset of vortex formation. It remains laminar up to ReSchlichting = 868 and TaSchlichting = 387. Since ReSchlichting and TaSchlichting at 25rpm and 45C and 65C are greater than 868 and 387, respectively; it has then been shown that the fluid flow for the RCE used in this thesis is turbulent according to Schlichting. However, Silverman (cited in Section 2.4 above) states that the Taylor number defined by Schlichting appears to be valid for narrow distances between the concentric cylinders (annular gap) only, i.e., 0.588mm.

The fluid flow for wider annular gaps such as used in this work (d=3.2cm) appears to be better described by Reynolds and Taylor numbers described by J. Newman, Electrochemical Systems, 1991. Newmand states that the fluid flow becomes instable at Re and Ta greater than 200 and 1708, respectively. It is therefore concluded that the fluid flow at the RCE is laminar with vortices since ReNewman at 25 rpm and 45C and 65C are 205 and 289, respectively. The TaylorNewman at 45C and 65C are 223,537 and 1.78 x 10^6, respectively. The onset of turbulence is at Ta 3 x 10^6 according to J. Newman.

3. CALCULATION OF THE LIMITING CURRENT DENSITY (iL) ACCORDING TO M. EISENBERG ET AL. AND J. NEWMAN CITED ABOVE.

3.1 Calculation of the Limiting Current Density According to J. Newman (Electrochemical Systems, 2004, pp. 398) when dR (rotating) = di (limiting CD electrode). The original equation was derived by Eisenberg et al. cited above.

$$iL_i := 0.0791\left[n \cdot F \cdot D_i \frac{Co}{di} \cdot \left(\frac{\omega_i \cdot di^2}{2\nu_i}\right)^{0.7} \left(Sc_i\right)^{0.356}\right]*$$

$$iL = \begin{pmatrix} 18 \\ 21 \\ 31 \\ 48 \\ 61 \\ 76 \\ 91 \\ 108 \\ 126 \end{pmatrix} \frac{mA}{cm^2}* \qquad Reynolds = \begin{pmatrix} 658 \\ 734 \\ 1246 \\ 2058 \\ 2809 \\ 3699 \\ 4659 \\ 5788 \\ 7138 \end{pmatrix} \qquad T = \begin{pmatrix} 20 \\ 25 \\ 30 \\ 40 \\ 45 \\ 50 \\ 55 \\ 60 \\ 65 \end{pmatrix}$$

The diffusion layer thickness, δ

$$\delta Newman_i := \frac{n \cdot F \cdot Co \cdot D_i}{iL_i}*$$

$$\delta Newman = \begin{pmatrix} 363 \\ 369 \\ 280 \\ 230 \\ 197 \\ 174 \\ 156 \\ 142 \\ 130 \end{pmatrix} \mu m*$$

3.4 Calculation of the Limiting Current Density and Diffusion Layer Thickness Using Arvia et al.'s Equation cited above

$$iLArvia_i := 0.0791\left(\frac{di}{\nu_i}\right)^{-0.30} \cdot \left(U_i\right)^{0.70} \cdot \left(\frac{do}{di}\right) \cdot \left(Sc_i\right)^{-0.644} \cdot n \cdot F \cdot Co$$

$$iLArvia = \begin{pmatrix} 67 \\ 77 \\ 117 \\ 178 \\ 228 \\ 282 \\ 340 \\ 403 \\ 472 \end{pmatrix} \frac{mA}{cm^2} \qquad Reynolds = \begin{pmatrix} 658 \\ 734 \\ 1246 \\ 2058 \\ 2809 \\ 3699 \\ 4659 \\ 5788 \\ 7138 \end{pmatrix} \qquad RPM = \begin{pmatrix} 10 \\ 10 \\ 15 \\ 20 \\ 25 \\ 30 \\ 35 \\ 40 \\ 45 \end{pmatrix} \qquad T = \begin{pmatrix} 20 \\ 25 \\ 30 \\ 40 \\ 45 \\ 50 \\ 55 \\ 60 \\ 65 \end{pmatrix}$$

SUMMARY
The DLT obtained from Eisenberg's equation is relatively higher than that obtained from Arvia's Equation. The Eisenberg Eq. was determined using hexacyanoferrate (II) and hexacyanoferrate (III) in 2M NaOH as supporting electrolyte. Arvia et al. obtained it using 1.5-3.5g/L copper in 1.5M sulfuric acid and also worked with a fixed cathode as the outer cylinder and a *stirred anode as the inner cylinder*.

3.6 Calculation of the Diffusion Layer Thickness at 10 and 25RPM and 45C and 64C Using Arvia's LCD and Nernst Equation.

$$\delta Arvia_i := \frac{n \cdot F \cdot Co \cdot D_i}{iLArvia_i} * \qquad \delta Arvia = \begin{pmatrix} 97 \\ 99 \\ 75 \\ 62 \\ 53 \\ 46 \\ 42 \\ 38 \\ 35 \end{pmatrix} \mu m \qquad RPM = \begin{pmatrix} 10 \\ 10 \\ 15 \\ 20 \\ 25 \\ 30 \\ 35 \\ 40 \\ 45 \end{pmatrix} \qquad T = \begin{pmatrix} 20 \\ 25 \\ 30 \\ 40 \\ 45 \\ 50 \\ 55 \\ 60 \\ 65 \end{pmatrix}$$

3.7 Calculation of Diffusion Layer Thickness at 10RPM AND 45C. The results of the LCD and δ are plotted in Figure 3.

$$iLArvia1045 := 0.0791 \left(\frac{di}{\nu_4} \right)^{-0.30} \cdot \left(U_1 \right)^{0.70} \cdot \left(\frac{do}{di} \right) \cdot \left(Sc_4 \right)^{-0.644} \cdot n \cdot F \cdot Co \qquad iLArvia1045 = 1198 \frac{A}{m^2}$$

$$\delta Arvia1045 := \frac{n \cdot F \cdot Co \cdot D_4}{iLArvia1045} * \qquad \delta Arvia1045 = 100 \mu m$$

3.8 Calculation of Diffusion Layer Thickness at 10RPM and 65C

$$iLArvia1065 := 0.0791\left(\frac{di}{\nu_8}\right)^{-0.30}\cdot\left(U_1\right)^{0.70}\cdot\left(\frac{do}{di}\right)\cdot\left(Sc_8\right)^{-0.644}\cdot n\cdot F\cdot Co \qquad iLArvia1065 = 1648\,\frac{A}{m^2}$$

$$\delta Arvia1065 := \frac{n\cdot F\cdot Co\cdot D_8}{iLArvia1065^*} \qquad \delta Arvia1065 = 100\,\mu m$$

3.9 Calculation of Diffusion Layer Thickness at 25RPM and 45C

$$iLArvia2545 := 0.0791\left(\frac{di}{\nu_4}\right)^{-0.30}\cdot\left(U_4\right)^{0.70}\cdot\left(\frac{do}{di}\right)\cdot\left(Sc_4\right)^{-0.644}\cdot n\cdot F\cdot Co \qquad iLArvia2545 = 2276\,\frac{A}{m^2}$$

$$\delta Arvia2545 := \frac{n\cdot F\cdot Co\cdot D_4}{iLArvia2545^*} \qquad \delta Arvia2545 = 53\,\mu m \qquad iLArvia_4 = 2276\,\frac{A}{m^2}$$

3.10 Calculation of Diffusion Layer Thickness at 25RPM and 65C

$$iLArvia2564 := 0.0791\left(\frac{di}{\nu_8}\right)^{-0.30}\cdot\left(U_4\right)^{0.70}\cdot\left(\frac{do}{di}\right)\cdot\left(Sc_8\right)^{-0.644}\cdot n\cdot F\cdot Co \qquad iLArvia2564 = 3129\,\frac{A}{m^2}$$

$$\delta Arvia2564 := \frac{n\cdot F\cdot Co\cdot D_8}{iLArvia2564^*} \qquad \delta Arvia2564 = 52\,\mu m$$

3.9 Comparison of Limiting Current Densities

iL = iLNewman = iLEisenberg = ILGabe

$$iL = \begin{pmatrix} 181 \\ 207 \\ 313 \\ 476 \\ 609 \\ 756 \\ 910 \\ 1079 \\ 1264 \end{pmatrix}\frac{A}{m^2} \qquad RPM = \begin{pmatrix} 10 \\ 10 \\ 15 \\ 20 \\ 25 \\ 30 \\ 35 \\ 40 \\ 45 \end{pmatrix} \qquad T = \begin{pmatrix} 20 \\ 25 \\ 30 \\ 40 \\ 45 \\ 50 \\ 55 \\ 60 \\ 65 \end{pmatrix} \qquad iLArvia = \begin{pmatrix} 675 \\ 774 \\ 1168 \\ 1776 \\ 2276 \\ 2823 \\ 3400 \\ 4030 \\ 4721 \end{pmatrix}\frac{A}{m^2}$$

SUMMARY

The LCD data obtained from the Eq. of Eisenberg et al. is lower than that obtained from the Arvia et al. Eq. The equation for the LCD (iL) was obtained using hexacyanoferrate (II) and hexacyanoferrate (III) in 2M NaOH at 25C. Howeve, LCD iLArvia was obtained using 1.5-3.5g/L cupric ions and 1.5M sulfuric acid at 18C and the *rotating* electrode was the *anode* operating as *inner electrode*. This electrode set up is opposite to that used for this thesis.

Moreover, the diffusion coeficient for cupric ions for Arvia's study was 5.22 x 10^-6 cm^2/s and the kinematic viscosity was 1.279 x 10^-2 cm^2/s at 18C. These overall conditions do not exactly replicate to the conditions under which the data for this thesis were obtained. Therefore, Arvia's data will be used as a reference only.

4.0 Experimental Limiting Current Density and Diffusion Layer Thickness at 0, 10 and 25rpm and 45C and 65C

This experimental LCD was sourced from Chapter 3 - Section 3.2.3 - Table 3.2 to calculate the experimental diffusion layer thickness. The LCD data and δ results are plotted in Figure 3.

4.1 DLT at Zero RPM (Free Convection) at 45C and 65C

iLXXYY, XX=RPM and YY=temperature.

$iL0045 := 1037 \frac{A}{m^2}$ $\quad \delta 0045 := n \cdot F \cdot Co \cdot \frac{D_4}{iL0045}$ $\quad \delta 0045 = 116 micron$

$iL0065 := 1432 \frac{A}{m^2}$ $\quad \delta 0065 := n \cdot F \cdot Co \cdot \frac{D_8}{iL0065}$ $\quad \delta 0065 = 115 \mu m$

4.2 DLT at 10 RPM at 45C and 65C

$iL1045 := 1118 \frac{A}{m^2}$ $\quad \delta 1045 := n \cdot F \cdot Co \cdot \frac{D_4}{iL1045}$ $\quad \delta 1045 = 108 \mu m$

$iL1065 := 1497 \frac{A}{m^2}$ $\quad \delta 1065 := n \cdot F \cdot Co \cdot \frac{D_8}{iL1065}$ $\quad \delta 1065 = 110 \mu m$

4.3 DLT at 25 RPM at 45C and 65C

$iL2545 := 1150 \frac{A}{m^2}$ $\quad \delta 2545 := n \cdot F \cdot Co \cdot \frac{D_4}{iL2545}$ $\quad \delta 2545 = 105 micron$

$iL2565 := 1660 \frac{A}{m^2}$ $\quad \delta 2565 := n \cdot F \cdot Co \cdot \frac{D_8}{iL2565}$ $\quad \delta 2565 = 99 micron$

Table 2: summarizes the calculated (using Arvia et al.'s equation) and the experimental diffusion layer thickness

TABLE 2

Calculated and Experimental Diffusion Layer Thickness at 0, 10 and 25 RPM and 45C and 65C

			Calculated		Experimental	
	RPM	Temp. C	DiffLT, μm	LCD	DiffLT, μm	LCD
Result :=						
0	0	45	0	0	97	$1.037 \cdot 10^3$
1	0	65	0	0	115	$1.432 \cdot 10^3$
2	10	45	94	$1.07 \cdot 10^3$	90	$1.118 \cdot 10^3$
3	10	65	99	$1.655 \cdot 10^3$	110	$1.497 \cdot 10^3$
4	25	45	49	$2.032 \cdot 10^3$	87	$1.15 \cdot 10^3$
5	25	65	52	$3.143 \cdot 10^3$	99	$1.66 \cdot 10^3$

$j := 0..5$ $\quad RPMData := Result^{\langle 0 \rangle}$ $\quad TempData := Result^{\langle 1 \rangle}$ $\quad ExpDiffLT := (Result \cdot micron)^{\langle 4 \rangle}$

$DiffLT := (Result \cdot micron)^{\langle 2 \rangle}$ $\quad LCD := \left(Result \cdot \frac{A}{m^2} \right)^{\langle 3 \rangle}$ $\quad ExpLCD := \left(Result \cdot \frac{A}{m^2} \right)^{\langle 5 \rangle}$

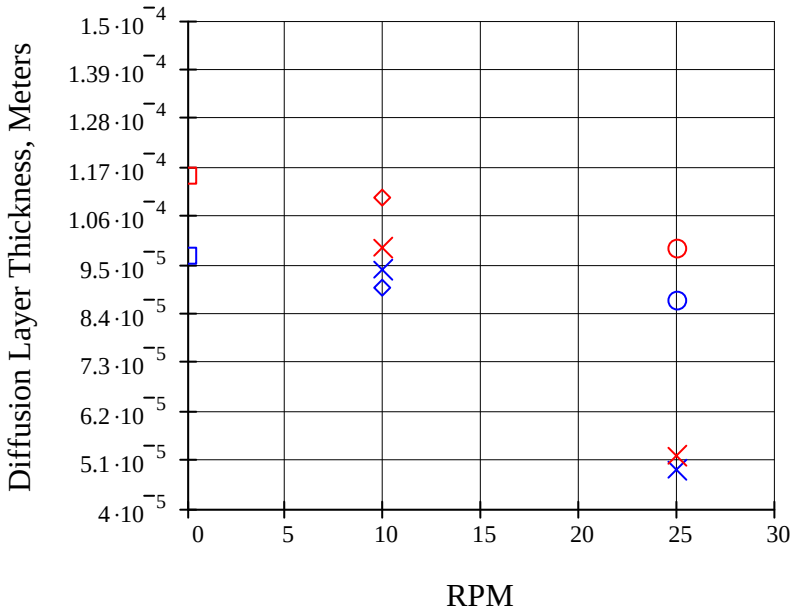

Figure 3: Calculated and Experimental Diffusion Layer Thickness at 0, 10 and 25 RPM and 45C and 65C

Legend: blue=45C; red=65C; squares=Free Convection; x = calculated using Arvia et al.'s LCD Eq. and Nernst Eq.

REFERENCES

1. Price D, Davenport W. *Physico-Chemical Properties of Copper Electrorefining and Electrowinning Electrolytes*. Metallurgical & Materials Transactions B-Process Metallurgy & Materials Processing Science 1981;12B:639-643.

2. Uceda D. Determination of Mass Transfer Characteristics in the Electrolysis of Copper [PhD Thesis]. Missouri-Rolla: University Missouri-Rolla; 1988.

3. Dutra A, O'Keefe T. *Copper Nucleation on Titanium for Thin Film Applications*. Journal of Applied Electrochemistry 1999;29:1217-1227.

4. Newman J, Thomas-Alyea KE. *Electrochemical Systems*. Third ed. Hoboken, New Jersey: John Wiley & Sons, Inc.; 2004.

5. Gabe D. *Rotating Electrodes for Use in Electrodeposition Process Control*. Plating & Surface Finishing 1995;9:69-76.

6. Eisenberg M, Tobias C, Wilke C. *Ionic Mass Transfer and Concentration Polarization at Rotating Electrodes*. Journal of the Electrochemical Society 1954;101(6):306-319.

7. Arvia AJ, Carrozza JSW. *Mass Transfer in the Electrolysis of Cuso4-H2so4 in Aqueous Solutions under Limiting Current and Forced Convection Employing a Cylindrical Cell with Rotating Electrodes*. Electrochimica Acta 1962;7:65-78.

8. Barkey D, Muller R, Tobias C. *Roughness Development in Metal Electrodeposition I. Experimental Results*. Journal of the Electrochemical Society 1989;138(8):2199-2207.

9. Silverman DC. *The Rotating Cylinder Electrode for Examining Velocity-Sensitive Corrosion - a Review*. Corrosion 2004;60(11):1003-1022.

10. Schlichting H. *Boundary-Layer Theory*. Sydney: McGraw-Hill; 1968.

11. Wang L, Olsen M, Vigil R. *Reappearance of Azimuthal Waves in Turbulent Taylor-Couette Flow at Large Aspect Ratio*. Chemical Engineering Science 2005;60:5555-5568.

12. Newman J. *Electrochemical Systems*. Second ed. London: Prentice-Hall International; 1991.

APPENDIX B

ELECTROCHEMICAL IMPEDANCE SPECTROCPY DATA USING GUAR AT -490mV vs. MSE AND 45^{o}C

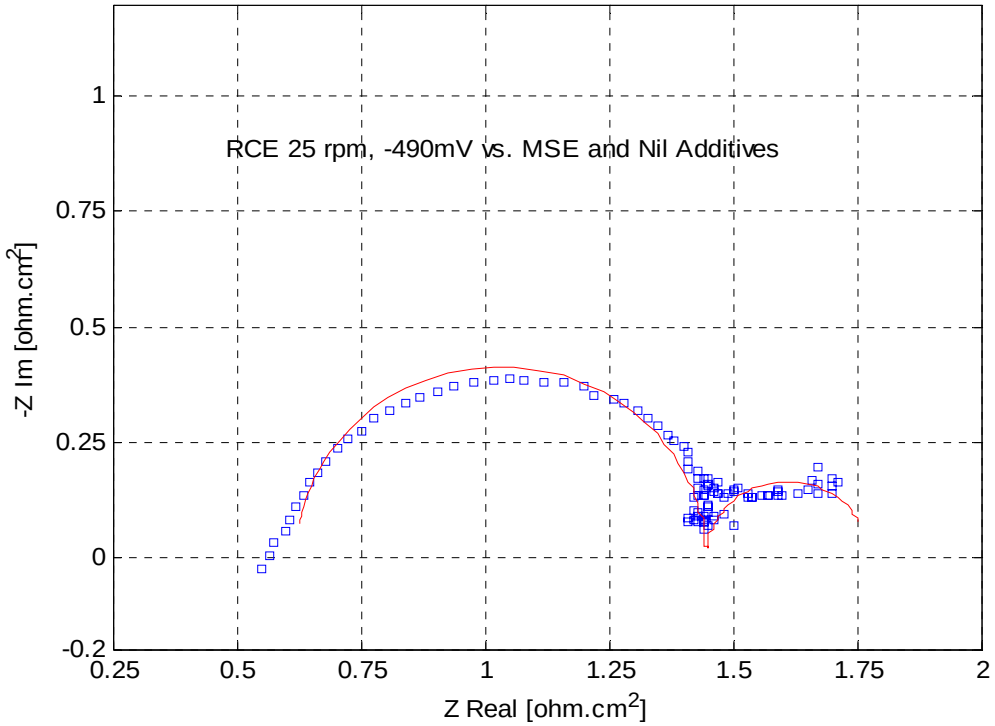

Figure 1: Complex-Plane Plot of Experimental and Simulated Impedance Spectra at 45^{o}C in the Absence of Guar at -490mV vs. MSE

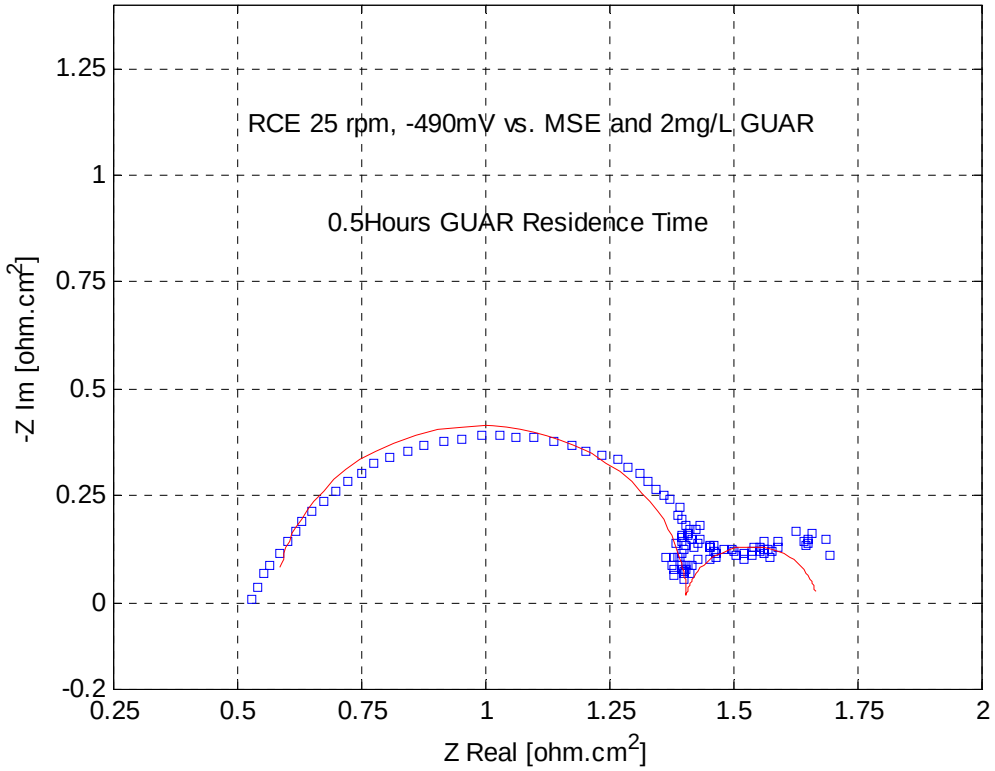

Figure 2: Complex-Plane Plot of Experimental and Simulated Impedance Spectra at 45^{o}C in the Presence of Guar at -490mV vs. MSE and 0.5Hours Residence Time

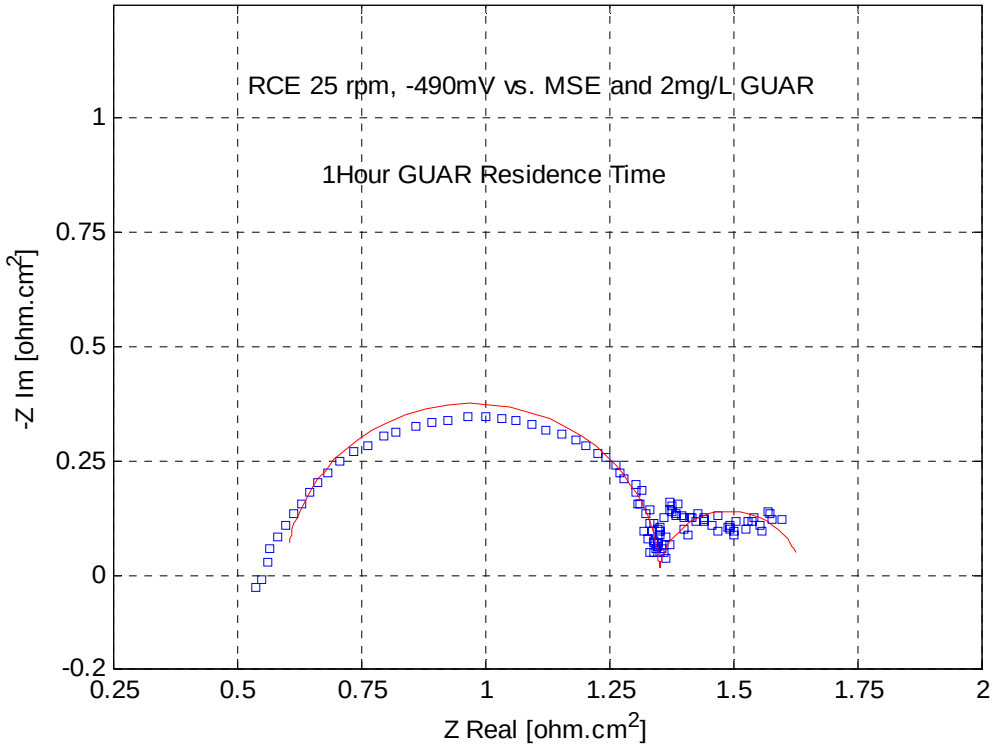

Figure 3: Complex-Plane Plot of Experimental and Simulated Impedance Spectra at 45°C in the Presence of Guar at -490mV vs. MSE and 1Hour Residence Time

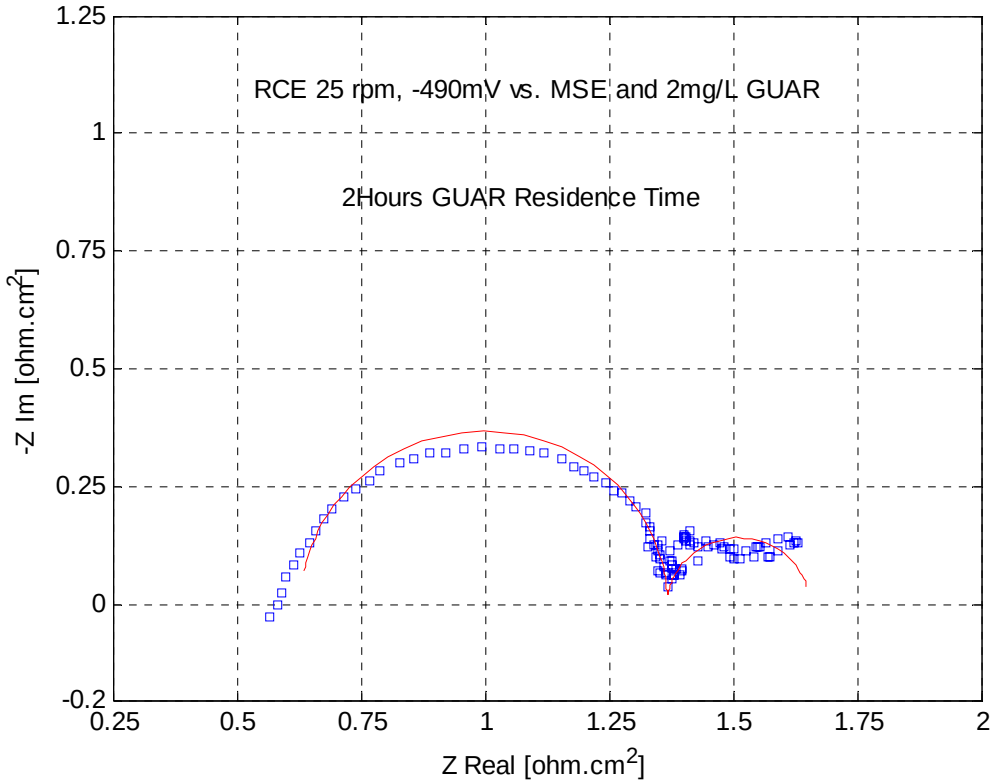

Figure 4: Complex-Plane Plot of Experimental and Simulated Impedance Spectra at 45°C in the Presence of Guar at -490mV vs. MSE and 2Hours Residence Time

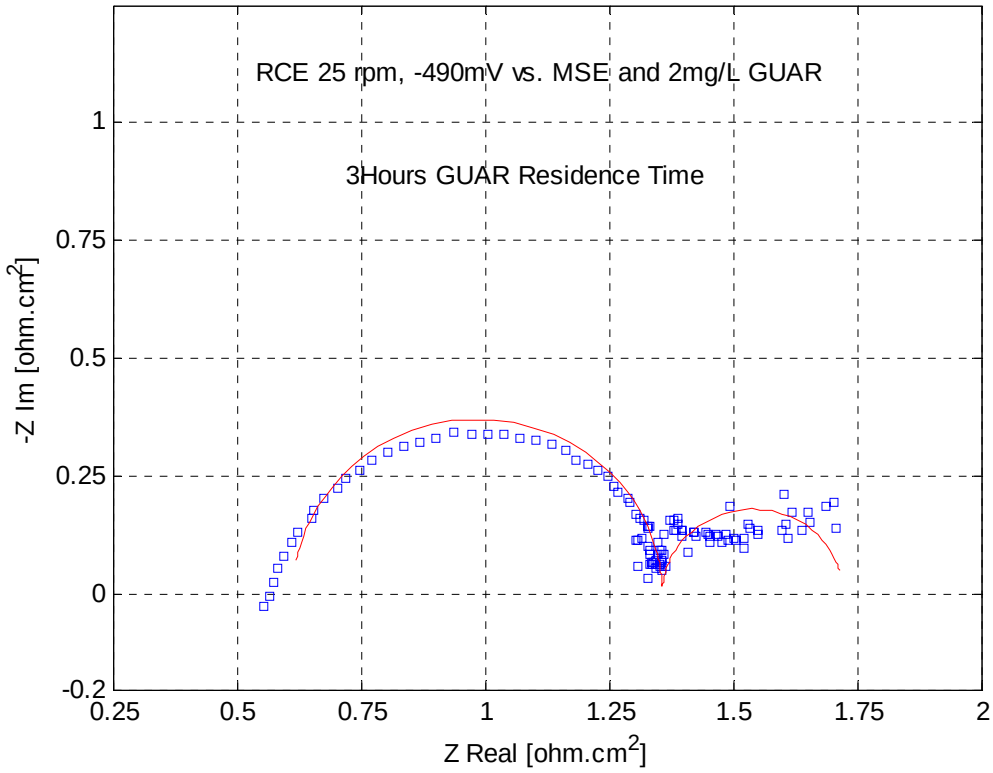

Figure 5: Complex-Plane Plot of Experimental and Simulated Impedance Spectra at 45°C in the Presence of Guar at -490mV vs. MSE and 3Hours Residence Time

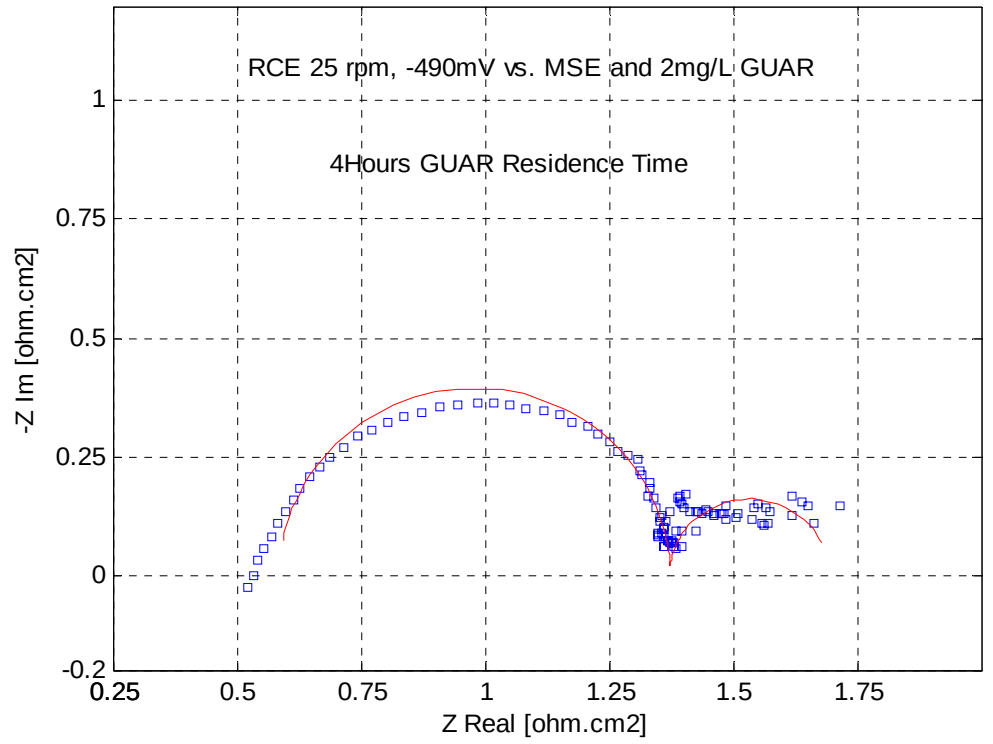

Figure 6: Complex-Plane Plot of Experimental and Simulated Impedance Spectra at 45°C in the Presence of Guar at -490mV vs. MSE and 4Hours Residence Time

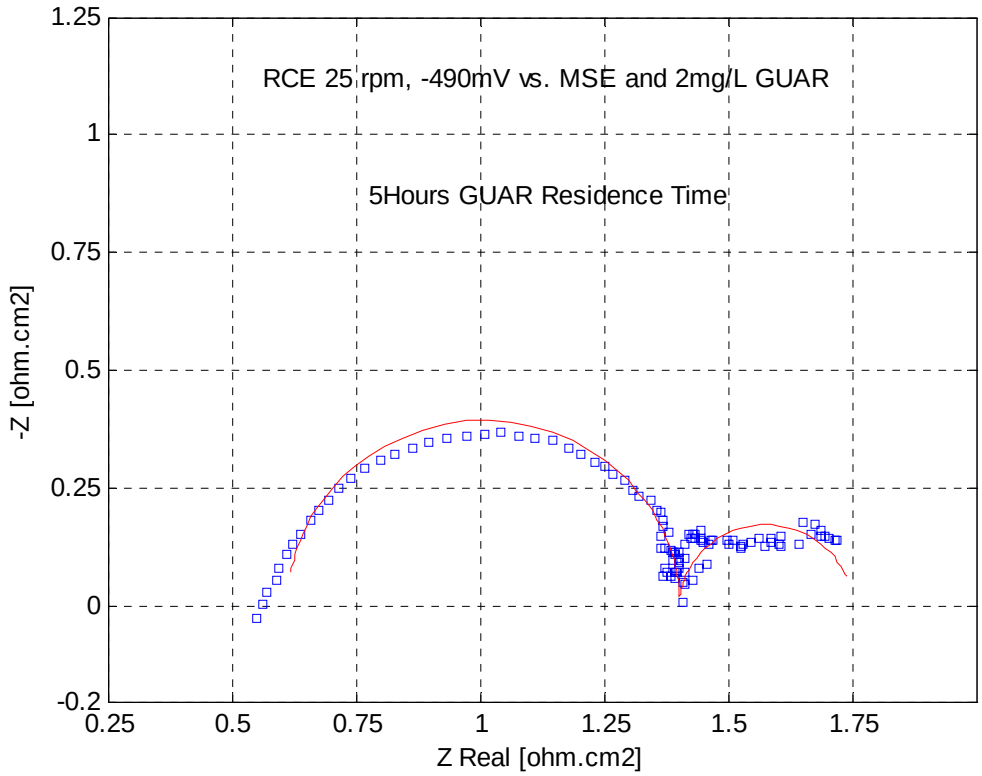

Figure 7: Complex-Plane Plot of Experimental and Simulated Impedance Spectra at 45^{o}C in the Presence of Guar at -490mV vs. MSE and 5Hours Residence Time

ELECTROCHEMICAL IMPEDANCE DATA USING APAM AT -470mV vs. MSE AND 45^{o}C

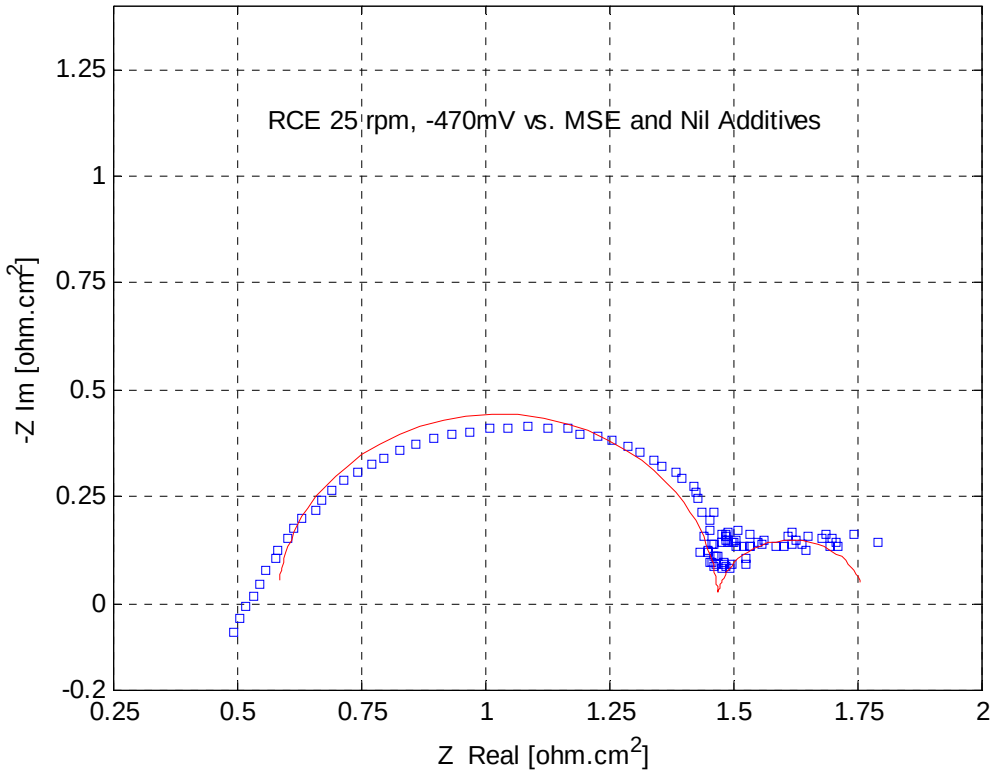

Figure 8: Complex-Plane Plot of Experimental and Simulated Impedance Spectra at 45°C in the Absence of APAM at -470mV vs. MSE

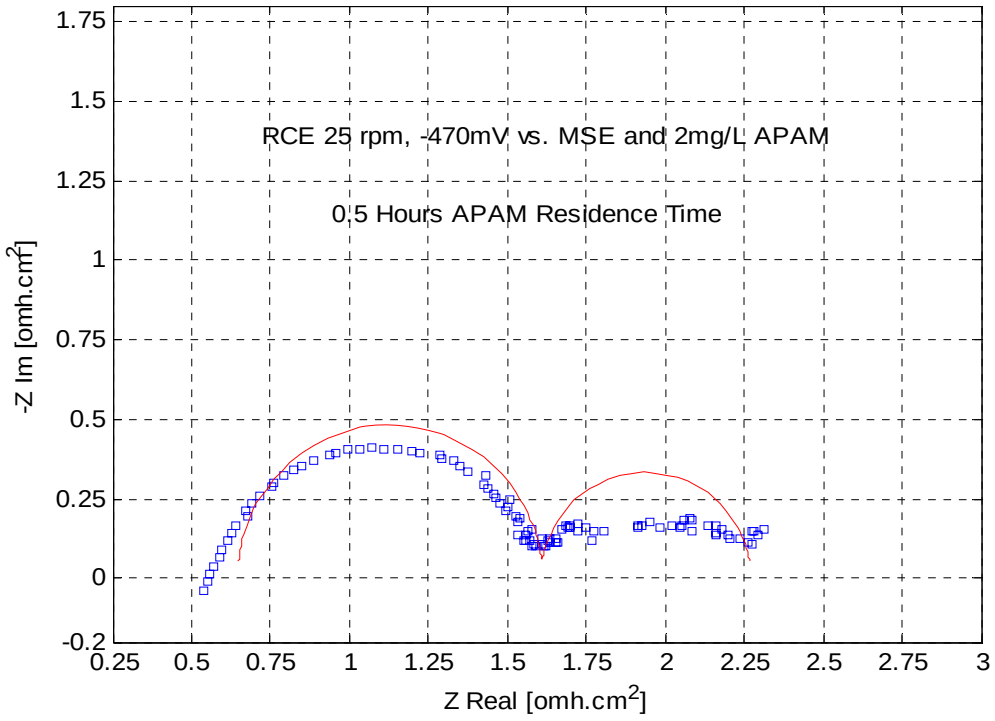

Figure 9: Complex-Plane Plot of Experimental and Simulated Impedance Spectra at 45°C in the Presence of APAM at -470mV vs. MSE and 0.5Hours Residence Time

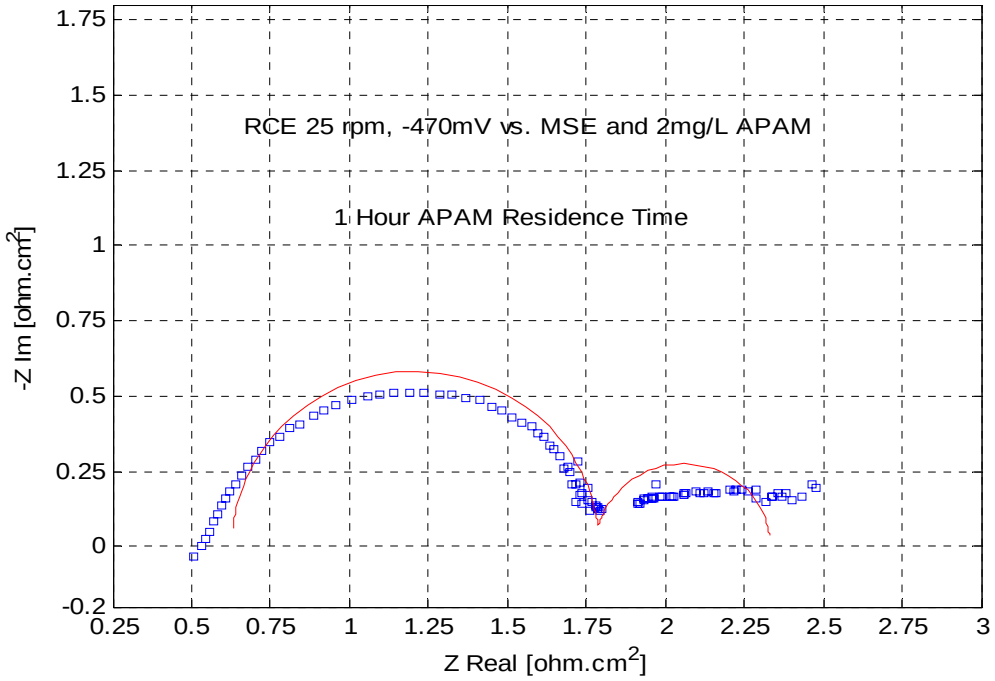

Figure 10: Complex-Plane Plot of Experimental and Simulated Impedance Spectra at 45°C in the Presence of APAM at -470mV vs. MSE and 1Hour Residence Time

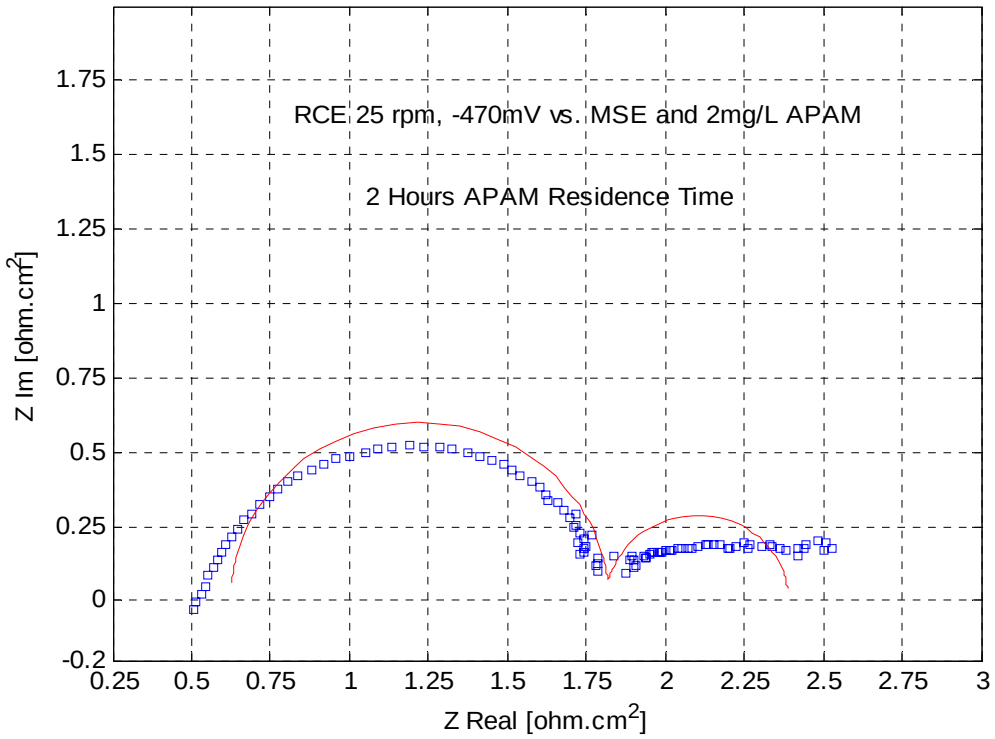

Figure 11: Complex-Plane Plot of Experimental and Simulated Impedance Spectra at 45°C in the Presence of APAM at -470mV vs. MSE and 2Hours Residence Time

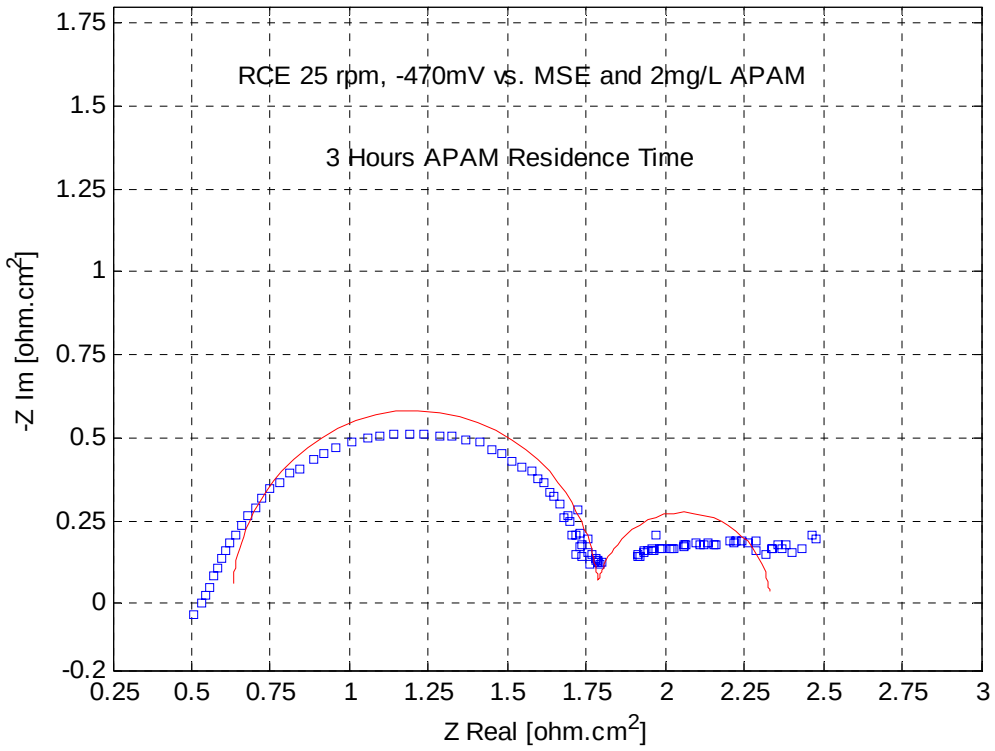

Figure 12: Complex-Plane Plot of Experimental and Simulated Impedance Spectra at 45°C in the Presence of APAM at -470mV vs. MSE and 3Hours Residence Time

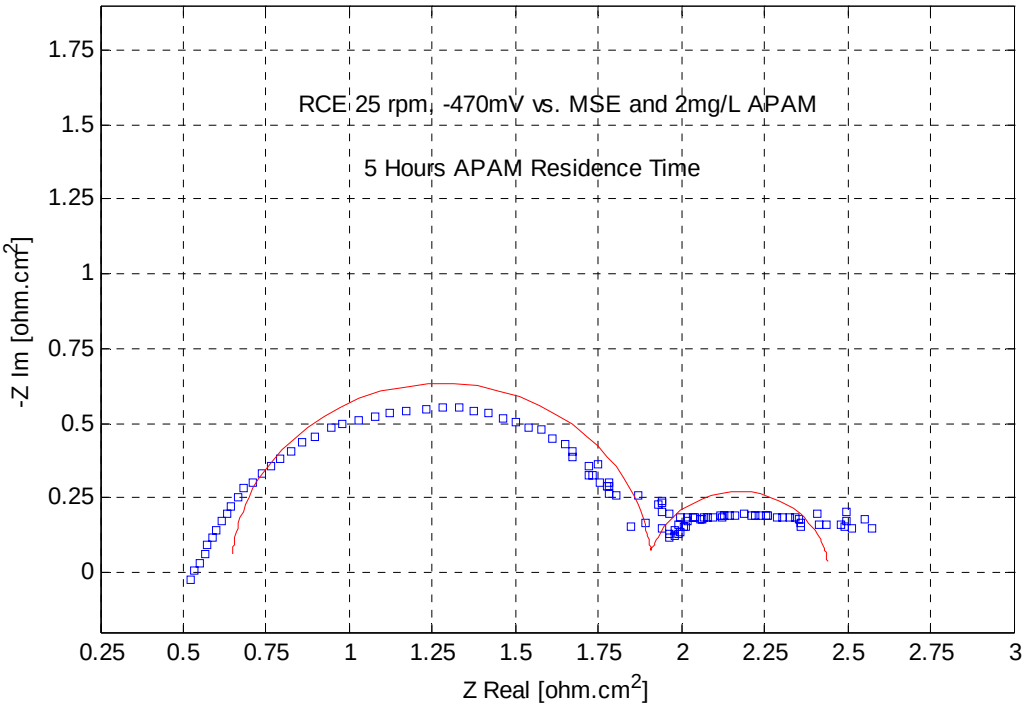

Figure 13: Complex-Plane Plot of Experimental and Simulated Impedance Spectra at 45°C in the Presence of APAM at -470mV vs. MSE and 5Hours Residence Time

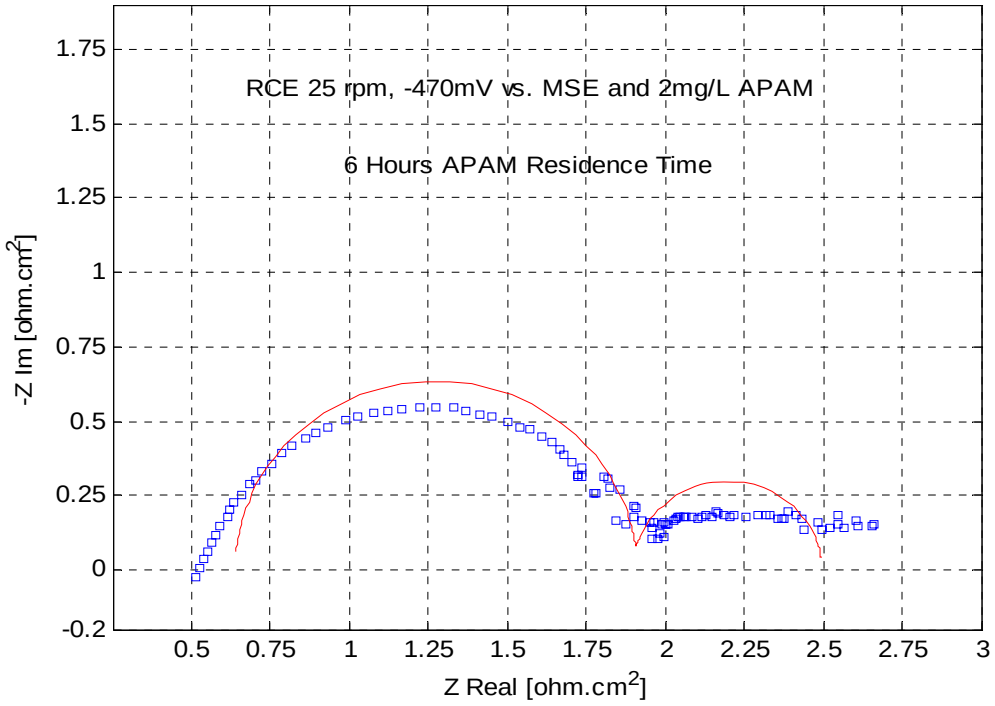

Figure 14: Complex-Plane Plot of Experimental and Simulated Impedance Spectra at 45°C in the Presence of APAM at -470mV vs. MSE and 6Hours Residence Time

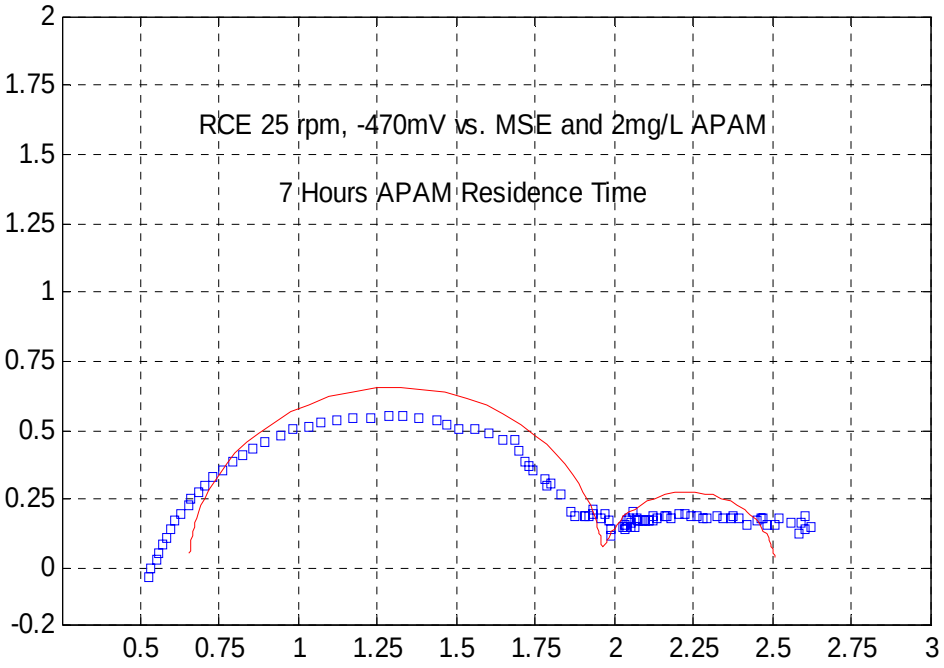

Figure 15: Complex-Plane Plot of Experimental and Simulated Impedance Spectra at 45°C in the Presence of APAM at -470mV vs. MSE and 7Hours Residence Time.

ELECTROCHEMICAL IMPEDANCE DATA USING APAM AT -490mV vs. MSE AND 45^{o}C

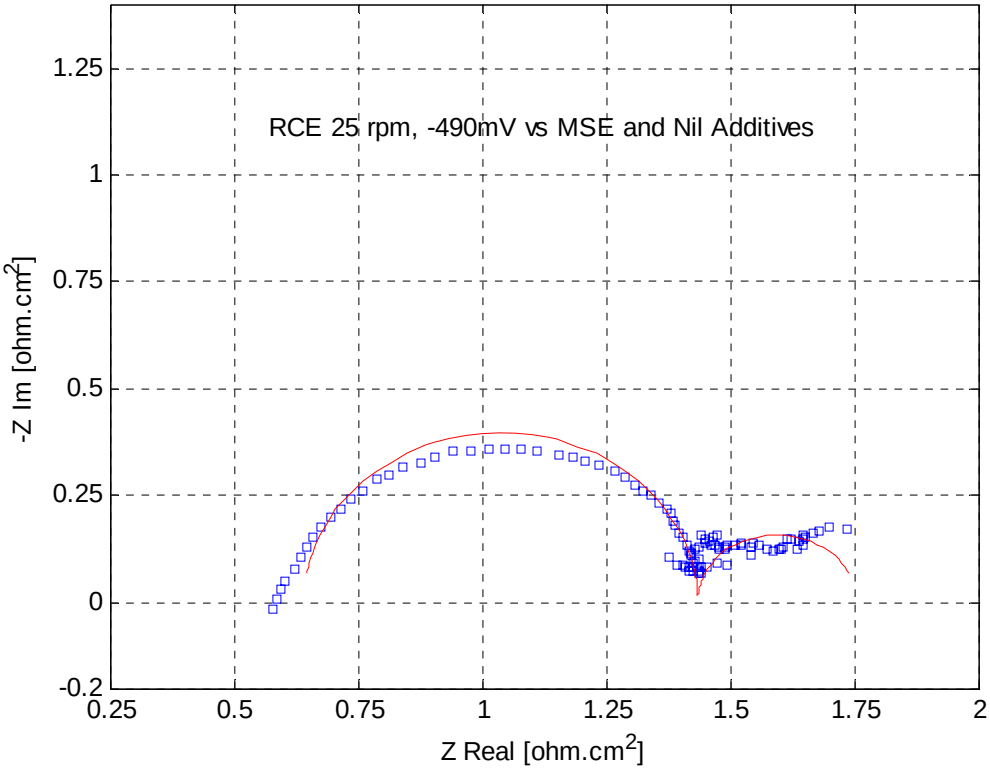

Figure 16: Complex-Plane Plot of Experimental and CNLS Simulated Impedance Spectra in the Absence of APAM at 45°C and -490mV versus MSE

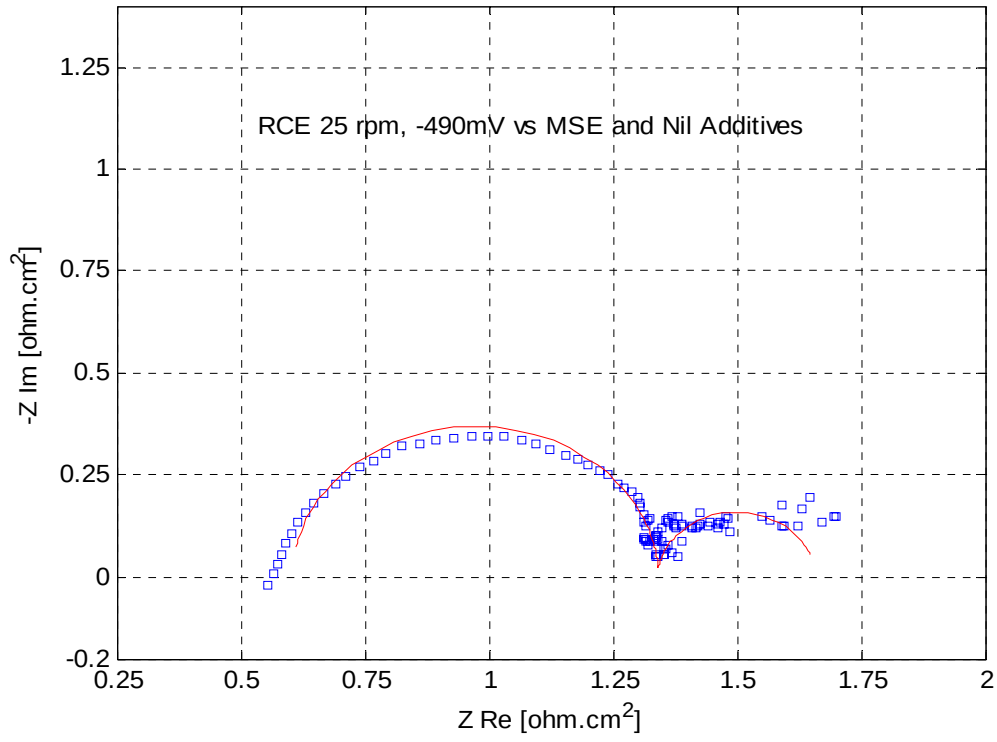

Figure 17: Complex-Plane Plot of Experimental and CNLS Simulated Impedance Spectra in the Absence of APAM at 45°C and -490mV versus MSE

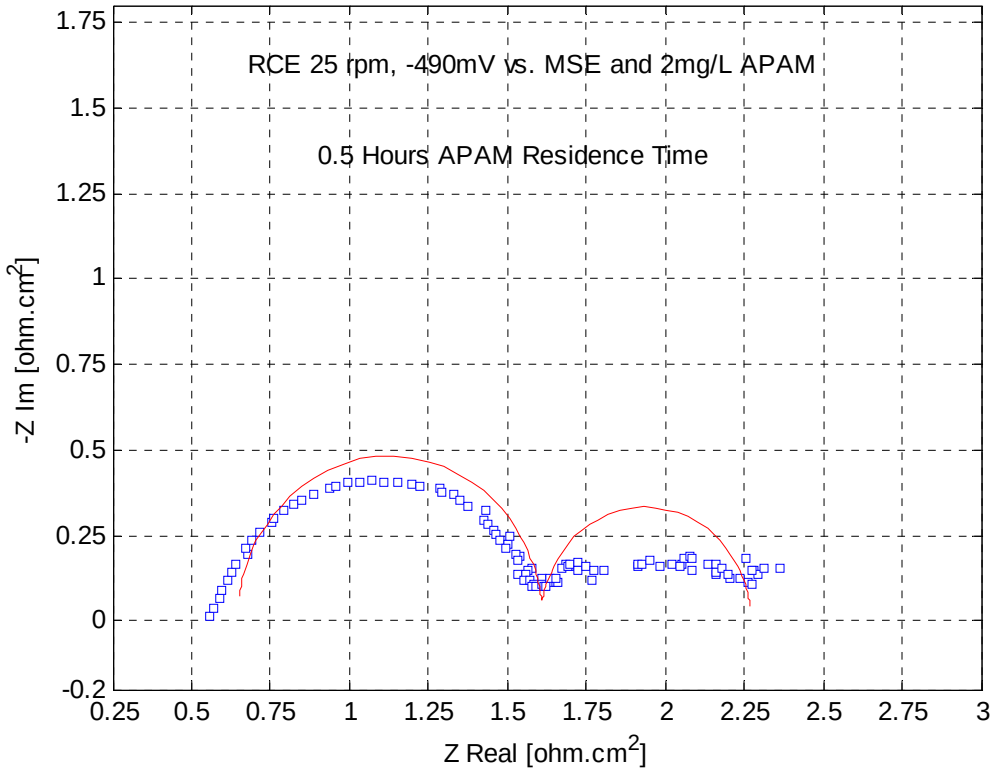

Figure 18: Complex-Plane Plot of Experimental and Simulated Impedance Spectra at 45°C in the Presence of APAM at -490mV vs. MSE and 0.5Hours Residence Time.

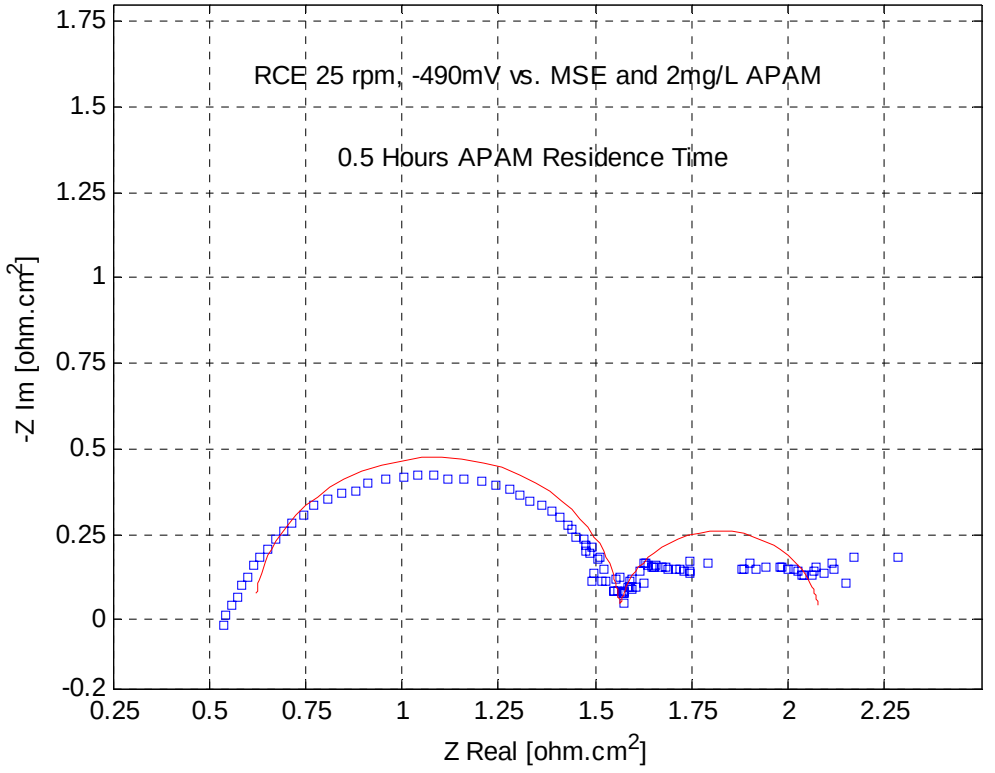

Figure 19: Complex-Plane Plot of Experimental and Simulated Impedance Spectra at 45°C in the Presence of APAM at -490mV vs. MSE and 0.5Hours Residence Time.

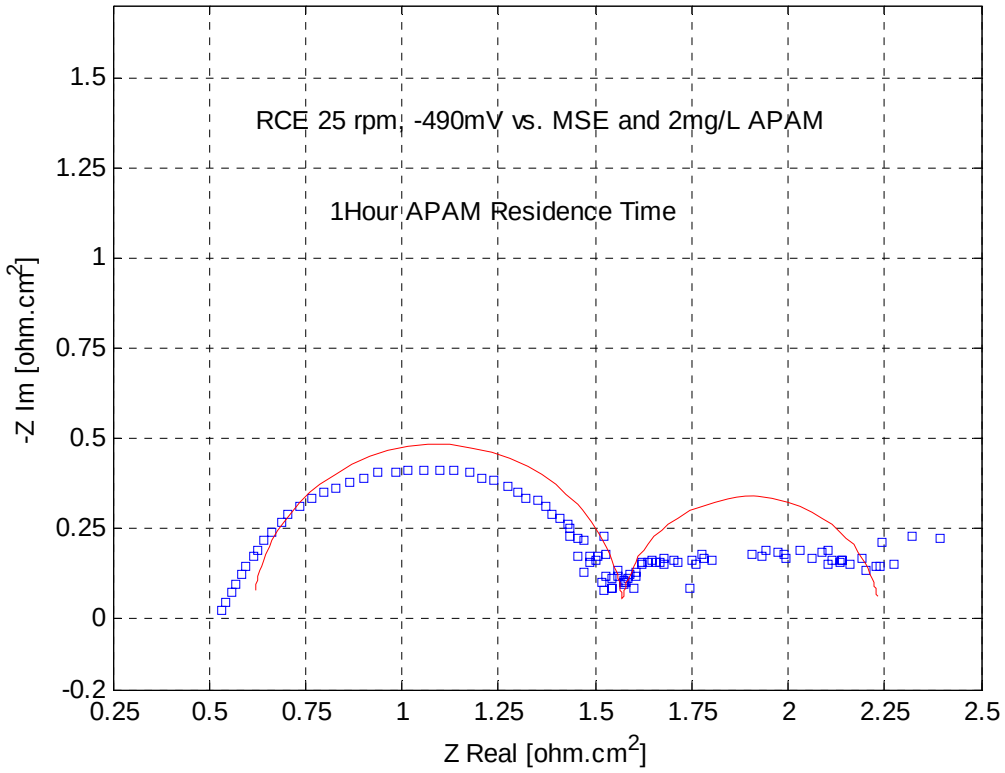

Figure 20: Complex-Plane Plot of Experimental and Simulated Impedance Spectra at 45°C in the Presence of APAM at -490mV vs. MSE and 1Hour Residence Time.

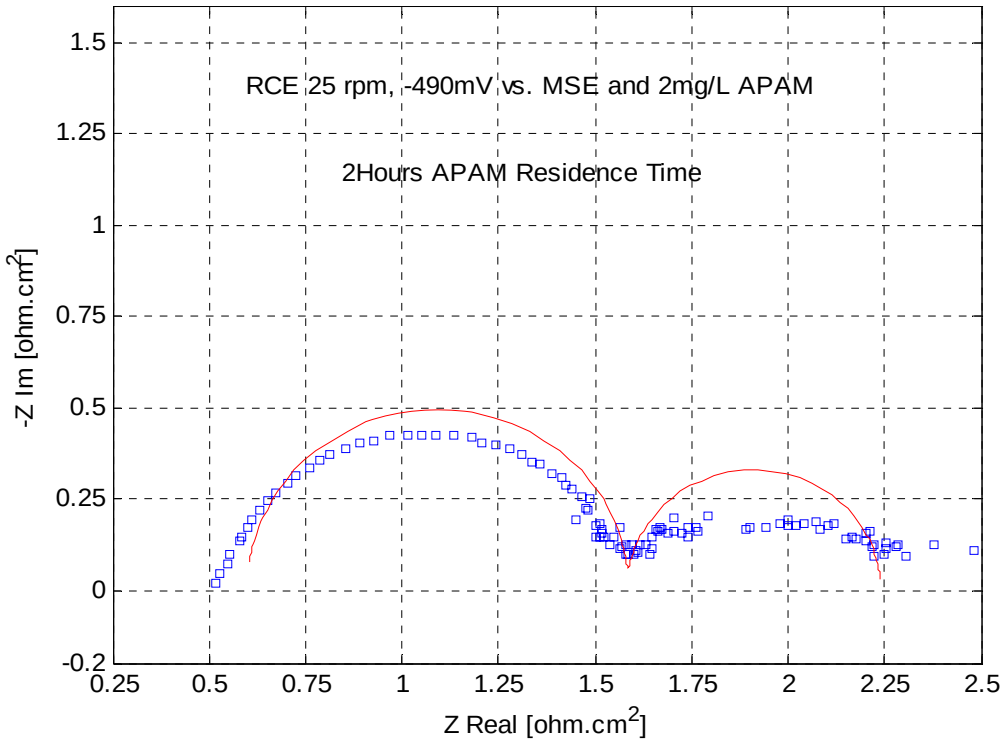

Figure 21: Complex-Plane Plot of Experimental and Simulated Impedance Spectra at 45°C in the Presence of APAM at -490mV vs. MSE and 2Hours Residence Time.

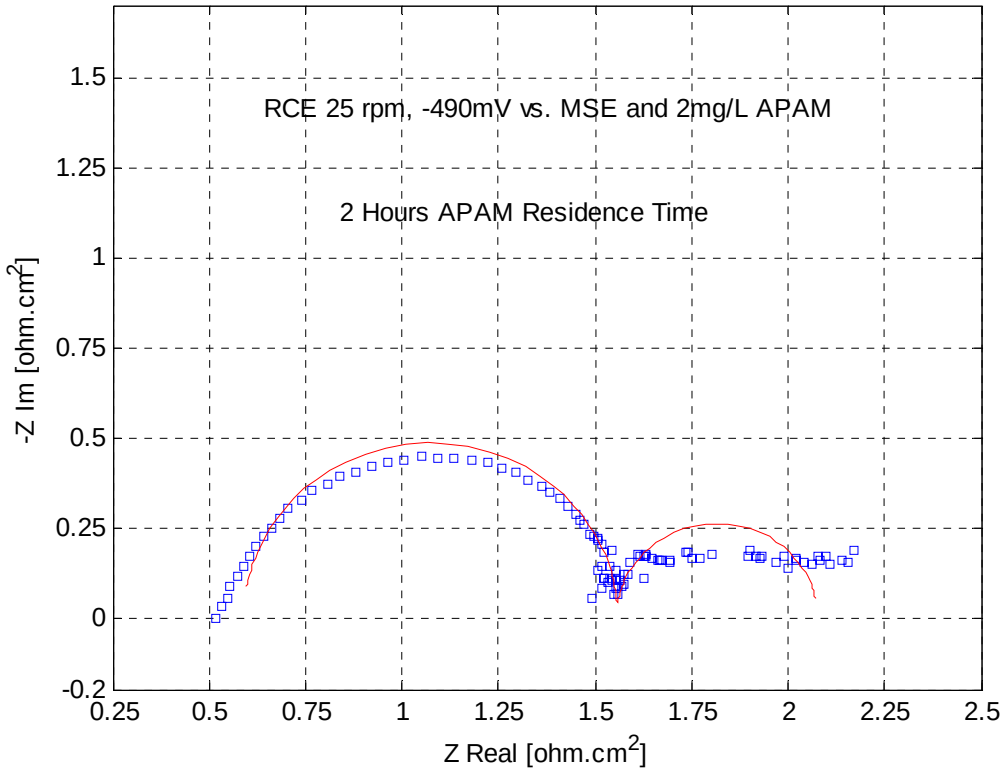

Figure 22: Complex-Plane Plot of Experimental and Simulated Impedance Spectra at 45°C in the Presence of APAM at -490mV vs. MSE and 2Hours Residence Time (T2)

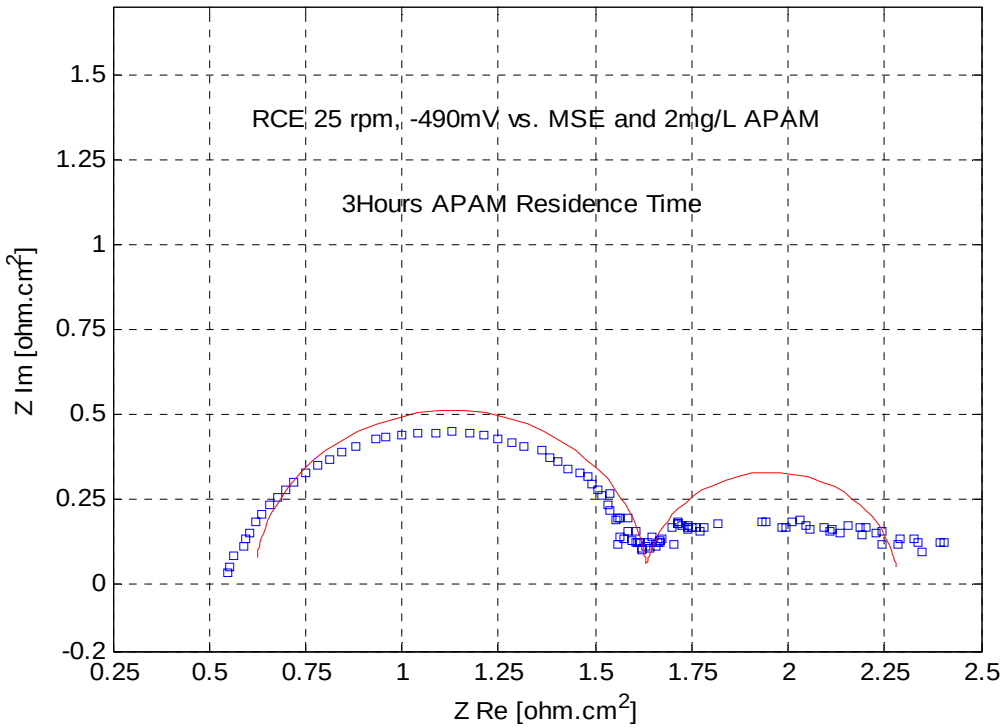

Figure 23: Complex-Plane Plot of Experimental and Simulated Impedance Spectra at 45°C in the Presence of APAM at -490mV vs. MSE and 3Hours Residence Time

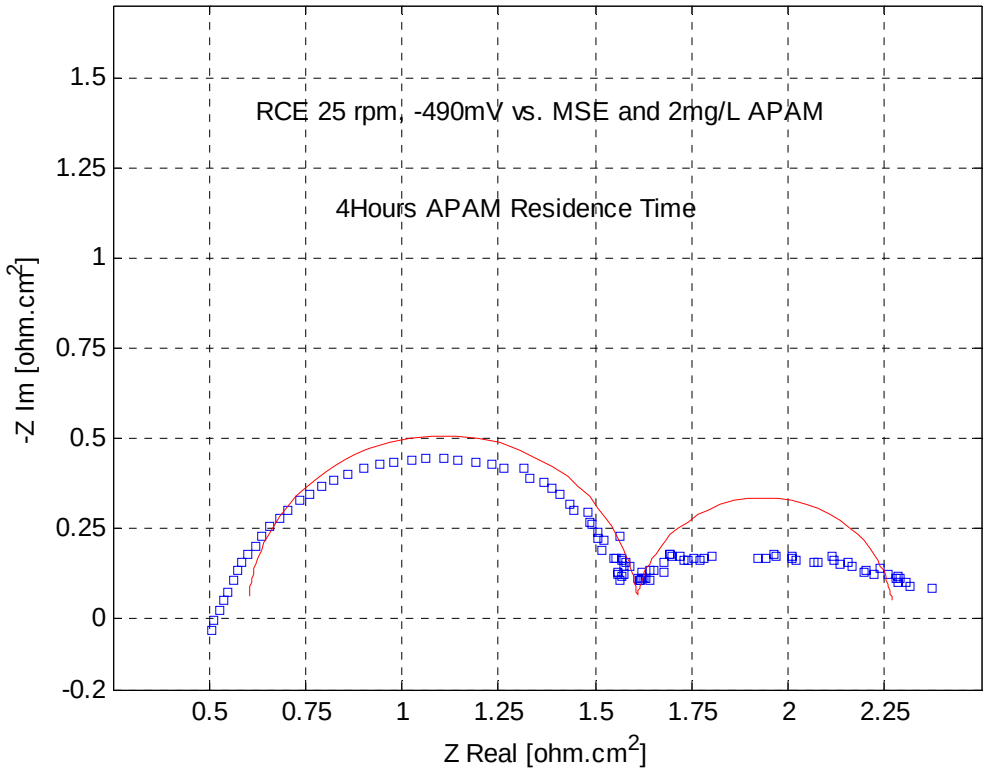

Figure 24: Complex-Plane Plot of Experimental and Simulated Impedance Spectra at 45°C in the Presence of APAM at -490mV vs. MSE and 4Hours Residence Time.

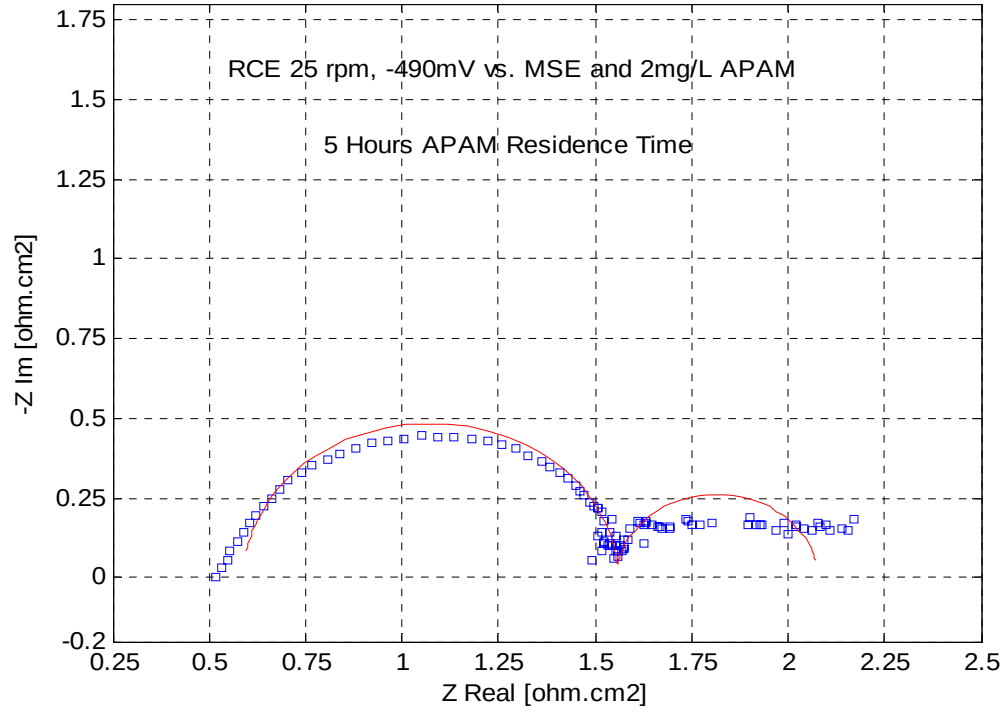

Figure 25: Complex-Plane Plot of Experimental and Simulated Impedance Spectra at 45°C in the Presence of APAM at -490mV vs. MSE and 5Hours Residence Time

ELECTROCHEMICAL IMPEDANCE DATA USING APAM AT -445mV vs. MSE AND 64^{o}C

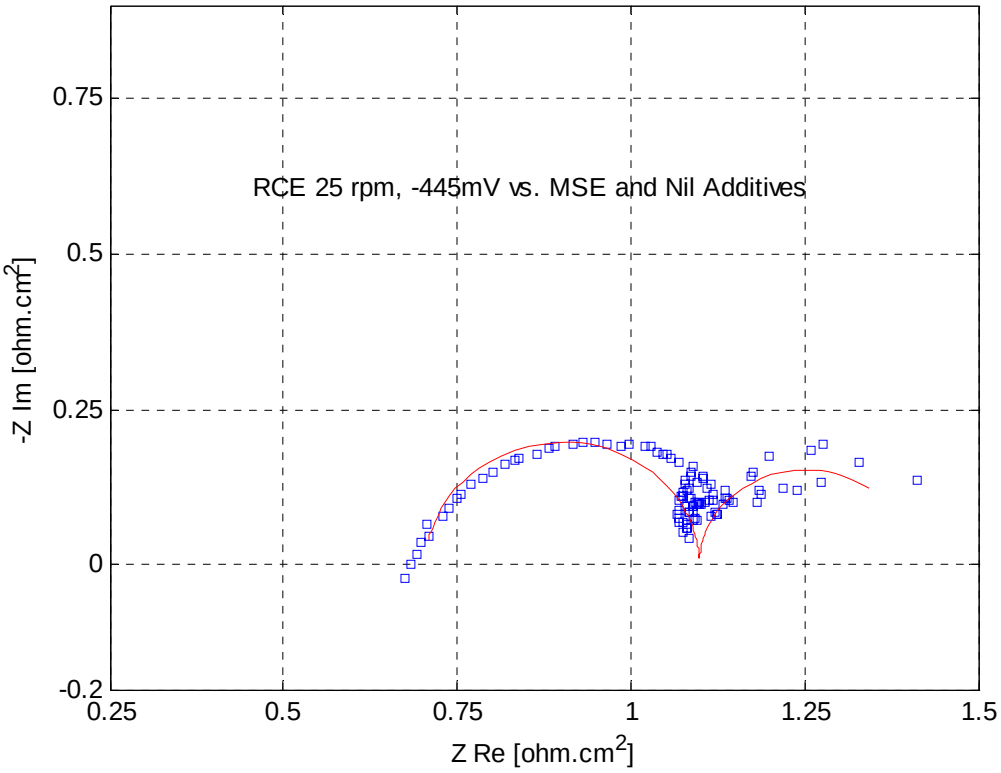

Figure 26: Complex-Plane Plot of Experimental and Simulated Impedance Spectra at 64°C in the Absence of APAM at -445mV vs. MSE

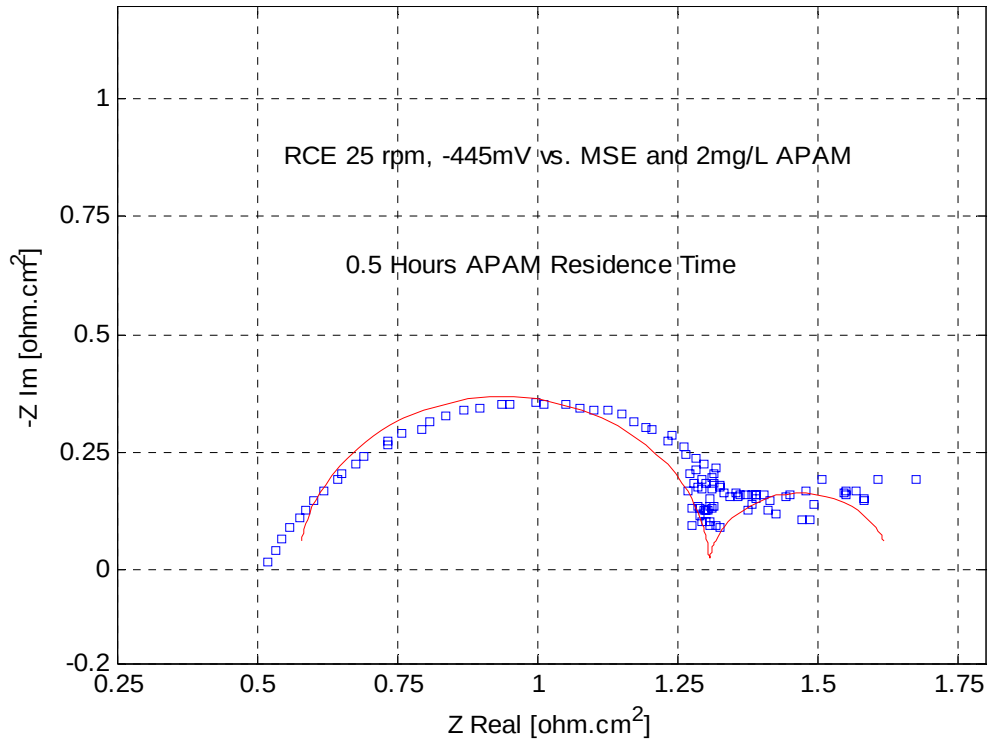

Figure 27: Complex-Plane Plot of Experimental and Simulated Impedance Spectra at 64°C in the Presence of APAM at -445mV vs. MSE and 0.5Hours Residence Time

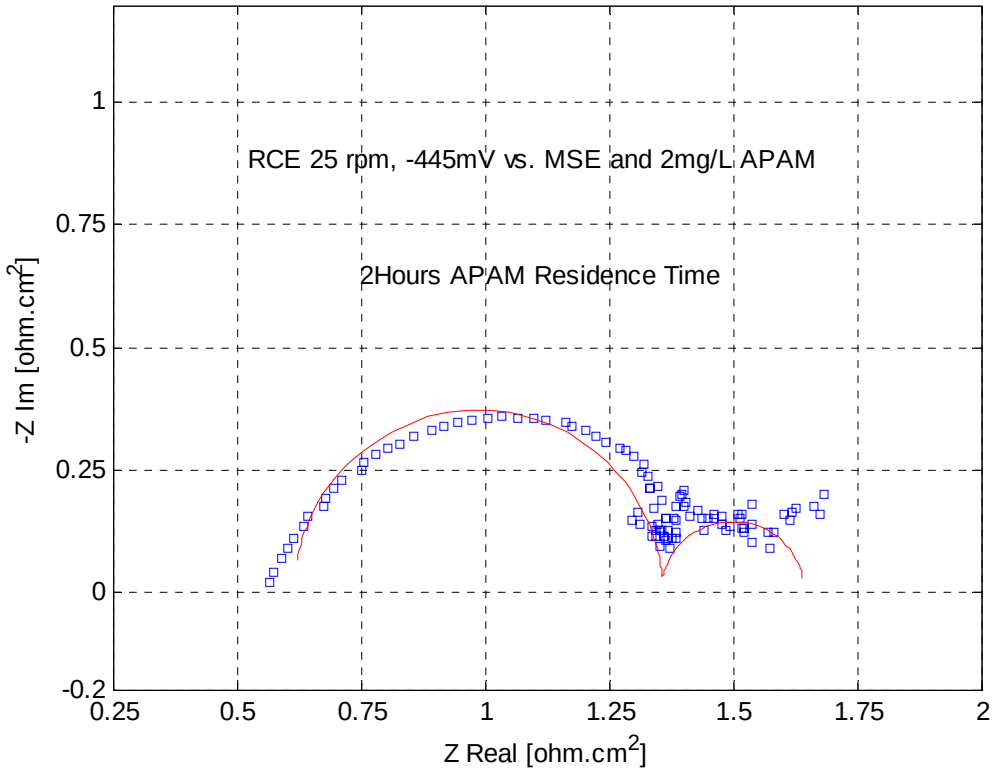

Figure 28: Complex-Plane Plot of Experimental and Simulated Impedance Spectra at 64°C in the Presence of APAM at -445mV vs. MSE and 2Hours Residence Time

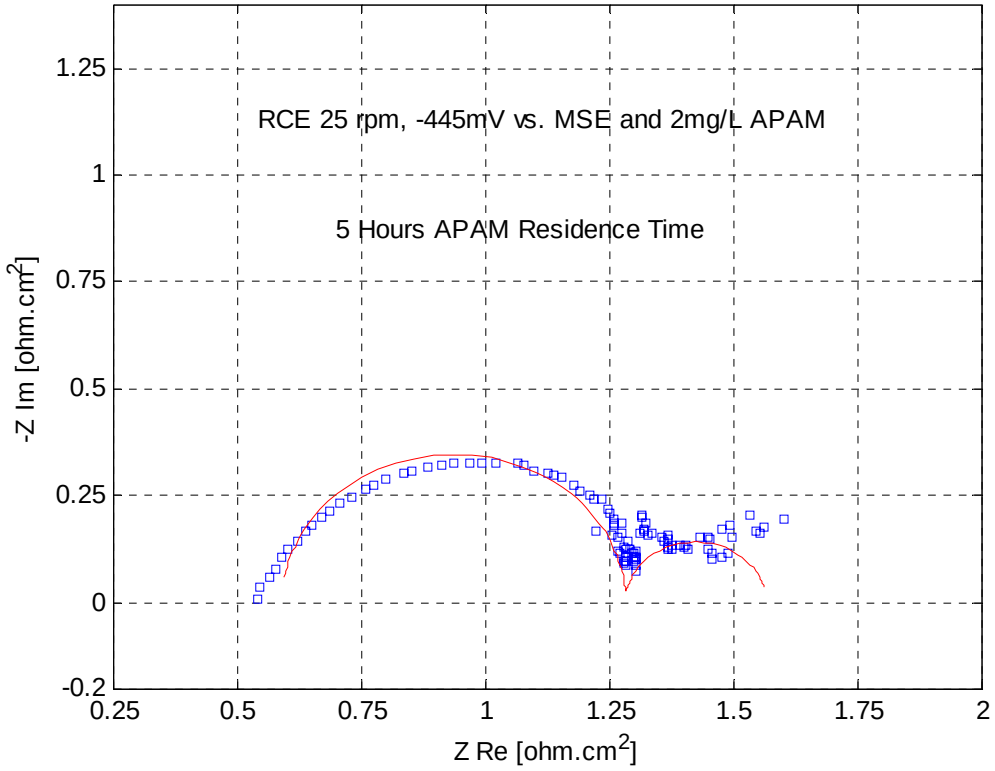

Figure 29: Complex-Plane Plot of Experimental and Simulated Impedance Spectra at 64°C in the Presence of APAM at -445mV vs. MSE and 5Hours Residence Time

ELECTROCHEMICAL IMPEDANCE DATA USING A ROTATING DISC ELECTRODE AT 25 RPM

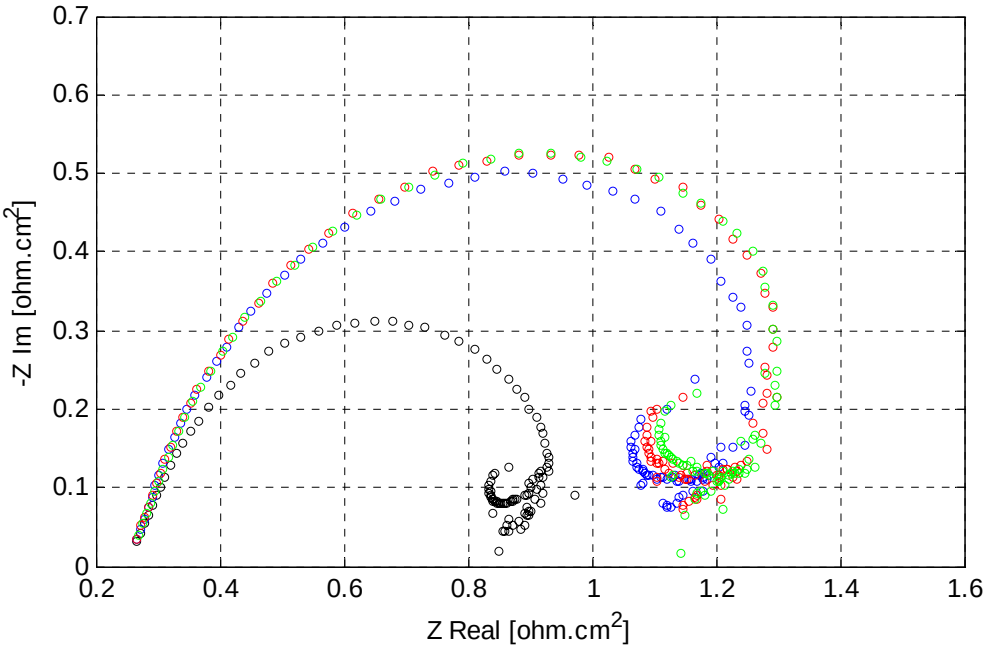

Figure 30: Complex-Plane Plot using RDE at 25 rpm and 45°C (50kHz-0.2Hz). Black – Control without APAM, Blue – 1 Hrs, Red – 3Hrs. and Green – 6Hrs.

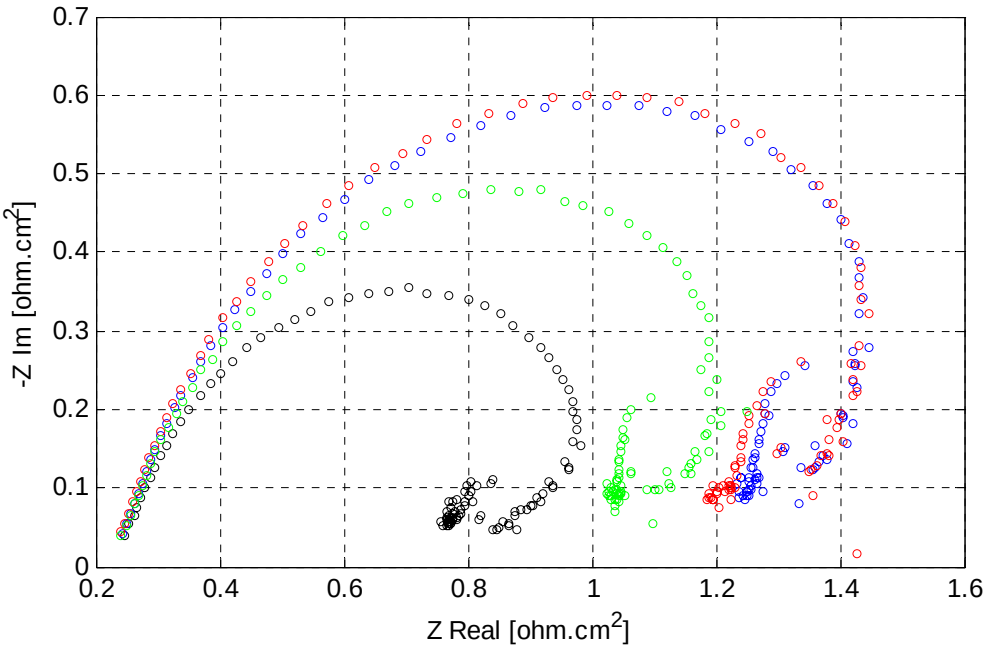

Figure 31: Complex-Plane Plot using RDE at 25 rpm and 64°C (50kHz-0.2Hz). Black – Control without APAM, Blue – 1 Hrs, Red – 3Hrs. and Green – 6Hrs.

<HYDROMETALLURGY 2003: 5th INTERNATIONAL SYMPOSIUM IN HONOR OF PROFESSOR IAN RITCHIE> *< Edited by C.A. Young, A.M. Alfantazi, C.G. Anderson, D.B. Dreisinger, B. Harris and A. James>*
TMS (The Minerals, Metals & Materials Society, <2003>

DETERMINATION OF CRYSTALLITE SIZE AND SURFACE ROUGHNESS OF COPPER DEPOSITS FOR ELECTROWINNING IN THE PRESENCE OF AN ORGANIC ADDITIVE

Cesimiro Fabian[a,b], Michael Ridd[b], Sharon Ness[c], Thomas Lancaster[d*] and Gregory Griffin[a]

[a]School of Engineering, James Cook University, Townsville, QLD., Australia
[b]School of Pharmacy and Molecular Sciences, James Cook University, Townsville, QLD., Australia,
[c]Advanced Analytical Center, James Cook University, Townsville, QLD., Australia,
[d*]Mount Gordon Operations, Western Metals Copper Limited, Gunpowder via Mount Isa, QLD., Australia,

Abstract

The crystallite size of copper electrodeposits was determined by X-Ray powder diffraction analysis using a General Area Detector Diffraction Solution (GADDS) diffractometer. Crystallite size was calculated for copper thin films which were deposited on a 316 stainless steel rotating cylinder electrode (RCE) in the presence and absence of additive "A". The crystallite size was calculated from a corrected full width at half maximum (FWHM) of the [110] peak profile using the Scherrer equation. The test of significant difference on crystallite size was derived using Kruskal-Wallis method. It was found that in the absence of the additive the median crystallite size was 426Å, which decreased to 364Å in the presence of the additive. As the additive degraded, the crystallite size increased to a size similar to that observed in the absence of additive.

1. Introduction

In the past 10 years, a lot of effort has been committed to understanding the role of additives in copper electrodeposition for the fabrication of interconnects in the microelectronics industry. However, relatively little has been published for copper deposition used in electrorefining and electrowinning. Both copper deposition in electrorefining and fabrication of interconnects requires dosing of organic additives into the electrolyte bath. The additives, commonly known as leveling agents, surfactants, grain refiners and brighteners produce smooth deposits by reducing dendrite growth or, in other terms, to promote superconformal growth for the fabrication of interconnects.

The role of the leveling agent is to reduce the charge transference at the entrances of the vias, protrusions or peaks and consequently to increase charge transference in the vias or valleys to attain smooth deposit or superconformal growth. The role of the grain refiner is to create new nucleates to form new crystallites that possibly enhance new microcurrent distribution.

---

*Present address: Straits Resources, WA, Australia

In this paper, we present a new technique (GADDS) to yield the mean crystallite dimensions of electrowon copper and limited information about their size distribution as well. This process control tool indicates that precision in terms of reproducibility is more important than absolute accuracy. This tool could be useful for quality-control comparisons to evaluate an additive system for the fabrication of interconnects, electrorefining and electrowinning.

The initial stages of 2D and 3D metal phase formation under electrochemical conditions are well understood on an atomic level and these nucleation processes depend on the nature and concentration of the leveling agent[(1)]. In metal deposition, nucleation is a very important process; the first step of metal deposition is the formation of nuclei of the depositing metal on a foreign substrate and on a substrate of the native metal. It is stated by Budevski[(1)] that the competition between nucleation and growth determines the smoothness of the deposit: the higher the nucleation rate; the finer the crystal grains (crystal size) . Conversely, the forms of the growing crystals determine the physical appearance and structure: for a higher growth rate of the crystal grains normal to the substrate, a more fibrous structure is obtained. A brightening effect can be achieved from large developed crystal faces parallel to the substrate. Therefore, the kinetics of nucleation and growth play a dominant role in determining the overall deposition kinetics, as well as the appearance, structure and properties of the deposit.

A randomly-oriented dispersion (RD) type corresponds to an increased inhibition of the crystallization process by increasing the cathodic overvoltage. The additive system for the

fabrication of interconnects often referred to in the literature[2, 3] consists of polyethylene glycol (PEG) of 3350 molecular weight, Janus Green B (JGB), bis (3-sulfopropyl) disulfide (SPS) and chloride ions in 24 g/L copper and 180 g/L sulfuric acid at room temperature. The other additive system also often referred to consists of PEG, thiol (3-mercapto-1-propanesulfonate, MPSA) and chloride ions[2, 3]. It was reported that PEG, MPSA and chloride ions were required to produce a clear hysteresis from cycle voltammographs from which a superconformal growth was also achieved. In comparison, the leveling agent used throughout the *electrorefining* industry is animal (protein) glue; the grain refiner is thiourea and chloride ions in 40-50 g/L copper and 150-180 g/L sulfuric acid at 62°C. Glue is a long-chain amino acid compound undergoing constant degradation by which the long-chain becomes shortened and protonated. The additions of fresh glue, thiourea and chloride ions are closely monitored in electrorefining plants and the dosing ratio of thiourea/glue are kept almost constant at about two.

The mechanism of the leveling effect of glue is thought to be due to the protonated ends of the glue becoming attached predominantly to the protrusions or peaks of the copper cathode. Therefore the mass transference of copper is minimized on these protrusions producing a rounded/smoothed deposit. The grain refiner, thiourea, also undergoes constant degradation, forming complexes with cuprous and cupric ions and its role is to create new nuclei on the deposit to possibly facilitate the growth of new crystals. In contrast, copper deposition in *electrowinning* uses only guarfloc (guar), a polysaccharide, and chloride ions as the additive system. It is known[4] that polysaccharides act as brighteners and that guar is a weaker leveling agent or weaker polarizer than animal glue.

In this paper we report the results of a study that investigates the use of a recently developed X-ray diffraction (XRD) spectrometer, General Area Detector Diffraction Solution (GADDS) diffractometer which allows for the collection of a large number of XRD spectra from electrowon copper sample over a small area. Using GADDS, it is possible to measure the effect of organic additives on crystallite sizes of electrowon copper and to assess the efficacy of the organic additive.

1.1 Line Broadening Principles for Crystallite Size

It is widely known that copper deposits as face centered cubic (fcc) crystals and a crystallite is the smallest diffracting domain in a material. It is important to note that the crystallite size is therefore different from, but maybe related to, particle size measured, for example with an electron microscopy.

In the absence of lattice of lattice strains or other imperfections in significant amounts, the breadth β of the pure diffraction profile can be used to calculate the crystallite size of a sample[5, 6]. The Sherrer equation (4) can be used to estimate the mean crystallite dimensions.

$$L = \frac{K.\lambda}{\beta.\cos\theta} \qquad \textbf{[1]}$$

where θ and λ are the Bragg angle and x-ray diffraction wavelength in angstroms (Å), respectively. β is the line breath, commonly known as the full width at half maximum (FWHM) intensity of the peak in radians corrected for instrumental broadening using a Gaussian profile fit ($\beta^2 = U^2 – S^2$; U = copper sample, S = standard)[5]. K, λ and θ are 0.9, 1.54184 and 15 degrees, respectively.

The Scherrer equation shows an inverse relationship between crystallite size and peak profile width: the wider the peak, the smaller the crystallites and a particle may be comprised of many crystallites.

1.2 Derivation of Diffusion Layer Thickness

A program was developed using Mathcad2001i[7] to derive the diffusion layer thickness for the RCE. The physicochemical properties of the electrolyte was obtained from the data of Price and Davenport[8, 9]. The equation for the rotating cylinder electrode is formulated as[10, 11]:

$$i_L = 0.079 \frac{nFDC_b}{d} \mathrm{Re}^{0.7}\, Sc^{0.356} \qquad [2]$$

where i_L is the limiting current density; d is the diameter of the inner cylinder, the rotating cylinder; Re, the Reynolds number ($d^2*\omega/\nu$) and Sc the Schmidt number (ν/D). n is the number of electrons transferred in the electrode reaction; F, Faraday's constant; D, diffusion coefficient of electrolyte, cm^2/s and C_b copper concentration, mol/cm^3. Finally, the Nernst diffusion model was applied to calculate the diffusion layer thickness[12].

2. Experimental

A rotating cylinder electrode (RCE) was constructed in-house similar to the test unit described by Barkey, Muller and Tobias[11] and the electrowinning tests were conducted using this rotating cylinder electrode made of 316L stainless steel as cathode and a dimensionally stable anode (DSA) sourced from ELTECH Systems Corporation, USA. The active area of the RCE was $28cm^2$ and 12,000 coulombs were applied to each test. The electrode gap was 40mm and the RPM of the RCE was controlled using a Movitrac controller and 0.37kW motor (RF27D17104) with gear box both from SEW Eurodrive.

The initial concentrations of the components of the electrolyte were: copper, 36 g/L; sulfuric acid, 160 g/L and chloride ions, 25 mg/L and the initial electrolyte volume was 3.75L. Additive "A" was dissolved in 16-fold diluted synthetic electrolyte for two hours at 50°C to promote its degradation, unless otherwise stated. Additive "A" was dosed to the electrolyte at 1mg/L, and thoroughly mixed in the electrolyte for approximately 20 minutes before a potential was applied to the EW cell.

The surface roughness of the deposit copper was measured using a Mahr Perthometer M1 using a 2μm stylus tip and calibrated with its PGN-3 (Rz = 2.9 μm) standard. The surface roughness measurement was conducted before the copper deposit was detached from the RCE at 8 equidistantly distributed areas along the height of the electrode.

X-Ray diffraction data was collected using a Siemens/Bruker General Area Detector Diffraction Solution, GADDS diffractometer at the Advanced Analytical Center of James Cook University. The instrumental parameters such as collimator size, detector resolution and beam divergence critically affect line broadening for the determination of peak broadening. Table 1 summarizes the instrumental parameters used to determine the peak broadening.

The GADDS diffractometer was set up to automatically map out 2cm^2 surface area from the 28 cm^2 copper deposits obtained from the electrowinning tests. It read in steps of 0.5mm until the full length of the Y-axis is completed and then it moved 0.5mm in the X-axis to read another full length of the Y-axis and successively to produce about 1450 readings per sample unless otherwise stated. Therefore, surface heterogeneity can be detected from the small and representative surface area to be analyzed from its XRD pattern.

Table 1: GADDS Diffractometer Parameters

Radiation	Cu
Sample-detector distance	30 cm
Collimator	500μm
kV, mA	40, 52
Data collection time/reading	60 sec
2θ, ω	70, 30
Step size, mm	0.5
Copper plate mapped area, cm^2	~2

2.1 Correction for Instrumental Line Broadening

Lanthanum hexaboride powder (LaB_6, 660a), line position and line shape standard, from the National Institute of Standards and Technology (NIST) was selected as the standard reference material (SRM). The NIST certificate states that the *Fundamental Parameters Approach* analysis for homogeneity testing and also for refinement of the FWHM using a Lorentzian profile indicated that LaB_6 displayed no strain broadening and the domain size was 2.0μm. Under the conditions stated above, the FWHM obtained for the LaB_6 SRM was 0.274 degrees, a value used to correct the FWHM of copper sample data for the effect of instrumental line broadening.

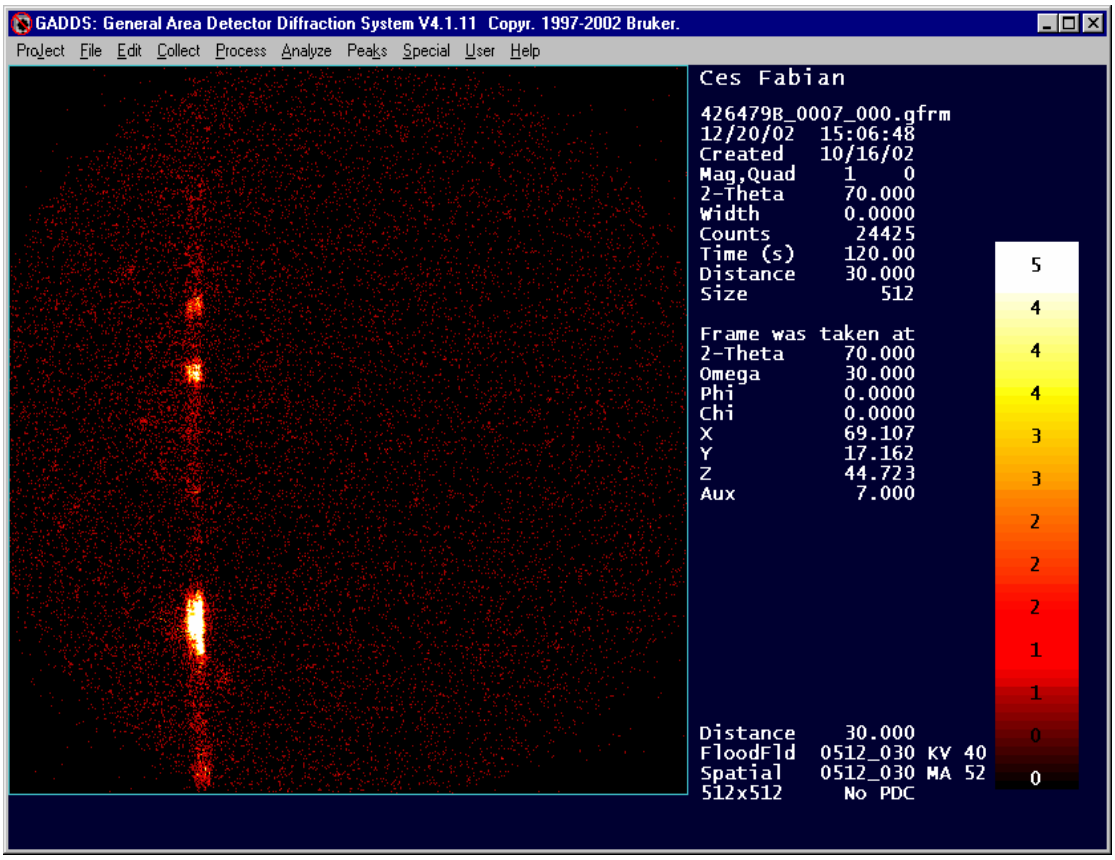

Figure 1: Typical frame from GADDS

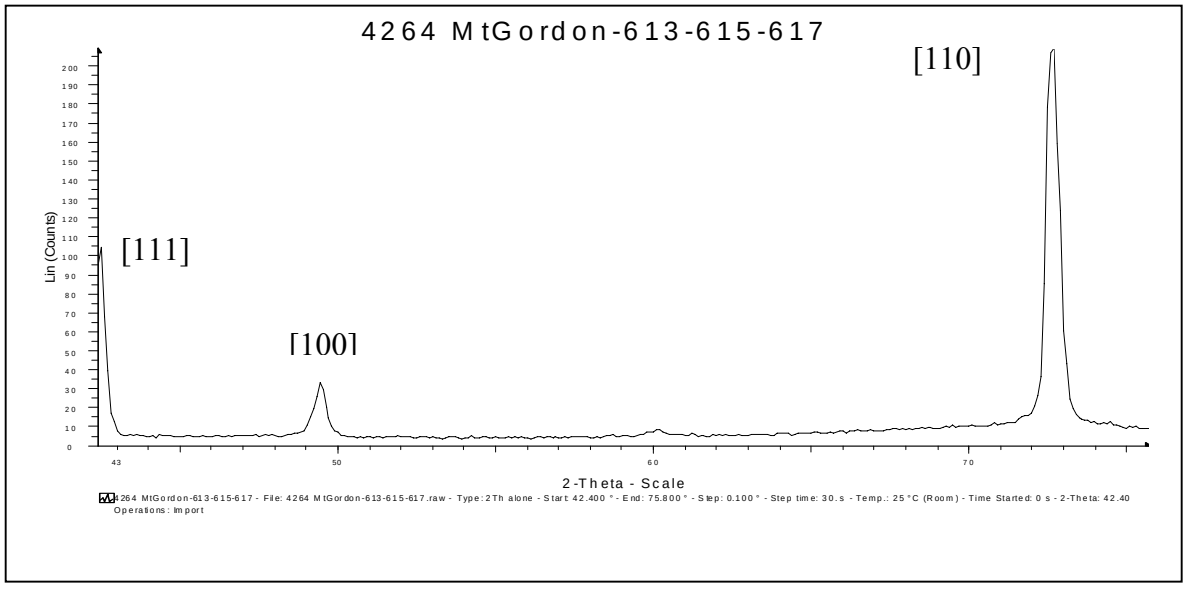

Figure 2: Typical preferred orientation profile: [110] >> [111] > [100]

The large spots in Figure 1 represent large crystallite sizes. The preferred orientation throughout this testwork was [110]>>[111]>[100] as observed in Figure 2. Ilgar and O'Keefe[13] has observed a similar orientation pattern in the presence of 20 mg/L chloride ions. Therefore the full width at half maximum was determined from the highest peak, i.e., the most common crystal orientation, the [110] preferred orientation.

The Full Width at Half Maximum (FWHM) was calculated from each profile using the EVA software from Bruker AXS.

3. Experimental Results

Table 2 shows the electrowinning conditions and surface roughness values obtained in the presence and absence of additive "A". It is noted that Tests 2 and 4 were conducted with the same electrolyte (3.75 L) and consequently, the small variations in concentration of both cupric and sulfuric acid insignificantly affected the deposition process.

Table 2: Electrowinning Conditions and Surface Roughness

Test No.	1	2	3	4
Additive "Ä" Qualitative Description	Nil	fresh	degraded	old
Additive "A" preparation, hrs		2	2	2
Additive "A" in electrolyte, hrs.		0-4	8-12	18-22
RCE rpm	10	10	10	10
EW time, hrs	4	4	4	4
Electrolyte temperature, ^{o}C	50	50	50	50
Current density, mA/cm^2	30	30	30	30
Surface roughness, Ra, µm	5.51±0.41	4.92±0.25	5.50±0.66	4.94±0.39

It is noted that the surface roughness in the absence of additive "A" at 10 RPM, equivalent to a 234 µm diffusion layer thickness and at 50^{o}C was 5.51 ± 0.41 µm. This value concurs with the range of values presented by Ilgar and O'Keefe[13] who studied the effect of 20 mg/L chloride ions on surface roughness in copper electrowinning and reported for 175 and 65 µm diffusion layer thicknesses with unstirred and stirred solutions, respectively. The values reported for unstirred solutions vary from 6.4 to 12.5 ± 0.50 µm at 30 and 40^{o}C, 25 and 35 mA/cm^2 and 6000 coulombs. The surface roughness for 65 µm diffusion layer thickness was reported to be 3.9 ± 0.50 µm. It is noted that although the copper and sulfuric acid concentrations were 36g/L and 160 g/L, respectively in the Ilgar and O'Keefe[13] study and this work, the concentration of chloride ions was 25 mg/L in this study and the electrowinning cell type was different in both studies. Therefore, the hydrodynamic equations to derive the diffusion layer thickness were also different.

In the presence of additive "A", the surface roughness from the present work appeared to be slightly lower than 5.51 ± 0.41 µm. It is noted that Tests 2 and 4 were conducted with the same electrolyte bath and it can be seen that the surface roughness for these tests slightly increases including their standard deviations.

Table 3 presents a summary of the results of the analysis of the GADDS data for each of the four electrowinning experiments. The FWHM data was analyzed using the Kruskal-Wallis nonparametric method to test significance of the difference between multiple groups using SPSS version 11.5 (2002 version). The Kruskal-Wallis test is a one-way analysis of variance by ranks; in contrast to ANOVA, it assumes nothing about the distribution of the test variable and it can be used to test ordinal variables. It tests the null hypothesis that multiple independent samples come from the same population.

As the crystallites above 4500Å in size could not be quantified due to instrument and standard limitations, the percentage of this unprocessed FWHM data is also presented in Table 3.

Table 3: Kruskal-Wallis Test Results for Crystallite Size Data

Test No.	1	2	3	4
FWHM No. Readings, N	1428	156	1479	1493
Crystallite Size No. Processed, N	1040	133	913	1102
Crystallites percentage > 4500 Å, %	27	15	38	26
Crystallite Size Mean Rank	1657	1333	1414	1716
Asymptotic. Sig., Monte Carlo Sig., 99% CI, lower and upper bounds	p = .0000			
Median Crystallite Size, Å	426	364	398	438

The Kruskal-Wallis test results indicate that the mean crystallite size differs between the four tests at the 99% confidence level. Thus it can be concluded that at least one of the four samples differs from the others. Inspection of Table 3 shows that the crystallite size mean rank and the median crystallite size decreased in the presence of additive "A' except for experiment 4 when the additive had undergone degradation at 50^{o}C for 18-22 hours and had become inactive.

It can be seen from Table 3 that the proportion of crystallites larger than 4500Å varied between the tests. When additive 'A' was degraded slightly smaller crystallites but distinctly more crystallites greater than 4500 Å were formed compared with nil additive, fresh additive and old additive. The data for Test 3 are consistent with the formation with the formation of relatively large proportion of small crystallites formed on top of large crystals.

Figure 3 shows the FWHM histograms and indicates that Test 3 has two distinct frequencies. The frequency conformed by FWHM values less than 0.274 degrees 2θ possibly represent crystallites greater than 4500Å.

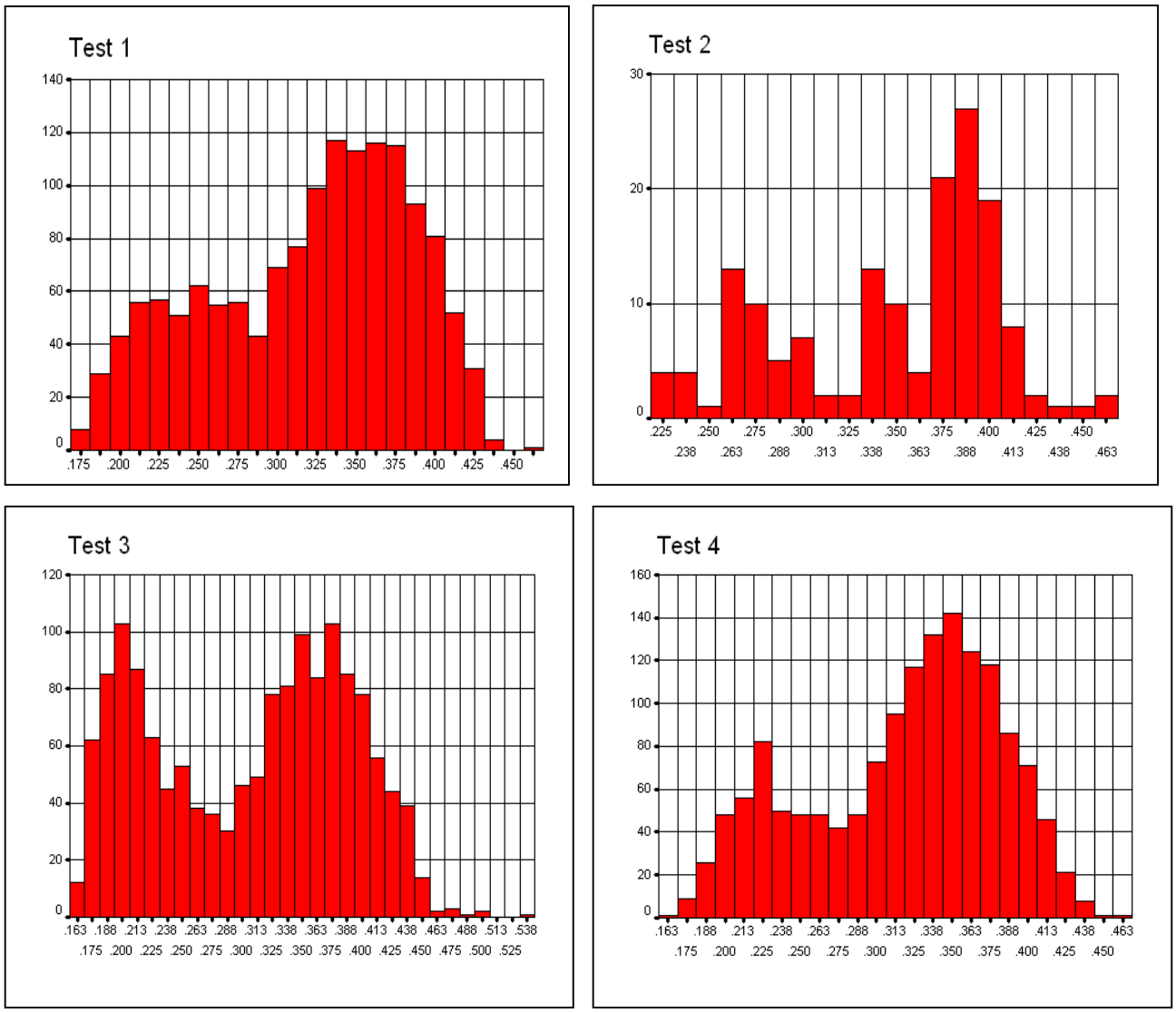

Figure 3 : FWHM Histograms

Figure 4 depicts the crystallite size mean rank results from the Kruscal-Wallis calculations and it indicates that Test 2 with fresh additives produces the smallest average crystallite size followed by Test 3 conducted with degraded additive, then Test 1 with no additive and finally Test 4 with an old additive as it would be expected. Figure 5 shows the median of crystallite size for all tests and confirms the above observation.

A comparison between the results in Tables 2 and 3 shows that while the surface roughness decreases in concert with a decrease in crystallite size between Tests 1 and 2; (as might be expected if crystallite size and particle size are closely related), the increases in surface roughness observed in Test 3 was not reflected in an increase in crystallite size. We are unable at this stage to explain this observation.

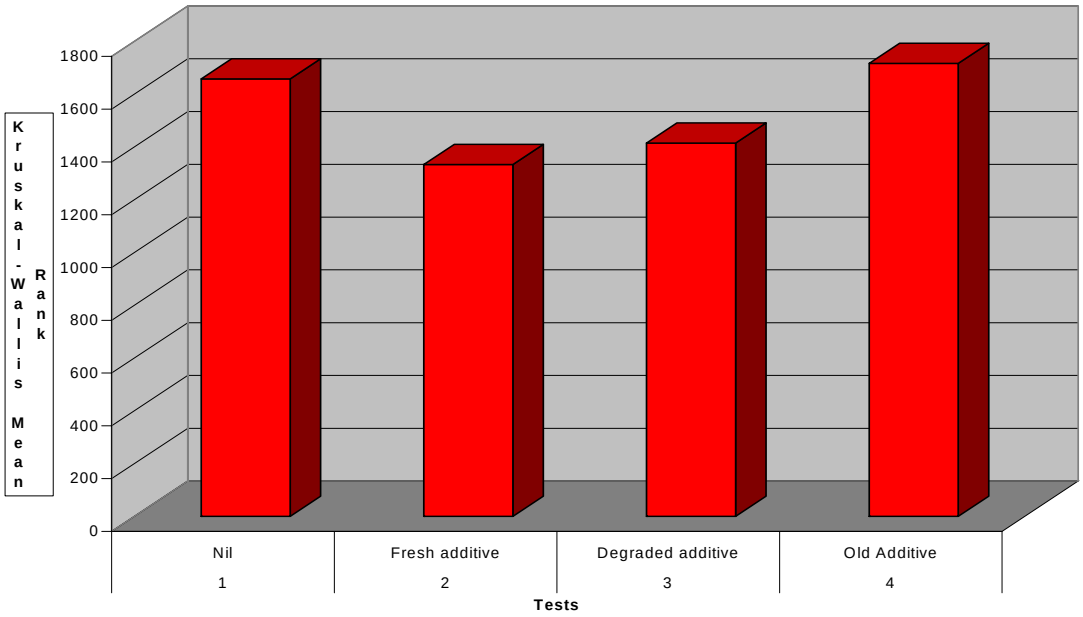

Figure 4: Kruskal-Wallis Mean Rank Results for Crystallite Size

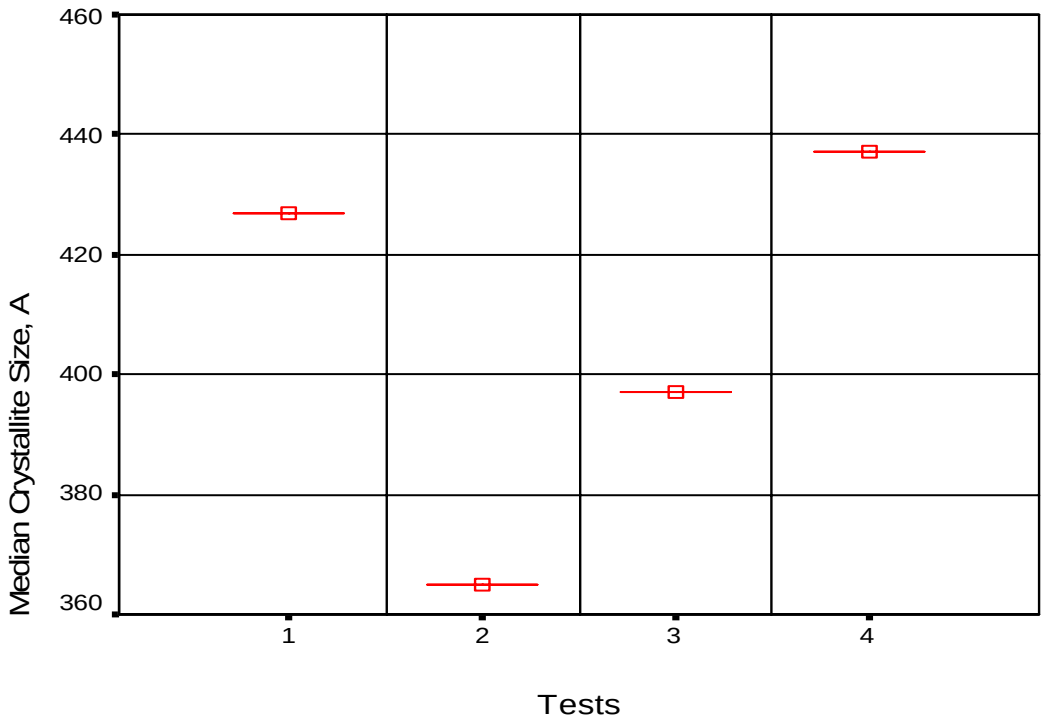

Figure 5: Median of Crystallite Size

Figure 6 shows the 3-D mapping of FWHM and crystallite size distribution for about 1450 readings per test for 2cm^2 surface area; except for Test 2 which had 150 readings on 1cm^2 area. It is noted that Test 3 indicates the predominance of smaller crystallite size. This figure demonstrates the ability of GADDS to obtain a map of crystallite sizes on electrowon deposits, a capability which potentially allows for a detailed study of spatially heterogeneous deposits.

Figure 8 shows a SEM micrograph of a polished sample of the electrowon copper in Test 3. It can be seen that a typical grain size as observed is of the order of 20μm. The median crystallite size for Test 3 measured by GADDS was 0.04μm indicating that for this sample an aggregation factor of the order of 500 is need to convert Scherrer crystallite size to the observable grain size.

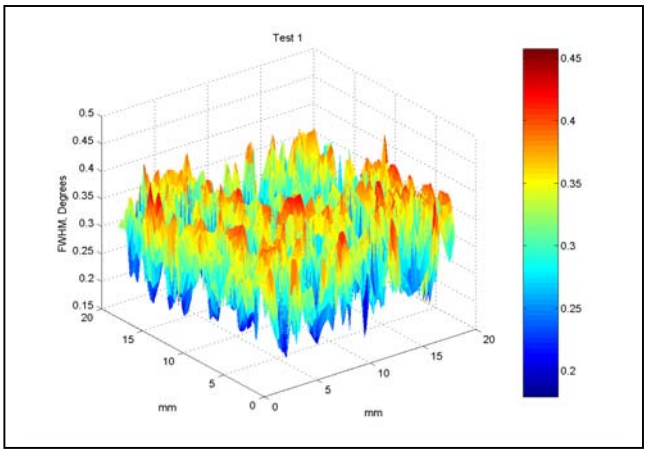
Test 1
FWHM, Degrees
mm
mm

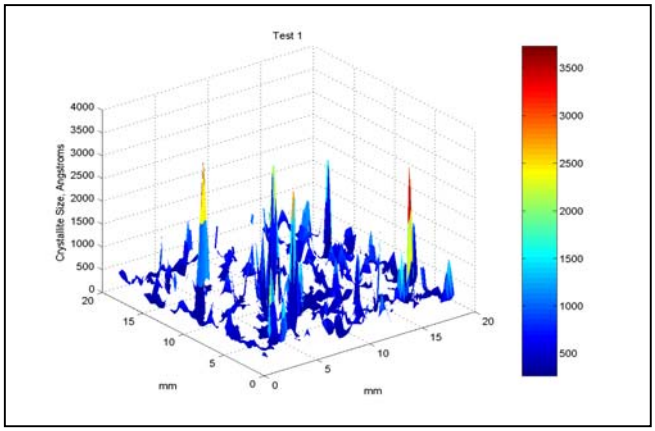
Test 1
Crystallite Size, Angstroms
mm
mm

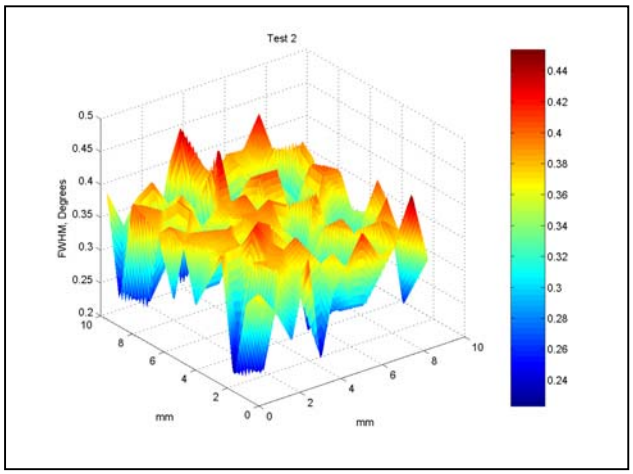
Test 2
FWHM, Degrees
mm
mm

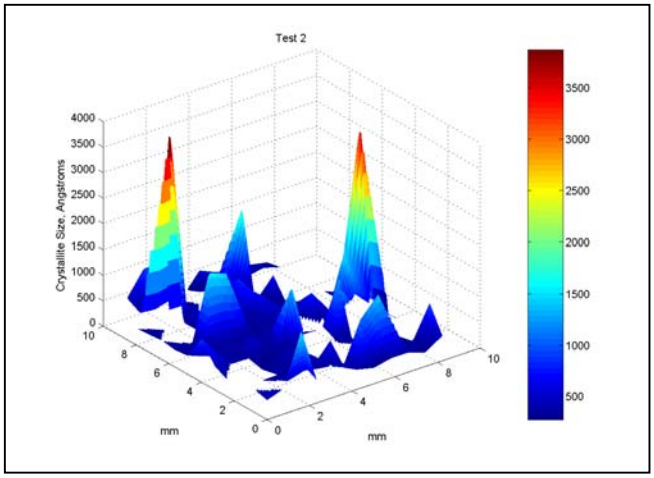
Test 2
Crystallite Size, Angstroms
mm
mm

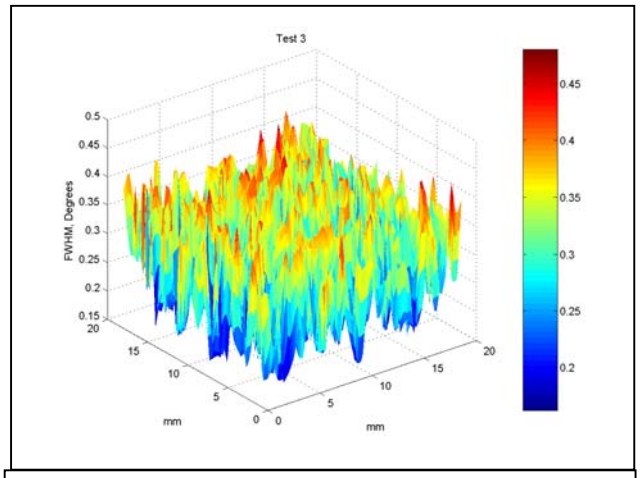
Test 3
FWHM, Degrees
mm
mm

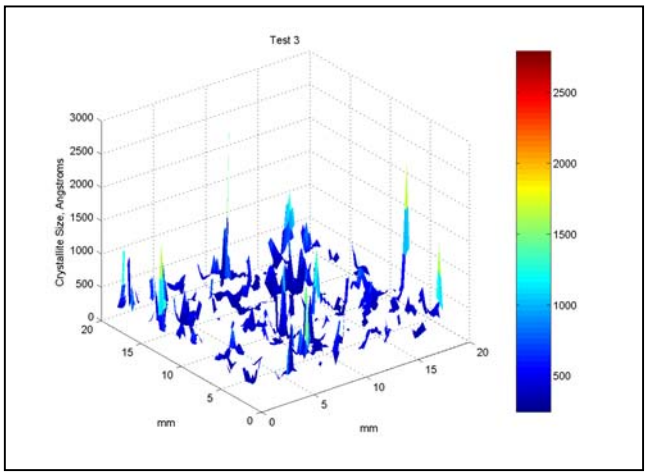
Test 3
Crystallite Size, Angstroms
mm
mm

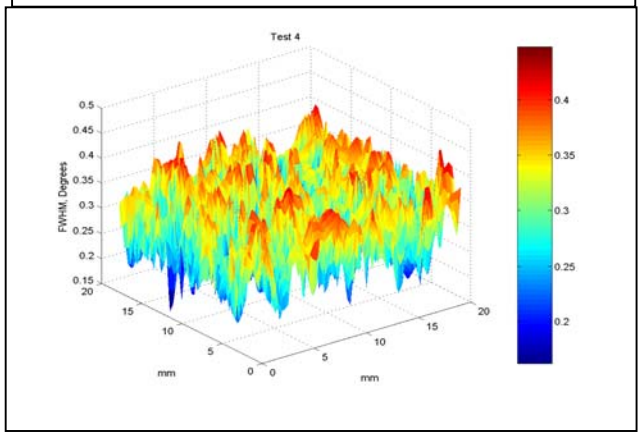
Test 4
FWHM, Degrees
mm
mm

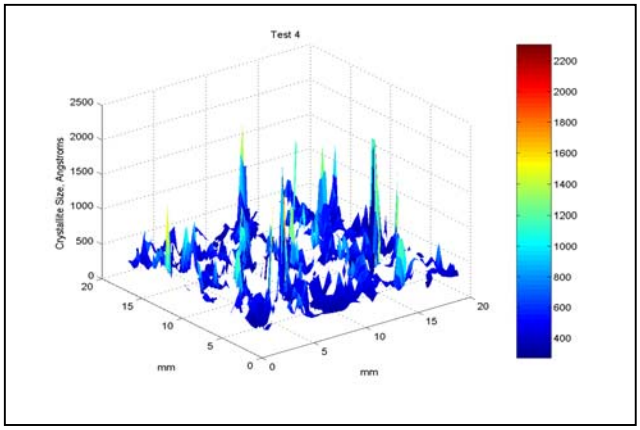
Test 4
Crystallite Size, Angstroms
mm
mm

Figure 6: 3D Mapping of FWHM and Crystallite Size

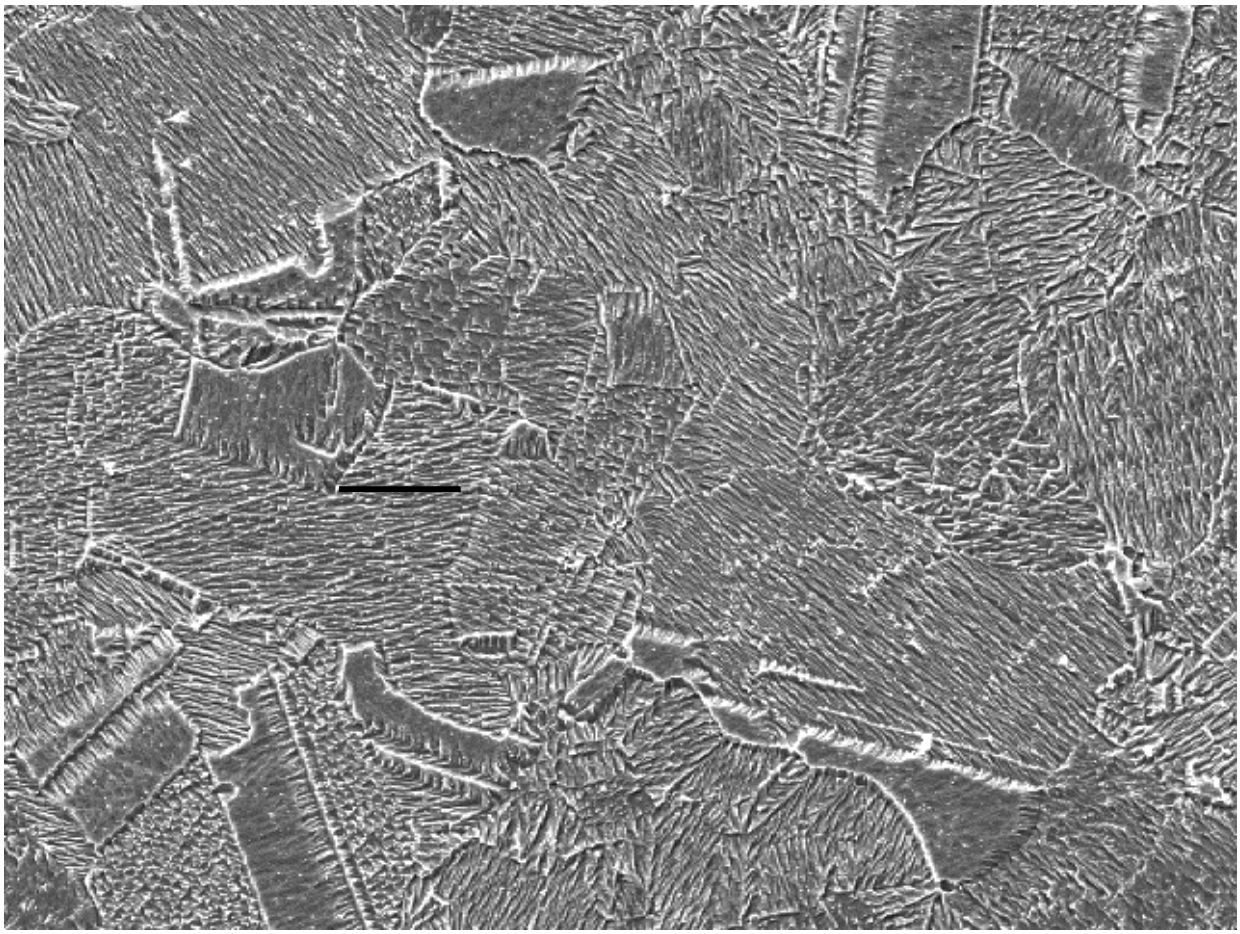

Figure 3: Test 3 Crystallite Size of Electrolyte-Side Polished (line = 20 μm)

Conclusions

In this paper we have demonstrated that GADDS, a non-destructive, in-situ technique is capable of detecting the effect of an additive on the crystallite size of electrowon copper. It was also shown that while there is some correlation between surface roughness and crystallite size, the correlation is relatively weak. In addition it has been demonstrated that GADDS allows for a study of spatial heterogeneity in crystallite dimension by allowing a 'map' of the crystallite size to be prepared.

Finally, additive "A" may be used as grain refiner in copper electrowinning and the GADDS technique may be used as a process control tool among other techniques, i.e., electrochemical, to select a new reagent system for copper electrodeposition in electrowinning, electrorefining and in the fabrication of interconnects.

Acknowledgements: we should like to acknowledge Mount Gordon Operations of Western Metals Copper Limited, Australia for supporting this research.

References

1. Budevski E, Staikov G, Lorenz W. Electrochemical Phase Formation and Growth, An Introduction to the Initial Stages of Metal Deposition. New York: VCH; 1996.
2. Moffat T, Bonevich J, Huber W, Stanishevsky A, Kelly D, Stafford G, et al. Superconformal electrodeposition of copper in 500-90 nm features. J. Electrochem. Soc. 2000;147(12):4524-4535.
3. Radisic A, West A, Searson P. Influence of Additives on Nucleation and Growth of Copper on n-Si(111) from Acidic Sulfate Solutions. Journal of the Electrochemical Society 2002;149(2):C94-C99.
4. Chassaing E. Effect of Organic Additives on the Electrocrystallization and the Magnetoresistance of Cu-Co Multilayers. Journal of the Electrochemical Society 2001;148(10):C690-C694.
5. Siemens, Bruker. GADDS Introduction Manual; 2001.
6. Klug H, Alexander L. X-Ray Diffraction Procedures for Polycrystalline and Amorphous Materials. Second ed. Sydney: John Willey & Sons; 1974.
7. MathSoft. Mathcad 2001i. In; 2002.
8. Price DC, Davenport WG. Densities, Electrical Conductivities and Viscosities of $CuSO_4/H_2SO_4$ Solutions in the Range of Modern Electrorefining and Electrowinning Electrolytes. Metallurgical & Materials Transactions B-Process Metallurgy & Materials Processing Science 1980;11B:159-163.
9. Price D, Davenport W. Physico-Chemical Properties of Copper Electrorefining and Electrowinning Electrolytes. Metallurgical & Materials Transactions B-Process Metallurgy & Materials Processing Science 1981;12B:639-643.
10. Baker DR, Verbrugge MW, Newman J. A transformation for the treatment of diffusion and migration. Application to the simulation of electrodeposition onto microelectrode geometries. Proceedings - Electrochemical Society 1992;92-3(Proc. Int. Symp. Electrochem. Microfabr., 1st, 1991):279-90.
11. Barkey D, Muller R, Tobias C. Roughness Development in Metal Electrodeposition I. Experimental Results. Journal of the Electrochemical Society 1989;138(8):2199-2207.
12. Uceda D. Determination of Mass Transfer Characteristics in the Electrolysis of Copper [PhD Thesis]. Missouri-Rolla: University Missouri-Rolla; 1988.
13. Ilgar E, O'Keefe T. Surface Roughening of Electrowon Copper in the Presence of Chloride Ions. In: Dreisinger D, editor. Aqueous Electrotechnologies: Progress in Theory and Practice; 1997: The Minerals Metals and Materials Society; 1997. p. 51-62.